



The University of
Nottingham

UNITED KINGDOM • CHINA • MALAYSIA

**FORMULATION, GASTROINTESTINAL TRANSIT STUDIES
AND ABSORPTION OF AMPHOTERICIN B-CONTAINING
SOLID LIPID NANOPARTICLES IN RATS**

Hilda Amekyeh, BPharm, MPhil Pharmaceutics

*Thesis submitted to the University of Nottingham in fulfilment of the requirements
for the Degree of Doctor of Philosophy*

May 2016

To my loving mother Lydia Gertrude Akyen.

You are dearly missed.

This thesis is the result of the author's original work except for quotations and citations, which have been duly acknowledged. It has not been previously or concurrently submitted for any degree at the University of Nottingham Malaysia Campus or any other institution.

Hilda Amekyeh

Date:

ACKNOWLEDGEMENTS

I would like to first thank God for His continued grace, protection and provision.

I would like to extend my deepest gratitude to my supervisor Prof. Nashiru Billa for his valuable guidance and patience throughout this research period. His exceptional supervision immensely contributed to the success of this project. You are well appreciated for your dedication to your students. I would also like to thank my co-supervisor Prof. Clive Roberts (Head, School of Pharmacy) for his support, time and advice during my stay at the University of Nottingham, UK campus (UNUK) which have contributed to the success of this project.

I would like to thank Prof. Stephen Doughty (Vice-Provost for Teaching and Learning, University of Nottingham Malaysia Campus, UNMC) for his invaluable advice and for his role as my internal assessor. I would like to thank Prof. Andrew Morris (Head, School of Pharmacy, UNMC) who in one way or another contributed to the success of this project. Your advice during the development of my HPLC method was well taken. My thanks also goes to the Graduate School of UNMC for the programmes organised for both training and information, which were very useful during my research.

My heartfelt gratitude goes to Prof. Kah-Hay Yuen (University Sains Malaysia, USM) for allowing me to use his laboratory for all the animal studies conducted in this project. His welcoming nature, expertise and guidance enabled me to achieve the main objectives of this study. A big thank you also goes to Dr. Sherlyn Chin, Mr. Song Thai and Ms. Nasiba for their assistance during my work at USM.

Many thanks to Dr. Christopher Parmentia, Dr. David Scurr, Prof. Chen, Paul Cooling and Thomas Booth, all of UNUK, for assisting me with various aspects of my work.

Many thanks to the lab technicians, and the academic and administrative staff of the School of Pharmacy, UNMC for the various ways they contributed to the success of my project and stay at UNMC.

I would also like to extend my sincere thanks to the Ministry of Science, Technology & Innovation of Malaysia (MOSTI) as well as the Ghana Education Trust Fund (GETFund) for the financial support they provided throughout the research project.

I would like to thank all my colleagues at the Drug Delivery Lab (UNMC), Yamina Boukari and Enas Ali Mahmoud Alkhader, as well as former colleagues Dr. Yaa Asantewaa, Dr. Hui Ling Lau, Dr. Adeyinka Temitope Aina and Dr. Manish Gupta for their valuable contributions and encouragement.

To my dearest late Mom, all your hard work, encouragement and prayer helped immensely to bring me this far. My dearest siblings, Richfield, Sussie and Rebecca, your love and faith in me have always kept me going. Many thanks to my dearest Olayinka Olafare for all his support and care. Lastly, I would like appreciate my cherished friends, Christopher, Perpetual, Daniel, Maud, James, Samuel, Paapa Osman and Aliyu Siise, for being there for me during the tough times; I could not have asked for better friends.

TABLE OF CONTENTS

	Page
DEDICATION	I
DECLARATION	II
ACKNOWLEDGEMENTS	III
TABLE OF CONTENTS	V
LIST OF TABLES	X
LIST OF FIGURES	XII
LIST OF EQUATIONS	XVIII
LIST OF ABBREVIATIONS	XIX
ABSTRACT	XXI
CHAPTER 1: INTRODUCTION AND BACKGROUND	1
1.1 General overview	1
1.2 Amphotericin B	4
1.2.1 Physicochemical properties	4
1.2.2 Pharmacokinetics	4
1.2.3 Mechanism of action	6
1.2.4 Toxicity	7
1.2.5 Available formulations of amphotericin B	9
1.3 Nanoparticle formulations	10
1.4 Lipid Nanoparticles	11
1.5 Solid lipid nanoparticles (SLNs)	13
1.5.1 Influence of formulation and processing variables on SLN quality	14
1.5.1.1 Lipids and emulsifiers	14
1.5.1.2 Particle size	15
1.5.2 Advantages of SLNs over other particulate drug delivery systems	16
1.5.3 Methods of preparing SLNs	17
1.5.3.1 High pressure homogenisation (HPH)	17
1.5.3.1.1 Hot homogenisation	17
1.5.3.1.2 Cold homogenisation	18
1.5.3.2 High speed stirring and/or ultrasonication	19
1.5.3.3 Emulsification solvent diffusion	19
1.5.3.4 Emulsification solvent evaporation	21
1.5.3.5 Supercritical fluid (SCF) method	21
1.5.3.6 Microemulsion-based method	22
1.5.3.7 Double emulsion method	23
1.5.3.8 Film-ultrasound dispersion method	24
1.5.4 Characterisation of SLNs	24

1.5.4.1	Particle size	24
1.5.4.2	Zeta potential (ZP)	27
1.5.4.3	Particle shape, morphology and topography	29
1.5.4.4	Crystallinity of lipid and drug	31
1.5.4.5	Drug localisation within SLNs	32
1.5.4.6	Drug release from SLNs	35
1.5.5	Oral absorption and bioavailability of SLNs	36
1.5.5.1	Dosage forms for oral SLNs	36
1.5.5.2	Mechanisms of oral absorption of SLNs	37
1.5.5.3	Bioavailability of SLNs	40
1.5.5.4	Metabolism of SLNs	41
1.5.6	Potential of SLNs in reducing toxicity and side effects of drugs	42
1.6	Gastrointestinal transit of pharmaceutical dosage forms	43
1.7	Aim of the study	45
1.8	Specific objectives	45
 CHAPTER 2: FORMULATION AND CHARACTERISATION OF AMPHOTERICIN B, PARACETAMOL AND SULPHASALAZINE SOLID LIPID NANOPARTICLES		46
2.1	Introduction	46
2.2	Materials	48
2.3	Methods	49
2.3.1	Formulation of AmB, PAR and SSZ SLNs	49
2.3.2	Scanning electron microscopy (SEM)	50
2.3.3	Optimised procedure for preparing AmB, PAR and SSZ SLNs	50
2.3.4	Characterisation of the optimised SLNs	50
2.3.4.1	Relative density and viscosity determinations	50
2.3.4.2	Gel electrophoresis	51
2.3.4.3	Photon correlation spectroscopy (PCS)	52
2.3.4.4	SEM analyses	53
2.3.4.5	Atomic force microscopy (AFM)	53
2.3.4.6	Fourier transform infrared spectroscopy (FTIR)	53
2.3.4.7	Differential scanning calorimetry (DSC)	54
2.3.4.8	HPLC method for <i>in vitro</i> analyses	54
2.3.4.9	Encapsulation efficiency (%EE)	55
2.3.4.10	Drug release studies	55
2.3.4.11	Determination of drug release kinetics	56
2.3.4.12	Statistical analyses	57
2.4	Results and discussion	58
2.4.1	Physical appearance of the SLNs	58

2.4.2	SEM analyses of the SLNs	59
2.4.3	Physical appearance of the optimised SLNs	61
2.4.4	Relative density and viscosity	61
2.4.5	Gel electrophoresis	62
2.4.6	PCS studies	63
2.4.7	SEM analyses	66
2.4.8	AFM analyses	68
2.4.9	FTIR analyses	72
2.4.10	DSC studies	79
2.4.11	HPLC analyses	84
2.4.12	Encapsulation efficiency (%EE)	88
2.4.13	Drug release studies	89
2.4.13.1	Drug release kinetics	95
2.4.14	Stability of the SLNs after freeze-drying and storage	98
2.4.14.1	Freeze-drying of the SLNs	98
2.4.14.2	Storage temperature and light conditions	102
2.5	Conclusions	110
 CHAPTER 3: STABILITY OF THE SOLID LIPID NANOPARTICLES AND SURFACE CHEMISTRY ANALYSES IN SIMULATED GASTROINTESTINAL FLUIDS		111
3.1	Introduction	111
3.2	Materials	114
3.3	Methods	114
3.3.1	Preparation of drug-free, AmB, PAR and SSZ SLN formulations	114
3.3.2	Stability of the SLNs in simulated GI fluids	115
3.3.3	PCS studies	115
3.3.4	NTA studies	115
3.3.5	ToF-SIMS analyses	116
3.4	Results and discussion	117
3.4.1	PCS analyses	117
3.4.2	NTA studies	131
3.4.3	ToF-SIMS analyses	142
3.5	Conclusions	160

CHAPTER 4: DEVELOPMENT AND VALIDATION OF HIGH-PERFORMANCE LIQUID CHROMATOGRAPHY METHOD	161
4.1 Introduction	161
4.2 Materials	163
4.3 Methods	164
4.3.1 HPLC instrumentation and conditions	164
4.3.2 Plasma standards	165
4.3.3 Plasma sample preparation	165
4.3.4 Specificity	165
4.3.5 Linearity and range	166
4.3.6 Precision	166
4.3.7 Accuracy	167
4.3.8 Recovery	167
4.3.9 Limits of detection and quantification	167
4.4 Results and discussion	168
4.4.1 Selection of internal standard (IS)	168
4.4.2 Mobile phase composition and elution method	169
4.4.3 Effect of deproteinising agent	176
4.4.4 HPLC method validation	180
4.4.4.1 Specificity	180
4.4.4.2 Effect of plasma (matrix effect)	184
4.4.4.3 Linearity and range	188
4.4.4.4 Precision	191
4.4.4.5 Accuracy	191
4.4.4.6 Recovery	192
4.4.4.7 LOD and LOQ	193
4.5 Conclusions	198
 CHAPTER 5: PILOT GASTROINTESTINAL TRANSIT STUDY	 199
5.1 Introduction	199
5.2 Materials and methods	202
5.2.1 Preparation of AmB, PAR and SSZ SLN formulations	202
5.2.2 <i>In vivo</i> study	202
5.2.2.1 Animals	202
5.2.2.2 Procedural care of the rats	203
5.2.2.3 Drug administration and blood sampling	203
5.2.3 Data and statistical analyses	204
5.3 Results and discussion	204
5.3.1 Selection of animal model	204

5.3.2	Improved absorption of AmB after its incorporation into SLNs	206
5.3.3	Absorption of PAR from SLNs and suspension	210
5.3.4	Absorption of SP from SSZ	213
5.3.5	Pilot GI transit study	216
5.3.6	Considerations for the main GI transit study	217
5.4	Conclusions	218
CHAPTER 6: EFFECT OF FOOD STATUS ON THE GASTROINTESTINAL TRANSIT OF AMPHOTERICIN B-CONTAINING SOLID LIPID NANOPARTICLES		220
6.1	Introduction	220
6.2	Methods	224
6.2.1	Preparation of SLN formulations	224
6.2.2	Animals	224
6.2.3	Drug administration and blood sampling	224
6.2.4	Estimation of gastric transit time (GTT)	225
6.2.5	Estimation of small intestinal transit time (SITT)	225
6.2.6	Estimation of caecal arrival time (CAT) and colonic transit time (CTT)	226
6.2.7	Estimation of AmB absorption in the stomach, small intestine and colon	226
6.2.8	Statistical analyses	226
6.3	Results and discussion	227
6.3.1	Improved oral bioavailability of AmB using SLNs	227
6.3.2	Gastric transit of the AmB SLNs	231
6.3.3	Small intestinal transit of the AmB SLNs	236
6.3.4	CAT and CTT of the AmB SLNs	238
6.3.5	Estimated AmB absorption in the stomach, small intestine and colon	241
6.4	Conclusions	247
CHAPTER 7: SUMMARY AND GENERAL CONCLUSIONS		248
CHAPTER 8: SUGGESTIONS FOR FUTURE WORK		251
LIST OF PUBLICATIONS FROM THE PRESENT WORK		254
REFERENCES		255

LIST OF TABLES

		Page
2.1	Composition of the SLNs	49
2.2	Models for drug release kinetics	57
2.3	Z-averages, PDIs and ZPs of freshly prepared SLN formulations	64
2.4	Melting peaks and enthalpies of TO and BW in the bulk lipids and the SLNs	82
2.5	Nonlinear fits of AmB, PAR and SSZ released from the respective SLNs	96
4.1	Gradient elution method for analysing AmB, PAR, SP and IS	171
4.2	Improved gradient elution method for HPLC analyses of AmB, PAR, SP and IS	174
4.3	Optimum gradient elution method for the HPLC analyses	174
4.4	Summary of HPLC method validation parameters for AmB	195
4.5	Summary of HPLC method validation parameters for PAR	196
4.6	Summary of HPLC method validation parameters for SP	197
5.1	Pharmacokinetic data for AmB SLNs and AmB suspension in rat plasma	207
5.2	Pharmacokinetic data for PAR SLNs and PAR suspension in rat plasma	211
5.3	Pharmacokinetic data for SP from SSZ SLNs and SSZ suspension in rat plasma	215

6.1	Pharmacokinetic data for AmB SLNs and AmB suspension in fasted and fed rats	228
6.2	Pharmacokinetic data for PAR SLNs and PAR suspension in fasted and fed rats	232
6.3	Individual values of T_{10P} , T_{90P} and GTT, estimated from plasma PAR profiles under fasted and fed states (n = 3)	235
6.4	Individual values of T_{max} , T_{10S} , CAT and SITT, estimated from plasma SP profiles under fasted and fed states (n = 3)	237
6.5	Estimated percentage absorption of AmB from SLNs in the stomach, small intestine and colon (n = 3)	245

LIST OF FIGURES

	Page	
1.1	Chemical structure of AmB	5
1.2	Structural similarities between cholesterol and ergosterol	7
1.3	Typical SLN structure	13
1.4	Schematic diagram for preparing nanoparticles using emulsification solvent diffusion method	20
1.5	Diagrammatic representation of the distribution of ions around a charged nanoparticle in a dispersion	27
1.6	Possible drug localisation in SLNs	34
1.7	Summary of SLN absorption after oral administration: A. Intercellular/paracellular pathway, B. M cell uptake via Peyer's patches, and C. chylomicron-assisted enterocyte absorption [SLN models: SS-Solid solution; CSM-DES-Core-shell model, drug-enriched shell; CSM-DEC-Core-shell model, drug-enriched core]	38
1.8	Diagram showing an M cell of a Peyer's patch	39
1.9	Typical gamma scintigraphic images from a GI transit study in a human volunteer	44
2.1	Gel electrophoresis set-up	52
2.2	Physical appearance of the SLNS	59
2.3	SEM images of the SLNs	60
2.4	Physical appearances of the optimised SLNS	61
2.5	Agarose gel (a) before and (b, c) after voltage application [b-normal photograph; c-image obtained from viewing gel under UV light]	63
2.6	Particle size distribution by intensity of the freshly prepared SLNs (n = 3)	65

2.7	SEM images of the optimised SLNs	67
2.8	AFM (a) surface topographic (b) phase and (c) 3D images of AmB SLNs	69
2.9	AFM (a) surface topographic (b) phase and (c) 3D images of PAR SLNs	70
2.10	AFM (a) surface topographic (b) phase and (c) 3D images of SSZ SLNs	71
2.11	Chemical structures of AmB, PAR and SSZ	72
2.12	FTIR spectra for pure AmB and AmB SLNs	75
2.13	FTIR spectra for pure PAR and PAR SLNs	76
2.14	FTIR spectra for pure SSZ and SSZ SLNs	77
2.15	FTIR spectra for AmB SLNs, PAR SLNs and SSZ SLNs	79
2.16	DSC thermograms of theobroma oil (TO), beeswax (BW), lecithin soy (LS), sodium cholate (SC), drug-free SLNs and drug-loaded SLNs	80
2.17	DSC thermograms of the pure drugs and their respective SLN formulations	81
2.18	Representative chromatograms for AmB at 405 nm, and PAR and SSZ at 254 nm [50 µg/mL each in a pure solution]	85
2.19	Standard calibration curves for pure solution of (a) AmB, (b) PAR and (c) SSZ	87
2.20	Encapsulation efficiencies of AmB, PAR and SSZ in their respective SLNs (n = 3)	89
2.21	Cumulative release profiles of AmB, PAR and SSZ in PBS (pH 7.4) from their respective freshly prepared and freeze-dried SLNs	90
2.22	Drug release profiles of AmB, PAR and SSZ from their respective SLNs	94
2.23	Images of the freeze-dried SLNs	99
2.24	Particle size distribution by intensity of the freeze-dried SLNs (n = 3)	100

2.25	SEM images of the freeze-dried SLNs	101
2.26	Particle size distribution by intensity of the SLNs after 24 months of storage (n = 3)	105
2.27	Z-averages and PDIs of the fresh SLNs, after storage for 24 months, and after freeze-drying (n = 3)	107
2.28	ZPs of the fresh SLNs, after storage for 24 months, and after freeze-drying (n = 3)	108
3.1	Particle size distribution by intensity of drug-free SLNs, before (fresh sample) and after their incubation in simulated GI fluids (n = 3)	118
3.2	Z-averages and PDIs of the SLNs before (fresh sample) and after their incubation in simulated GI fluids (n = 3)	121
3.3	ZPs of the SLNs before (fresh sample) and after their incubation in simulated GI fluids (n = 3)	122
3.4	Particle size distribution by intensity of AmB SLNs, before (fresh sample) and after their incubation in simulated GI fluids (n = 3)	124
3.5	Particle size distribution by intensity of PAR SLNs, before (fresh sample) and after their incubation in simulated GI fluids (n = 3)	126
3.6	Particle size distribution by intensity of SSZ SLNs, before (fresh sample) and after their incubation in simulated GI fluids (n = 3)	128
3.7	Size distribution by particle concentration of drug-free SLNs, before (fresh sample) and after their incubation in simulated GI fluids (n = 3)	133
3.8	Mean particle sizes (using NTA) of the SLNs, before (fresh sample) and after their incubation in simulated GI fluids (n = 3)	134
3.9	Size distribution by particle concentration of AmB SLNs, before (fresh sample) and after their incubation in simulated GI fluids (n = 3)	136
3.10	Size distribution by particle concentration of PAR SLNs, before (fresh sample) and after their incubation in simulated GI fluids (n = 3)	138
3.11	Size distribution by particle concentration of SSZ SLNs, before (fresh sample) and after their incubation in simulated GI fluids (n = 3)	140

3.12	The chemical structure of AmB with the portions representing the diagnostic peaks demarcated: (a) $[\text{C}_{20}\text{H}_{27}\text{O}_2]^-$ at m/z 299.20; (b) $[\text{C}_{20}\text{H}_{29}\text{O}_2]^-$ at m/z 301.22; and (c) $[\text{C}_{17}\text{H}_{21}\text{NO}_4]^-$ at m/z 303.23	143
3.13	Negative ion ToF-SIMS spectra of pure AmB, drug-free SLNs, fresh AmB SLNs and AmB SLNs incubated in simulated GI fluids	144
3.14	Negative ion ToF-SIMS spectra showing AmB on the surface of AmB SLNs, before and after their incubation in simulated GI fluids	146
3.15	The chemical structure of PAR with a demarcation of the portion representing the diagnostic peak $[\text{C}_7\text{H}_7\text{O}]^-$ at m/z 107.05	147
3.16	Negative ion ToF-SIMS spectra of pure PAR, drug-free SLNs, fresh PAR SLNs and PAR SLNs incubated in simulated GI fluids	148
3.17	Negative ion ToF-SIMS spectra showing PAR on the surface of PAR SLNs, before and after their incubation in simulated GI fluids	150
3.18	Negative ion ToF-SIMS spectra of pure SSZ, drug-free SLNs, fresh SSZ SLNs and SSZ SLNs incubated in simulated GI fluids	152
3.19	Negative ion ToF-SIMS spectra showing SSZ on the surface of SSZ SLNs, before and after their incubation in simulated GI fluids	154
3.20	Molecular ion depth profiles for $[\text{C}_{20}\text{H}_{27}\text{O}_2]^-$, $[\text{C}_{20}\text{H}_{29}\text{O}_2]^-$ and $[\text{C}_{17}\text{H}_{21}\text{NO}_4]^-$ obtained from the AmB SLNs	156
3.21	Molecular depth profile for $[\text{C}_7\text{H}_7\text{O}]^-$ obtained from the PAR SLNs	157
3.22	Molecular depth profile for $[\text{C}_{18}\text{H}_{13}\text{N}_4\text{O}_5\text{S}]^-$ obtained from the SSZ SLNs	158
4.1	Chromatogram for piroxicam and α -naphthol (125 $\mu\text{g}/\text{mL}$ each), showing piroxicam as the preferred IS for the HPLC analyses	169
4.2	Chromatograms for (a) PAR and SP at 254 nm and (b) AmB at 405 nm, using the gradient method in Table 4.1	172
4.3	Chromatograms for (a) PAR, SP and IS at 254 nm; and (b) AmB and IS at 405 nm, using the gradient method in Table 4.2	175
4.4	Chromatograms showing the effects of deproteinising agent on peak shape and symmetry at 254 nm	179

4.5	Chromatograms of a pure solution of the analytes showing (a) PAR, SP and IS at 254 nm; and (b) AmB and IS at 405 nm	181
4.6	Chromatograms showing the separation selectivity of phenol, benzoic acid and p-toluic acid for acetonitrile and methanol [Shimadzu, 2015]	183
4.7	Chromatograms of the methanol-ethanolic extract of blank rat plasma at (a) 254 nm and (b) 405 nm	185
4.8	Chromatograms of spiked plasma showing (a) PAR, SP and IS at 254 nm; and (b) AmB and IS at 405 nm	186
4.9	Standard calibration curve of the peak response ratios of (a) AmB to IS, (b) PAR to IS, and (c) SP to IS, each versus the corresponding concentration of AmB, PAR or SP ($\mu\text{g/mL}$) in rat plasma	190
5.1	Mean plasma concentration-time curves of AmB after a single oral dose administration of AmB SLNs, PAR SLNs and SSZ SLNs; and a suspension of AmB, PAR and SSZ to fasted rats ($n = 3$)	206
5.2	Mean plasma concentration-time curves of PAR after a single oral dose administration of AmB SLNs, PAR SLNs and SSZ SLNs; and a suspension of AmB, PAR and SSZ to fasted rats ($n = 3$)	211
5.3	Splitting of the azo bond in SSZ to release SP and 5-aminosalicylic acid	213
5.4	Representative HPLC chromatograms showing the appearance of SP in plasma at 2 hr and peaking at 8 hr post dosing in one rat	214
5.5	Mean plasma concentration-time curves for SP after a single dose oral administration of AmB SLNs, PAR SLNs and SSZ SLNs; and a suspension of AmB, PAR and SSZ to rats ($n = 3$)	215
5.6	Plasma drug concentration-time profiles for AmB, PAR, and SP following simultaneous administration of AmB SLNs, PAR SLNs and SSZ SLNs at a dose of 10 mg/kg each ($n = 3$)	217
6.1	The mean plasma concentration-time curve of AmB in fasted rats after a single 10 mg/kg oral dose of AmB suspension; and 10 mg/kg dose each of AmB SLNs, PAR SLNs and SSZ SLNs	228

6.2	The mean plasma concentration-time curve of AmB in fed rats after a single 10 mg/kg oral dose of AmB suspension; and 10 mg/kg dose each of AmB SLNs, PAR SLNs and SSZ SLNs	229
6.3	Effect of food on the absorption of PAR SLNs in fasted and fed rats (n = 3)	232
6.4	Mean PAR absorption versus time curves in the fasted and fed rats (n = 3)	234
6.5	Effect of food on the absorption of SP from SSZ SLNs in rat colon (n = 3)	239
6.6	Mean SP absorption versus time curves in the fasted and fed rats (n = 3)	240
6.7	Absorption of AmB SLNs in the stomach, small intestine and colon in fasted rats	242
6.8	Absorption of AmB SLNs in the stomach, small intestine and colon in the fed rats	242
6.9	Cumulative percentage absorption of AmB under fasted and fed conditions	244

LIST OF EQUATIONS

		Page
2.1	$\%EE = \frac{\text{Amount of drug in precipitate}}{\text{Amount of drug used in formulation}} \times 100\%$	55
2.2	Zero order $Q = Kt$	57
2.3	First order $\log Q_R = \frac{Kt}{2.303}$	57
2.4	Higuchi $Q = K(t)^{\frac{1}{2}}$	57
2.5	Hixson – Crowell $Q_0^{1/3} - Q_t^{1/3} = Kt$	57
2.6	Korsmeyer – Peppas $\log Q = \log K + n \log t$	57
3.1	Stokes – Einstein equation ... $\overline{(x, y)^2} = \frac{2k_B T}{3r_h \pi \eta}$	112
4.1	$\%CV = \frac{\text{Standard deviation (SD)}}{\text{Mean concentration}} \times 100\%$	166
4.2	Relative error (E_r) = $\frac{\bar{x} - x_t}{x_t} \times 100\%$	167
4.3	$\%Recovery = \frac{\text{Concentration of drug in spiked plasma}}{\text{Concentration of pure drug solution}} \times 100\%$	167

LIST OF ABBREVIATIONS

3D	3-dimensional
AFM	Atomic force microscopy
AmB	Amphotericin B
ANOVA	Analysis of variance
AUC	Area under plasma drug concentration-time curve
BW	Beeswax
CAT	Caecal arrival time
CTT	Colonic transit time
DLS	Dynamic light scattering
DMSO	Dimethyl sulphoxide
DSC	Differential scanning calorimetry
EE	Encapsulation efficiency
FTIR	Fourier transform infrared spectroscopy
GE	Gastric emptying
GI	Gastrointestinal
GTT	Gastric transit time
HPLC	High-performance liquid chromatography
IS	Internal standard
NTA	Nanoparticle tracking analysis
PAR	Paracetamol
PBS	Phosphate-buffered saline
PCS	Photon correlation spectroscopy
PDI	Polydispersity index
SC	Sodium cholate

SD	Standard deviation
SEM	Scanning electron microscopy
SITT	Small intestinal transit time
SLN	Solid lipid nanoparticle
SP	Sulphapyridine
SSZ	Sulphasalazine
T _{10P}	Time for 10% PAR absorption
T _{10S}	Time for 10% SP absorption
T _{90P}	Time for 90% PAR absorption
T _{90S}	Time for 90% SP absorption
TEM	Transmission electron microscopy
TO	Theobroma oil
ToF-SIMS	Time-of-flight secondary ion mass spectrometry
ZP	Zeta potential

ABSTRACT

Successful delivery of pharmaceuticals orally requires a firm understanding of how dosage forms behave during their passage through the gastrointestinal (GI) tract. In this study, the GI transit time and absorption of amphotericin B (AmB) solid lipid nanoparticles (SLN) were investigated in rats, using paracetamol (PAR) and sulphapyridine (SP) as indirect markers. A high encapsulation efficiency of 91.2% was obtained for the AmB SLNs. The SLNs were exhaustively characterised with regards to size, zeta potential (ZP), viscosity, density, migration propensity within agarose gel, *in vitro* drug release and morphology, to ensure similar disposition in the GI tract after simultaneous oral administration. Freeze-drying did not significantly alter the size or ZP of the AmB SLNs, and *in vitro* drug release from fresh and freeze-dried SLNs were identical. AmB, PAR and sulphasalazine (SSZ) (the latter being the prodrug of SP) were individually formulated into SLNs using beeswax and theobroma oil as the lipid matrix. The z-averages, polydispersity indices and ZPs of the SLNs ranged from 206.5-224.8 nm, 0.161-0.218 and |61.90|-|71.90| mV, respectively. Gel electrophoresis studies indicated a similar movement propensity among the three SLNs as their migration distances were identical (22.2-22.4 mm) within agarose gel. Scanning electron and atomic force microscopy studies revealed that all three SLNs were spherical in morphology and with similar surface characteristics. The SLNs were assessed for changes in size and surface charge on exposure to simulated GI fluids using dynamic light scattering (DLS) and nanoparticle tracking analysis (NTA). On contact with the fluids, the particles had a slight increase in size due to ingress of the dissolution media. NTA results were found to be more beneficial than DLS as the latter was biased towards larger particles that were present possibly due to aggregation. After incubation in simulated gastric fluid followed by simulated intestinal fluid (mimicking gastric emptying), all the SLNs were found to be less than 350 nm in size and neutral in charge,

which are optimal attributes for intestinal absorption. Time-of-flight secondary ion mass spectroscopic (ToF-SIMS) analyses revealed minimal drug amounts on the surfaces of the particles indicating that drug location was in the core of the SLNs. A developed and validated high-performance liquid chromatography (HPLC) method for simultaneous assay of the drugs in rat plasma using piroxicam as internal standard was found to be sensitive, accurate and precise, with drug recovery from plasma exceeding 92% in each case. A pilot GI transit study conducted in rats showed that the HPLC method was appropriate for the study. In the main study, the effects of food on the transit and absorption of the AmB SLNs were investigated. The presence of food slowed the transit of the SLNs in the GI tract. The gastric transit time of the AmB SLNs was estimated indirectly using PAR and was obtained as 1.71-2.25 hr. Caecal arrival time (CAT) of the AmB SLNs was estimated using SP detection in plasma as SSZ metabolism to produce SP occurs predominantly by the activity of colonic flora. In both fasted and fed states, CAT was 1.80-1.90 hr whereas transit time through the small intestine was 1.65-1.79 hr. A delayed rate of AmB absorption was observed in the fed state however, the extent of absorption was not affected by food. The percentage AmB absorption during the fasted state in the stomach, small intestine and colon were not significantly different from absorption within the respective regions in the fed state. In both states however, absorption was highest in the colon and appeared to be a summation of small intestinal absorption plus absorption proper within the colon. The study indicated that AmB SLNs irrespective of food status were slowly but predominantly taken up by lymphatic absorption, and the small intestine was the most favourable site for their absorption. The data indicate that it is possible to enhance the bioavailability of AmB through its incorporation into SLNs. Further enhancement of AmB bioavailability can be achieved through appropriate formulation interventions aimed at slowing transit of the SLNs in the small intestine. Finally, being a lipid-based system, the SLNs may have a potential to reduce the nephrotoxic effects of AmB.

CHAPTER 1

INTRODUCTION AND BACKGROUND

1.1 General overview

Amphotericin B (AmB) is a broad-spectrum antifungal drug, chiefly used for treating life-threatening systemic fungal infections. Its therapeutic efficacy is however limited due to poor aqueous solubility, and serious side effects mainly nephrotoxicity [Nahar *et al.*, 2008; Kleinberg, 2006]. A micellar suspension of the sodium deoxycholate salt of AmB (Fungizone[®]) is currently the conventional formulation that is used clinically [Wong-Beringer *et al.*, 1998].

Lipid-based drug delivery is a favourable approach used to enhance the absorption and bioavailability of poorly water-soluble drugs [Wagner *et al.*, 2001; Pouton and Porter, 2008; Jawahar *et al.*, 2012]. Three lipid formulations of AmB are currently available on the market, following persistent efforts aimed at formulating to improve its tolerability and increase its efficacy. These are AmB lipid complex (ABLC), (Abelcet[®]); AmB colloidal dispersion (ABCD), (Amphocil[®]); and liposomal AmB (L-AmB) (AmBisome[®]). These formulations are all administered intravenously but are still associated with serious side effects such as fever, chills, rigors, malaise, headache, generalised aches, nausea, vomiting and hypoxia [Kleinberg, 2006; Patel, 2000].

One lipid-based delivery system receiving much attention lately is the solid lipid nanoparticle (SLN), which is used to improve the oral bioavailability of hydrophobic drugs. In addition, studies have shown that the side effects imposed by AmB are potentially minimised when administered as a lipid-based oral formulation [Risovic *et al.*, 2003; Gershkovich *et al.*, 2009; Jain *et al.*, 2012].

An oral SLN formulation of AmB is therefore a sensible approach for the delivery of AmB. However, it is imperative that the absorption behaviour of the SLN formulation within the GI tract is studied to ensure that the formulation manifests maximum therapeutic efficacy.

A review of literature indicates that a huge amount of work has been done on the development of nanoparticulate drug delivery systems, aimed at addressing the issue of poor efficacy/absorption. However, not much work is directed towards establishing the uptake mechanisms or transit properties of these nanoparticles after oral administration.

Monitoring the absorption and gastrointestinal (GI) transit of pharmaceuticals provides vital information on their design and development. GI transit studies give an indication of a drug's 'absorption window', which is the optimal site of absorption of orally administered dosage forms. For the design and delivery of therapeutic agents that are known to have poor bioavailability, this information is vital. Gamma scintigraphy is a useful technique that may be used. However, the gamma camera is rather expensive and suitable radionuclides may not be readily available. Indirect methods which employ suitable marker drugs may be used in obtaining data on gastric emptying and oro-caecal transit properties of dosage forms *in lieu of* gamma scintigraphy [Peh and Yuen, 1996; Rahman *et al.*, 2005].

The absorption of paracetamol (PAR) (which is preferential in the small intestine) is related to the rate of gastric emptying after oral delivery [Heading *et al.*, 1973; Clements *et al.*, 1978]. Its rate of appearance in blood is therefore useful as a measure of the gastric emptying rate of simultaneously administered dosage forms. After oral administration, sulphasalazine (SSZ) is hydrolysed by the large bowel flora to produce sulphapyridine (SP) and 5-aminosalicylic acid. The SP is rapidly absorbed from the large bowel thus, measuring SP in the blood can be used to

determine the arrival of an SSZ-containing dosage form at the large bowel and hence, the oro-caecal transit time can be estimated [Kellow *et al.*, 1986; Staniforth *et al.*, 1987]. These two compounds therefore provide a cheaper alternative to gamma scintigraphy in monitoring the GI transit behaviour of a drug formulation [Peh and Yuen, 1996; Rahman *et al.*, 2005].

In this study, it was aimed to use PAR and SP (SP to be released from SSZ hydrolysis in the large intestine) as marker drugs to monitor the GI transit behaviour of AmB SLNs in relation to its absorption. The three drugs (AmB, PAR and SSZ) were therefore formulated into individual SLNs. The SLNs were evaluated for similarities in their physical properties and then subjected to a pilot GI transit study using Sprague-Dawley rats as the animal model. The pilot study provided the basis for a main transit study in which the effect of food on the oral absorption of AmB-containing SLNs was studied.

1.2 Amphotericin B

AmB is a fungicidal agent that was initially isolated from *Streptomyces nodosus*. It has a broad spectrum of activity and is efficacious in candidiasis, cryptococcosis, aspergillosis, histoplasmosis, blastomycosis, coccidioidomycosis, zygomycosis, sporotrichosis, fusariosis and phaeohyphomycosis [Klepser, 2011]. Some fungi including rare pathogens such as *Trichosporon spp.*, *Aspergillus terreus*, *Scedosporium spp.* and *Malassezia furfur* are intrinsically resistant to AmB. AmB is also effective against the protozoan parasite *Leishmania donovani* [Walsh *et al.*, 1990; Walsh *et al.*, 1992].

1.2.1 Physicochemical properties

AmB is a mixture of antifungal polyenes (polyunsaturated organic compounds) produced by growing certain strains of *Streptomyces nodosus*. AmB ($C_{47}H_{73}NO_{17}$ = 924.1; structure shown in Figure 1.1) is a yellow to orange powder which gradually decomposes above 170°C [Moffat *et al.*, 2005]. It is practically insoluble in water, ethanol, chloroform and ether, but it is soluble in dimethylformamide (1 in 200), dimethyl sulphoxide (1 in 20) and propylene glycol. It has a pK_a value of 5.5.

1.2.2 Pharmacokinetics

Due to its hydrophobicity, AmB is poorly absorbed after oral, intramuscular or subcutaneous administration [Moffat *et al.*, 2005]. It is slowly excreted in the urine (about 40%), and less than 10% of the administered dose is excreted unchanged in 24 hr with traces still detectable in urine

several days after treatment has ended. AmB has a plasma half-life about 24 to 48 hr and a volume of distribution of about 4 L/kg. In plasma, about as high as 90 to 97% of the drug is protein bound.

AmB is a class IV drug according to the Biopharmaceutics Classification System, which means that, it has low solubility and low membrane permeability. These two properties in addition to its poor stability in acidic media are the key factors that contribute to the poor oral bioavailability of AmB. Generally, class IV compounds have poor bioavailability and are minimally absorbed over the intestinal mucosa with high variability. The low stability of AmB in acidic media can be addressed through enteric-coating of orally destined formulations but the poor aqueous solubility and membrane permeability remain significant challenges to oral delivery [Amidon *et al.*, 1995; Gershkovich *et al.*, 2009].

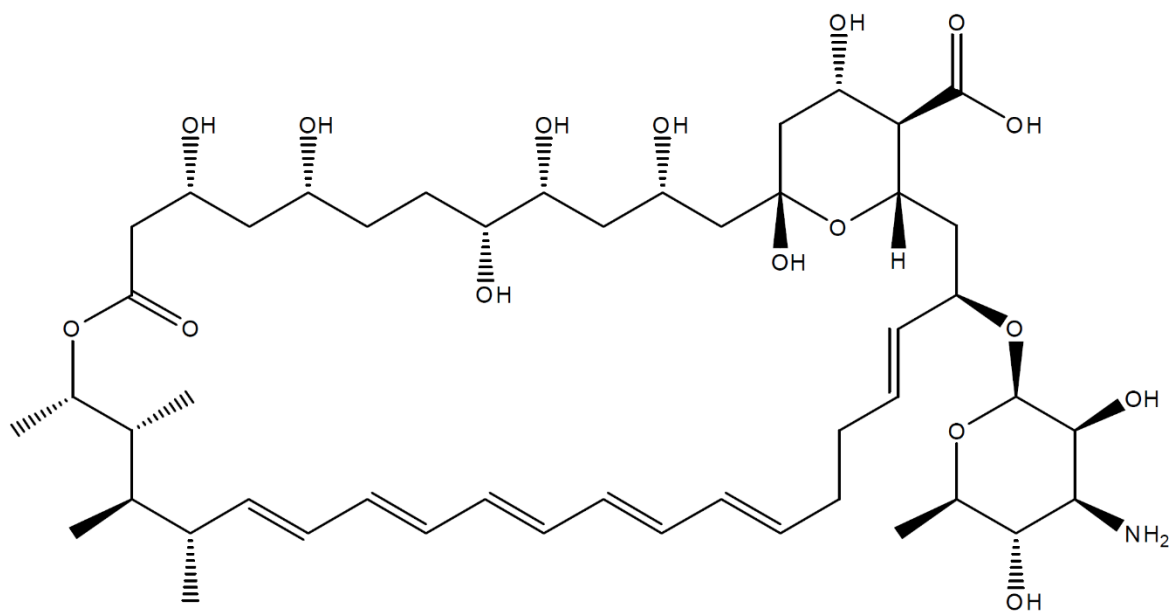


Figure 1.1 Chemical structure of AmB

1.2.3 Mechanism of action

In the presence of ergosterol in fungal cell membrane, AmB monomers nucleate to form an AmB multimeric pore with the lipophilic polyene chains arrayed on the outside of the multimer in contact with the fungal membrane lipids [Kleinberg, 2006]. The hydrophilic polyhydroxyl chains of AmB form the inner walls of an aqueous pore. These pores increase the permeability of the fungal membrane to small intracellular cations such as potassium, which are necessary for cell metabolism, thereby promoting their leakage. The rapid depletion of these ions finally results in fungal cell death. Although AmB has a slightly higher affinity for ergosterol in the fungal cell membrane, it can also bind to the cholesterol in mammalian cell membranes due to the structural similarity of the two sterols (Figure 1.2); this is the cause of the cytotoxicity associated with AmB therapy. A study by Baginski *et al.* (2002) showed that the channels/pores formed by AmB interaction with ergosterol were larger in size with a more prominent pattern of stable intermolecular hydrogen bonds compared with those formed with cholesterol, resulting in higher ion conductance in fungi than in mammals [Baginski *et al.*, 2002].

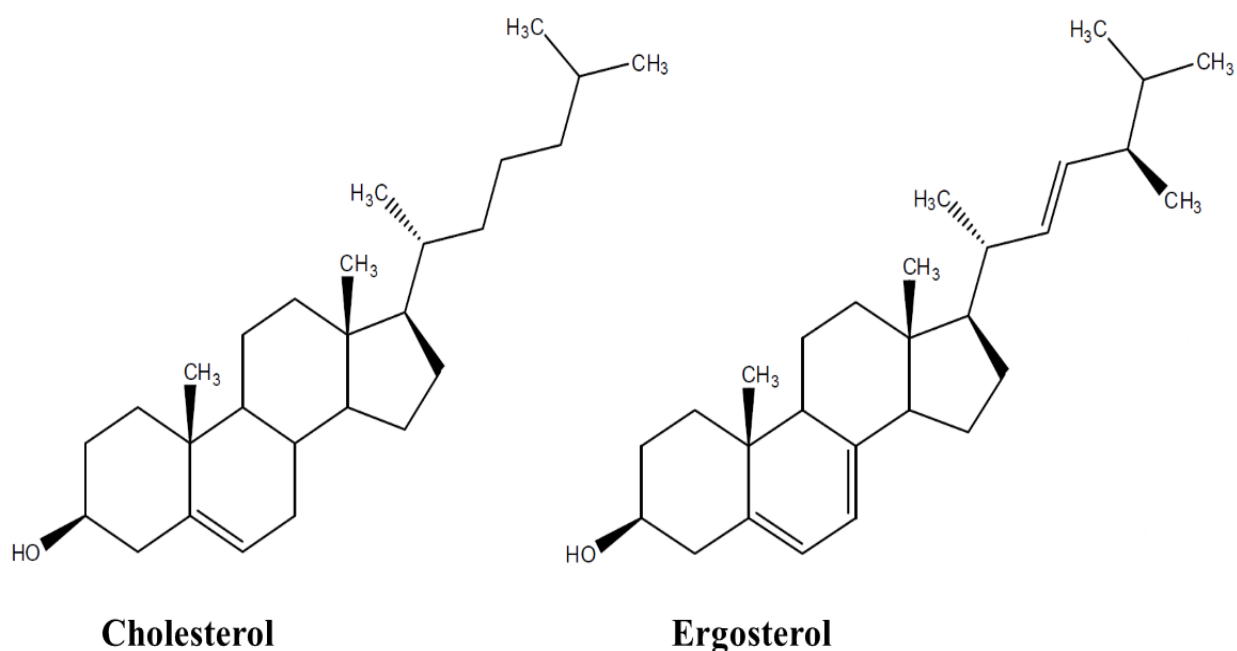


Figure 1.2 Structural similarities between cholesterol and ergosterol

1.2.4 Toxicity

Although AmB has broad-spectrum antifungal activity, its clinical use is limited by its toxicity. It shows two main toxicities, acute or infusion-related toxicity and chronic (end organ) toxicity [Patel, 2000]. The latter essentially affects the kidneys (nephrotoxicity) and may lead to permanent renal impairment especially when AmB is co-administered with other nephrotoxic drugs. The infusion-related adverse events are characterised by fever, thrombophlebitis, chills, rigors, malaise, headache, generalised aches, nausea, vomiting and hypoxia [Ellis *et al.*, 1992; Khoo *et al.*, 1994; Patel, 2000]. Hypotension/hypertension, hypothermia, cardiac arrhythmia and pulmonary infiltrates have also been reported when AmB is administered with leukocyte transfusions. Some strategies used to reduce the nephrotoxicity include saline loading, slowing the infusion rate,

alternate-day dosing and dose reduction; however, the two latter strategies are inappropriate if a patient is suffering a life-threatening infection.

The toxic reactions to AmB may be related to the induction of pro-inflammatory cytokines produced by AmB and the release of TNF-alpha from macrophages [Chia and McManus, 1990; Arning *et al.*, 1995]. Premedication with analgesics, antihistamine drugs and low-dose hydrocortisone may help decrease these effects [Khoo *et al.*, 1994].

The AmB-associated nephrotoxicity causes lengthy hospitalisation and increased mortality (49-65%) especially in patients requiring haemodialysis [Deray, 2002]. There is attendant duplication of baseline creatinine levels; vasoconstriction which leads to ischemic injury and direct interaction with epithelial cell membranes causing tubular dysfunction. Risk factors for AmB nephrotoxicity include high daily average and total cumulative doses, dehydration, abnormal baseline renal function (e.g. compromised glomerular filtration rate (GFR) in very ill and elderly patients), simultaneous use of nephrotoxic drugs (e.g. cyclosporine and vancomycin) and patients in a high-risk category such as bone marrow transplant patients [Wingard *et al.*, 1999; Deray, 2002]. A 25% increase in creatinine values (i.e. a 50% decrease in GFR) results in nephrotoxicity except the drug is stopped; but this may not be probable if large cumulative doses (> 4 g) have already been given. High doses of AmB (up to 2 mg/kg/day) can be tolerated by continuous infusion but AmB has a concentration-dependent mode of action therefore, the adverse effects may be more pronounced [Deray, 2002; Imhof *et al.*, 2003].

1.2.5 Available formulations of amphotericin B

Due to the toxicities from AmB therapy highlighted above, efforts have been directed towards reformulations to improve tolerability and increase efficacy [Vyas and Gupta, 2006]. Fungizone[®], which is a micellar dispersion of AmB with sodium deoxycholate (AmBD) has been available since 1958 and is usually referred to as the classical AmB formulation. However, its use is associated with a number of the aforementioned acute side effects in about 80% of patients, with about 30% of patients also experiencing renal malfunction [Torrado, 2008; Baginski, 2009]. Fungizone[®] extensively associates with low-density lipoproteins (LDL) and is then taken up by LDL receptors in the kidneys. This process is believed to be the cause of its dose-dependent nephrotoxicity.

Three parenteral lipid formulations of AmB have been approved by the FDA: AmB lipid complex (ABLCL), composed of AmB complexed with dimyristoylphosphatidylcholine and dimyristoylphosphatidylglycerol (Abelcet[®]); AmB colloidal dispersion (ABCD), which is formed from AmB complexed with cholesteryl sulphate (Amphocil[®]); and liposomal AmB, L-AmB (AmBisome[®]), which is composed of AmB complexed with hydrogenated soy phosphatidylcholine, distearoyl, phosphatidylglycerol and cholesterol [Kleinberg, 2006]. These formulations are used only intravenously as intramuscular administration of AmB is not ideal because of irritation and poor absorption from the intramuscular route [Khoo *et al.*, 1994].

These lipid formulations differ in various aspects such as their lipid composition, shape/design, physicochemical properties, pharmacokinetic parameters and clinical efficacy; nonetheless, they are less nephrotoxic than conventional AmB, which was the purpose of their development. They also show different accumulation rates in various tissue components [Herbrecht, 2003].

ABL-C is used at a dosage of 5 mg/kg/day in patients of all ages. It offers equal or better efficacy compared with AmBD, coupled with improved tolerability. There are no differences in efficacy or mortality compared with L-AmB, and it can be given safely to patients with existing renal failure (including that caused by AmBD use) to improve renal function [Walsh *et al.*, 1998; Martino, 2004].

ABCD is used at a dosage of 3-4 mg/kg/day. It is the least studied lipid formulation however, it has equal efficacy with the other formulations. It is much less nephrotoxic (50% less) than AmBD but associated with more frequent infusion-related toxicity (i.e. chills and fever) [White *et al.*, 1998; Bowden *et al.*, 2002].

L-AmB is a single-bilayer liposomal drug-delivery system used for treating infections refractory to AmBD, or used in patients in whom renal impairment or unacceptable toxicity precludes the use of AmBD [Ostrosky-Zeichner *et al.*, 2003; Antoniadou and Dupont, 2005]. L-AmB accumulates well in the kidneys but it is the least nephrotoxic of the lipid formulations however, dose-limiting renal toxicity may still be observed. Its approved dosage is 3 mg/kg/day for empiric therapy in neutropenic patients, 6 mg/kg/day for cryptococcal meningitis in patients with HIV infection and 3-5 mg/kg/day for systemic fungal infections.

1.3 Nanoparticle formulations

Nanoparticles range from 10 to 1000 nm in diameter and may be formulated using polymers or lipids, in which a therapeutic agent can be entrapped, adsorbed, or chemically coupled with [Panyam and Labhasetwar, 2003; Sahoo and Labhasetwar, 2003]. Their submicron size offers

several advantages over microparticles such as having a relatively higher intracellular uptake. For instance, a study indicated that nanoparticles of size 100 nm showed 2.5-fold greater intracellular uptake compared to 1- μm sized particles, and a 6-fold higher uptake compared to 10- μm particles in a Caco-2 cell line [Desai *et al.*, 1997]. Similar data was obtained using a rat *in situ* intestinal loop model, in which the uptake of 100 nm sized particles was 15- to 250-fold more than that of 1 and 10 μm sized particles [Desai *et al.*, 1996].

The selection of a suitable delivery system for a drug is based on the physicochemical properties of the drug, the disease state and the location of the disease in the body [D'mello *et al.*, 2009]. The size and mode of delivery of a drug can affect the therapeutic outcomes of a disease; this is because permeability and passive membrane diffusion are effected for drugs with small size. Therefore, entrapping a drug in a nanoparticle could result in better cellular uptake or drug targeting to specific tissues in addition to possibly controlling the drug release.

The use of nanoparticles may however be limited by physical instability (e.g. aggregation) and/or chemical instability (e.g. hydrolysis of the drug carrier, drug leakage and chemical reactivity) when they are stored for a long time [Auvillain *et al.*, 1989; Chacon *et al.*, 1999] but these can be controlled or avoided by optimising the formulation parameters.

1.4 Lipid nanoparticles

Lipid nanoparticles are colloidal nanoparticles made from solid lipids or a combination of solid and liquid lipids [Müller *et al.*, 2002]; these are known as solid lipid nanoparticles (SLNs) and nanostructured lipid carriers (NLCs), respectively. The key difference between them is the

composition and physical state of the lipids, which serve as the core of their structures [Saupe *et al.*, 2005].

In SLNs, the drug is incorporated between the voids in the crystal lattice of the solid lipid [Müller *et al.*, 2000] while in NLCs, the liquid lipids added to solid lipids offer flexibility in controlling drug encapsulation and drug release [Sauto and Müller, 2007]. The solid-liquid lipid matrix of NLCs has more imperfections and could make higher drug encapsulation possible depending on the drug and lipid properties [Müller *et al.*, 2007]. Drug location in the core or shell of the lipid nanoparticle depends on the lipid nature, drug properties, drug solubility in the lipid and the method of nanoparticle preparation employed [Sauto and Müller, 2007].

Lipid nanoparticles have superior physical stability as compared with other disperse systems such as liposomes [Saupe *et al.*, 2005]. In liposomes and emulsions, the drug can diffuse and partition between the oil and the aqueous phase unlike in lipid nanoparticles where the solid lipid shell prevents this, thus reducing drug leakage and degradation [Müller *et al.*, 2000; Sauto and Müller, 2007]. Lipid nanoparticles offer benefits over other lipid carriers. For example, because of the increased surface area from the lipids in a nanoparticulate system for transdermal drug delivery, adhesiveness to the skin is improved. In addition, an occluding film is formed on the skin, which increases skin hydration and penetration of the drug. The lipids in the nanoparticle can also interact with the lipids in the skin and act further as penetration enhancers [Wissing *et al.*, 2001; Sauto and Müller, 2007].

Lipid nanoparticles can also be used to control drug release through gradual drug diffusion out of the lipid matrix [Müller *et al.*, 2000]. As a result of this, drug release can be moderated by altering the composition of the lipids [Lippacher *et al.*, 2001; Sauto and Müller, 2007].

1.5 Solid lipid nanoparticles (SLNs)

SLNs are composed of physiological lipids usually dispersed in an aqueous surfactant solution (Figure 1.3) and are solid at room temperature. Consequently, mobility of the incorporated drug is reduced, which is favourable for controlled drug release [Müller and Lucks, 1996; zur Mühlen *et al.*, 1998]. SLNs are an alternative to polymeric particulate systems and are suitable carriers for hydrophobic drugs, peptides, proteins and antigens; however, for hydrophilic drugs, a high encapsulation efficiency into the hydrophobic matrix is not usually achieved [Almeida and Souto, 2007].

The unique properties of small size (large surface area) and high drug loading capacity give SLNs the potential to enhance the performance of lipophilic pharmaceuticals [Saupe and Rades, 2006; Uner and Yener, 2007].

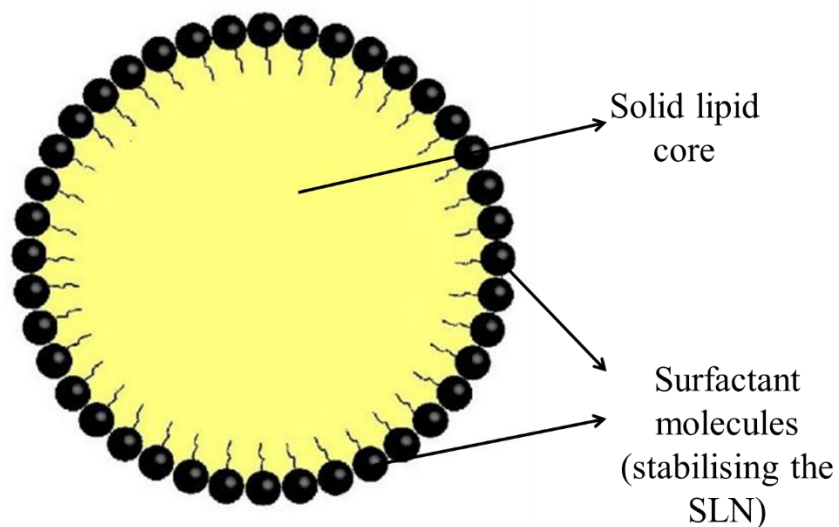


Figure 1.3 Typical SLN structure

1.5.1 Influence of formulation and processing variables on SLN quality

1.5.1.1 Lipids and emulsifiers

The ingredients used in preparing SLNs include biocompatible/biodegradable solid lipid(s), emulsifier(s), coemulsifier(s) and water. The lipids used are safe (reducing the risk of acute and chronic toxicity), inexpensive and can be obtained in high purity; they include triglycerides (e.g. tristearin), partial glycerides (e.g. Imwitor), fatty acids (e.g. stearic acid), steroids (e.g. cholesterol and cholesterol butyrate) and waxes (e.g. cetyl palmitate, carnauba wax, beeswax, emulsifying wax) among others [Loxley, 2009; Severino *et al.*, 2012]. The choice of the lipid is based on the assessment of its polymorphic nature, crystallinity, miscibility/solubility in solvents and physicochemical properties.

All classes of emulsifiers (with respect to charge and molecular weight) can be used to stabilise the lipid dispersion [Mehnert and Mäder, 2001]. A blend of emulsifiers prevents particle agglomeration more efficiently but the choice depends on the route of administration for instance, using the parenteral route requires careful selection and limited use of emulsifiers due potential toxicity. Surfactant/surfactant mixture concentration can strongly affect the SLN particle size. Generally, smaller particle sizes are obtained when a higher surfactant to lipid ratio is employed and *vice versa* [zur Mühlen, 1996].

It has also been investigated that when a blend of ‘same-class’ surfactants are used than either surfactant used alone at the same concentration, they seem to compete for interface sites [Tan *et al.*, 2010]. This competition leads to a relatively thinner Helmholtz layer, resulting in a higher zeta potential and hence, a higher colloidal stability. In addition, the electrostatic repulsion produced

from using ionic surfactants is more vital in imparting stability to lipid nanoparticles during storage as compared with the steric hindrance from non-ionic surfactants.

In the hot homogenisation method of preparing SLNs, particle size increases with higher melting lipids. Other factors linked to the type of lipid and SLN quality are the velocity of lipid crystallisation, lipid hydrophilicity (which influences self-emulsifying properties) and the shape of the lipid crystals [Siekmann and Westesen, 1992; Siekmann and Westesen, 1994; zur Mühlen, 1996]. Increasing SLN lipid content over 5-10% produces larger particles with a broader size distribution in most cases, which is undesirable.

1.5.1.2 Particle size

Particle size can considerably affect the physical stability of the formulation, the biofate of the particles, as well as the release profile of the loaded drug. Therefore, particle size must be well controlled; ideally, size distribution must be narrow and in the submicron range [Siekmann and Westesen, 1994; Mehnert and Mäder, 2001]. The final particle size of lipid nanoparticles is affected by several factors such as the constituents of the formulation (i.e. surfactant/surfactant mixture, lipid properties and the drug), production methods and variables (such as time, temperature, pressure, number of cycles and equipment) and other procedures like sterilisation and lyophilisation (freeze-drying) if required. For example, larger particle sizes are achieved at lower processing temperature. Additionally, the hot homogenisation technique produces SLNs of smaller sizes (< 500 nm) with a narrow size distribution as compared with cold homogenisation however, high temperature is not suitable for thermolabile drugs or lipids/carriers. Again, mean particle size and polydispersity index increase with increasing homogenisation pressure (beyond 1500 bar) and

number of homogenisation cycles (beyond 3-5 cycles) due to the increased kinetic energy of the particles.

1.5.2 Advantages of SLNs over other particulate drug delivery forms

- Their small size makes them suited for intravenous drug delivery and for the crossing of biomacromolecules into the lymphatic system after oral delivery.
- In some production methods of SLNs, the use of organic solvents could be avoided.
- They can be produced on a large scale with excellent reproducibility.
- Drug release can be controlled if desired.
- Drug targeting to specific areas in the body by coating/attaching ligands to their surfaces can be achieved.
- SLN formulations can be optimised to have increased stability of several months.
- The lipids used are biodegradable; therefore, SLNs have a better biocompatibility.
- Higher drug loading, as well as high bioavailability of entrapped drugs.
- Chemical protection of incorporated drugs is offered by the solid lipid core.

[Müller *et al.*, 2000; Gohla and Dingler, 2001; Mehnert and Mäder, 2001; Lockman *et al.*, 2003; Saupe and Rades, 2006; Mukherjee *et al.*, 2009]

1.5.3 Methods of preparing SLNs

1.5.3.1 High pressure homogenisation (HPH)

HPH is a reliable method for preparing SLNs, in which scaling up presents no problems as the other techniques do [Lippacher *et al.*, 2000]. In HPH, homogenisers are operated at high pressures (100-2000 bar), which causes acceleration of fluids to a very high velocity (over 1000 km/h) resulting in particle size reduction to the submicron range. The lipid content in the formulation is usually 5-10% but higher amounts of up to 40% can also be used.

There are two approaches for the homogenisation step in the production of SLNs by HPH, cold and hot. In each case, the primary step requires drug incorporation into the molten lipid.

1.5.3.1.1 Hot homogenisation

This is carried out at temperatures above the melting point of the lipid used [Lander *et al.*, 2000]. A pre-emulsion is produced from the drug-loaded lipid melt and an aqueous solution of the emulsifier (both at the same temperature) with the aid of a high-shear mixing device, followed by HPH. It is necessary to obtain a pre-emulsion of good quality and with droplet size in the range of only a few micrometres to produce a final product of high quality. When smaller particle sizes are desired, higher temperatures are employed to decrease the viscosity of the inner phase but this could also increase the rate of degradation the drug and/or the lipid carrier. More than one cycle of homogenisation (about 3-5 cycles at 500-1500 bar) can be done, noting that HPH by itself increases the sample temperature by about 10°C for 500 bar [Jahnke, 1998].

The primary product of the hot homogenisation process is a nanoemulsion. Solid particles are then formed by cooling the hot nanoemulsion to room temperature or below. Due to the small particle size and the presence of emulsifiers, the chances of lipid crystallisation occurring is highly slowed, enabling the sample to remain intact for several months [Bunjes *et al.*, 1998].

1.5.3.1.2 Cold homogenisation

Cold homogenisation on the other hand is carried out with the lipid in the solid state. Good temperature control is needed to ensure the unmolten state of the lipid because there is temperature increase during homogenisation [Jahnke, 1998]. This technique overcomes some problems associated with the hot homogenisation technique such as temperature-induced drug degradation, drug distribution into the aqueous phase during homogenisation and complexity of the crystallisation step of the nanoemulsion (which leads to some alterations and/or supercooled melts) [zur Mühlen, 1996].

The first step is the same as in the hot homogenisation technique, which is dissolving or dispersing the drug in the melted lipid [zur Mühlen, 1996]. The drug-containing lipid melt is then cooled rapidly (using either dry ice or liquid nitrogen), which favours the homogenous distribution of the drug within the lipid matrix. The solid lipid-drug complex thus obtained is ball or mortar milled into microparticles (50-100 μm). The cooling step increases the brittleness of the lipid thereby favouring particle comminution. The microparticles are then dispersed in a chilled emulsifier solution and subjected to high pressure homogenisation at or below room temperature.

Compared with hot homogenisation, larger particle sizes and a broader size distribution are obtained [zur Mühlen, 1996]. In addition, thermal exposure of the sample is decreased, but not evaded due to the initial step of melting the lipid [Mehnert and Mäder, 2001].

1.5.3.2 High speed stirring and/or ultrasonication

Ultrasonicators and stirring equipment are common in the laboratory but both instruments have the disadvantage of producing particles with a broad particle size distribution that ranges into the micrometre range [Mukherjee *et al.*, 2009]. This results in physical instabilities like particle growth upon storage. There may also be metal contamination from the probe due to the ultrasonication step. In order to make a stable formulation, a high stirring speed and ultrasonication are used in combination at a high temperature in making the pre-emulsion for formulating the SLNs.

The large-sized particles obtained by this method are not a problem for oral drug delivery however, if the formulation is intended for intravenous administration, a high concentration of emulsifiers can be used for particle size reduction, but this may also increase the risk of toxicity [Mehnert and Mäder, 2001].

1.5.3.3 Emulsification solvent diffusion

This method (summarised in Figure 1.4) was first described by Quintanar-Guerrero *et al.* (1996) in preparing polymeric nanoparticles. In this technique, the organic solvent (partially water-miscible) is saturated with water to achieve preliminary thermodynamic equilibrium between the

two liquids. The organic solvent containing the dissolved carrier (polymer/lipid) and the drug is emulsified in an aqueous surfactant solution using a high-speed homogeniser (a stabilising agent may be added) at the melting point of the lipid (or about 5°C higher). Excess water is then added to the oil-in-water (o/w) emulsion formed with continuous stirring thus causing phase transformation and outward diffusion of the solvent from the internal phase to the external phase. This leads to the precipitation of the polymer/lipid and the formation of colloidal nanoparticles. The solvent is then removed by vacuum or steam distillation or evaporation. The concentration and the nature of the lipid and surfactant, stirring rate and the processing temperature are critical variables in this technique [Quintanar-Guerrero *et al.*, 1996; Trotta *et al.*, 2003].

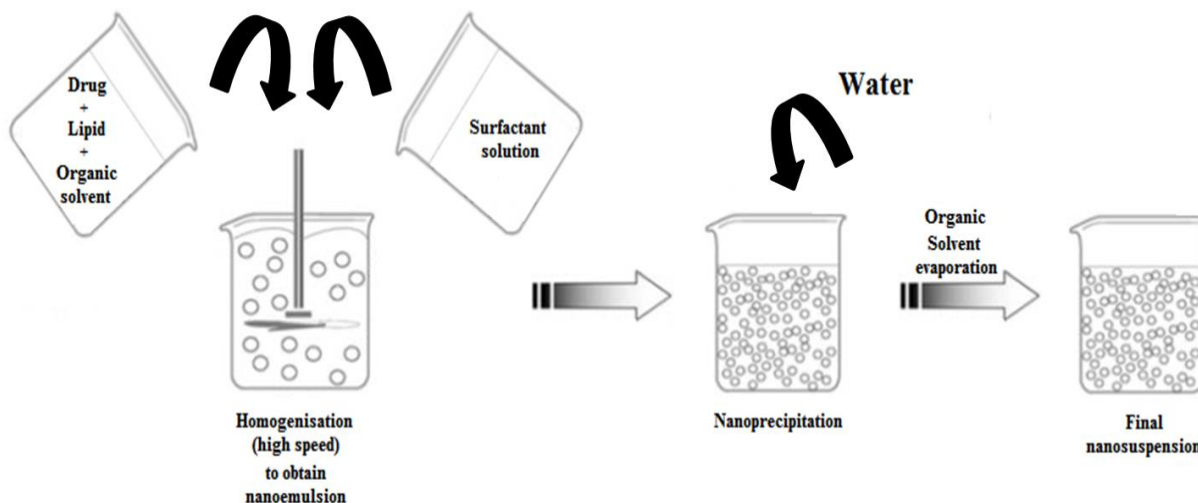


Figure 1.4 Schematic diagram for preparing nanoparticles using emulsification solvent diffusion method [modified from Jelvehgari and Montazam, 2012].

1.5.3.4 Emulsification solvent evaporation

This method involves obtaining nanoparticles by precipitation from o/w emulsions. The lipophilic material (that is the drug and the lipid) is dissolved in a water-immiscible organic solvent (e.g. cyclohexane, ethyl acetate) and then emulsified in an aqueous phase using mechanical stirring [Mehnert and Mäder, 2001]. The solvent is then evaporated causing precipitation of the lipid nanoparticles in the aqueous medium.

Sjöström and Bergenståhl (1992) used this method to obtain a mean particle size of 25 nm using cholesterol acetate as model drug and a lecithin/sodium glycocholate blend as emulsifier. The lipid concentration in the organic phase determines the mean particle size; that is, very small particles are obtained with low lipid content (about 5%). In addition, as the lipid content increases, the efficiency of the emulsification declines because the viscosity of the dispersed phase increases. The avoidance of any heat stress is beneficial in this procedure over cold homogenisation while the main drawback is the use of organic solvents [Mehnert and Mäder, 2001].

1.5.3.5 Supercritical fluid (SCF) method

There are several procedures in SCF technology for producing micro/nanoparticles. These include rapid expansion of supercritical solution (RESS), particles from gas-saturated solutions (PGSS), gas/supercritical antisolvent (GAS/SAS), aerosol solvent extraction system (ASES) and solution enhanced dispersion by supercritical fluids (SEDS) [Jung and Perrut, 2001; Jovanoviæ *et al.*, 2004; Rodrigues *et al.*, 2004].

SCF technology is a useful alternative for producing solvent-free particulate drug carriers. Carbon dioxide (CO₂) is almost exclusively the solvent employed for reasons such as its low toxicity, relatively low critical temperature and moderate critical pressure and low cost [Sellers *et al.*, 2001]. The advantages of this method are the mild processing conditions, possible sterilising properties of supercritical CO₂, possibility of producing nanoparticles as dry powders and the feasibility of scaling-up [Jovanoviæ *et al.*, 2004].

A modified PGSS process has been used to produce insulin SLNs, where the drug was dissolved in dimethyl sulphoxide (DMSO) and the solution incorporated into a melted mixture of tristearin, phosphatidylcholine and dioctyl sulphosuccinate [Caliceti *et al.*, 2006]. The lipid matrix was mixed with compressed CO₂ and atomised to produce SLNs < 500 nm in size. The formulation had sustained release properties and preserved the biological activity of the insulin. However, the use of the DMSO compromised the aim of solvent-free SCF processing, especially as the particles were intended for parenteral purposes.

1.5.3.6 Microemulsion-based method

This is based on the dilution of a microemulsion, where the lipid nanoparticles are prepared by stirring an optically transparent mixture comprising of a low melting fatty acid (e.g. stearic acid), an emulsifier (e.g. polysorbate 20), co-emulsifiers (e.g. butanol) and water at 65-70°C. The hot microemulsion produced is then diluted in cold water (2-3°C) in a ratio range of 1:25 to 1:50, respectively, with stirring, which causes the lipid droplets in the microemulsion to solidify into lipid nanoparticles [Gasco, 1993; Cavalli *et al.*, 1996; Joresa *et al.*, 2004]. The temperature gradient and pH define the quality of the product obtained but the former facilitates rapid lipid

crystallisation thus preventing particle aggregation. The dilution stage considerably lowers the lipid content as compared with SLNs produced by the HPH method. The possibility of scaling up from laboratory size to industrial size batch is an advantage of this method as there is no need for high shear machinery.

Major drawbacks include high production costs and sensitivity to minor changes in the formulation composition or thermodynamic variables, which can result in phase transitions [Gasco, 1993]. In addition, the dilution step reduces particle concentration to below 1%, requiring a large amount of water to be removed for processing to a final dosage form. Lastly, a high concentration of surfactant is used which can cause toxicity but the excess can be removed by ultracentrifugation, ultrafiltration or dialysis.

1.5.3.7 Double emulsion method

This is based on the emulsification solvent evaporation method for preparing SLNs for hydrophilic drugs [Cortesi *et al.*, 2002]. The drug and a stabiliser (e.g. gelatin, poloxamer-407) are encapsulated in the internal water phase of a w/o/w double emulsion to avoid drug partitioning into the external water phase during solvent evaporation. This is then emulsified in melted lipid to give a primary emulsion, which is then dispersed in another aqueous phase containing a hydrophilic emulsifier (e.g. PVA). The double emulsion thus obtained is stirred and isolated by filtration. SLNs containing sodium cromoglycate (a hydrophilic compound) have been prepared using this method. Prior to this, the solvent evaporation method was employed which gave a low encapsulation efficiency (2% w/w); which was increased to 50% w/w when the w/o/w double emulsion technique was used except that larger-sized particles were obtained.

1.5.3.8 Film-ultrasound dispersion method

In this method, the lipid and the drug are dispersed in an appropriate organic solution(s). A lipid film is obtained by rotating the organic solution in a suitable vessel and evaporating the solvent, after which an aqueous solution containing the emulsifier is added [Ekambaram *et al.*, 2012]. SLNs with small and uniform particle sizes are then produced with the aid of an ultrasound probe. Wang *et al.* (2007) used this technique to produce oleanolic acid SLNs with mean diameter of 62 nm and encapsulation efficiency of 98.29%.

1.5.4 Characterisation of SLNs

1.5.4.1 Particle size

(I) Photon correlation spectroscopy (PCS) and laser diffraction (LD) are the dominantly employed techniques for routine particle size measurements [Sinha *et al.*, 2010]. PCS is based on dynamic laser light scattering (DLS) due to Brownian motion of particles in a solution/suspension, and is suitable for assessing particle sizes from 3 nm to 3 μm . PCS diameters (hydrodynamic diameters) are obtained by measuring the fluctuation of scattered light from particles. The PCS device comprises a light source, a temperature-controlled sample cell and a photomultiplier for detecting the scattered light. PCS uses the scattered light and diffusion data from the Brownian motion of particles in the Stokes-Einstein equation to give the radius of a particle (average particle size) along with the size distribution in a fairly dilute sample [Sinha *et al.*, 2010]. An improvement of PCS for higher concentrated/opaque samples (e.g. emulsions) is photon cross-correlation spectroscopy (PCCS).

Laser diffraction (LD) alternatively measures particle size in the range of 0.1-180 μm and is based on the dependence of diffraction angle on particle size (Fraunhofer spectra); that is, smaller particles cause more intense scattering at higher angles than larger particles [Sinha *et al.*, 2010].

Phase sensitive-intensity-difference-scattering technology has very much enhanced the sensitivity of LD to smaller particles however, it is advisable to use PCS with LD. PCS and LD are however not very useful in analysing samples comprising various populations of different sizes [Garti and Sato, 1988; Müller *et al.*, 2000].

Nanoparticle formulations are usually polydisperse systems, so polydispersity index (PDI) is used as a measure of the particle size distribution. Ideally, the PDI for a monodisperse system is zero whereas for polydisperse systems PDI must be less than 0.5 because, a value greater than the latter indicates a very broad particle size distribution system [Jawahar *et al.*, 2012].

(II) Nanoparticle tracking analysis (NTA) is a commercialised equipment by NanoSight Ltd (Amesbury, UK) and provides visualisation of samples in real time. NTA measures the absolute size distribution of particles with diameters ranging from 50 nm to 1 μm . The particles suspended in a suitable dispersion medium are illuminated by a laser beam and they scatter light or exhibit fluorescence. A dark-field microscope is then used to determine the position of single particles in constant motion due to Brownian motion. The movements of each particle are tracked and the mean squared velocity, which depends on the particle diameter is calculated. An absolute size distribution of the particles in suspension can be obtained after the system has been calibrated with beads of known concentration. NTA can be used to determine the zeta potential as well by applying an electric field across the suspension and measuring the velocity of single particles due to electrophoresis [Carr *et al.*, 2008; Dragovic *et al.*, 2011].

(III) Field flow fractionation (FFF) is another technique that is used in particle size characterisation [Jawahar *et al.*, 2012]. FFF is centered on the elution of small particles in a parabolic flow profile. The scattering signal produced by the eluted components are then evaluated by multi-angle light scattering (MALS) with the aid of a photometer which records and computes the size-weighted radius within the range of 10 nm to 1 μ m. Flow FFF is the most sensitive of the available FFF techniques as it can measure particle size as small as 1 nm. Small particle size differences could be very well resolved using FFF unlike in PCS. Additionally, FFF can be used for separating particles for further characterisation.

Samples have to be diluted well for FFF analysis like most other nanoparticle analytical procedures but this may alter some sample properties (e.g. removal of surfactants from the particle surface) and result in erroneous data [Mehnert and Mäder, 2001].

(IV) Acoustic spectroscopy is useful for obtaining data on particle size using relevant equations and measuring the attenuation of sound waves [Garud *et al.*, 2012]. The oscillating electric field produced by moving charged particles under the influence of acoustic energy could also be used to obtain information on the surface charge of particles.

Laser diffraction is the commonly used technique for determining particle size in suspensions, emulsions, dry powders and aerosols, but it requires light transmission, which limits its application to dilute samples [Alba *et al.*, 1999]. Sound waves interact with particles in a similar fashion to light but the former has the benefit of being able to travel through concentrated samples. Sound-based particle size analysis has been in existence for years but it is limited in size ranges and only works well with dense, rigid particles. Acoustic attenuation spectroscopy overcomes these restrictions. It employs ultrasonic transducer technology and digital signal processing which are

centred on classical acoustical principles to permit analysis of highly concentrated particle systems with sizes in the range of 0.01 μm to 1000 μm .

1.5.4.2 Zeta potential (ZP)

A nanoparticle having a net surface charge attracts a layer of oppositely charged ions which moves with the nanoparticle [Escubed Ltd., 2015]. There is however a point beyond which the attracted ions do not move with the particle which is called the ‘slipping plane’. The layer of both the surface charge and oppositely charged ions is referred to as the electrical double layer (EDL). The EDL consists of an inner region of strongly bound ions known as the ‘stern layer’ and an outer layer of loosely associated ions called the ‘diffuse layer’ (depicted in Figure 1.5).

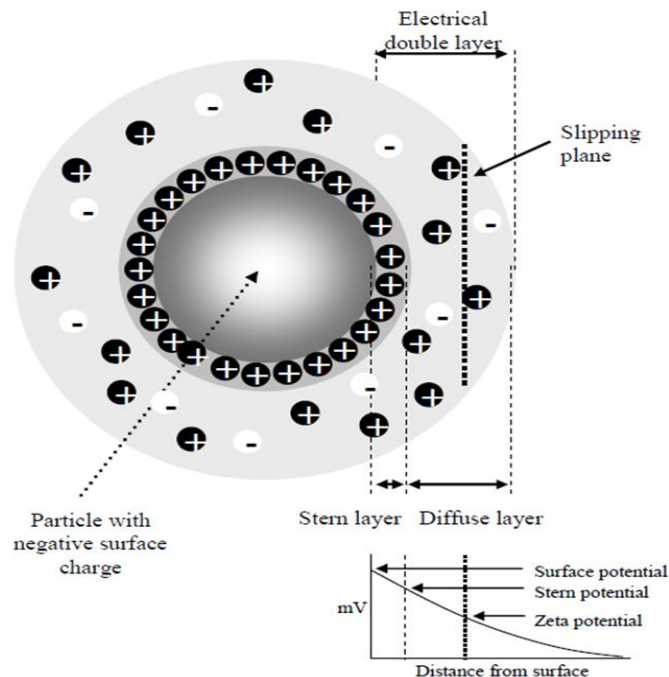


Figure 1.5 Diagrammatic representation of the distribution of ions around a charged nanoparticle in a dispersion [Escubed Ltd., 2015]

Zeta potential (electrokinetic potential) is a measure of the potential difference between the medium in which the particle is dispersed and the layer of fluid containing the oppositely charged ions [Escubed Ltd., 2015; Nanocomposix, 2015]. ZP is therefore, the electric potential at the EDL boundary. Particles with ZP bind to oppositely charged surfaces. The magnitude of ZP (usually ranging from -100 mV to +100 mV) gives information on the stability of a colloidal dispersion. Nanoparticles with higher ZP values exhibit increased electrostatic repulsion (from ionic surfactants) and are therefore stable over time while those with lower magnitudes ultimately aggregate due to van der Waals inter-particle attractions. This is however not applicable to formulations containing steric stabilisers because the latter reduce particle aggregation by adsorption onto the particle surface and decrease ZP in the process [Müller, 1996]. This indicates that a formulation containing a steric stabiliser will show good stability despite having a low ZP magnitude. The following ZP values (absolute) give an indication of the stability behaviour of colloidal dispersions according to Riddick (1968):

- 0-3 mV : Maximum agglomeration and precipitation
- 3-5 mV : Strong agglomeration and precipitation
- 10-15 mV : Threshold of agglomeration
- 16-30 mV : Threshold of delicate dispersion
- 31-40 mV : Moderate stability
- 41-60 mV : Fairly good stability
- 61-80 mV : Very good stability
- 81-100 mV : Extremely good stability

It is worth noting that the magnitude of charge on the surface of a nanoparticle is affected by the pH of the dispersion medium. The net charge on a nanoparticle can be reduced to zero at its

isoelectric point however, this may not be desired as the dispersion becomes highly unstable at this point with a high probability of flocculation.

ZP is usually measured in a cell that has two gold electrodes [Nanocompositix, 2015]. Voltage is applied to the electrodes to cause the particles to move towards the oppositely charged electrode and particle velocity is then measured as a function of voltage. The particles move through a laser beam passing through the cell and the intensity of scattered light fluctuates at a frequency proportional to the particle speed. The latter is measured at multiple voltages and the data obtained is used to calculate the ZP.

1.5.4.3 Particle shape, morphology and topography

(I) Electron microscopy

Transmission electron microscopy (TEM) and scanning electron microscopy (SEM) are examples of direct methods for physical characterisation of SLNs [Liu *et al.*, 2007]. Electron microscopy employs electrons instead of light for visualising particles in the nanometre range. SEM detects scattered electrons from the surface of the particles and visualises the surface while TEM detects electrons transmitted through the sample.

When performing TEM on nanoparticles, it must be considered that they can be vulnerable to the high energetic electron beam [Bentley *et al.*, 2005] so for susceptible samples, a low electron beam current should be used. TEM however is costly, and there may be image overlapping during analysis [Smith, 2007]. Sample preparation is also a bit tedious and time-consuming, involving dehydration, staining and conductive coating steps, which may cause changes that could affect the

resulting shape of the nanoparticles [Liu *et al.*, 2007]. High-resolution TEM (HRTEM) uses electron beam interference by the sample rather than the absorbance of the beam as with ordinary TEM, thereby giving a higher resolution.

SEM is also used for shape and morphological examination of nanoparticles by using a high-energy electron beam however, the beam is scanned over the sample surface and the backscattering of the electrons is looked at [Jawahar *et al.*, 2012]. The sample has to be under a vacuum (like TEM) and electrically conductive (non-conductive samples can be sputter-coated for conductivity) at the surface.

(II) Atomic force microscopy (AFM)

AFM employs the force acting between a sample surface and a probing tip to provide qualitative and/or quantitative information about the physical properties of nanoparticles such as size, morphology, surface texture and roughness (topography) [Drake *et al.*, 1989; Kirby *et al.*, 1995]. The benefit of AFM is that the sample is easily prepared by placing a drop of dilute solution/dispersion on a clean microscope slide or a mica substrate, and the sample may be dried prior to analysis. In addition, vacuum is not a requirement, the sample does not need to be conductive and images are obtained rapidly.

Submicron particles move rapidly, as such preparatory steps such as solvent removal may be crucial depending on the analysis being conducted however, this may also cause significant modifications in the molecular structure of the sample [Kumar and Randhawa, 2013]. Sample dehydration may result in changes such as cluster formation, particle shrinkage and lipid crystallisation, all of which can affect the results obtained.

1.5.4.4 Crystallinity of lipid and drug

Studying the degree of lipid crystallinity and modification in lipid nanoparticles is essential as these are highly related to drug incorporation and release rates. Differential scanning calorimetry (DSC) and X-ray scattering are commonly used for this purpose.

DSC is based on the fact that various modifications (such as polymorphs) of a lipid have different melting points and enthalpies [Müller *et al.*, 2000]. It gives data on the nature, melting and crystallisation characters of both the solid and liquid constituents of a sample by providing data on their glass transition temperatures, as well as their melting points and enthalpies. Thermodynamic stability and lipid packing density are both inversely related to drug incorporation rates but the extent depends on the particular modification/polymorphic form (supercooled melt, alpha (α)-modification, beta prime (β')-modification and beta (β)-modification) of the lipid. The main polymorphic forms have been reported to be in the following order of increasing stability, melting point and packing density: $\alpha < \beta' < \beta$. A supercooled melt is formed when lipid crystallisation/solidification (initiated by crystallisation nuclei) does not occur although a lipid in its liquid/molten state is stored below its melting point. Crystallisation is a size dependent process so the tendency to form supercooled melts increases with decreasing particle size. After crystallisation, triglycerides tend to pack into very specific structural arrangements with characteristic symmetries, and the latter depends on the type of unit cell present in the crystals. The packing arrangement of atoms within the crystal defines the type of unit cell structure present in the crystal [Boistelle, 1988; Müller *et al.*, 2000; Marangoni, 2011].

Polymorphism is mainly a property of triacylglycerols and other lipids, and is their ability to crystallise into different crystal types but essentially maintaining their chemical composition

[Marangoni, 2011]. It is a form of physical degradation that can affect the stability of dosage forms because although chemically identical, polymorphs may have different thermodynamic properties such as melting point, X-ray diffraction pattern, infrared spectral signature, Raman spectra and solubility characteristics [Martin *et al.*, 1983; Marangoni, 2011]. It is therefore important to understand the particular polymorphic shifts of both lipids and drugs in a drug product, if any.

It is however worth noting that, because emulsifiers are included in SLN preparation, lipid crystallisation and changes due to lipid modifications are greatly slowed [Suresh *et al.*, 2007; Vivek *et al.*, 2007; Jawahar *et al.*, 2012].

X-ray diffraction (XRD) is used to evaluate the length of the long and short spacings of a lipid lattice but it is necessary to analyse the whole SLN dispersion instead of only the lipid. This is because solvent removal may lead to changes in the sample [Westesen *et al.*, 1993].

Both single crystals and polycrystalline materials can be analysed using XRD, which involves evaluation of the interference of scattered x-rays from the atoms in a sample using Bragg's Law. XRD dimensions are stated in angstroms ($1 \text{ \AA} = 0.1 \text{ nm}$). XRD is very beneficial but it can be time-consuming and also, a large amount of sample is usually required.

1.5.4.5 Drug localisation within SLNs

The amount of drug incorporated in SLNs may affect the characteristics of drug release. The amount of encapsulated drug in an SLN can be ascertained after the free drug and the lipid(s) have been separated from the aqueous medium. This separation can be achieved through ultracentrifugation, centrifugation, filtration or gel permeation chromatography. The amount of the

drug is then determined by a suitable standard analytical technique such as spectrophotometry, spectrofluorometry, high-performance liquid chromatography (HPLC) or liquid scintillation counting [Magenheim and Benita, 1991]. In this regard, the selected analytical method must be sensitive, selective and precise for the drug.

Factors influencing drug loading in a lipid are drug solubility in/miscibility with the melted lipid, chemical/physical structure of the solid lipid matrix and the polymorphic state of the lipid. For adequate drug loading, drug solubility in the lipid melt must be sufficiently high, which can generally be achieved by using mono- and diglycerides. Complex lipids like mixtures of mono-, di- and triglycerides and also lipids with fatty acids of different chain lengths form less perfect crystals, which offer voids to contain the drugs to enhance drug loading [Mehnert *et al.*, 1997; Müller *et al.*, 2000].

The incorporation of drugs into SLNs has been summarised (Figure 1.6) to be by one of the following models:

- (I) Solid solution: This model is produced during the initial stages of cold homogenisation. After dissolution in the molten lipid, the drug becomes molecularly dispersed within the lipid matrix when the drug-lipid mixture is rapidly cooled [zur Mühlen *et al.*, 1998].
- (II) Core-shell model, drug-enriched shell: This model results from hot homogenisation, as the drug repartitions into the SLN shell (superficial layers) during the cooling stage of SLN preparation.
- (III) Core-shell model, drug-enriched core: This is formed when a drug is dissolved in the lipid melt at or close to its saturation solubility and it precipitates before the lipid recrystallises

during the cooling stage of preparing the nanoemulsion. The cooling results in supersaturation and crystallisation of the drug preceding lipid crystallisation, which leads to the formation of a drug-enriched core surrounded by a lipid shell.

[Schwarz, 1995; zur Mühlen, 1996; Mehnert *et al.*, 1997; zur Mühlen and Mehnert, 1998]

- (IV) Drug particles could also be attached/adsorbed onto the surface of the SLN [Svilenov and Tzachev, 2013]. Several techniques such as electron spectroscopy (e.g. X-ray photoelectron spectroscopy (XPS)), ion-based techniques (e.g. secondary ion mass spectrometry (SIMS)), and scanning probe microscopy (SPM) (e.g. AFM and scanning tunnelling microscopy (STM)) are available for the characterisation of SLN surfaces. Any of these can be useful in studying the presence of drug particles on the surface of a particle.

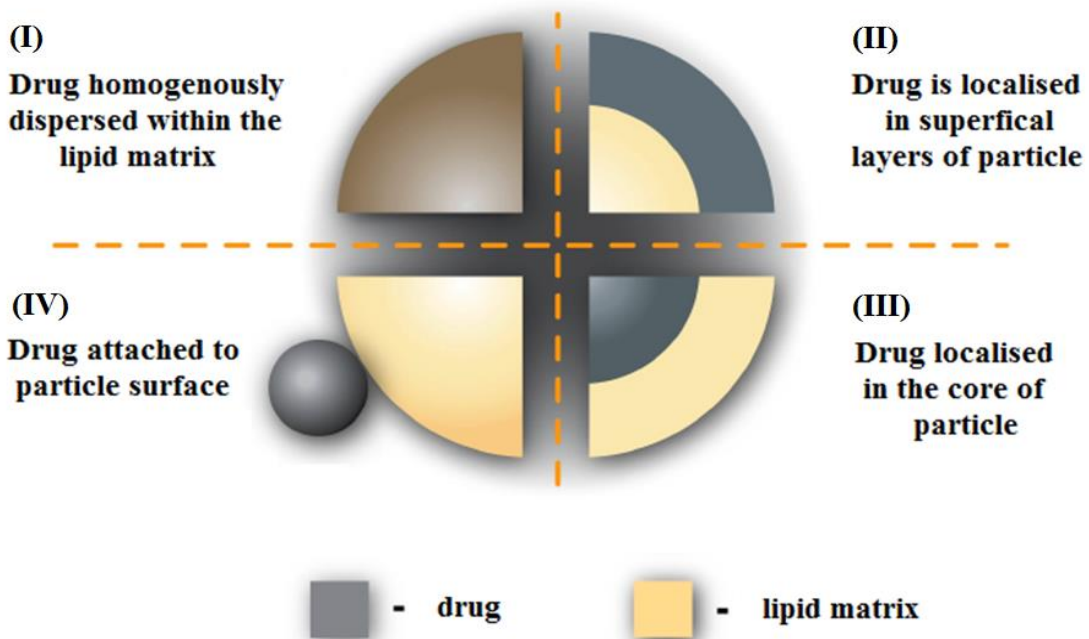


Figure 1.6 Possible drug localisation in SLNs [Svilenov and Tzachev, 2013]

1.5.4.6 Drug release from SLNs

Drug release is a key factor worth considering before and after preparing a successful SLN system [Dhawan *et al.*, 2004]. The rate of drug release depends on the solubility characteristics of the drug, desorption of surface-bound/adsorbed drug, drug diffusion through the SLN and erosion/degradation of the SLN matrix. If drug diffusion occurs faster than erosion of the matrix, then the drug release mechanism is largely by diffusion.

Some *in vitro* and *in vivo* data on SLNs have shown prolonged drug release up to 80 hr [Reddy *et al.*, 2006; Li *et al.*, 2009; Dodiya *et al.*, 2011; Dwivedi *et al.*, 2014]. An *in vitro* study conducted on prednisolone SLNs showed drug release up to 35 days [zur Mühlen and Mehnert, 1998]. It is possible to modify drug release profiles based on the lipid, type and amount of surfactant, as well as the production parameters (e.g. temperature) [zur Mühlen and Mehnert, 1998; zur Mühlen *et al.*, 1998] used in formulating SLNs. However, sufficient hydrophobicity of the drug is also necessary to keep the latter preferentially entrapped within the lipid matrix to achieve a prolonged release. All the aforementioned factors are key in determining the shape/outline of the release profiles of drugs from carrier systems.

A problem of ‘burst release’ (initial high drug release) is sometimes observed with lipid nanoparticulate systems when particles with drug-enriched shells are produced [zur Mühlen *et al.*, 1998]. This property can be exploited to deliver an initial high dose if desired or avoided if prolonged drug release is desired. Differences in lipid melting and homogenisation temperatures are considered as the main parameters that determine the structure of the SLN matrix and hence, how drug release may occur.

Drug release profiles for SLNs can be explained by drug partitioning between the lipid and aqueous surfactant phases, especially during the production stage [Müller *et al.*, 2000]. For instance during hot homogenisation, varying amounts of the drug partitions into the aqueous phase. This partitioning and the extent to which it happens depend on the drug's solubility characteristics, temperature of the aqueous phase and the surfactant concentration. High drug solubility, high temperature and increasing surfactant amount result in higher drug partitioning into the aqueous phase. On cooling the o/w nanoemulsion, drug solubility in the water phase decreases causing re-partitioning of the drug back into the lipid phase. Due to the decreasing temperature, solid lipid cores also start forming thereby encapsulating the drug until they become crystallised/solidified. As a result, the remaining drug concentrates in and/or on the outer shell of the SLNs and is subsequently released in the form of a 'burst', while the drug within the SLN core is released gradually over an extended period [zur Mühlen and Mehnert, 1998; Müller *et al.*, 2000].

A good way to avoid undesired burst release is to prepare SLNs at a low temperature, and either with a low concentration of surfactants or with surfactants which do not solubilise the drug, to keep the drug within the lipid matrix [zur Mühlen and Mehnert, 1998; Müller *et al.*, 2000].

1.5.5 Oral absorption and bioavailability of SLNs

1.5.5.1 Dosage forms for oral SLNs

SLNs can be orally administered as an aqueous dispersion or in the traditional solid dosage form such as tablets, pellets, capsules or powders. An aqueous SLN formulation can be used as the granulation fluid for making tablets or it can be spray-dried or lyophilised into powder form and

added as part of the powder mix for tableting. SLNs can also be administered as pellets by using the former as a wetting agent in the extrusion process [Pinto, 1999]. SLN powders or pellets can as well be filled into hard gelatin capsules for oral delivery. Alternatively, SLNs can be formulated in liquid PEG 600 and filled into soft gelatin capsules for use [Yang, 1999].

1.5.5.2 Mechanisms of oral absorption of SLNs

There are two possible mechanisms of uptake of SLNs as illustrated in Figure 1.7.

(I) Microfold (M) cells of Peyer's patches in the gut (Figure 1.8):

This is an intracellular uptake route by which drugs are transported into systemic circulation, through the intestinal lymphatics and the thoracic lymph duct [Arahamian *et al.*, 1987]. The intercellular junctions between endothelial cells of lymphatic capillaries are more open as compared to blood capillaries, which results in molecular sieving of nanoparticles of large sizes directly into lymphatic vessels. M cell uptake of nanoparticles is therefore size-dependent (i.e. the smaller the size, the higher the uptake). Thus, nanoparticulate systems can effectively improve drug bioavailability to enhance therapeutic efficacy. Lymphatic delivery is helpful not only for absorption of poorly soluble drugs but also for targeting drug carriers to the lymphatics.

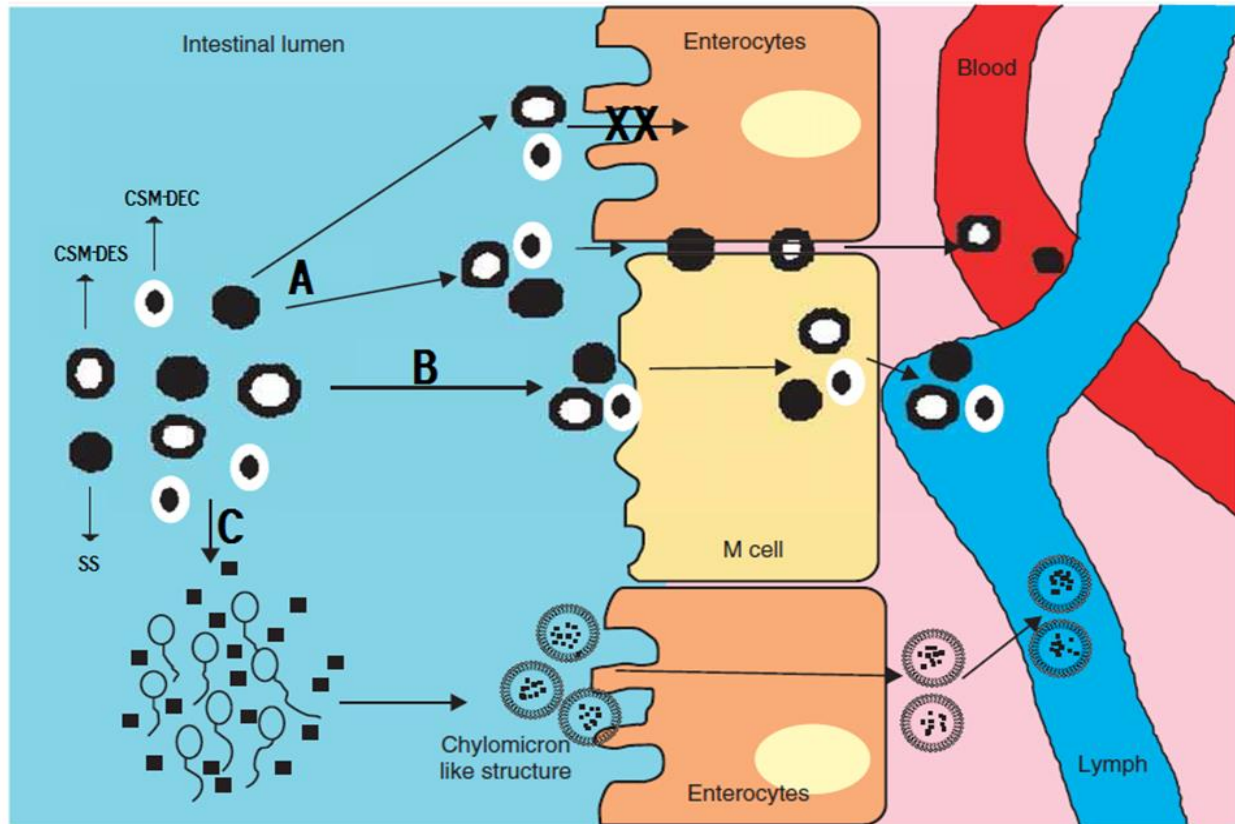


Figure 1.7 Summary of SLN absorption after oral administration:
 A. Intercellular/paracellular pathway, B. M cell uptake via Peyer's patches, and C. chylomicron-assisted enterocyte absorption [SLN models: SS-Solid solution; CSM-DES-Core-shell model, drug-enriched shell; CSM-DEC-Core-shell model, drug-enriched core] [Harde *et al.*, 2011]

(II) Intercellular/paracellular uptake:

Paracellular uptake transports SLNs directly into blood through capillary vessels or between intestinal epithelial cells [Aprahamian *et al.*, 1987]. Nanoparticles have been found in intercellular spaces and in larger defects of the mucosa 10 to 15 min after intraluminal injection into the intestines of anaesthetised beagle dogs. The nanoparticles were subsequently found in the small capillaries near the intestinal epithelium and then finally in the capillaries of the core of the villus.

After 30 min, the nanoparticles were quite numerous at the inner surface of the vascular epithelium where they generally formed clusters.

In addition to M cell and paracellular uptake of SLNs, lipase-mediated chylomicron formation followed by lymphatic absorption can enhance SLN absorption. Chylomicrons are physiological carriers (lipoproteins) that transport lipids from the intestines to the lymph [Bargoni *et al.*, 1998; Sanjula *et al.*, 2009]. Lipase-mediated chylomicron formation aids in the dissolution and assimilation of hydrophobic drugs in the lipid core of SLNs to promote drug absorption. Involvement of chylomicrons and transport via the Peyer's patches offer SLNs a direct transport into the lymphatic system, which allows for drug targeting to lymph [Bargoni *et al.*, 1998].

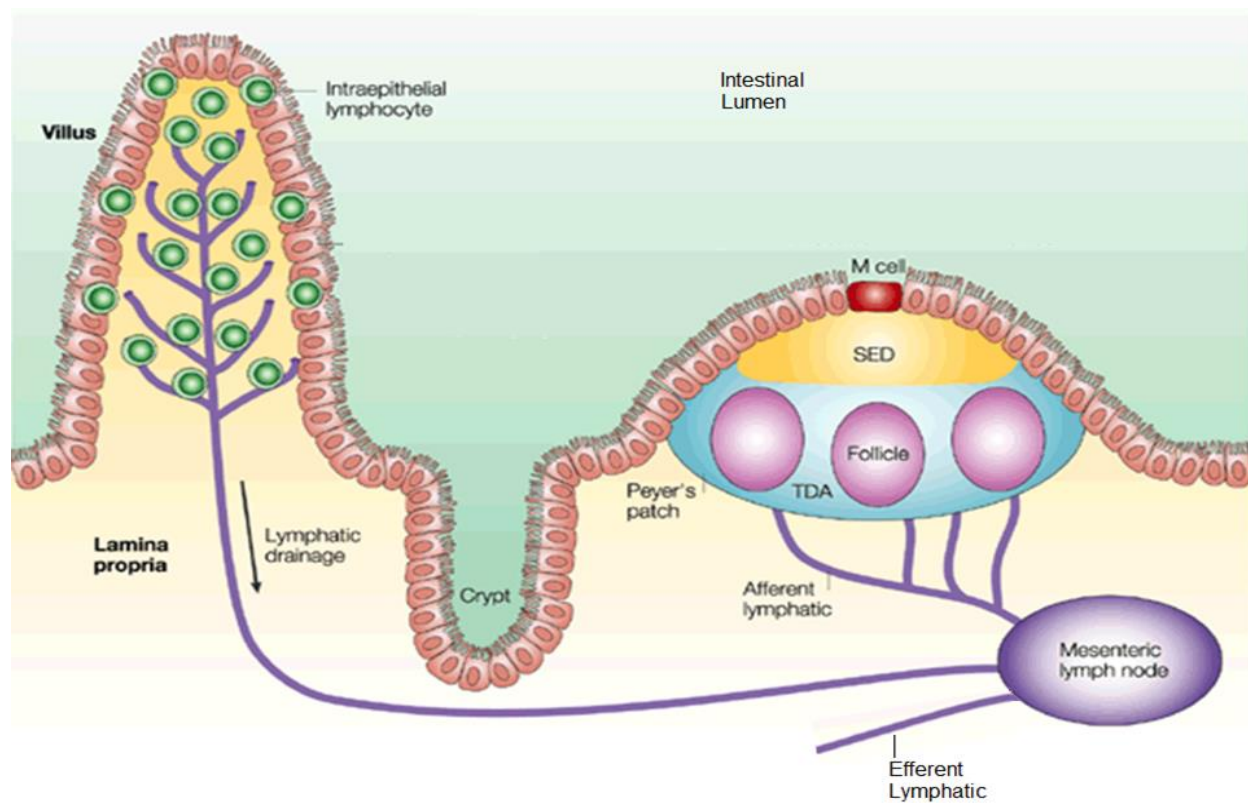


Figure 1.8 Diagram showing an M cell of a Peyer's patch [Mowat, 2003]

1.5.5.3 Bioavailability of SLNs

The oral bioavailability of drugs depends on their solubility/dissolution rate and degradation in the GI tract, absorption across transmembrane barriers and transporters such as P-gp [Cai *et al.*, 2010]. Lipid-based drug delivery systems such as SLNs enhance the oral bioavailability of hydrophobic drugs by keeping the drugs in a solubilised state. In addition, triglycerides of SLNs are digested by lipases to produce surface-active mono- and diacylglycerols, which induce the secretion of endogenous phospholipids and bile salts to facilitate the formation of mixed micelles and thereby improve oral absorption of poorly soluble drugs [Müller *et al.*, 2006; Porter *et al.*, 2007]. SLNs of several drugs have shown significant improved oral bioavailability compared with their respective drug suspensions [Li *et al.*, 2009; Sanjula *et al.*, 2009; Hu *et al.*, 2010; Varshosaz *et al.*, 2010(a, b); Luo *et al.*, 2011; Zhang *et al.*, 2012; Xue *et al.*, 2013; Dwivedi *et al.*, 2014].

A factor that contributes to the absorption enhancing property of SLNs is their small size, which considerably increases their surface area and results in ample and steady absorption from the GI tract [Hanafy *et al.*, 2007]. Because very fine particles are generally adhesive, SLNs can adhere to the gut wall to prolong their residence time thereby enhancing their oral absorption [Tarr and Yalkowsky, 1989; Müller *et al.*, 2000; Müller *et al.*, 2006]. Again, SLNs can enhance lymphatic delivery of drugs (Section 1.5.5.2) contributing to their bulk oral bioavailability. Lipids can stimulate lipoprotein formation and intestinal lymphatic lipid flux to increase the extent of lymphatic drug transport, but this is influenced by the type of lipid [Paliwal *et al.*, 2009] and the amount of surfactants [Sanjula *et al.*, 2009] used in preparing the SLNs. For instance, a study by Paliwal *et al.* (2009) revealed that Compritol® 888 ATO-based SLNs showed better drug loading and release characteristics, better oral bioavailability and higher concentration of methotrexate in the lymph, as compared with the stearic acid-, glycerol monostearate- or tristearin-based SLNs.

Sanjula *et al.* (2009) have also reported that increasing the concentration of the surfactant poloxamer 188 resulted in a decreased bioavailability of carvedilol SLNs, after intraduodenal administration of the SLNs to rats.

Uptake of intact SLNs via M cells and the lymphatic route plays an important role in SLN absorption, as evidenced by some studies. TEM analyses of blood and lymph after duodenal administration of SLNs to rats have shown the presence of intact SLNs. It was also observed that the size of the SLNs prior to administration and that found later in the lymph were about the same [Bargoni *et al.*, 1998; Cavalli *et al.*, 2003]. Yuan *et al.* (2007) also used fluorometry to confirm that about 77.9% of fluorescein isothiocyanate-labelled stearic acid SLNs were absorbed into systemic circulation through the lymphatic route after oral administration of the SLNs to rats.

1.5.5.4 Metabolism of SLNs

The solid lipids in SLNs are degraded enzymatically by pancreatic lipases after oral administration however, the rate of degradation is affected by the type of lipid matrix as well as the type and amount of surfactant [Müller *et al.*, 1996]. In an *in vitro* lipase assay, it was found that using bile salts in low concentrations promoted SLN degradation while poloxamer 188 inhibited SLN degradation due to steric stabilisation. The rate of lipase degradation of long fatty acid chains was also slower than that of shorter ones. Again, larger SLNs (≥ 800 nm) were degraded slowly as compared with smaller particles (180-330 nm) [Olbrich *et al.*, 2002(a,b)].

Due to the improved lymphatic transport of SLNs, incorporated drugs avoid first-pass metabolism. As a result, lower doses of drugs affected by first-pass metabolism can be administered in the form

of SLNs, which serves to improve tolerance to drugs with narrow therapeutic windows. The bioavailability of drugs loaded into SLNs is therefore further enhanced via evading first-pass effect due to lymphatic transport, adding on to the aforementioned mechanisms of improved absorption [Hu *et al.*, 2010; Varshosaz *et al.*, 2010(a)].

1.5.6 Potential of SLNs in reducing toxicity and side effects of drugs

The encapsulation of drugs into SLNs and the resulting controlled drug release from the particles reduce direct exposure of the encapsulated drugs to the body, which to an extent decreases drug-induced systemic toxicities. Some studies have compared the toxic effects of lipid-based formulations of AmB with those of aqueous suspensions containing only the drug. The results indicated that the lipid formulations, compared to the free drug, showed significantly lesser renal toxicity in rats [Risovic *et al.*, 2003; Gershkovich *et al.*, 2009; Jain *et al.*, 2012], as well as reduced *in vitro* haemolysis [Jain *et al.*, 2012; Gupta *et al.*, 2013] in mammalian cells. In the former set of studies, renal toxicity was assessed based on changes in plasma creatinine levels after drug administration compared with baseline values.

Triptolide has limited clinical use due to its poor aqueous solubility and oral bioavailability. It also causes hepatotoxicity. However, oral administration of triptolide SLNs to rats led to an improved bioavailability and reduced toxicity of triptolide [Mei *et al.*, 2005; Zhang *et al.*, 2013]. An *in vitro* study by Ezzati *et al.* (2014) on alendronate sodium also indicated that loading the drug into SLNs resulted in a considerably lower cytotoxicity as compared with the free drug. SLNs therefore serve as a promising system for reducing drug-related toxicities.

1.6 Gastrointestinal transit of pharmaceutical dosage forms

The small intestine is considered the main site of drug absorption in man due to its high and effective surface area [Davis *et al.*, 1986]. If any, drug absorption from the stomach is minimal, and some drugs may be absorbed to a limited extent from the large intestine. The general consideration therefore is that drugs should be formulated so they can be principally absorbed from the small intestine.

Ho *et al.* (1977) and Higuchi *et al.* (1981) introduced the 'reserve length' concept for drug absorption, which is the anatomical length over which complete drug absorption occurs. The reserve length depends on physiological factors such as bulk flow rate, spreading of the dosage form in the small intestine and drug permeability through the intestinal mucosa.

Factors such as particle size, stress, posture, calorific value of meals and specific effects of fats/lipids have been shown to affect gastric emptying of markers, food and dosage forms [Kelly, 1981; Dubois and Castell, 1984; Fell and Digenis, 1984; Fara, 1985]. For instance, smaller-sized drug [Sugito *et al.*, 1992] and food [Olausson *et al.*, 2008] particles are emptied from the stomach faster than larger ones in human subjects. Some studies have also indicated that lying down may slow down peristalsis [Steingoetter *et al.*, 2006] and delay gastric emptying [Gruber *et al.*, 1958]. In a study by Zheng *et al.* (2009), gastric emptying was found to be delayed when rats were acutely stressed (single stress), and then completely restored after chronic stress (repeated single stress for 5 consecutive days) was applied using a restraint stress model. The presence of lipids in the duodenum [Hölzer *et al.*, 1994] and consumption of meals of high caloric values [Calbet and MacLean, 1997] have also been found to delay gastric emptying.

Several methods are available to measure intestinal transit time of orally administered formulations. These include radiography, the use of metabolisable markers (hydrogen breath test) and gamma scintigraphy, with each having its benefits and shortcomings. The nature of the method employed, such as the use of a high osmolarity preparation (lactulose solution) in the hydrogen breath test [Read *et al.*, 1980], or the present condition of the subject, such as intubation [Read *et al.*, 1983], may alter the normal physiological processes in a subject. Gamma scintigraphy has mostly been used over the years for investigating the transit pattern (movement and disintegration) and intestinal transit time of dosage forms [Wilson *et al.*, 1984; Christensen *et al.*, 1985; Billa *et al.*, 2000; Honkanen *et al.*, 2004]; however, this procedure requires the use of expensive equipment, radionuclides and harmful radiation. Figure 1.9 illustrates how the position of a radiolabelled dosage form in the GI tract was monitored in gamma scintigraphy; noting that, the times of arrival of the dosage form at various points of the GI tract could also be estimated.

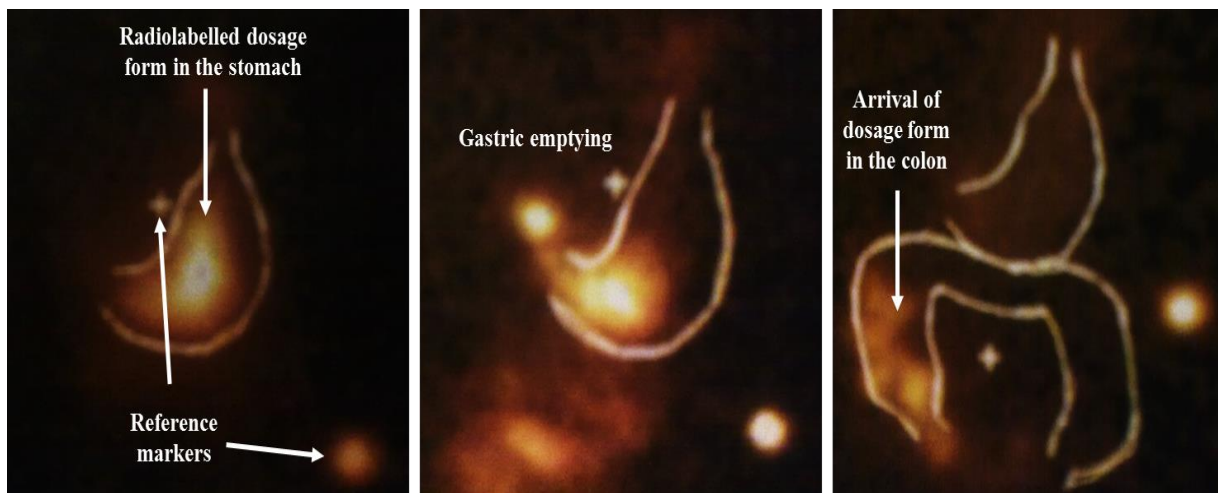


Figure 1.9 Typical gamma scintigraphic images from a GI transit study in a human volunteer

[Reference markers: Firmly attached to the skin at left lobe of liver and lower left costal margin to aid repositioning of the volunteer for image acquisition]

[Billa *et al.*, 2000]

1.7 Aim of the study

To formulate and characterise an amphotericin B-containing solid lipid nanoparticulate formulation, and to study the gastrointestinal transit behaviour and absorption of the formulation in rats.

1.8 Specific objectives

1. To formulate and optimise an AmB-containing solid lipid nanoparticle (SLN) formulation.
2. To formulate paracetamol (PAR) SLNs and sulphasalazine (SSZ) SLNs.
3. To characterise the formulated SLN preparations to ensure similarities in their physicochemical properties.
4. To develop and validate a high-performance liquid chromatography method to assay AmB, PAR and sulphapyridine (SP) simultaneously in rat plasma, using a suitable internal standard.
5. To investigate the gastrointestinal transit behaviour and absorption of the AmB-loaded SLNs using rats as the animal model.
6. To study the effect of food on the absorption of the AmB SLNs.

CHAPTER 2

FORMULATION AND CHARACTERISATION OF AMPHOTERICIN B, PARACETAMOL AND SULPHASALAZINE SOLID LIPID NANOPARTICLES

2.1 Introduction

Hydrophobic drugs such as AmB are poorly absorbed from the GI tract when administered orally; therefore, such drugs have to be administered in appropriate carrier systems to address the constraint of poor absorption in order to enhance their therapeutic efficacy. One main system proposed is the lipid-based delivery system (LBDS). Lipids increase drug absorption and thereby improve oral bioavailability by: facilitating the formation of solubilised species via particle size reduction, producing a solid-state solution within the carrier [Humberstone and Charman, 1997; Porter and Charman, 2001; Pouton and Porter, 2008; Jawahar *et al.*, 2012]; changing drug uptake, efflux and disposition by modifying enterocyte-based transport [Wilson and Mahony, 1997; Pramod *et al.*, 2010]; and enhancing lymphatic drug transport [Charman *et al.*, 1997; Driscoll, 2002; Porter *et al.*, 2007].

After oral delivery, nanoparticles as well as microparticles less than 5 μm in size have the potential to traverse the Peyer's patches along the GI tract, which drain into lymph and then eventually empty loaded drugs into systemic circulation [Jani *et al.*, 1989; Jani *et al.*, 1994; Shakweh *et al.*, 2005]. There is also evidence that lipid-based AmB formulations improve the oral bioavailability of AmB [Patel and Patravale, 2011; Jain *et al.*, 2012] and minimise its side effects, chiefly the nephrotoxicity [Risovic *et al.*, 2003; Gershkovich *et al.*, 2009; Jain *et al.*, 2012]. The triple-benefit of improved oral bioavailability, reduced renal toxicity and preclusion of infusion-related toxicity give oral AmB-containing SLN preparations a promising future in clinical use.

Adequate and proper characterisation of SLN dispersions is a prerequisite for the control of their quality. Characterisation of SLNs is however met with challenges due to their small size and the complexity and dynamic nature of the delivery system. The important parameters of SLNs that are usually evaluated include but are not limited to particle size, size distribution, zeta potential, degree of crystallinity and lipid properties, drug content, *in vitro* drug release and surface morphology [Mehnert and Mäder, 2001].

As the sizes of particles decrease to the submicron scale, their physicochemical properties begin to differ from those associated with their bulk forms/individual components [Baer *et al.*, 2010]; thus, particle size is usually the first feature that is determined after SLNs are prepared. In addition, the surface layers of nanoparticles, whether deliberately or accidentally formed may have important effects on formulations so there is the need to understand and characterise the particle surface [Grainger and Castner, 2008]. Nanoparticles may also be coated with surfactants or contaminants hence, it is necessary that these are adequately identified and characterised as their composition and structure may affect the properties and performance of the formulation as a whole, especially during storage or after environmental exposure [Baer *et al.*, 2010].

Many analytical tools cannot be used for direct measurement of freshly prepared undiluted SLN dispersions. Consequently, there is the possibility of changes within a sample prior to its characterisation, due to sample preparation procedures such as dilution, which results in the removal of emulsifiers from the particle surface. Additionally, removal of water during sample drying may induce crystallisation and lipid modifications [Mehnert and Mäder, 2001]. The aforementioned factors therefore have to be taken into consideration during characterisation of SLNs and other nanoparticulate systems.

In this chapter, the preparation and characterisation of individual SLN formulations containing AmB, PAR or SSZ are described. The characterisation studies precede a GI transit study in rats in the subsequent chapters, in which the PAR and SSZ (from which SP is released *in vivo*) serve as markers for estimating the gastric emptying and oro-caecal transit times respectively, of the AmB SLNs. The exhaustive characterisation of all three SLNs is to ensure similarity in their physicochemical properties with the assumption that, when administered simultaneously via the oral route, they would respond similarly to the hydrodynamics within the GI tract.

2.2 Materials

Beeswax (Acros Organics, Morris Plains, NJ, USA), theobroma oil (JB Cocoa Sdn Bhd, Gelang Patah, Johor, Malaysia), amphotericin B (Nacalai Tesque, Inc., Kyoto, Japan), sulphasalazine (Tokyo Chemical Industry Co. Ltd., Tokyo, Japan) and agarose (1st Base Laboratories Sdn Bhd, Seri Kembangan, Selangor, Malaysia) were purchased from the respective companies. Paracetamol, trehalose and phosphate-buffered saline (pH 7.4) were purchased from Sigma-Aldrich (St. Louis, MO, USA). Lecithin soy and sodium cholate were obtained from MP Biomedicals (Illkirch, France). Chloroform, ethyl acetate, methanol and hydrochloric acid were purchased from Fisher Scientific (Loughborough, UK). SYBR[®] Green and loading buffer were purchased from Thermo Fisher Scientific (Waltham, MA, USA). All reagents and solvents used were of analytical and HPLC grades, respectively. Water used was Milli-Q 18.2 M Ω ·cm at 25°C (Millipore Corp., Bedford, USA).

2.3 Methods

2.3.1 Formulation of AmB, PAR and SSZ SLNs

The SLNs were prepared as previously described by Tan *et al.* (2010) but without oleic acid (liquid lipid). Briefly, the drug (AmB, PAR or SSZ) and lecithin soy (LS) were first dissolved in a mixture of chloroform-methanol at a 2:1 ratio, along with theobroma oil (TO) and beeswax (BW) as indicated in Table 2.1. The solvent mixture was evaporated off using a Rotavapor[®] R-200/205 (Büchi Labortechnik AG, Flawil, Switzerland) at 50°C, leaving the drug embedded within the lipid matrix. The lipid matrix was melted in 10 mL of ethyl acetate (previously equilibrated with water for 10 min) at 70°C. At the same time, 20 mL of a 5% w/v sodium cholate (SC) solution was heated to the same temperature. Both phases were homogenised using a high-speed homogeniser (Ika-Turrax T 25[®], IKA[®], Staufen im Breisgau, Germany) at 9 500 rpm for 10 min. 80 mL of water at 70°C was then added slowly to the mixture with continuous stirring for a further 20 min. The organic solvent was then evaporated off using the rotary evaporator at 70°C.

Table 2.1 Composition of the SLNs

Drug	Amount of drug (mg)	Theobroma oil (mg)	Beeswax (mg)	Lecithin soy (mg)	Sodium cholate (mg/20 mL)	Water (mL)
AmB, PAR or SSZ	50	200	200	120	1000	80

2.3.2 Scanning electron microscopy (SEM)

The surface topography and morphology of the SLNs were determined using a Quanta 400 FE-SEM (FEI, Hillsboro, OR, USA). Prior to analysis, the samples were diluted with Milli-Q water. They were then placed on carbon tape and air-dried for 24 hr. Samples were then mounted on the stage and viewed under low vacuum mode at 20 kV.

2.3.3 Optimised procedure for preparing AmB, PAR and SSZ SLNs

The SLNs were prepared according to the procedure described in Section 2.3.1 with the following modifications. The chloroform-methanol mixture was used at a ratio of 1:1. The concentration of the SC solution was reduced to 2.5% w/v. The volumes of ethyl acetate and SC solution used, each at 70°C, were 20 mL and 40 mL, respectively. Homogenisation of the lipid and aqueous phases was done at 10 000 rpm for 6 min. The final steps were addition of 60 mL of water at 70°C to the nanoemulsion formed, followed by stirring the mixture for 20 min and then evaporation of the organic solvent.

2.3.4 Characterisation of the optimised SLNs

2.3.4.1 Relative density and viscosity determinations

The densities and viscosities of freshly prepared SLN dispersions were investigated using a density bottle and a viscometer (DV-I Prime, Brookfield Engineering Laboratories Inc., Middleboro, MA, USA), respectively. For the relative density determination, the mass of each formulation was divided by the mass of an equal volume of deionised water. The viscosity values on the other hand

were obtained directly from the viscometer readings. All determinations were made in triplicate and results expressed as mean \pm standard deviation (SD).

2.3.4.2 Gel electrophoresis

In order to gain an insight into the relative movement propensities of the three SLNs within a milieu as may be encountered in the GI tract, a gel electrophoresis was set up (Figure 2.1) and the distances travelled by the three SLNs, constrained within agarose gel were measured. Agarose was completely dissolved in 1 \times TBE (89 mM Tris base, 89 mM boric acid and 2 mM EDTA) buffer solution at a concentration of 1% w/v using microwave heating. The solution was allowed to cool slightly (before gelation), followed by the addition of 30 μ L of SYBR[®] Green dye. The mixture was poured into a casting plate and a gel comb was inserted to form wells. The gel was left to set at room temperature for 30 min. The running buffer, 1 \times TBE, was then poured into the gel tank to submerge the gel. A 10- μ L aliquot of each SLN sample was mixed separately with 2 μ L of the loading buffer (containing glycerol, bromophenol blue as dye and water) and then loaded into the wells within the gel in triplicates. The gel electrophoresis unit was run at +45 V for 45 min and then +39 V for 15 min. The migration of the SLNs within the gel was viewed under UV light (Bio-Rad, Hercules, CA, USA) and the distances travelled were measured using a calibrated ruler.

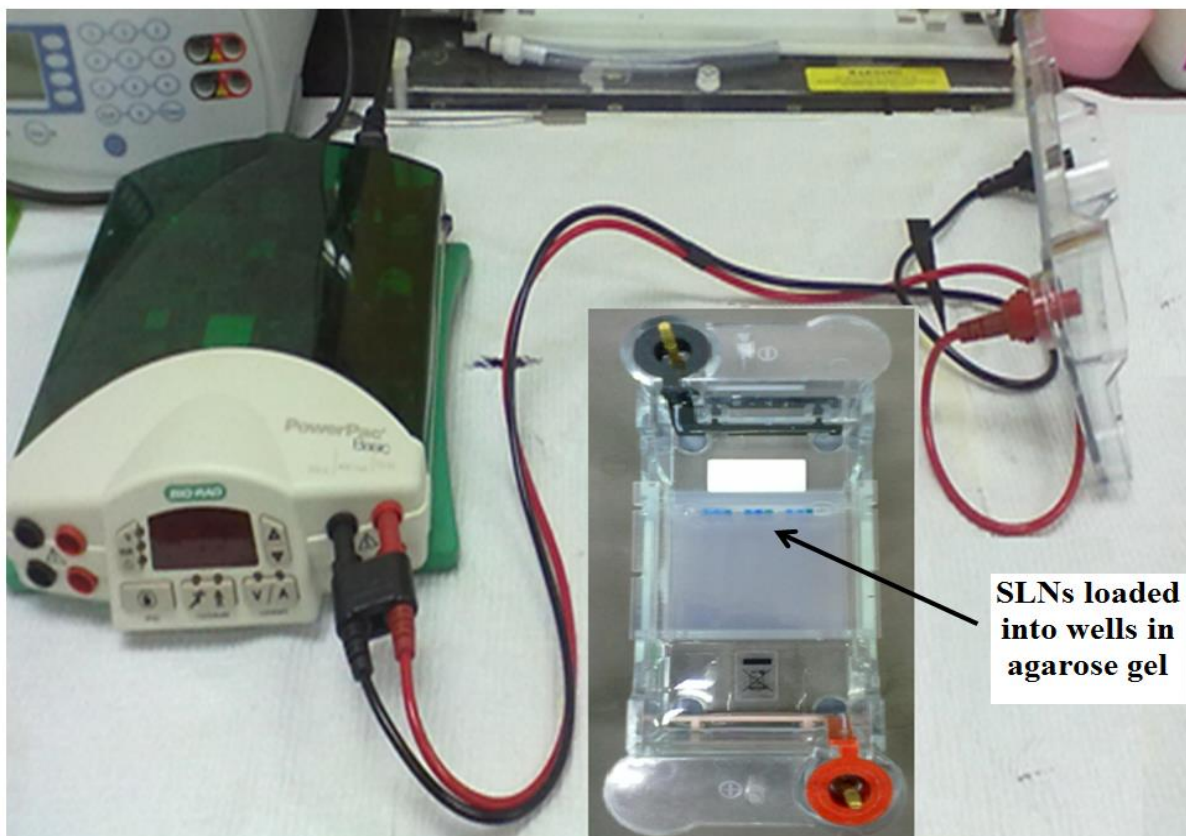


Figure 2.1 Gel electrophoresis set-up

2.3.4.3 Photon correlation spectroscopy (PCS)

PCS studies were carried out on the SLNs using a Zetasizer Nano ZS[®] (Malvern, UK) equipped with a 4 mW He-Ne laser (633 nm). The parameters measured were z-average, zeta potential and polydispersity index (PDI). Particle size analysis using PCS is evaluated using the intensity distribution of the particles; therefore, the z-average is the mean intensity diameter of the particle population. PDI, also known as heterogeneity index describes the width of variation within the sample size distribution. The zeta potential is the measurement of the net surface charge of the SLNs.

All SLN samples were diluted with Milli-Q water before analyses using a clear disposable zeta cell. Each analysis was carried out at 25°C and performed in triplicate. The data obtained were expressed as mean \pm SD.

2.3.4.4 SEM analyses

SEM analyses were performed as described in Section 2.3.2.

2.3.4.5 Atomic force microscopy (AFM)

AFM images were obtained from freshly prepared SLN samples using a scanning probe microscope (NTEGRA Prima, NT-MDT, Moscow, Russia). Prior to analysis, 50 μ L of each sample was diluted with 1 mL deionised water. A 40- μ L aliquot of this dilution was placed on a mica disc and air-dried after removing excess liquid with filter paper. Images were recorded in tapping mode using silicon cantilevers coated with aurum at a resonance frequency of 220 kHz.

2.3.4.6 Fourier transform infrared spectroscopy (FTIR)

This analysis was conducted to verify the possibility of interaction between the drugs and other components within the SLN formulations. Infrared spectra were obtained using an FTIR spectrophotometer (Spectrum RX I, Perkin Elmer, Waltham, MA, USA). To record the spectra, samples were ground with an appropriate amount of potassium bromide until a homogenous mix was obtained. A well-formed disc of the mixture was obtained by compressing the mixture at a

pressure of 5 tons for 5 min using a pellet press (Model 4350, Carver Inc., Wabash, IN, USA). The spectra were obtained over a wavenumber range of 4000-400 cm^{-1} .

2.3.4.7 Differential scanning calorimetry (DSC)

DSC thermograms of the drugs, bulk lipids and SLNs were obtained using a DSC Q2000 (TA instruments, New Castle, DE, USA) equipped with a TA Universal Analysis 2000 software. Approximately 5 mg of sample was placed in a standard aluminium pan, hermetically sealed and subjected to the analyses at a scan rate of 5°C/min from -20 to 250°C. The melting enthalpies of the samples were obtained by integration of their melting peaks with the TA Universal Analysis 2000 software. Analyses were run under a gentle stream of nitrogen (50 mL/min), using an empty pan as the reference.

2.3.4.8 HPLC method for *in vitro* analyses

A Perkin Elmer HPLC system (Series 200 auto-sampler, Series 200 UV/VIS detector) configured to TotalChrom[®] Navigator software was used with an Eclipse Plus[®] C18 (250 x 4.6 mm, 5 μm) column (ZORBAX, Agilent, Santa Clara, CA, USA). The mobile phase was filtered through a 0.45 μm membrane filter before use and comprised of acetate buffer (pH 4) [A], prepared by mixing 847 mL of 0.1 M acetic acid and 153 mL of 0.1 M sodium acetate trihydrate [Lambert and Muir, 1955]; and acetonitrile [B]. The mobile phase was run at a flow rate of 1 mL/min in gradient mode as follows: 100% A at 0-0.5 min; 60% A at 0.5-7 min; 20% A at 7-9 min; 60% A at 9-12 min and 100% A at 12-15 min. A wavelength of 254 nm was used to detect PAR and SSZ, and 405 nm used to detect AmB. Calibration curves for AmB, PAR and SSZ dissolved in a mixture of

methanol and dimethyl sulphoxide at ratios of 1:3, 3:1 and 1:1, respectively, were plotted (peak area against drug concentration) over a concentration range of 0.25-50 µg/mL for each drug. The coefficients of determination (R^2) and line equations were determined for each calibration curve.

2.3.4.9 Encapsulation efficiency (%EE)

The %EE of AmB, PAR or SSZ within the SLNs was determined following a slightly modified method [Tan *et al.*, 2010]. Briefly, a few drops of a 0.1 M HCl solution were added to 1 mL of SLN dispersion to precipitate the nanoparticles, followed by centrifugation at 14 000 rpm for 45 min using a microcentrifuge (Microfuge[®] 16, Beckman Coulter Inc., Brea, CA, USA). The supernatant was decanted and the precipitate washed with PBS (pH 7.4) to remove any free drug. The precipitate was then dissolved in 1 mL of a mixture of methanol and DMSO at a ratio of 1:3, 3:1, and 1:1 for AmB, PAR and SSZ SLNs, respectively. The above mixtures were heated to 70°C and then cooled to room temperature, followed by centrifugation at 14 000 rpm for 10 min to separate the lipid. The amount of drug in the solvent was determined using HPLC (Section 2.3.4.8).

The %EE was calculated using the following equation:

$$\%EE = \frac{\text{Amount of drug in precipitate}}{\text{Amount of drug used in formulation}} \times 100\% \dots\dots\dots\text{Equation 2.1}$$

2.3.4.10 Drug release studies

Cumulative *in vitro* drug release studies on both freshly prepared and freeze-dried (Alpha1-2 LD_{Plus} freeze-dryer, Osterode am Harz, Germany) SLNs were conducted using PBS (pH 7.4) as

the dissolution medium. SLNs containing 0.5 mg of drug were dispersed in the dissolution medium and incubated at 37°C in a WiseCube WIS-20[®] shaking incubator (PMI-Labortechnik GmbH, Grafstal, Switzerland) operated at 100 rpm. At predetermined time intervals (0, 1, 2, 4, 8 hr), 1 mL samples were withdrawn and the volume taken was replenished with the dissolution medium. The nanoparticles were then precipitated with 0.1 M HCl, followed by centrifugation at 14 000 rpm for 10 min using a microcentrifuge and the supernatant decanted. A 20- μ L aliquot of the supernatant, containing the released drug was then injected onto the HPLC (Section 2.3.4.8) and the cumulative amount of drug released with time calculated. The data obtained are expressed as mean \pm SD from triplicate measurements. The same procedure was followed for each SLN formulation.

The *in vitro* release of the SLNs was further evaluated up to 30 hr on individual seeded tubes and not cumulatively as described above. Several replicas of 100 μ L SLNs (either freshly prepared or a suspension of freeze-dried sample in deionised water) were placed in separate microcentrifuge tubes containing 1 mL of PBS (pH 7.4) and subjected to the same conditions (temperature and speed) as described above. The analyses were conducted for drug released in each tube. At predetermined times (0, 1, 2, 4, 8, 18 and 30 hr), a seeded tube was taken and subjected to the same procedure of SLN precipitation, centrifugation and analysis of supernatant as described above.

2.3.4.11 Determination of drug release kinetics

The release kinetics of the drugs from the SLNs were determined by fitting the *in vitro* release data into the equations presented in Table 2.2. The zero order kinetics corresponds to the percentage cumulative drug release versus time data. Values of the coefficients of determination (R^2) were calculated from the linear curves obtained by regression analyses of the plot for each formulation.

The kinetic model that best fitted the release data was then evaluated by comparing the R^2 values from using the various models. For the Korsmeyer-Peppas model, the value of n was also obtained.

Table 2.2 Models for drug release kinetics

Model	Expression
Zero order	$Q = Kt$ Equation 2.2
First order	$\log Q_R = \frac{Kt}{2.303}$ Equation 2.3
Higuchi	$Q = K(t)^{\frac{1}{2}}$ Equation 2.4
Hixson-Crowell	$Q_0^{1/3} - Q_t^{1/3} = Kt$ Equation 2.5
Korsmeyer-Peppas	$\log Q = \log K + n \log t$... Equation 2.6

Where: Q - percentage cumulative release; Q_R - percentage drug remaining; t - time in hours; K - constant (according to the respective models); n - release/diffusional exponent.

2.3.4.12 Statistical analyses

The properties of the AmB SLNs, PAR SLNs and SSZ SLNs were compared where appropriate using GraphPad Prism 5 software. Paired t -test was used to analyse statistical differences between freshly prepared and freeze-dried SLN samples. In all cases, statistical significance was indicated when p value < 0.05.

2.4 Results and discussion

2.4.1 Physical appearance of the SLNs

Figure 2.2 shows the appearances of the freshly prepared SLNs. The arrows in the diagram point to a small amount of sediment at the bottom of the AmB SLN vial, and areas of different opacities in the PAR and SSZ SLNs. The latter is clearly indicative of creaming phenomenon. Many emulsion-based formulations cream on standing [Attwood, 2001]. This is caused by the dispersed phase either rising to the top or sinking to the bottom of the preparation depending on its density relative to that of the continuous phase. The nanoparticles in the creamed layers of the SLNs did not coalesce, thus they were easily redispersed upon shaking however, creaming is not desirable as it increases the tendency of particle aggregation. One way of preventing creaming is to reduce the particle size of the dispersed phase, which can be achieved by homogenisation at an optimum speed and for an optimum time. This is because, although homogenisation results in particle size reduction, the kinetic energy imparted to the particles can result in particle collisions and cause aggregation and increase in particle size instead.

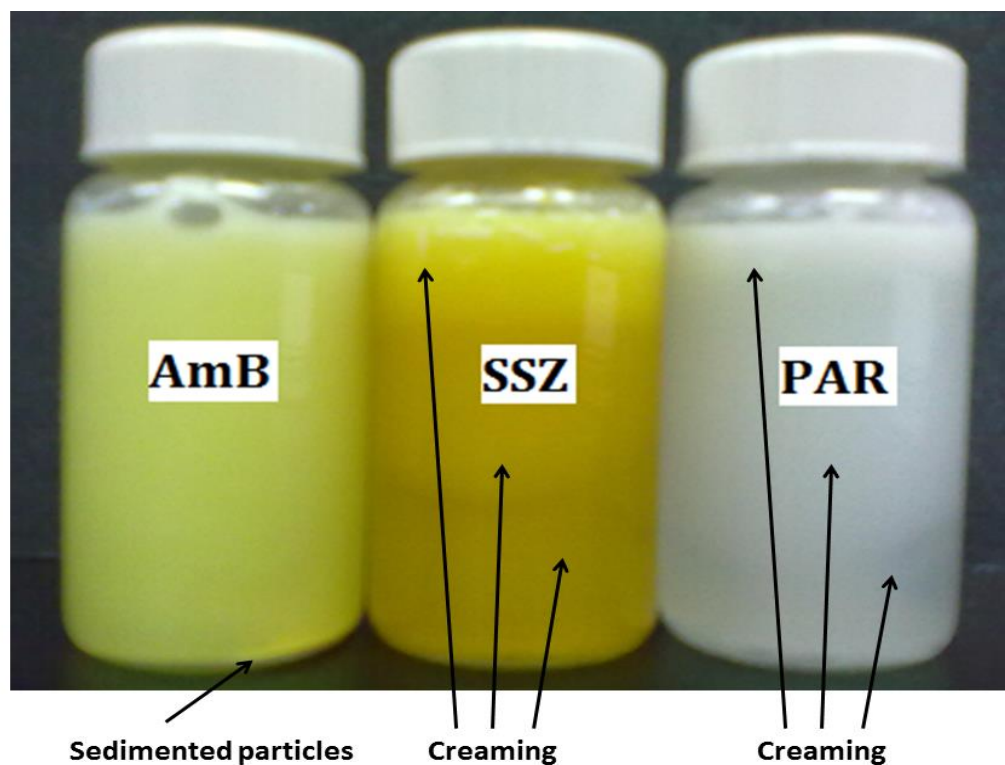


Figure 2.2 Physical appearance of the SLNS

2.4.2 SEM analyses of the SLNs

The images obtained from the SEM analyses of all the three SLNs as presented in Figure 2.3 showed that mostly spherical microparticles were formed instead of nanoparticles. These images, together with the physical appearance of the SLNs (Figure 2.2) necessitated that the SLNs be reformulated.

After optimisation, homogenisation at a speed of 10 000 rpm for 6 min was deemed favourable for formulating the SLNs to achieve particle size reduction to the submicron range.

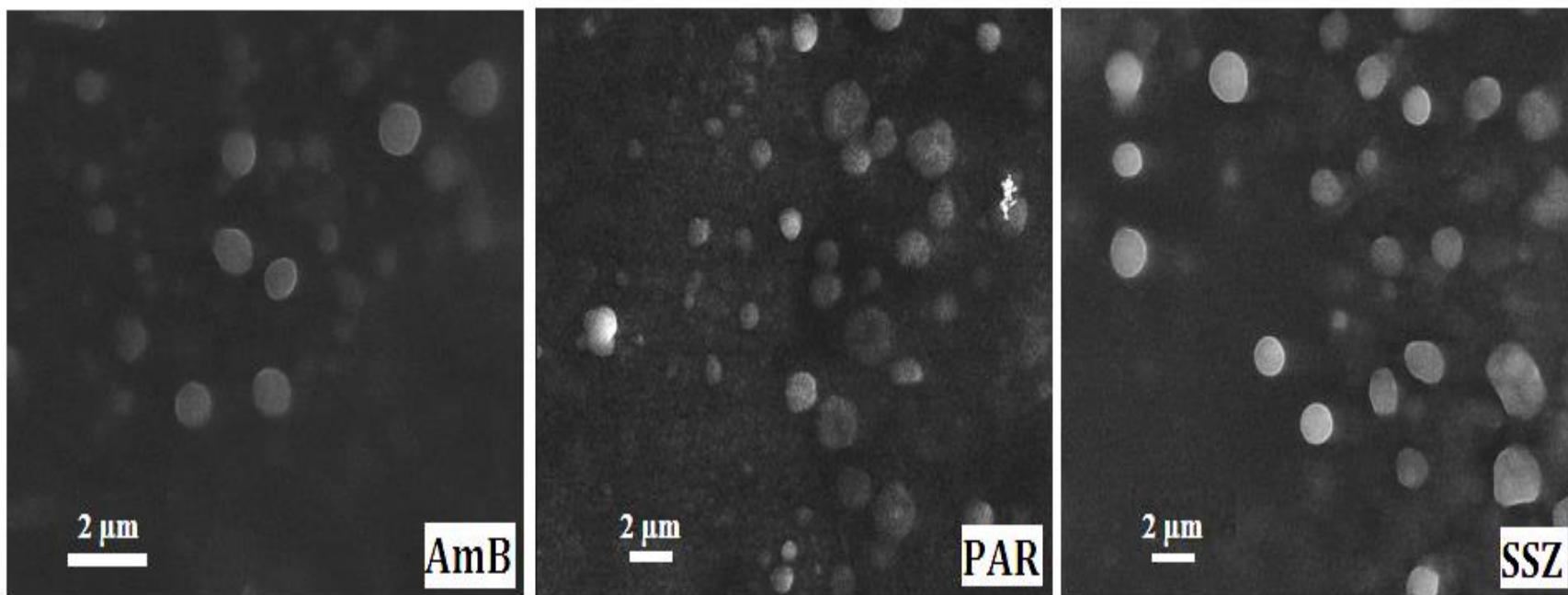


Figure 2.3 SEM images of the SLNs

2.4.3 Physical appearance of the optimised SLNs

The modified procedure stated in Section 2.3.3 was used in preparing the SLNs shown in Figure 2.4. The SLNs were easy to differentiate from each other as the final products took the colours of the incorporated drugs; yellow for the AmB SLNs, white for the PAR SLNs and bright yellow for the SSZ SLNs. The preparations were uniform in appearance without any signs of physical instability such as creaming, flocculation, coalescence or particle sedimentation.

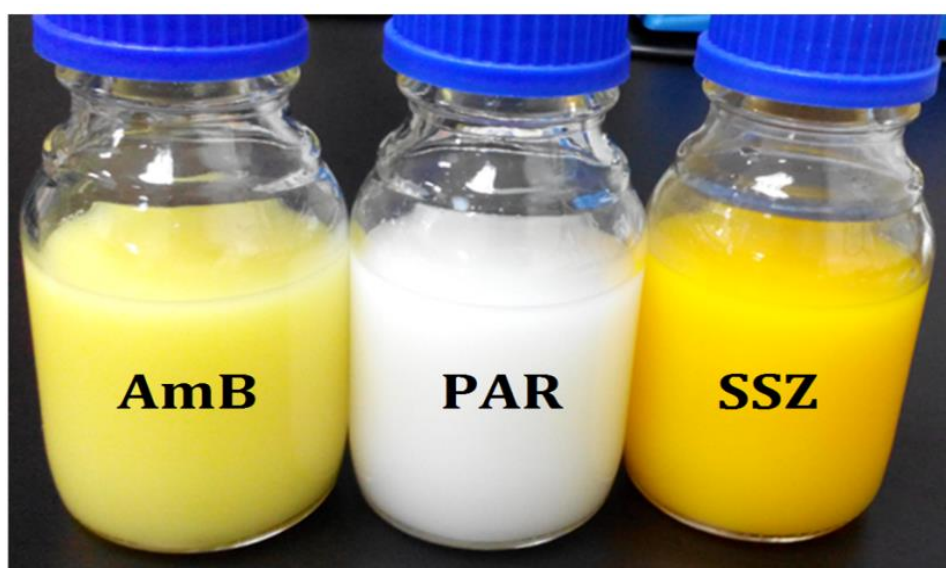


Figure 2.4 Physical appearances of the optimised SLNS

2.4.4 Relative density and viscosity

The mean values of relative densities were 1.00, 1.01 and 1.01 for AmB, PAR and SSZ SLNs respectively; and were not significantly different from each other ($p > 0.05$ in all cases). The mean viscosity values were 1.14 ± 0.16 cPs, 1.21 ± 0.06 cPs and 1.04 ± 0.12 cPs for AmB, PAR and SSZ SLNs respectively; also being not statistically different from each other ($p > 0.05$). Viscosity and

density play a significant role in the GI transit of dosage forms because generally, low viscosity liquid dosage forms offer advantages of elimination of fed-fasted effects, rapid drug absorption and increased bioavailability [Amidon *et al.*, 1991; Clarke *et al.*, 1993; Tuleu *et al.*, 1999; Bosch *et al.*, 2003]. It is therefore probable that the three SLNs would respond similarly to the hydrodynamics imposed by the GI tract due to the similarities in viscosity and density.

2.4.5 Gel electrophoresis

In order to further ascertain the relative propensities of the three SLNs to move within a milieu, the SLNs were subjected to gel electrophoresis and the distances migrated by each type of SLN towards the positive electrode were measured. The agarose gel matrix contains pores that are formed from random packing of the polymer, which consists of repeating agarobiose units. Agarobiose is a disaccharide derived from D-galactose and 3,6-anhydro-L-galactopyranose. Although the pores in the gel are small and the gel is stationary in contrast to what would be expected in the GI tract, the analyses nonetheless give an indication of the mobility propensities of the SLNs within a matrix such as chyme. Figure 2.5 illustrates images of the agarose gel before and after the application of voltage, and clearly show that the SLNs travelled similar distances along the gel. The distances migrated by the three types of SLNs were 22.2 ± 0.0 mm for AmB; 22.4 ± 0.4 mm for PAR and 22.3 ± 0.1 mm for SSZ, with the values not differing from each other significantly ($p > 0.05$). This study along with the density and viscosity data further suggest the possibility of similar dispositions amongst the three SLNs in response to GI hydrodynamics.

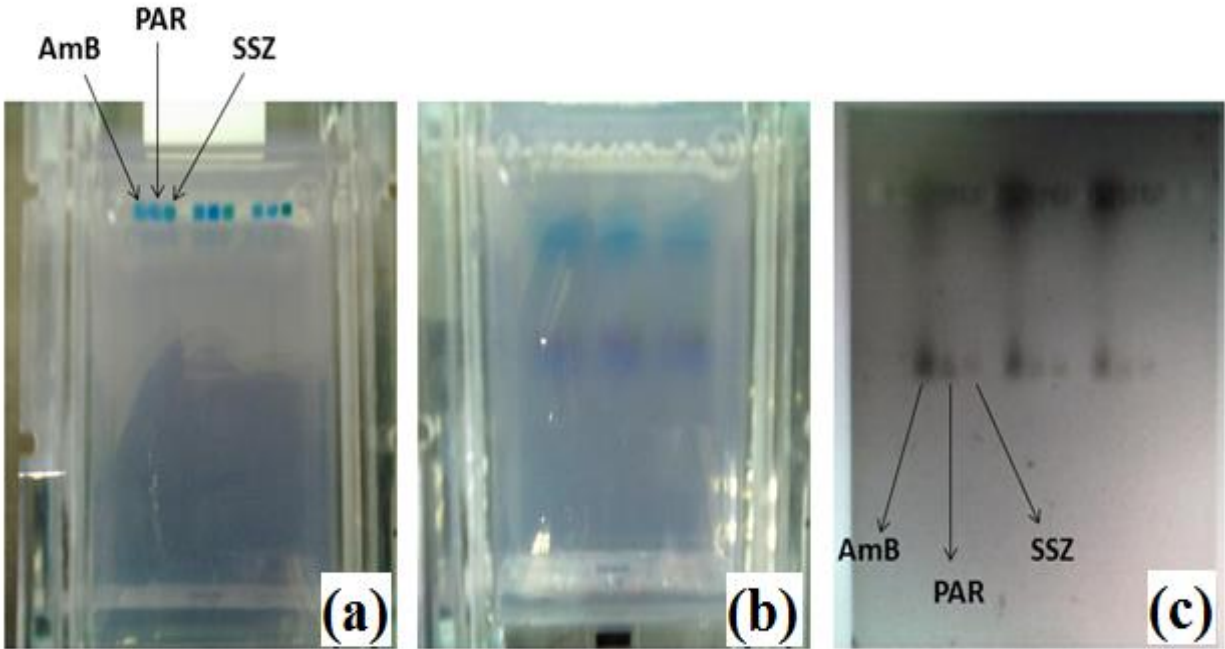


Figure 2.5 Agarose gel (a) before and (b, c) after voltage application [b-normal photograph; c-image obtained from viewing the gel under UV light]

2.4.6 PCS studies

The particle size distribution profiles for all three SLNs were mostly unimodal with negligible proportions of the particles having sizes above 1000 nm as depicted in Figure 2.6. From Table 2.3, it can be seen that there were no statistically significant differences among the z-averages of the three SLNs ($p > 0.05$), albeit a slightly higher value for SSZ (224.8 ± 3.3 nm) and PAR (210.1 ± 1.4 nm) compared with AmB (206.5 ± 1.7 nm) SLNs. All the PDI values obtained were well below 0.5, ranging from 0.16 ± 0.03 to 0.22 ± 0.01 , which indicates a mostly narrow particle size distribution. This is also evidenced by the narrow widths of the particle size distribution profiles.

The ZP values for all three SLNs showed that the surfaces of the particles were negatively charged. This is attributable to the use of sodium cholate, which is an anionic surfactant, in preparing the SLNs. The magnitude of ZP can be used to predict colloidal stability, with values greater than $|60 \text{ mV}|$ indicating very good stability resulting from high inter-particle electrostatic repulsion, which is of great importance during storage [Riddick, 1968]. The ZP for the three SLNs ranged from $-61.9 \pm 1.0 \text{ mV}$ to $-71.9 \pm 0.9 \text{ mV}$ indicating that particle aggregation during storage owing to van der Waals inter-particle attractions can be expected to be low.

Table 2.3 Z-averages, PDIs and ZPs of freshly prepared SLN formulations

Sample	Z-average (nm)	PDI	ZP (-mV)
AmB	210.1 ± 1.4	0.22 ± 0.01	61.9 ± 1.0
PAR	206.5 ± 1.7	0.16 ± 0.03	71.9 ± 0.9
SSZ	224.8 ± 3.3	0.19 ± 0.08	70.7 ± 0.6
<i>p</i> value	*	*	*

* $p > 0.05$ - the mean values do not significantly differ from each other statistically

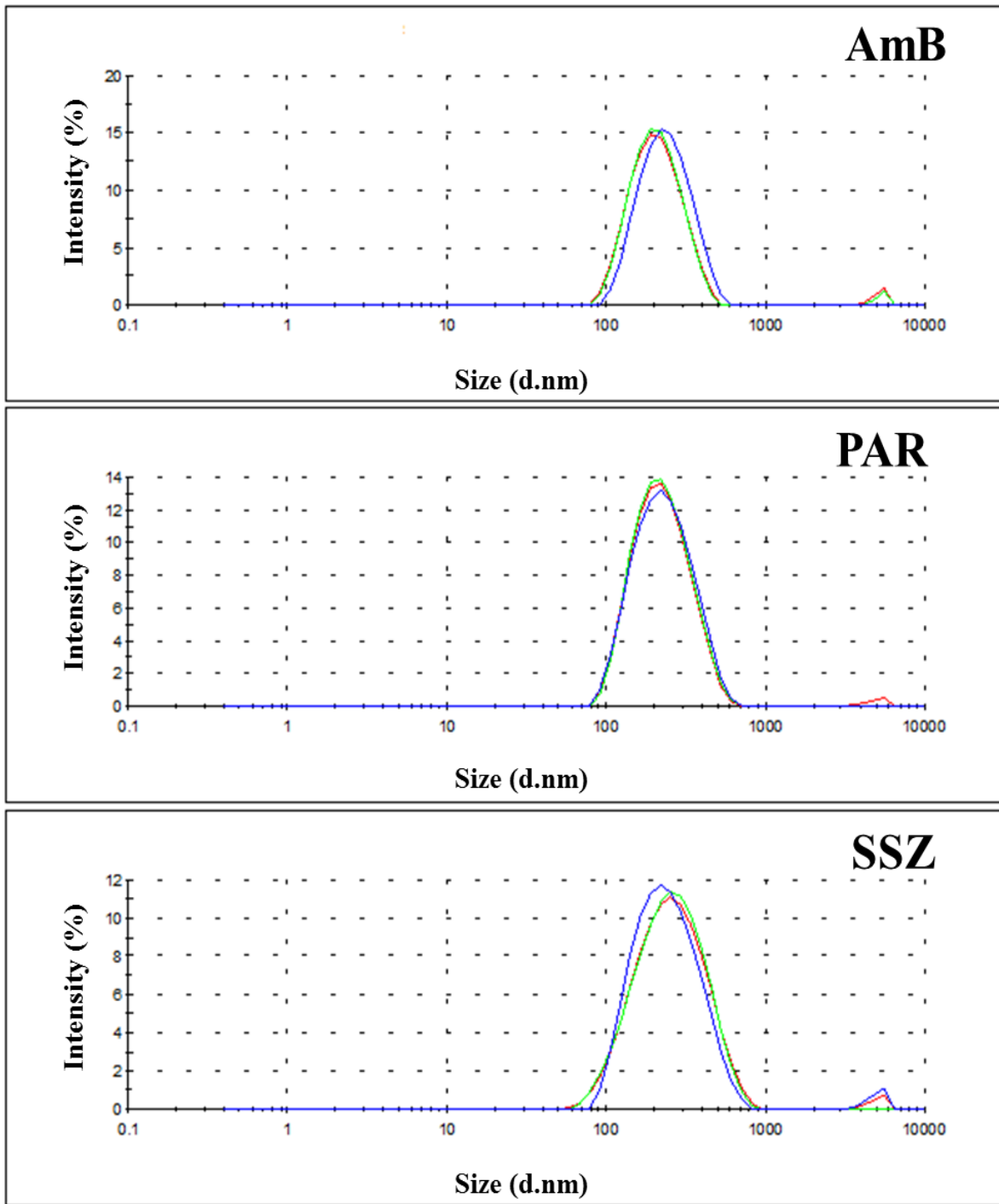


Figure 2.6 Particle size distribution by intensity of the freshly prepared SLNs (n = 3)

2.4.7 SEM analyses

The images obtained from the SEM are presented in Figure 2.7. All three SLNs showed uniform spherical particles with fairly smooth morphologies and generally appeared identical in outlook, with a tendency for agglomeration. The SEM images show homogenous particle sizes and corroborate the size data obtained in the PCS analysis. None of the images of the SLNs showed the presence of drug crystals.

It can also be seen that the particle sizes from the SEM data are lower than the z-average values obtained from the PCS analyses. The particle sizes in the SEM seem to be at the lower end of the size distribution profiles for all three SLNs, which is consistent with the findings of Dubes *et al.* (2003) who observed a similar pattern. This is because PCS measurements are based on DLS, and measure the hydrodynamic diameter of particles. DLS measurements depend on additional surface structures attached to particles due to the double layer of solvated ions that move with the particles when the latter are in Brownian motion in a liquid. Therefore, the sizes measured in PCS are relatively larger than those obtained from microscopic techniques since the latter do not use DLS. In addition, any hydration layers around the particles are removed during the drying step of sample preparation prior to analysis, if drying is required [Tscharnuter, 2000; Svilenov and Tzachev, 2013].

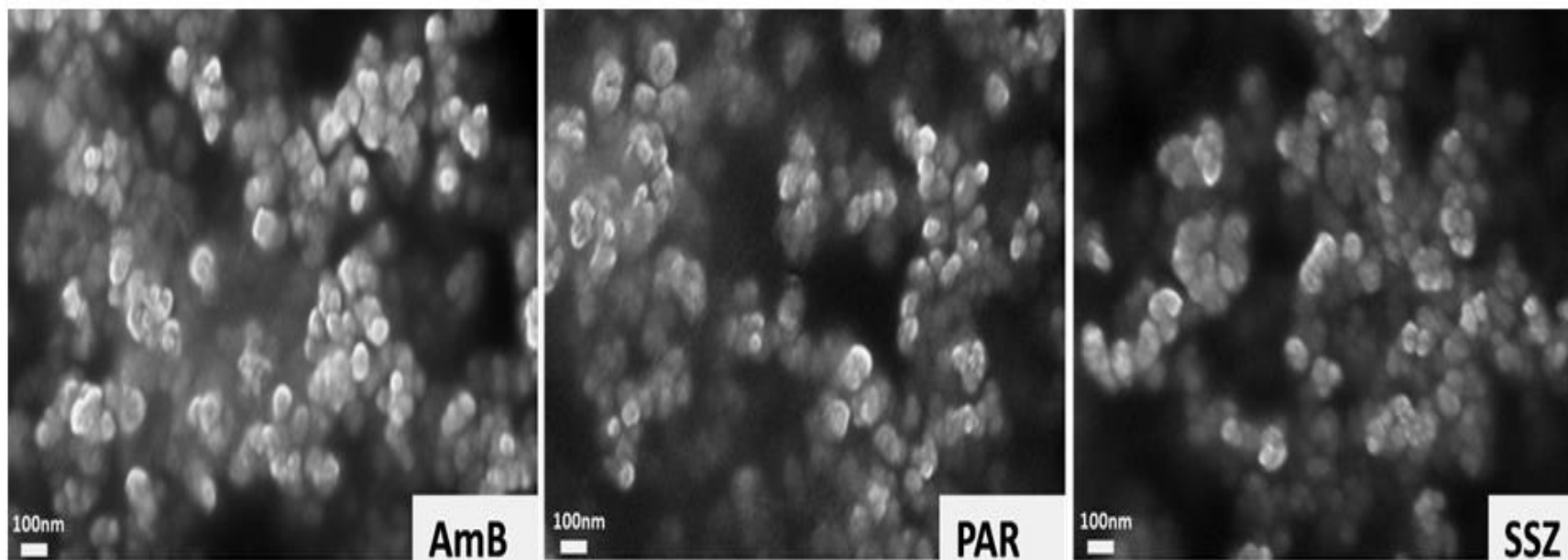


Figure 2.7 SEM images of the optimised SLNs

2.4.8 AFM studies

AFM analyses were done to further study the size, morphology and surface texture or roughness of the SLNs. Figures 2.8-2.10 show the phase, topographic and 3D images of the SLNs. The sample surface topographic and phase images for all three SLN formulations showed discrete particles, which were somewhat spherical in shape, and with sizes corroborating those obtained from the PCS and SEM analyses. The phase images showed that the SLNs have a homogenous appearance without a crystalline or rough appearance to suggest significant drug adsorption on the particle surfaces. The 3D images further reveal that the particles from all the formulations studied had somewhat smooth surfaces. Comparing the height of the particles (z-axis) with the width/diameter dimensions on the x- and y-axes, it was observed that the heights were below 50 nm with the diameters being up to about 200 nm. This indicates that the particles may be disc-like or platelet-like in shape or that they may have lost their sphericity during the sample preparation process however, non-spherical particles are seen in the topographic images as well. As with the particle sizes in the SEM images, it can be seen that the particle sizes obtained from the AFM analyses are smaller as compared with the z-average sizes obtained in the PCS analyses. This is because the SLN samples were air-dried prior to the analyses as was done for the SEM analyses, thereby removing any solvent layers, which contribute to the hydrodynamic particle diameters in PCS analyses. The disc-like shape and the difference between the diameter and height of the SLNs are in line with the findings of zur Mühlen *et al.* (1996) and Dubes *et al.* (2003). Dubes *et al.* (2003) also attributed smaller particle sizes from SEM analyses compared with PCS sizes to possible shrinking of particles during sample drying.

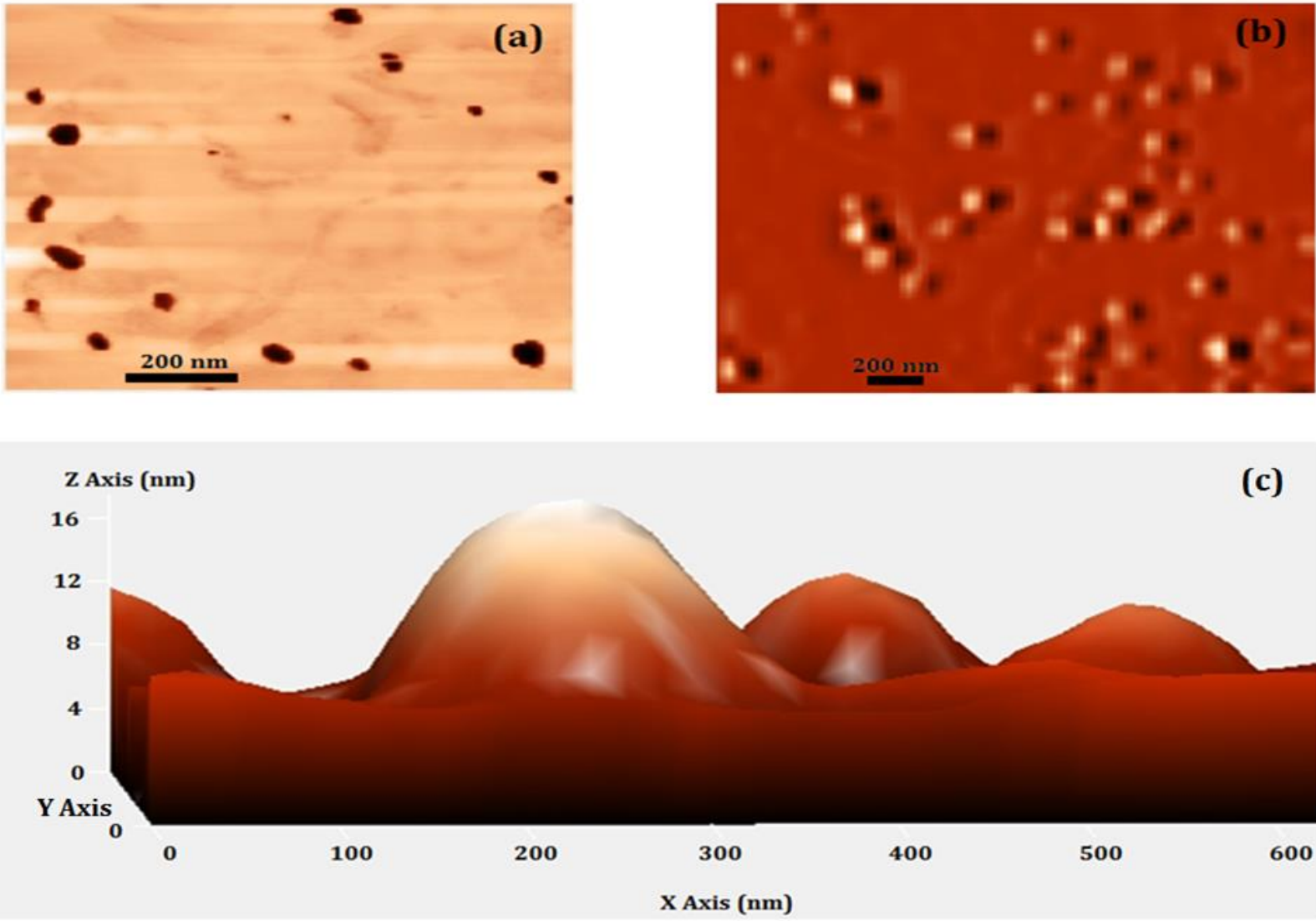


Figure 2.8 AFM (a) surface topographic (b) phase and (c) 3D images of AmB SLNs

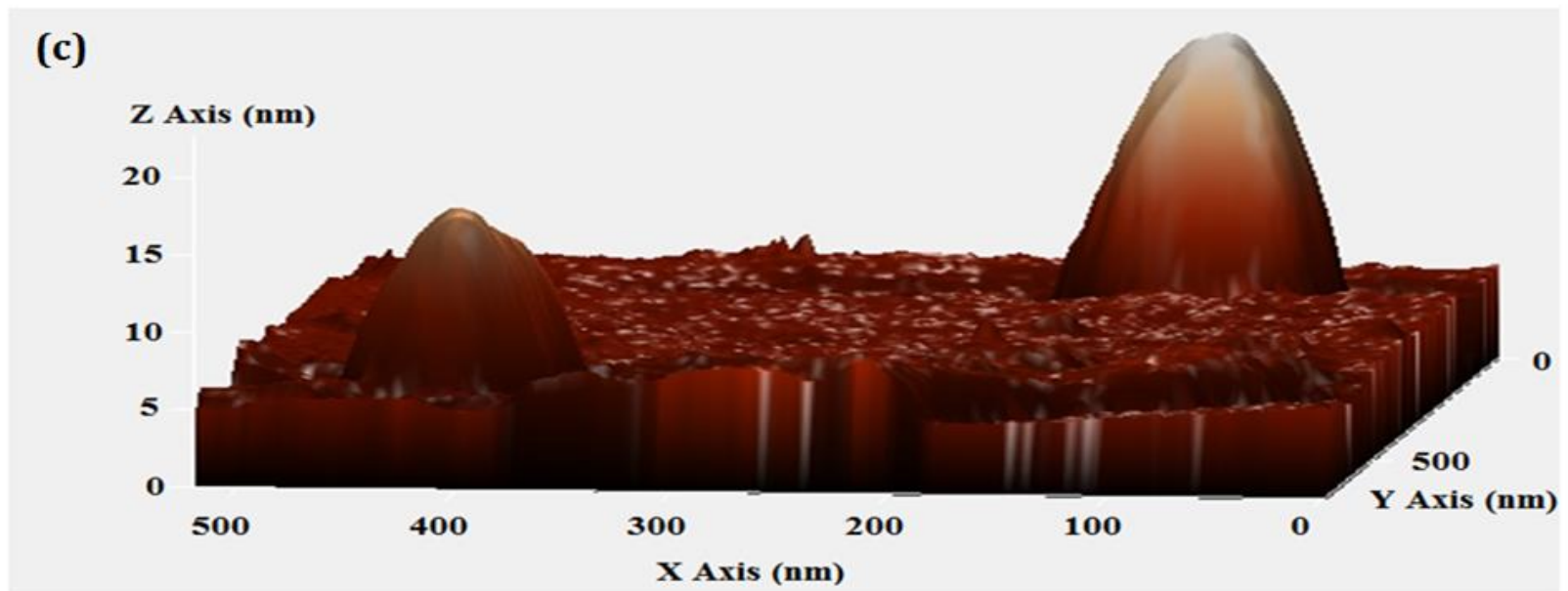
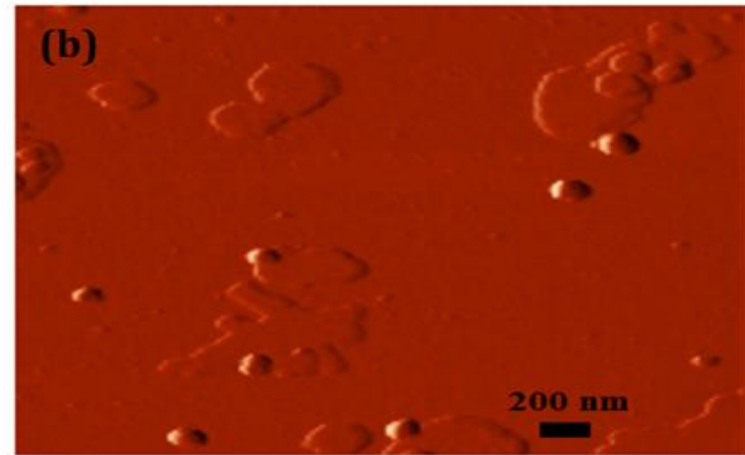
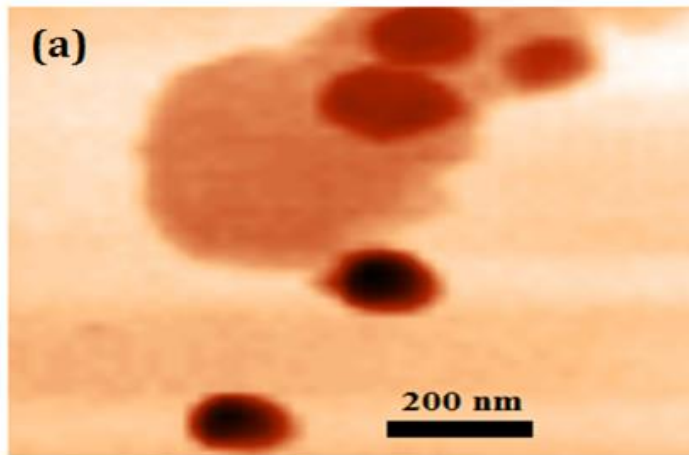


Figure 2.9 AFM (a) surface topographic (b) phase and (c) 3D images of PAR SLNs

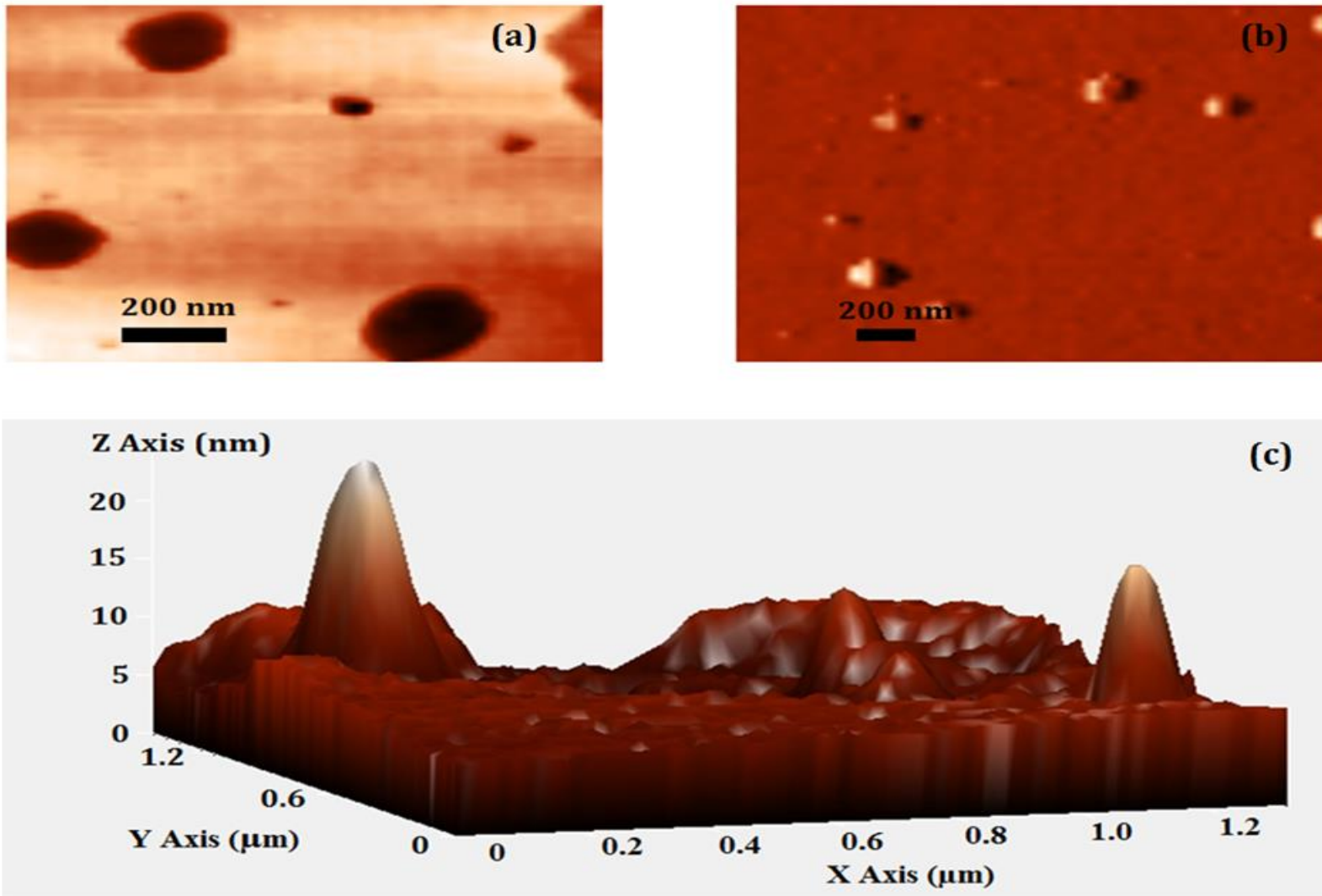


Figure 2.10 AFM (a) surface topographic (b) phase and (c) 3D images of SSZ SLNs

significant chemical interactions between the drugs and the excipients as characteristic drug peaks were still seen in the corresponding SLN spectra, indicating compatibility between the drugs and the excipients in the formulations.

Theobroma oil (TO) is an edible vegetable fat composed mainly of triglycerides of palmitic acid, stearic acid and oleic acid. TO has C-H and C=H stretching vibrations at approximately 719 and 1464 cm^{-1} ; and between 2800-3000 cm^{-1} , respectively. The O-C=O ester bond vibration found in triglycerides is also located 1177 and 1736 cm^{-1} [Goodacre and Anklam, 2001].

Beeswax (BW) is a wax formed from several compounds. Its main components are palmitate, palmitoleate and oleate esters of cerotic acid and long-chain (30-32 carbons) aliphatic alcohols such as triacontanyl alcohol. BW shows hydrocarbon vibrations at approximately 2918 and 1464 cm^{-1} . It has bands of esters (O-C=O) at about 1700 cm^{-1} and alcohols (O-H) at 1047 cm^{-1} . There have also been peaks detected at approximately 1338 cm^{-1} for amides and at 1219 and 728 cm^{-1} for amines [Zimnicka and Hacura, 2006].

Lecithin on the other hand is composed largely of phosphoric acid, choline, fatty acids, glycerol, glycolipids, triglycerides and phospholipids [Nzai and Proctor, 1998]. The phosphate stretches are evident at 1177, 1078 and 1047 cm^{-1} while the quaternary amine group is characterised by asymmetrical and symmetrical stretchings at 1046 and 1078 cm^{-1} , respectively. There is also a band between 1765-1720 cm^{-1} corresponding to a strong C=O stretching vibration in the phospholipid and a $(\text{CH}_3)_3\text{N}$ stretching band at 983 cm^{-1} .

Cholic acid is a bile acid. Sodium cholate shows characteristic bands for O-H stretching at about 3394 cm^{-1} and C-H vibrations at 2939 and 2863 cm^{-1} . There are also bands showing vibrations for

C-H in-plane bending, C=O and C-O-H at about 1403 cm^{-1} ; and C-C-O at 1082 cm^{-1} [Yang *et al.*, 2005].

It is evident from the above that a number of functional groups exist in the excipients in the SLN formulations. Some of the bands representing characteristic functional groups in the drugs were slightly shifted to lower or higher frequencies or showed differing band intensities or both, in their respective SLN spectrum. Other peaks also seem absent or merged with adjacent peaks to form larger bands. These are due to the many functional groups from both the drugs and excipients, resulting in the possibilities of merging of bands closely located in the spectra; as well as possible interactions between drug and lipid/excipients such as intermolecular hydrogen bonding.

Figure 2.12 shows the FTIR spectra for pure AmB and AmB SLN. The pure drug shows characteristic bands at 1692 , 1570 and 1010 cm^{-1} due to C=O stretch band and N-H₂ in-plane bend, polyene C=C stretch band, and C-H bend out-of-plane bend, respectively. The peak at 1040 cm^{-1} is also characteristic of the bending of N-H₂ out-of-plane and C-O-C symmetric stretching vibration due to the pyranose ring. The 1177 cm^{-1} band also represents a C-O-C asymmetric stretch for the β -glycosidic linkage. The C-H bend in the pyranose ring vibration is also represented by the 851 cm^{-1} peak. Comparing the spectra for AmB and AmB SLN, it can be seen that the majority of the aforementioned peaks are still present in the SLN except for the carbonyl-stretching band at 1692 cm^{-1} which seems to have merged with the peak at 1736 cm^{-1} in the SLN spectrum [Asher and Schwartzman, 1977; Nahar and Jain, 2009; AL-Quadeib *et al.*, 2015].

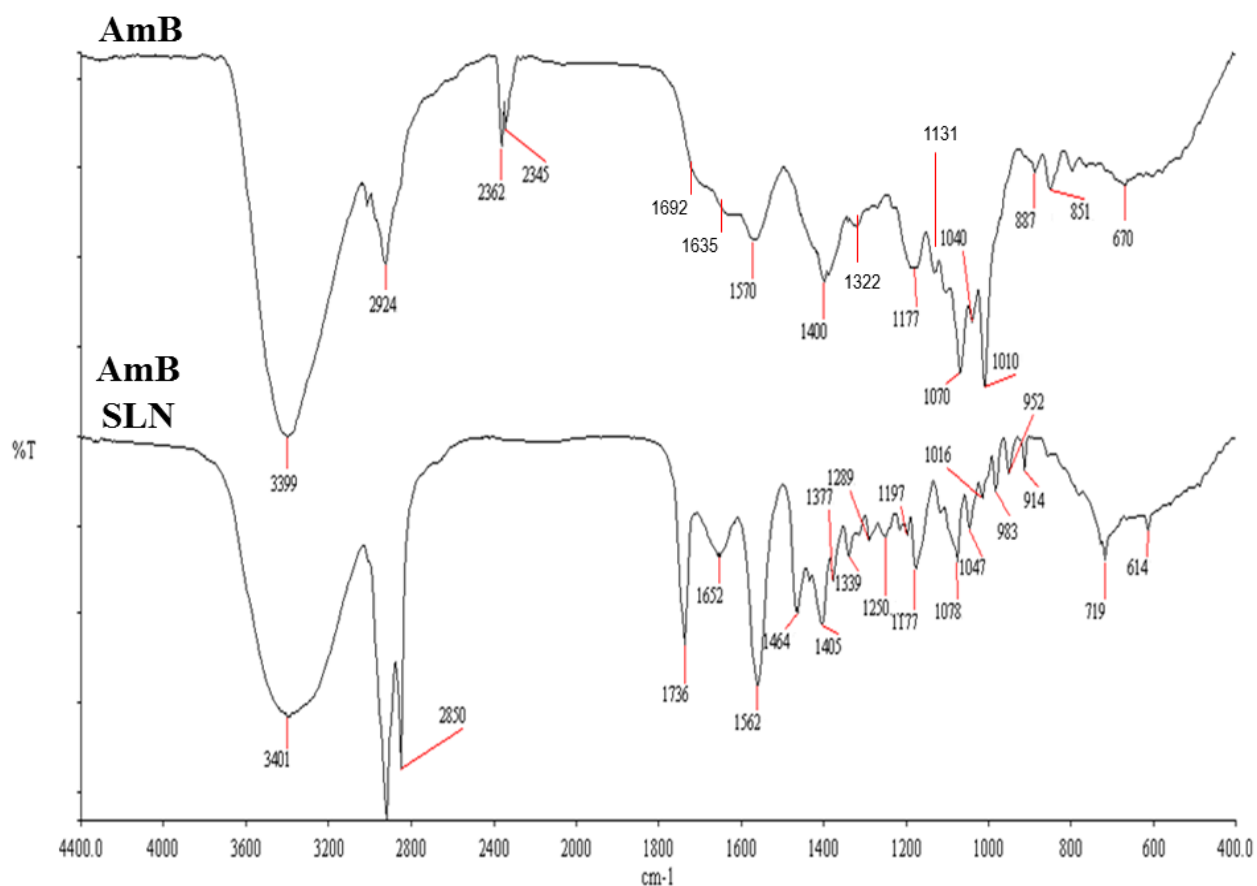


Figure 2.12 FTIR spectra for pure AmB and AmB SLN

Figure 2.13 shows FTIR spectra for PAR and PAR SLN. The main absorption bands for pure PAR are those at: 3326 cm^{-1} , which represents the N-H stretching vibration; 3162 cm^{-1} for the O-H group stretching vibration; 1655 cm^{-1} for the C=O group; 1564 cm^{-1} for the N-H in-plane bending; 1610 , 1506 and 1442 cm^{-1} for the aromatic ring; and 1327 cm^{-1} for O-H bending vibration [Wang *et al.*, 2002]. There is also a peak at 1260 cm^{-1} for the C-N stretching vibration. All these peaks are found present in the spectrum for PAR SLN except those at 3326 cm^{-1} and 3162 cm^{-1} . Instead, there is a single band at 3401 cm^{-1} in the SLN, which is characteristic of the O-H functional group

in PAR, BW and sodium cholate; and which also points to a possible intermolecular hydrogen bonding of the O-H group with the N-H group in PAR.

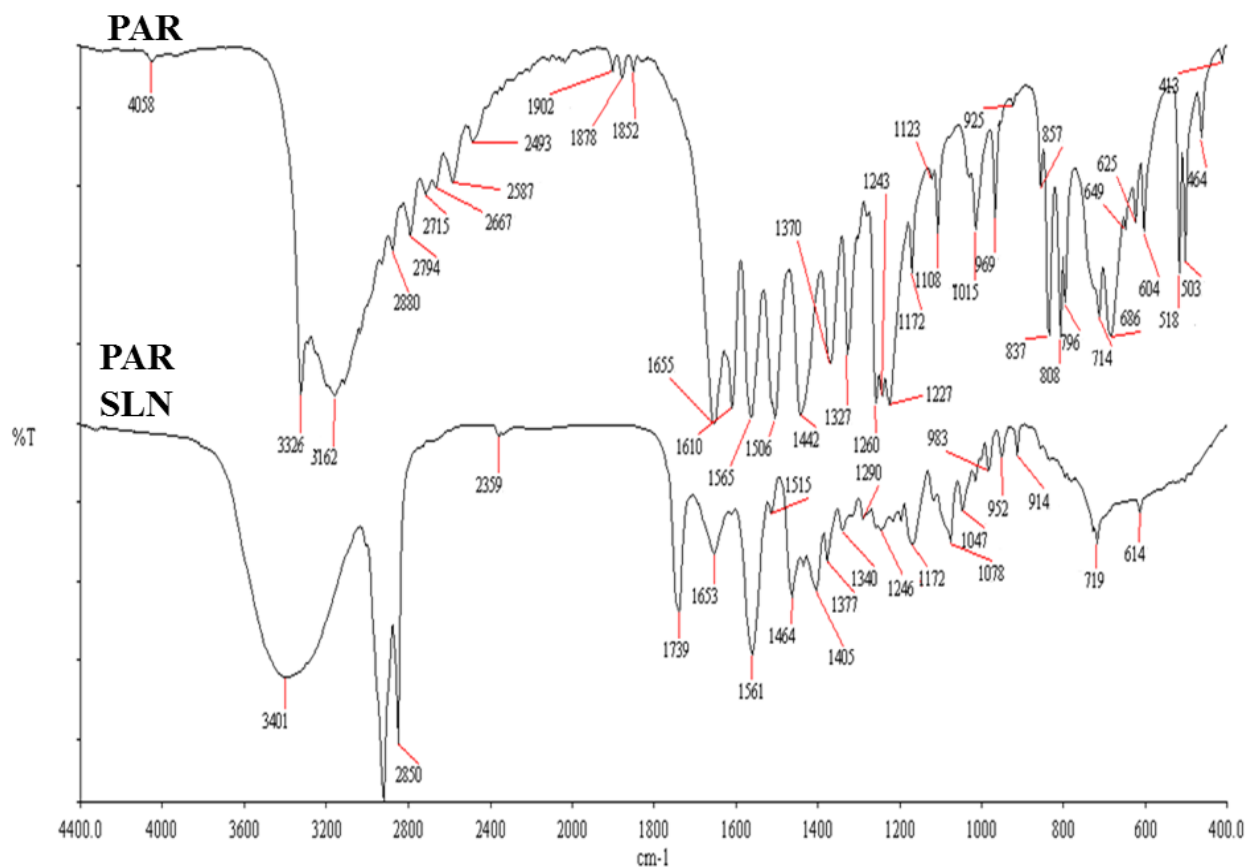


Figure 2.13 FTIR spectra for pure PAR and PAR SLNs

Figure 2.14 shows the FTIR spectra for pure SSZ and SSZ SLN. The spectrum for pure SSZ shows a medium broad band at 3438 cm⁻¹, which is attributed to the phenolic O-H and carboxylic O-H groups [Soliman *et al.*, 2005]. Other characteristic peaks are those at 1280, 1427 and 1618 cm⁻¹, representing the C=O bond in the phenolic group, and symmetric and asymmetric stretching vibrations of the carboxylate moiety, respectively.

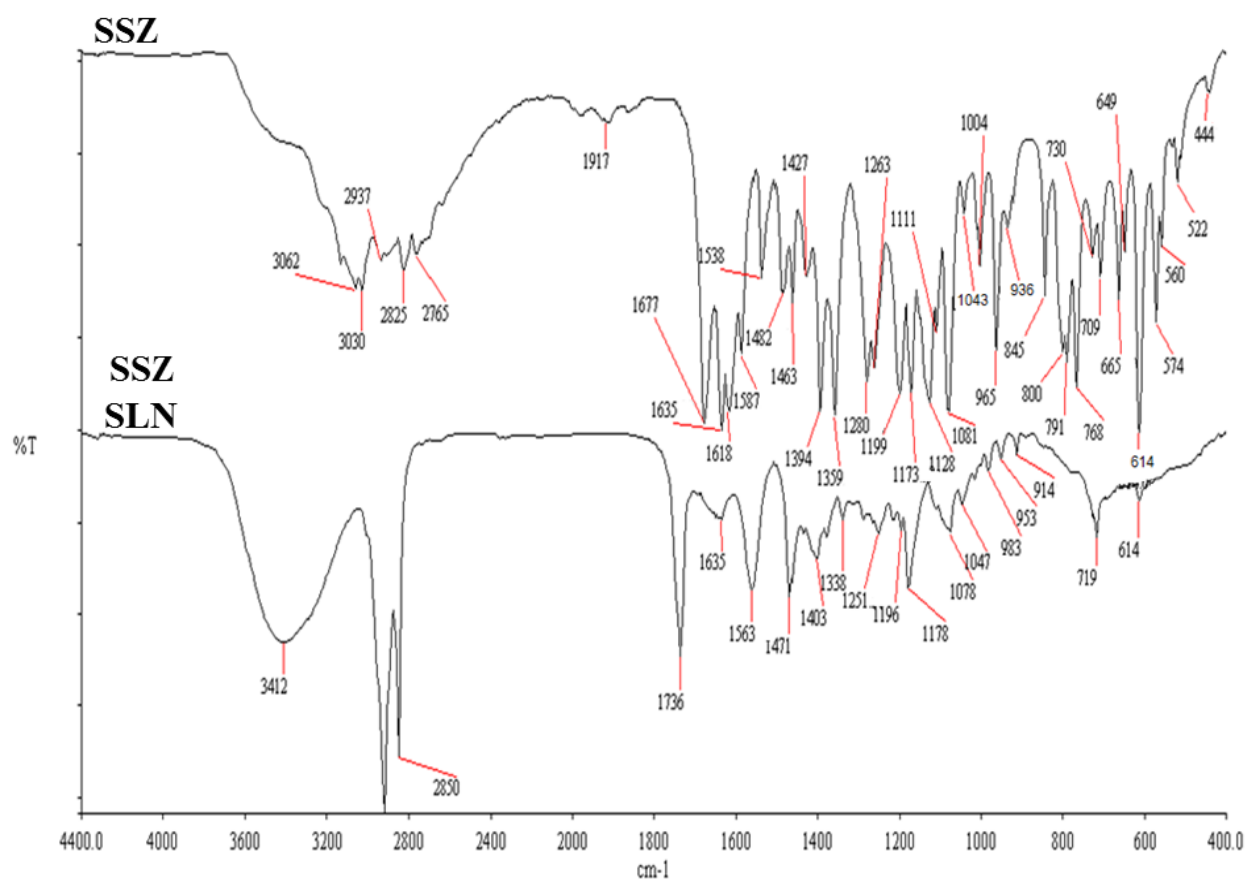


Figure 2.14 FTIR spectra for pure SSZ and SSZ SLNs

The peak located at 1587 cm^{-1} represents the stretching of the N=N group; while those at 1359 cm^{-1} and 1173 cm^{-1} represent asymmetric and symmetric stretching vibrations of the O=S=O group, respectively [Soliman *et al.*, 2005]. In-plane bending of O-H group occurs at 1394 cm^{-1} . The bands at 1618 and 1587 cm^{-1} assigned to the carbonyl and azo groups, respectively, are not apparent in the spectrum for the SSZ SLN, which is attributable to interactions with other functional groups in the formulation resulting in merged and broader bands shifted to 1635 and 1563 cm^{-1} , respectively. These two latter peaks are present at similar positions in the spectra for AmB SLN and PAR SLN as well so it cannot be established if a significant interaction had occurred between

SSZ and the excipients in the formulation. However, it could rather be explained that the two bands are largely due to functional group interactions in the excipients as neither peak points directly to a characteristic band in any of the excipients. Again, it can be observed that the peaks at 1635 and 1563 cm^{-1} are of higher intensities in the spectra for all three SLNs as compared with peaks at similar positions in the pure drugs, which further supports the preceding statement.

Figure 2.15 illustrates the FTIR spectra for the three SLNs only. The resemblance among the spectra is clearly seen, which is due to the same vibrations in the lipids and other excipients, as the SLNs were similarly formulated. The circled band in the spectrum for PAR SLN at 1515 cm^{-1} is the most visible peak clearly absent from the other spectra. The other main differences in the spectra are the shifts in frequencies and differences in shape and intensities of similar peaks, which clearly emphasise the effect of the different molecular vibrations in the three different drugs; and also the various interactions that may have occurred among the excipients or between the drugs and the excipients.

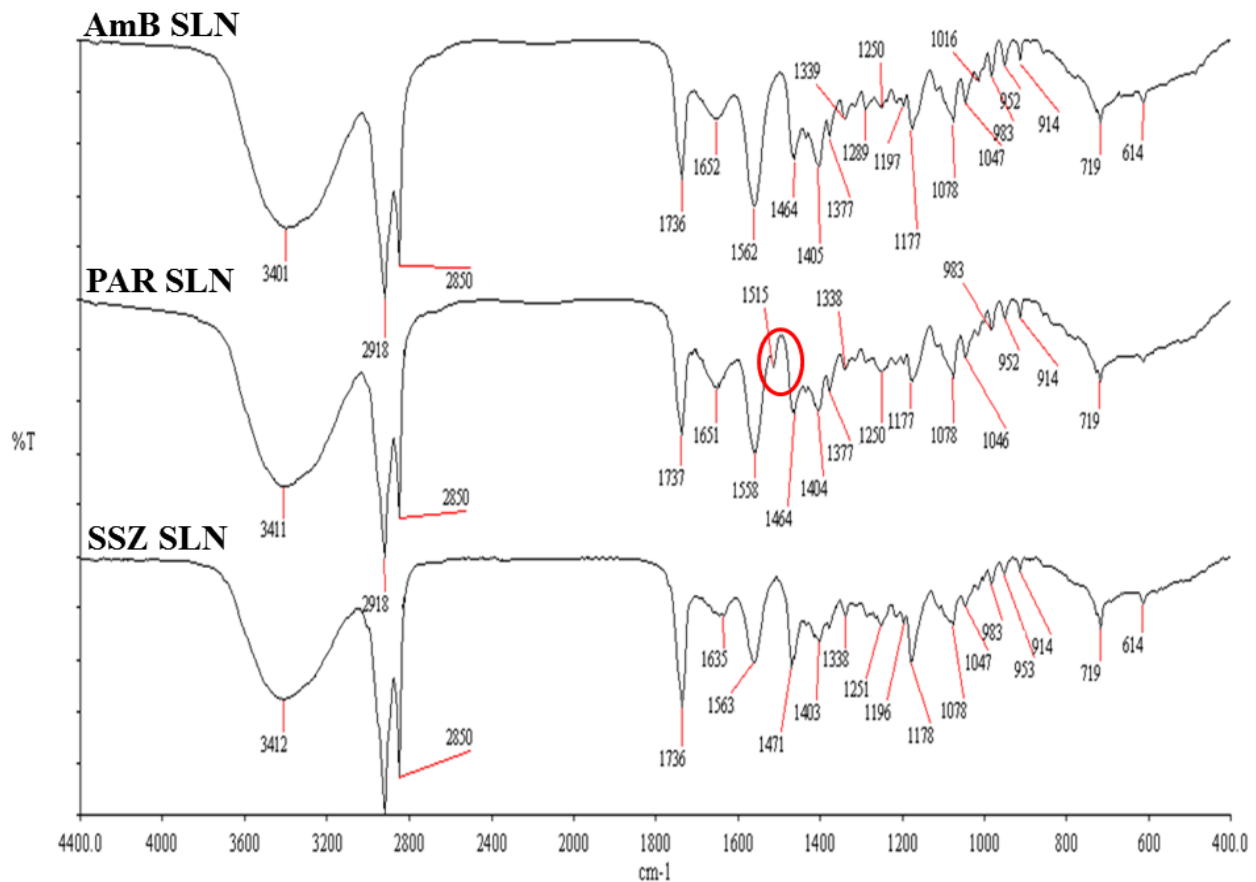


Figure 2.15 FTIR spectra for AmB SLNs, PAR SLNs and SSZ SLNs

[Circled band represents the most distinct peak in the PAR SLN, possibly due to the aromatic ring in PAR; and which is absent from the spectra for the AmB and SSZ SLNs]

2.4.10 DSC studies

DSC analyses were carried out in order to identify any interactions between the components of the SLN formulations, chiefly between the lipids and drugs, and to investigate the melting behaviour of the lipids. Figure 2.16 shows the DSC thermograms of the excipients (bulk lipids, lecithin soy and sodium cholate) overlaid on the thermograms of the various SLN formulations while Figure 2.17 shows thermograms of the pure drugs and the SLNs containing them.

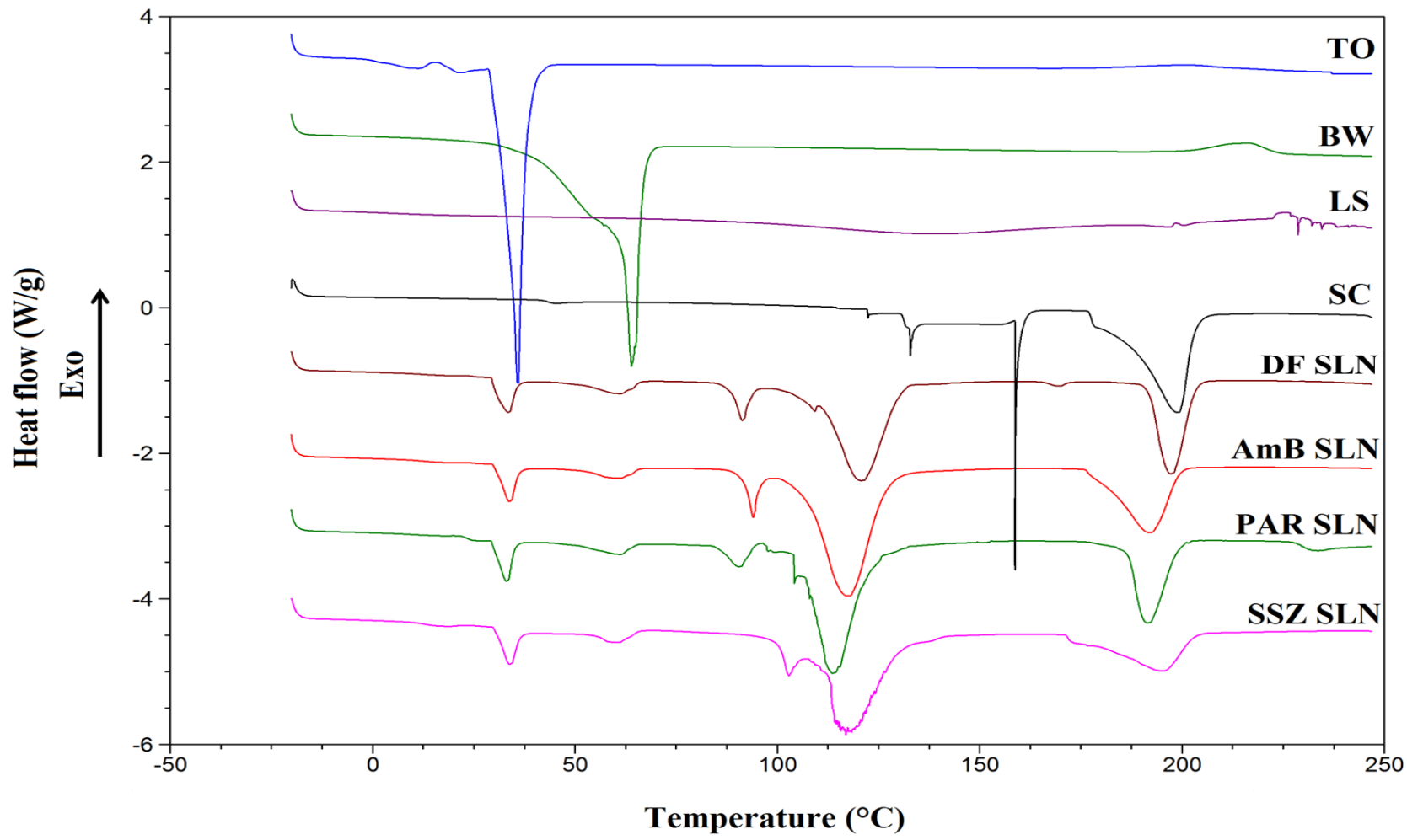


Figure 2.16 DSC thermograms of theobroma oil (TO), beeswax (BW), lecithin soy (LS), sodium cholate (SC), drug-free (DF) SLN and the drug-loaded SLNs

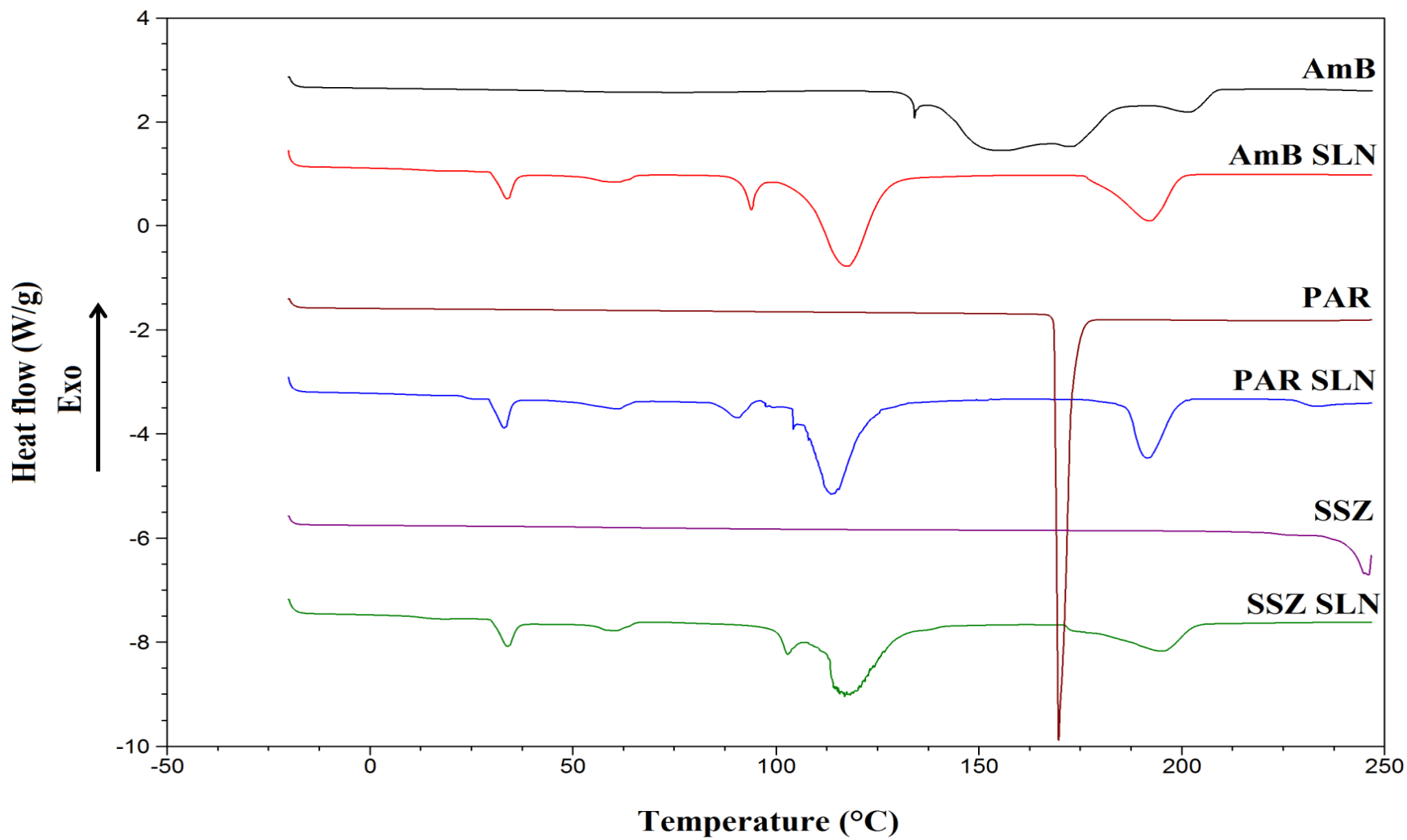


Figure 2.17 DSC thermograms of pure drugs and their respective SLN formulations

Table 2.4 also lists the melting temperatures and enthalpies of TO and BW in their bulk forms as well as within the SLNs.

Table 2.4 Melting peaks and enthalpies of TO and BW in the bulk lipids and the SLNs

Sample	TO		BW	
	Melting point (°C)	Melting enthalpy (J/g)	Melting point (°C)	Melting enthalpy (J/g)
Bulk lipid	35.1	156.1	63.3	176.7
Drug-free SLNs	33.1	13.32	61.8	3.47
AmB SLNs	33.1	5.95	61.5	3.76
PAR SLNs	32.9	8.55	61.9	4.07
SSZ SLNs	33.4	6.32	61.3	3.68

Overall, it can be seen that the melting peaks of TO and BW occurred at slightly lower temperatures (32.9-33.4°C for TO and 61.3-61.9°C for BW) in all the SLNs compared with that of their bulk counterparts (35.1°C for TO and 63.3°C for BW). It is also observed that the melting peaks corresponding to TO and BW in the SLN thermograms are broadened while those for the bulk lipids are sharper. These are largely due to the increased surface area resulting from the nanocrystalline size of the lipids in the SLNs as compared with the larger size and smaller surface

area of their bulk forms. The peak broadening is essentially due to the polydisperse nature of the particles, which causes different fractions to melt at slightly different temperatures [Westesen and Bunjes, 1995; Unruh *et al.*, 1999; Bunjes *et al.*, 2000]. It is clear from the results that the properties of the lipid cores in all the SLN formulations remained essentially the same as their bulk forms. This is because, any changes in the crystalline properties of the lipids after formulating the nanoparticles would have manifested as substantial changes in their melting temperatures; which would indicate that a polymorphic transformation has occurred.

Melting enthalpy is another indication of the crystal orderliness in lipids, aside melting point [Hou *et al.*, 2003]. Generally, substances in their less ordered crystal or amorphous state require less energy to melt as compared with their perfect crystalline forms, which need higher amounts of energy to overcome crystal lattice forces. The melting enthalpies of the bulk TO and BW were 156.1 and 176.7 J/g respectively; this suggests ordered lattice arrangements unlike in the SLNs in which they exist as their amorphous forms, resulting in lower melting enthalpies ranging 5.95-13.32 J/g and 3.47-4.07 J/g, respectively.

The melting peaks for the drugs: 153.7°C for AmB, 169.6°C for PAR and 245.9°C for SSZ, were absent from the thermograms of the respective SLNs containing them. This suggests that the drugs are dispersed in their amorphous forms within the SLNs and not in their crystalline states as in the bulk forms. This change in form occurred during preparation of the SLNs when the drugs were dissolved in the solvent-mix and the melted lipids, resulting in a homogenous distribution of the drugs in the latter. Again, the sodium cholate serving as surfactant keeps the drugs solubilised in the SLN structure; this prevents the drugs from crystallising out and keeps them in their amorphous states [Cavalli *et al.*, 1997; Cavalli *et al.*, 1999; Venkateswarlu and Manjunath, 2004]. These results are in line with other DSC studies in which drug peaks were absent from the respective

SLN thermograms but present when physical mixtures of the drugs and excipients were analysed [Yang and Zhu, 2002; Venkateswarlu and Manjunath, 2004; Reddy *et al.*, 2006; Zhang *et al.*, 2012; Yasir and Sara, 2014].

2.4.11 HPLC analyses

The amount of AmB, PAR and SSZ encapsulated within the respective SLNs as well as the amounts of each drug released from the particles during the *in vitro* studies were determined using HPLC, employing external standard calibration. A standard curve was constructed for each analyte from peak responses against known concentrations of standard solutions. The equations generated from the curves were then used in calculating unknown amounts of the respective analytes.

Identification and assignment of the peaks for the various analytes were done by repeatedly injecting standard solutions of the respective drug solutions under the same chromatographic conditions. In most HPLC analyses, quantitative calculations are done using peak areas; however, equivalent results can be achieved with peak heights for most cases [Crawford Scientific, 2015(a)]. The use of peak area is more suitable if there is peak tailing because the latter results in variations in peak heights while peak area values generally remain constant and are therefore more reproducible. Calculations using peak heights are usually preferred for trace analysis, in which the peaks of interest are very small owing to very low analyte concentrations [Lindholm, 2004; Crawford Scientific, 2015(a)]. In the present study, drug assays were conducted using peak areas. Figure 2.18 shows representative individual chromatograms obtained from separately injecting solutions of AmB, PAR and SSZ under the same chromatographic conditions.

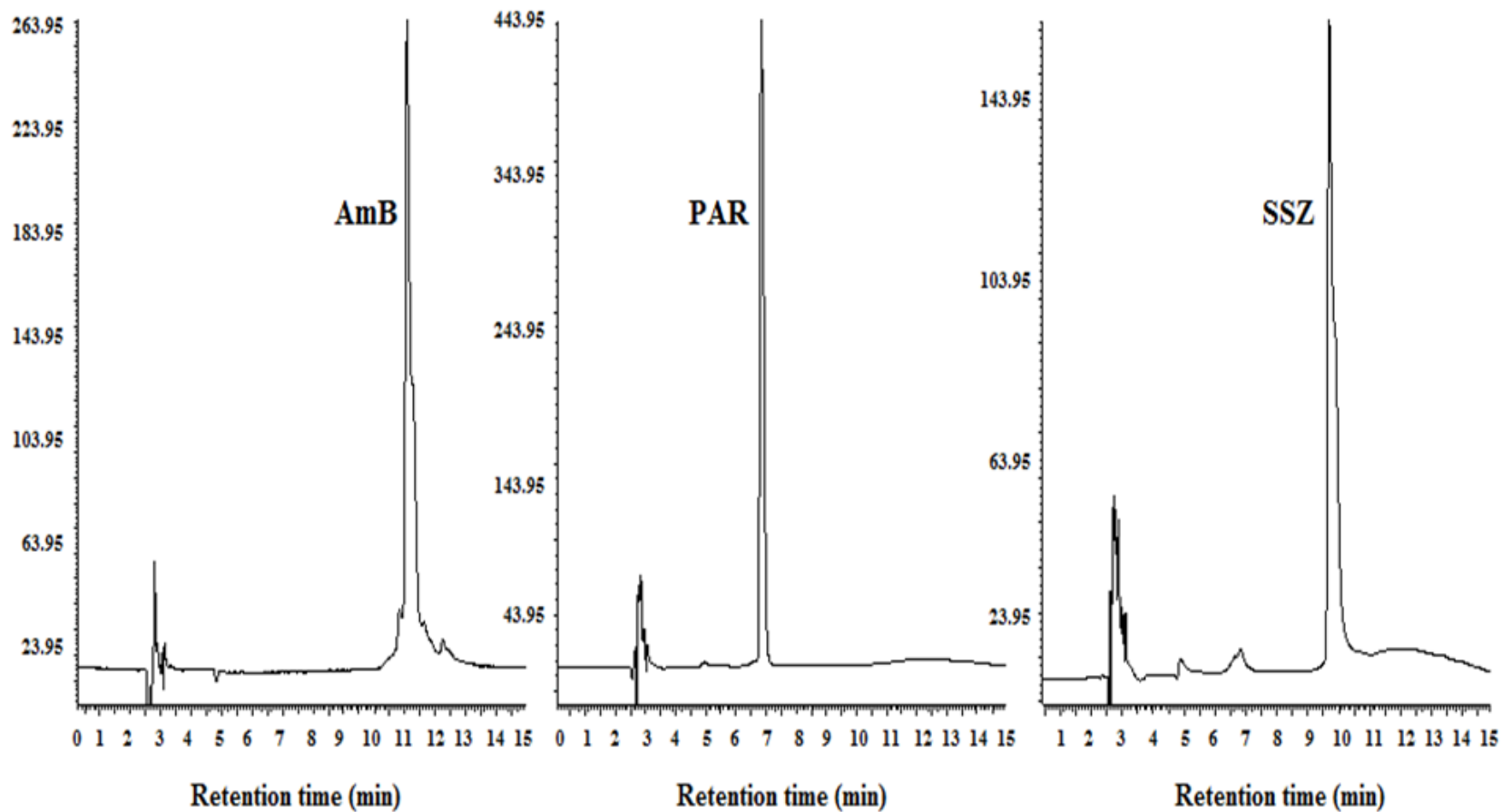


Figure 2.18 Representative chromatograms for AmB at 405 nm, and PAR and SSZ at 254 nm [50 µg/mL each in a pure solution]

It can be seen that all the peaks obtained are very well resolved without any interfering peaks. The retention times were obtained as 11 min for AmB at 405 nm; and as 6.6 min and 9.7 min for PAR and SSZ, respectively, at 254 nm. The calibration curves were found to be linear over the concentration range of 0.25-50 µg/mL for each drug (Figure 2.19). The coefficients of determination (R^2) were obtained to be 1, 1 and 0.9997, for AmB, PAR and SSZ, respectively, indicating very good linearity. The simple HPLC method and mobile phase system used can be applied in assaying AmB, PAR or SSZ in pharmaceutical formulations and the clear retention times of the analytes from each other also allows for their simultaneous assay.

There are several published data on the individual detection and assay of AmB, PAR and SSZ in various pharmaceutical dosage forms, chiefly for quality control and stability testing purposes. In an HPLC method for analysing SSZ, a retention time and run time of 14 min and 18 min, respectively, were obtained by Saini and Bansal (2014), which are both longer than those obtained in this study; 9.7 min and 15 min, respectively. Several HPLC studies on PAR [Chandra and Sharma, 2013; Chandra *et al.*, 2013; Gangishetty and Verma, 2013] and AmB [Wilkinson *et al.*, 1998; Eldem and Arican-Cellat, 2000; Balamuralikrishna and Syamasundar, 2010] as separate entities have produced shorter retention and run times than those obtained in the present work as only one compound was analysed in each case. In the current study however, a single HPLC method for analysing all three compounds is preferred for simplicity and rapidity in terms of instrumentation, mobile phase composition and other chromatographic conditions, as well as to make a simultaneous assay of the analytes possible since both PAR and SSZ were detected at the same wavelength of 254 nm.

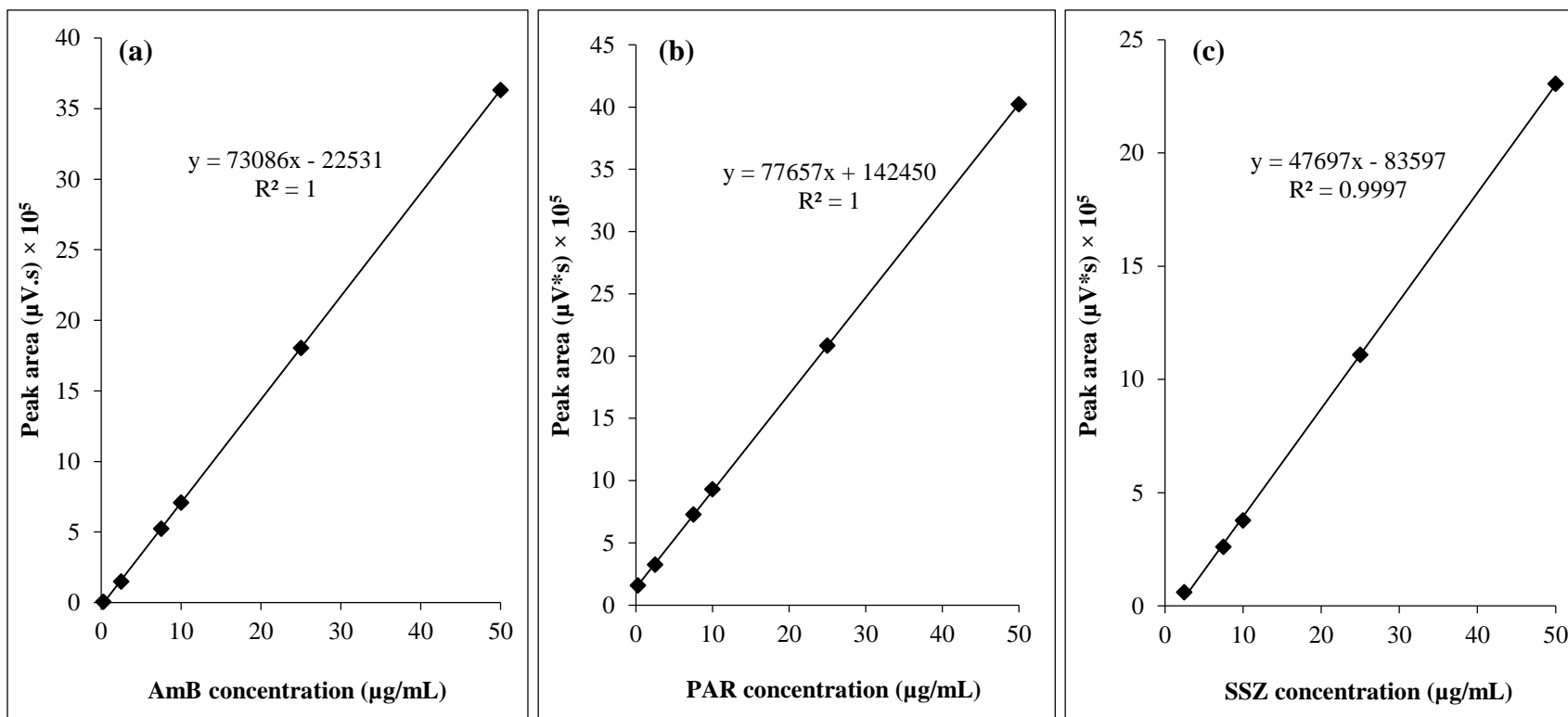


Figure 2.19 Standard calibration curves for pure solution of (a) AmB, (b) PAR and (c) SSZ

2.4.12 Encapsulation efficiency (%EE)

The %EEs of the freshly prepared AmB, PAR and SSZ SLNs were found to be $91.2\pm 3.04\%$, $60.7\pm 0.26\%$ and $78.4\pm 0.16\%$, respectively, and are illustrated in Figure 2.20. The higher encapsulation efficiency of AmB is attributable to its relatively high lipophilicity, being compatible with the lipid matrices. On the other hand, the %EE for PAR was the lowest and this can be linked to its hydrophilic nature. Nonetheless, the %EE for all three drugs were appreciably high and suggest that the emulsification solvent diffusion technique used in preparing the SLNs is suitable for encapsulating AmB and the marker drugs.

A search through literature does not reveal solid lipid nanoparticulate formulations of PAR or SSZ; due to the former's good oral bioavailability of about 70-90%, and the latter is partially although irregularly absorbed after oral administration [Moffat *et al.*, 2005]. AmB on the other hand is poorly absorbed orally; hence, there are various proposed formulations to help improve its absorption. Percentage encapsulation efficiencies of 34.5%, 50.6% and 75.9% have been achieved for AmB in poly (lactide-co-glycolide) [Italia *et al.*, 2009(a)], gelatin-coated [Jain *et al.*, 2012] and phospholipid-cholesterol [Jung *et al.*, 2009] nanoparticles, respectively. In the initial two studies, the drug loading in the formulations were 10% w/w and 6% w/w of the lipid/polymer weight, respectively. In the present study however, drug loading in each SLN formulation was 12.5% w/w of the total lipid used. Two SLN formulations of AmB have been prepared by Patel and Patravale (2011) (AmbiOnp) and Gupta *et al.* (2013) for which the drug loading and %EE were 12.5% w/w and 99.99%, and 1% w/w and 69.8%, respectively. The AmbiOnp formulation however had a PDI greater than 1 and required further treatments such as probe sonication and dialysis, to obtain smaller sized particles with a reduced PDI of 0.12. As a result, the whole procedure lasts longer

than 6 hr and is expensive. The AmB SLNs produced in this study however follows a simpler process and requires a shorter formulation time.

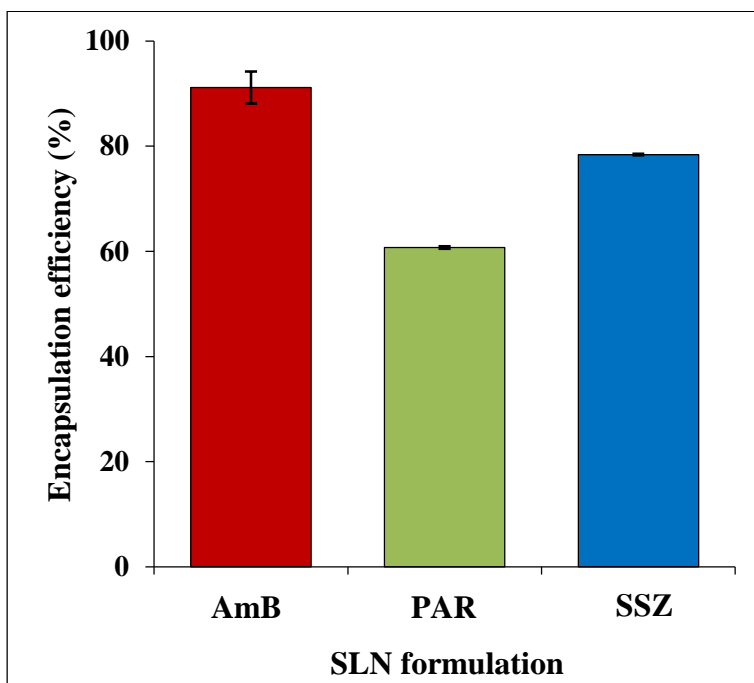


Figure 2.20 Encapsulation efficiencies of AmB, PAR and SSZ in their respective SLNs (n = 3)

2.4.13 Drug release studies

Cumulative drug release studies were conducted on both freshly prepared and freeze-dried SLNs and the results are illustrated in Figure 2.21. The data show that for the freshly prepared SLNs, only $11.80 \pm 0.4\%$ of AmB was released within the 8 hr study period, whereas the maximum amount of SSZ released was $31.40 \pm 1.95\%$. In contrast, $65.90 \pm 0.04\%$ of PAR was released within the study period.

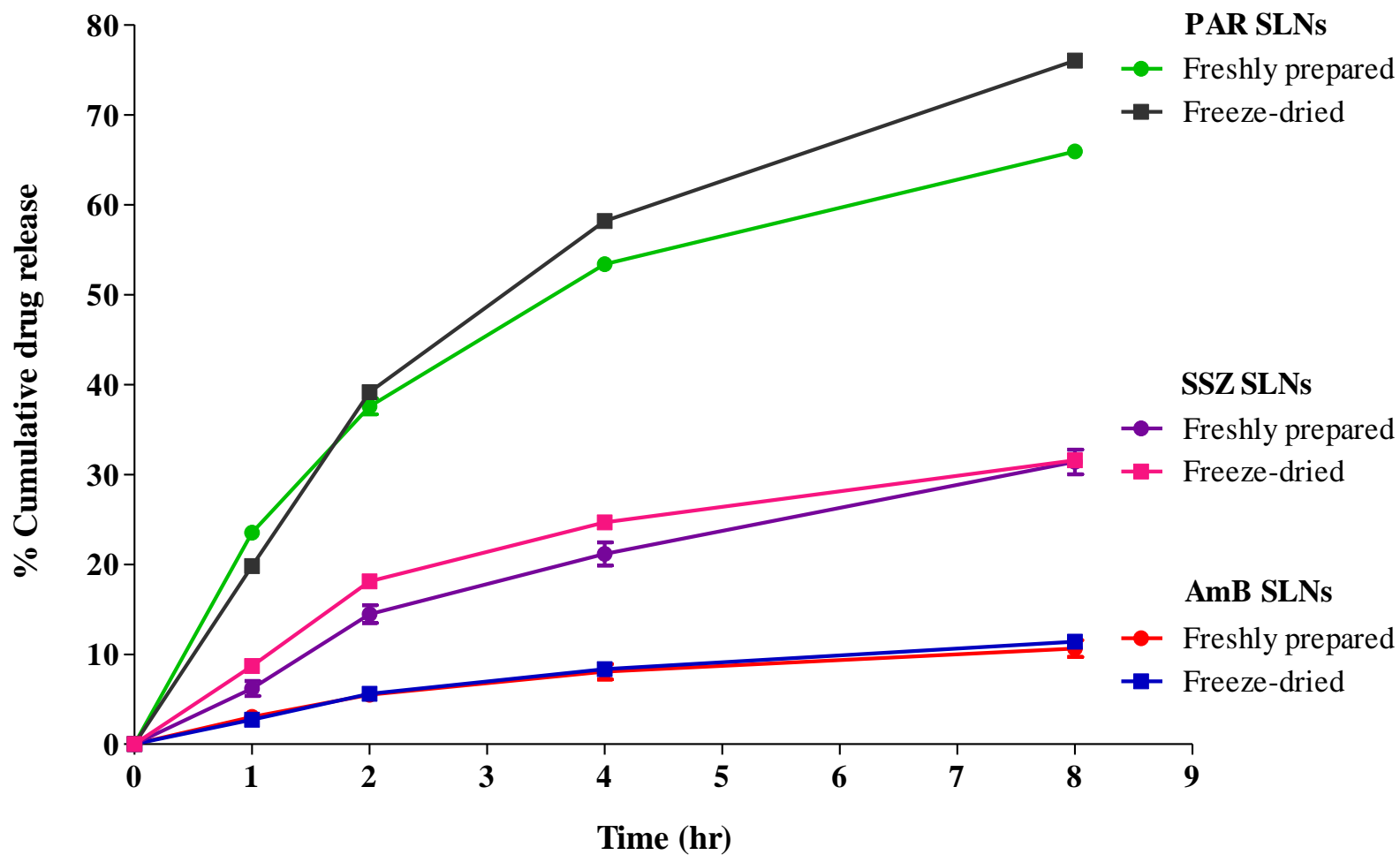


Figure 2.21 Cumulative release profiles of AmB, PAR and SSZ in PBS (pH 7.4) from their respective freshly prepared and freeze-dried SLNs

The percentage cumulative drug release from the freeze-dried AmB, PAR and SSZ SLNs were $11.4\pm 0.4\%$, $76.04\pm 0.21\%$ and $31.6\pm 0.33\%$, respectively. The differences in the amounts of drug released at the last time point, between each respective pair (fresh and freeze-dried SLNs) were not statistically significant (using *t*-test); 0.3894, 0.3351 and 0.0678 for AmB, PAR and SSZ, respectively. As such, whether as a fresh or freeze-dried formulation, drug release would remain essentially identical for all three SLNs.

The low drug release from AmB and SSZ SLNs relative to PAR SLNs are consistent with the biopharmaceutics classification system (BCS) for AmB and SSZ as class IV drugs, with low permeability and aqueous solubility. PAR has been assigned to either class I or III in several reports due to its high aqueous solubility and relatively good permeability. Essentially, both class I and III drugs have high aqueous solubility however, class I drugs have higher permeability. The implications of the *in vitro* release study is that, most of the PAR is likely to be released from the nanoparticles prior to absorption of the intact SLNs. On the other hand, there is likely to be a significant retention of AmB and SSZ within the SLNs prior to absorption in the GI tract; this is because of the higher $\log P$ values of AmB (1.16) and SSZ (2.67) relative to PAR (0.48). One of the significant advantages of SLNs is the fact that prolonged (slow) drug release is inherent because the particles are solid at room temperature hence, drug diffusion/mobility within the lipid matrix and then out of the particle is minimal [Reddy *et al.*, 2006]. Drug release is normally preceded by ingress of the dissolution medium into the carrier, followed by dissolution of the drug and then outward diffusion of the drug. In this context, the slow ingress of water into the lipid matrix becomes rate-limiting.

It is also likely that due to the slow release of AmB from the SLNs as observed in Figure 2.21, AmB is incorporated within the SLN as a drug-enriched matrix model. In this case, drug molecules must diffuse across a distance from within the lipid matrix to the outer shell, which further slows the drug release process. The slow *in vitro* drug release from the SLNs is therefore desirable because, a higher proportion of the drug is retained within the SLNs prior to uptake of the intact particles by M cells of the Peyer's patches and via the paracellular route. The drug-rich particles can also be digested and the drug incorporated into chylomicrons for uptake by the enterocytes. Since SLNs are reputed to be taken up principally by the Peyer's patches along the GI tract, a sustained drug release is desirable.

An extended drug release study was conducted on the respective pair of SLNs (freshly made and freeze-dried) up to 30 hr as depicted in Figure 2.22. In this study, the amount of drug released at each time point was assayed respectively hence, the plots are not cumulative. The release profiles of each of the three drugs from the pair of SLNs were identical as observed previously, albeit higher for the fresh formulation in each case. The statistical differences between drug release from freshly made and freeze-dried SLNs were mostly insignificant as the p values were > 0.05 at all the sampling points, except at the 2-hr time point for AmB where $p = 0.0468$, which although borderline, still indicates statistical significance.

In the case of AmB, there was a slight dip in release from the freeze-dried SLNs at 2 hr but thereafter, release remained essentially identical to the fresh sample until 30 hr. The release of PAR was largely sustained up until 8 hr after which there was a slight dipping. This dip in PAR release might signal some changes to the physical integrity of the SLNs after the freeze-drying process, so that the matrices are more tortuous. Tortuosity refers to the structure (such as curviness) of pores and channels in a matrix. High tortuosity will therefore impede diffusion of drug payloads

from such matrices. Substances that are soluble in the GI tract are sometimes used as channelling agents in waxy matrices so that, as they dissolve and leach into the GI fluids, tortuous capillaries are created to aid drug diffusion [Collett and Moreton, 2001]. Since PAR has good aqueous solubility, it could have acted as a channelling agent with its effect being higher in the freeze-dried formulation and hence, the observed drug release pattern. SSZ release from the SLNs followed a typical diffusion-limited profile, with a peak at 2 hr and a somewhat sustained trough thereafter. Comparing the profiles, it is noted that PAR being more hydrophilic than the other two drugs is expected to show increased drug release with time. Moreover, the pattern of AmB release is indicative of a gradually eroding matrix, which means that for an intact SLN, the path length followed via diffusion remains fairly constant.

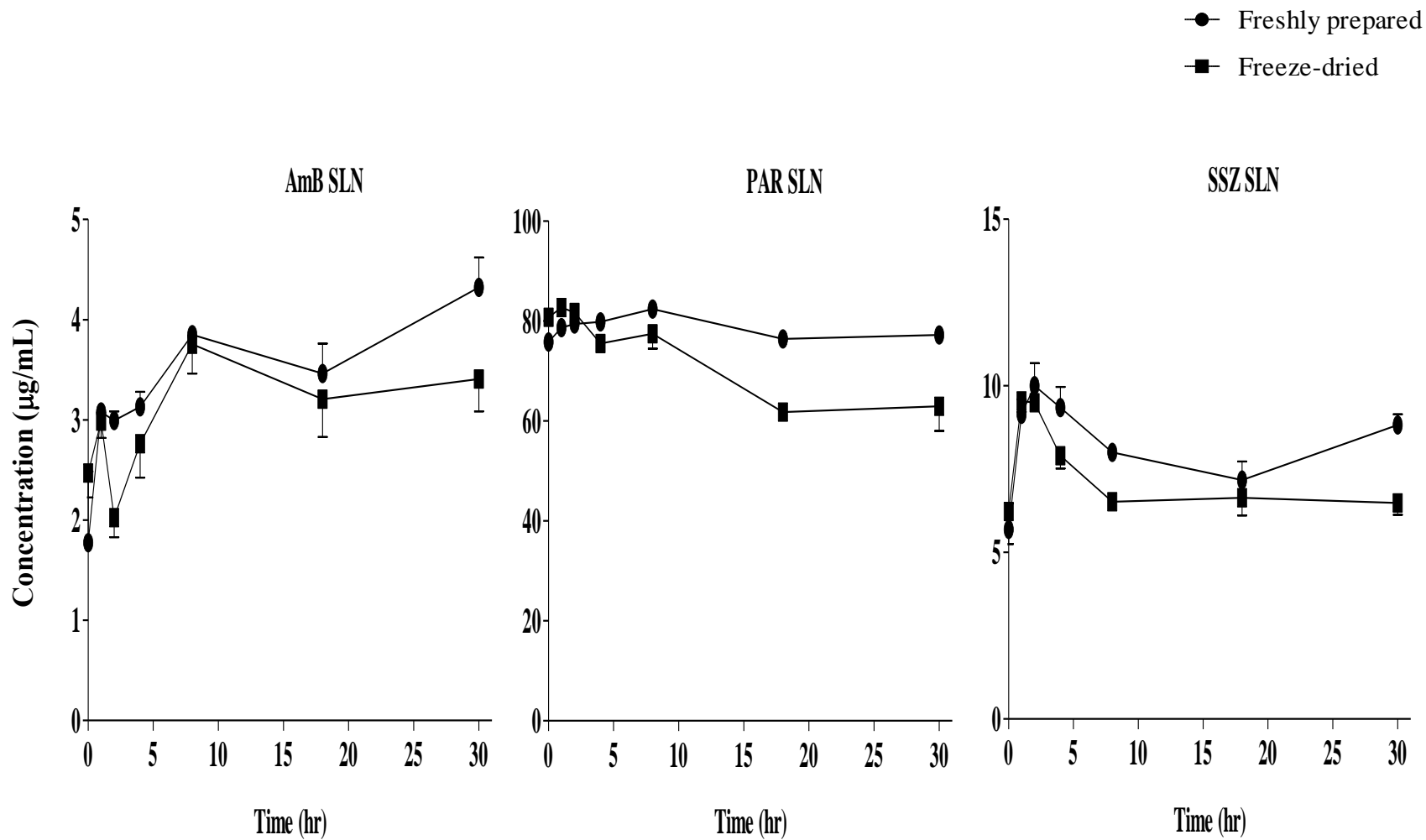


Figure 2.22 Drug release profiles of AmB, PAR and SSZ from their respective SLNs

2.4.13.1 Drug release kinetics

In order to shed more light on drug release from the lipid matrices, the kinetics of release from each SLN was investigated. Drug release refers to the process by which a drug solute migrates from an initial position in a delivery system to the outer surface and then into the surrounding release medium [Langer, 1990]. This may seem as a simple process however, it is affected by several complex factors such as the physicochemical properties of the drug, the structural characteristics of the delivery system, the release environment and possible interactions among these factors. Generally, solute diffusion as well as swelling and degradation of the delivery system are the main driving forces for solute transport from drug containing matrices [Langer, 1990; Artfin *et al.*, 2006].

The coefficient of determination (R^2) values obtained from the various equations generated using the release models are shown in Table 2.5. It can be seen that the values are highest for the Higuchi model for each formulation. Only the PAR freeze-dried sample gave an R^2 value for first-order release that was close to that for the Higuchi model albeit slightly higher for the latter; however, the model which best fits the release data by giving the highest R^2 value is selected. It could therefore be said that drug release from the SLNs followed the Higuchi model.

The mechanisms of drug release from dosage forms are conveniently used to categorise controlled release systems as diffusion-controlled, swelling-controlled or chemically-controlled [Siepmann and Peppas, 2011]. When the release data for a formulation fits well (very high R^2 value) with the Higuchi model, it indicates that drug release is diffusion-controlled [Higuchi, 1961].

According to the Higuchi model, the release of a solid drug from a matrix involves simultaneous penetration of the surrounding liquid, dissolution of the drug and leaching out of the drug through

interstitial channels or pores [Higuchi, 1961]. The model is based on several hypotheses. These include the following: initial drug concentration in the matrix is much higher than the drug's solubility, drug diffusion occurs only in one dimension and edge effect is negligible, drug particles are much smaller than the thickness of the carrier system, matrix swelling and dissolution are negligible, drug diffusivity is constant, and perfect sink conditions exists in the release environment.

Table 2.5 Nonlinear fits of AmB, PAR and SSZ released from the respective SLNs

SLN formulation	R ²				n value
	First order	Higuchi	Hixson- Crowell	Korsmeyer-Peppas	
AmB fresh	0.8997	0.9889	0.8964	0.9704	0.5960*
AmB freeze-dried	0.9206	0.9826	0.9174	0.9606	0.6740*
PAR fresh	0.9360	0.9858	0.9077	0.9728	0.4963
PAR freeze-dried	0.9820	0.9825	0.9592	0.957	0.6392
SSZ fresh	0.9631	0.9743	0.9559	0.9563	0.7565*
SSZ freeze-dried	0.8932	0.9765	0.8821	0.9297	0.6035*

* - data not applicable as drug release < 60% during the study period

Venkateswarlu and Manjunath (2004), Kushwaha *et al.* (2013), and Yasir and Sara (2014) also found the *in vitro* release of clozapine, raloxifene and haloperidol, respectively, from their SLNs to follow Higuchian release kinetics.

The value of n from the Korsmeyer-Peppas equation characterises the drug transport/release mechanism in the following manner: $n = 0.43$ signifies Fickian (case I) diffusion, $0.43 < n < 0.85$ signifies anomalous (non-Fickian) diffusion, $n = 0.85$ means a case II transport, and $n > 0.85$ indicates a super case-II transport. Fick's laws of diffusion postulate that a drug solute will move from a region of high concentration to a region of low concentration across a concentration gradient; and the change in concentration with time in a particular region is proportional to the change in concentration gradient at that point.

The value of n is however valid only when applied to the initial 60% of drug release, which makes it useful only for the release data obtained for the PAR SLNs. The n values for fresh and freeze-dried PAR SLNs were found to be 0.4963 and 0.6392, respectively, both of which designate non-Fickian diffusion.

In Fickian diffusion, drug release is diffusion-controlled whereas in case II, release is controlled by relaxation of the matrix. Anomalous diffusion behaviour is intermediate between Fickian and case II, in which the rates of drug diffusion and relaxation of the matrix are comparable, which indicate that drug release from the PAR SLNs were controlled by both mechanisms. In the present study, relaxation relates to possible changes in the volume-to-surface ratio of the lipid matrix of the SLNs due to permeability of the matrices to the release medium [Langer, 1990; Artifin *et al.*, 2006].

2.4.14 Stability of the SLNs after freeze-drying and storage

2.4.14.1 Freeze-drying of the SLNs

A study by zur Mühlen (1996) indicated that SLN formulations may be generally stable from 12 to 36 months however, various factors such as initial processing parameters, handling and storage may cause increase in particle size over a short period of time if not optimised. Freeze-drying is one way to improve the physical and chemical stabilities of SLNs. Freeze-drying also makes the incorporation of SLNs into solid dosage forms possible however, both the freezing and drying steps exert mechanical stresses on the particles and reduce the protective effects of surfactants. Cryoprotectants are therefore usually added to SLN dispersions at concentrations of 10-15% (of the total formulation) prior to freeze-drying to reduce the chances of particle aggregation as well as to ease redispersion of the freeze-dried product. Cryoprotectants prevent particle aggregation by preventing direct contact between adjacent lipid particles and by interacting with the polar groups of surfactants to act as a pseudo-hydration shell [Mobley and Schreier, 1994]. Cryoprotectants are usually sugars or polymers but the commonly used ones are mannitol, sorbitol, trehalose, glucose and polyvinylpyrrolidone. Trehalose has been described as the most efficient cryoprotectant for SLN formulations [Cavalli *et al.*, 1997; Schwarz and Mehnert, 1997; Heiati *et al.*, 1998; Mehnert and Mäder, 2001] and was used at a concentration of 10% in the present study.

The AmB, PAR and SSZ SLNs were freeze-dried without trehalose prior to the FTIR and DSC analyses in Section 2.3.4. *In vitro* release studies were conducted on the freeze-dried SLN samples in order to assess possible differences in drug release from freshly prepared SLN suspensions and the freeze-dried ones. Figure 2.23 shows images of the freeze-dried SLN powders. All three SLN

formulations produced fluffy powders, which tended to stick onto surfaces such as weighing paper, so they required very careful and swift handling during weighing and transfer into containers.

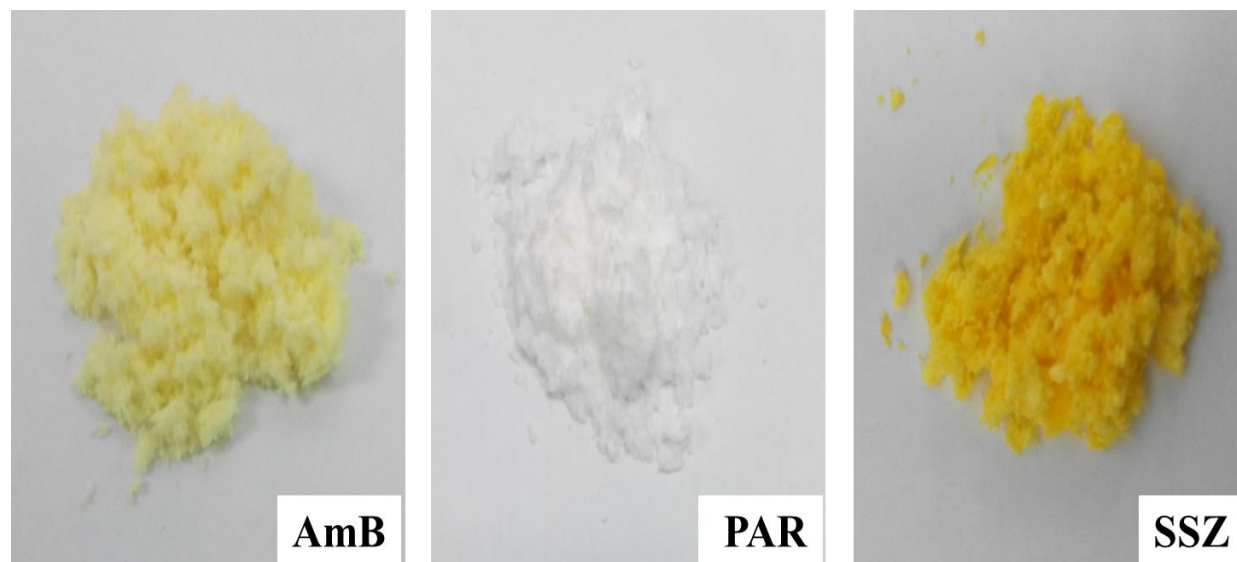


Figure 2.23 Images of the freeze-dried SLNs

Figure 2.24 illustrates the size distribution of the freeze-dried nanoparticles. It can be seen that only the AmB SLNs showed a more unimodal distribution. PAR and SSZ SLNs showed mostly bimodal size distribution profiles. The z-average diameters and PDIs for AmB, PAR and SSZ SLNs were 265.0 ± 40.7 nm and 0.40 ± 0.13 , 333.6 ± 56.8 nm and 0.53 ± 0.06 , and 283.6 ± 63.5 nm and 0.56 ± 0.10 , respectively. This shows that the freeze-drying procedure did not significantly alter the size of the nanoparticles. In general, the z-average values remained below 340 nm. Only the freeze-dried PAR SLNs showed more than a 100 nm increase in mean particle size, which could be due to the presence of the aggregates seen in its SEM image in Figure 2.25.

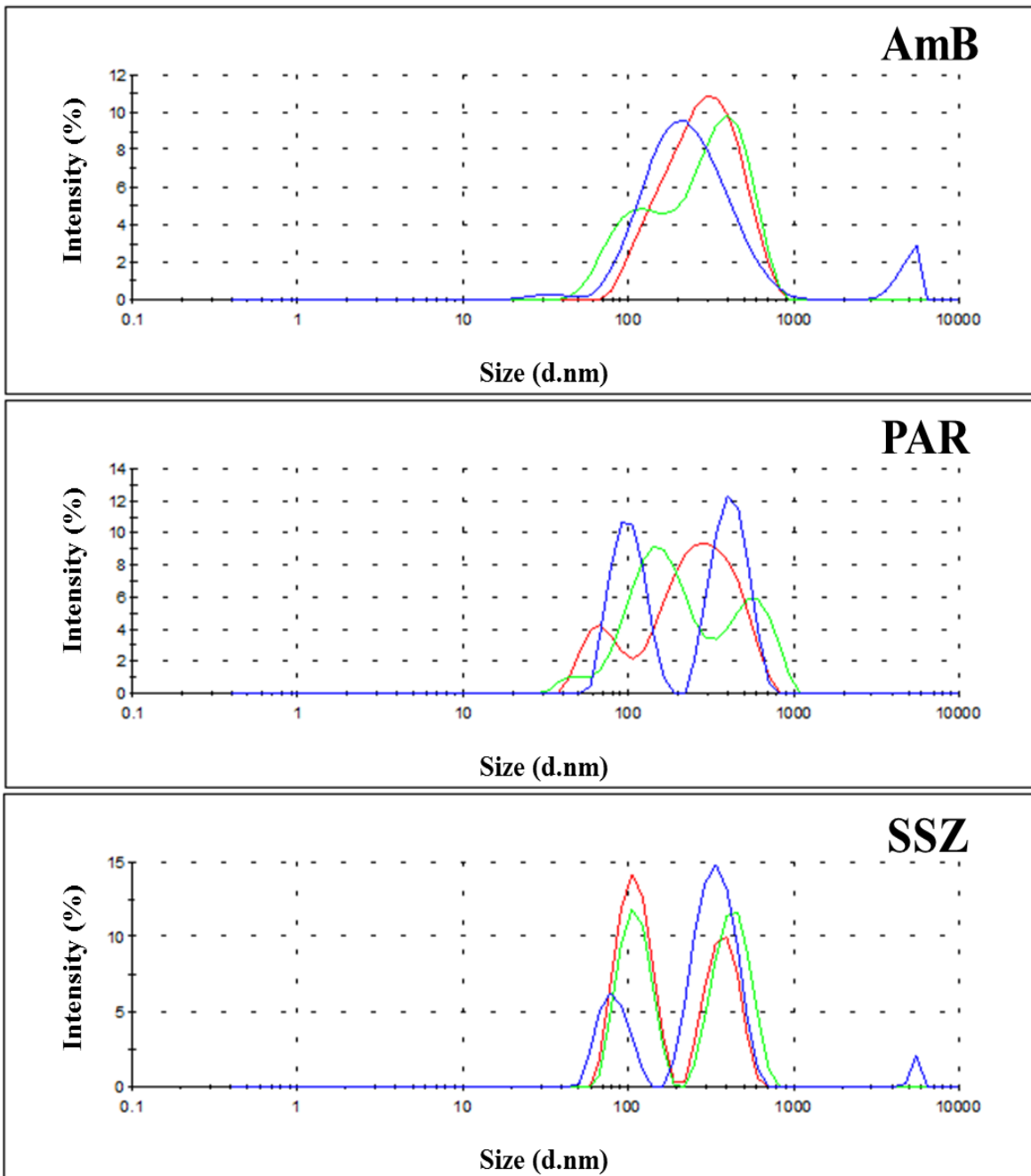


Figure 2.24 Particle size distribution by intensity of the freeze-dried SLNs (n = 3)

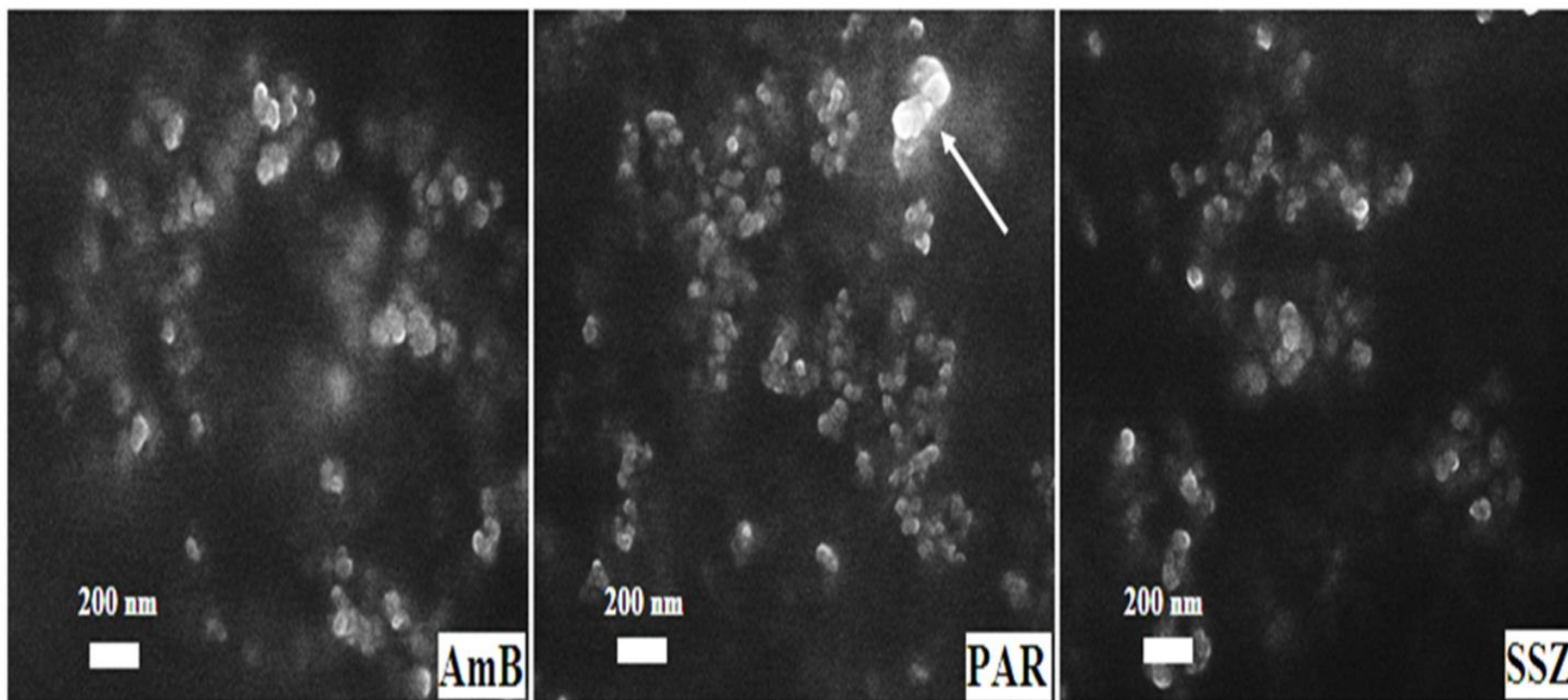


Figure 2.25 SEM images of the freeze-dried SLNs
[The arrow points to a large aggregate of the PAR SLNs]

The ZP values were obtained as -66.8 ± 2 mV, -70.8 ± 11.0 mV and -61.5 ± 13.0 mV for AmB, PAR and SSZ SLNs, respectively, indicating good colloidal stability [Riddick, 1968], and not differing much from the values obtained for the fresh samples. Figure 2.25 shows the SEM images of the freeze-dried SLNs in which the particles appear similar in outlook with those of the freshly prepared SLNs (Figure 2.7) except for some few aggregates in the former.

Polymorphic modifications of lipids may result from sample dehydration, as occurs in freeze-drying [Svilenov and Tzachev, 2013]. These can cause changes in particle shape and conformation with various consequences such as particle growth, since surfactant molecules can no longer offer sufficient coverage to newer surfaces formed; and changes in drug incorporation and release rates. These may have further effects on bioavailability and obvious changes in the aesthetic appearance of the formulation [Reddy *et al.*, 2006]. The results from the DSC experiments (Section 2.4.10), which were conducted on freeze-dried formulations indicated that the melting temperatures of the lipids in their bulk forms as well as within the SLNs remained relatively unchanged. The maximum difference in melting point observed was 2.2°C for TO in the PAR SLNs. This is a good indication that no polymorphic changes had occurred during the freeze-drying process, pointing to the stability of the dispersions.

2.4.14.2 Storage temperature and light conditions

Storage temperature can affect the stability of SLNs as well as drug formulations in general. Drug-loaded SLNs have been found to be more stable when stored at low temperatures such as refrigerated or room temperatures ($15\text{-}25^{\circ}\text{C}$). Storage at much higher or lower temperatures is associated with instabilities such as increase in particle size and PDI due to particle aggregation,

lipid modifications and high drug expulsion rates [Reddy *et al.*, 2006; Harde *et al.*, 2011; Kakkar *et al.*, 2011]. Again, it is important to store SLNs at temperatures lower than the melting point of the lipid to ensure that the latter remains in solid state to keep the drug encapsulated. Refrigerated temperature (4-8°C) was therefore selected as the storage temperature for both freshly prepared and freeze-dried AmB, PAR and SSZ SLNs; also because the freeze-dried SLNs were found to stick together and to their containing vessels when kept at room temperature, causing difficulty in handling.

Figure 2.26 shows the particle size distribution profiles of the three SLNs after storage at refrigerated temperature for 24 months. It can be seen that the profiles are similar with those obtained for the freshly prepared SLNs (Figure 2.6). The z-average diameters and PDIs for AmB, PAR and SSZ SLNs were obtained as 262.0 ± 3.5 nm and 0.20 ± 0.03 , 307.7 ± 2.7 nm and 0.25 ± 0.02 , and 256.6 ± 2.9 nm and 0.27 ± 0.03 , respectively. The ZP values obtained were -63.7 ± 5.4 mV, -67.8 ± 0.8 mV and -68.3 ± 0.9 mV for AmB, PAR and SSZ SLNs, respectively. It is apparent that these agree very much with the PCS data obtained for the freshly prepared SLNs as presented in Section 2.4.6. Since the particle sizes and ZPs of the AmB, PAR and SSZ SLNs remained relatively same after storage, it can be said that storage of the AmB, PAR and SSZ SLNs in the refrigerator was appropriate and maintained the stability of the SLNs.

The particle aggregation due to storing SLN dispersions at relatively high temperatures is attributed to increased particle kinetic energy from the input energy, which favours particle collisions and the resultant aggregation. Increasing temperatures may also cause changes in the protective film properties of surfactants on particles and result in particle aggregation [Reddy *et al.*, 2006]. At the storage temperature of the SLNs (4-8°C), it can be said that the particles were not energetic enough to undergo rapid Brownian motion to result in aggregation induced by

particle collisions. Again, with the melting points of TO and BW which form the protective solid lipid cores of the particles being at about 33°C and 61°C, respectively, for all three SLNs according to Table 2.4, it is convincing that the nanoparticles would be remain solid to keep the drugs encapsulated within the lipid matrices during refrigerated storage.

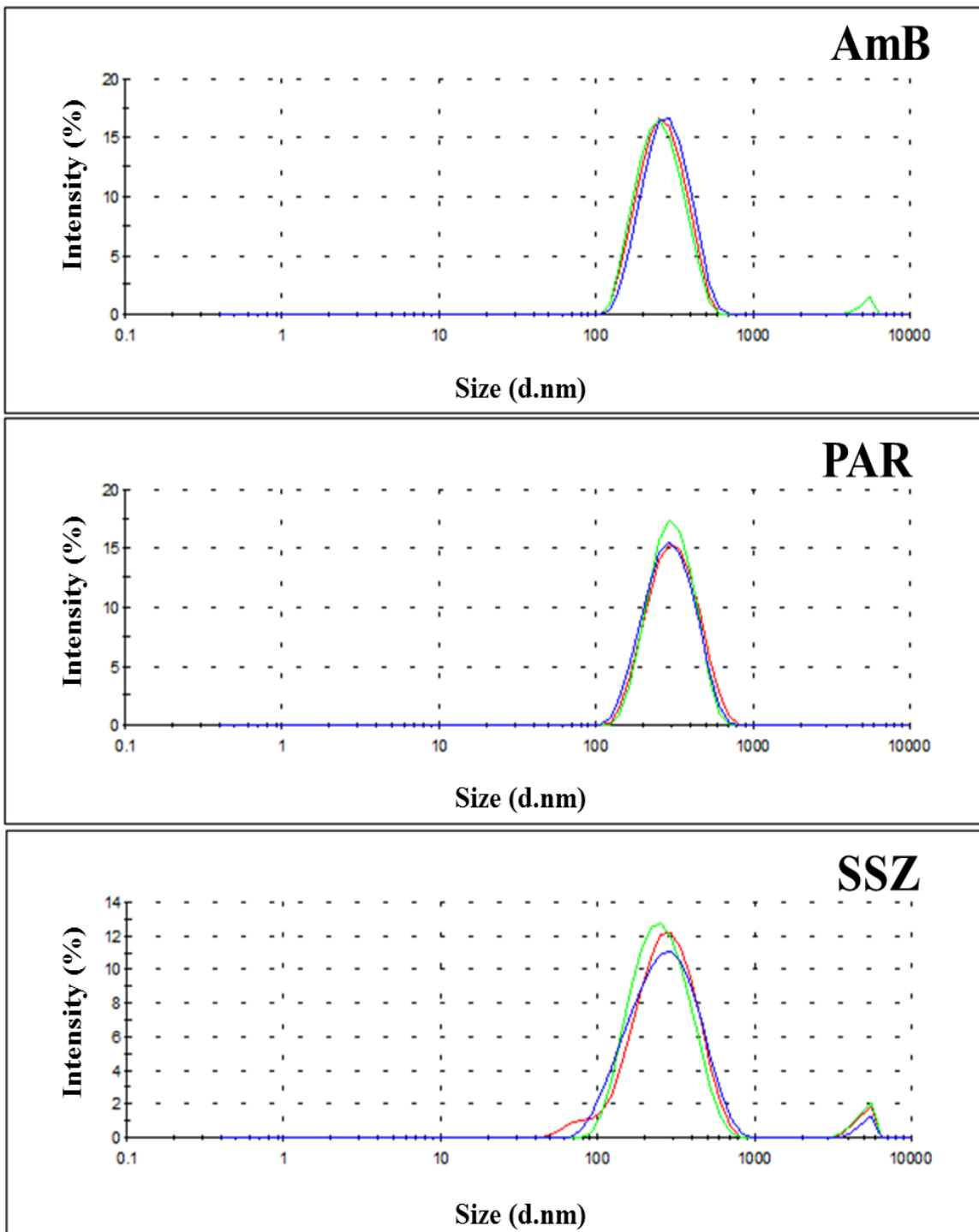


Figure 2.26 Particle size distribution by intensity of the SLNs after 24 months of storage (n = 3)

Figures 2.27 and 2.28 compare the z-average diameters, PDIs and ZPs of the freshly prepared, 24 months-stored and freeze-dried SLNs. It can be seen from the graphs that for all three SLNs, freeze-drying resulted in a slight increase in particle size (up to about 1.6-fold) and up to a 3-fold increase in PDI. Storage for 24 months also caused up to a 1.5-fold increase in the mean sizes of all three SLNs, and up to a 1.5-fold increase in the PDIs for PAR and SSZ SLNs, while the PDI for AmB remained almost unchanged. The ZP values however remained relatively the same with that of the freshly prepared SLNs, irrespective of storage time or freeze-drying. As stated in Section 1.5.4.2, ZP values $> |60 \text{ mV}|$, as obtained for all three SLNs indicate high colloidal stability. The results therefore clearly point to all three SLN dispersions being very stable systems irrespective of storage or freeze-drying. Also, there is the likelihood that the freeze-dried product will have a much longer shelf life given that it is a solid formulation, and hence hydrolysis of either the drugs or the excipients are checked.

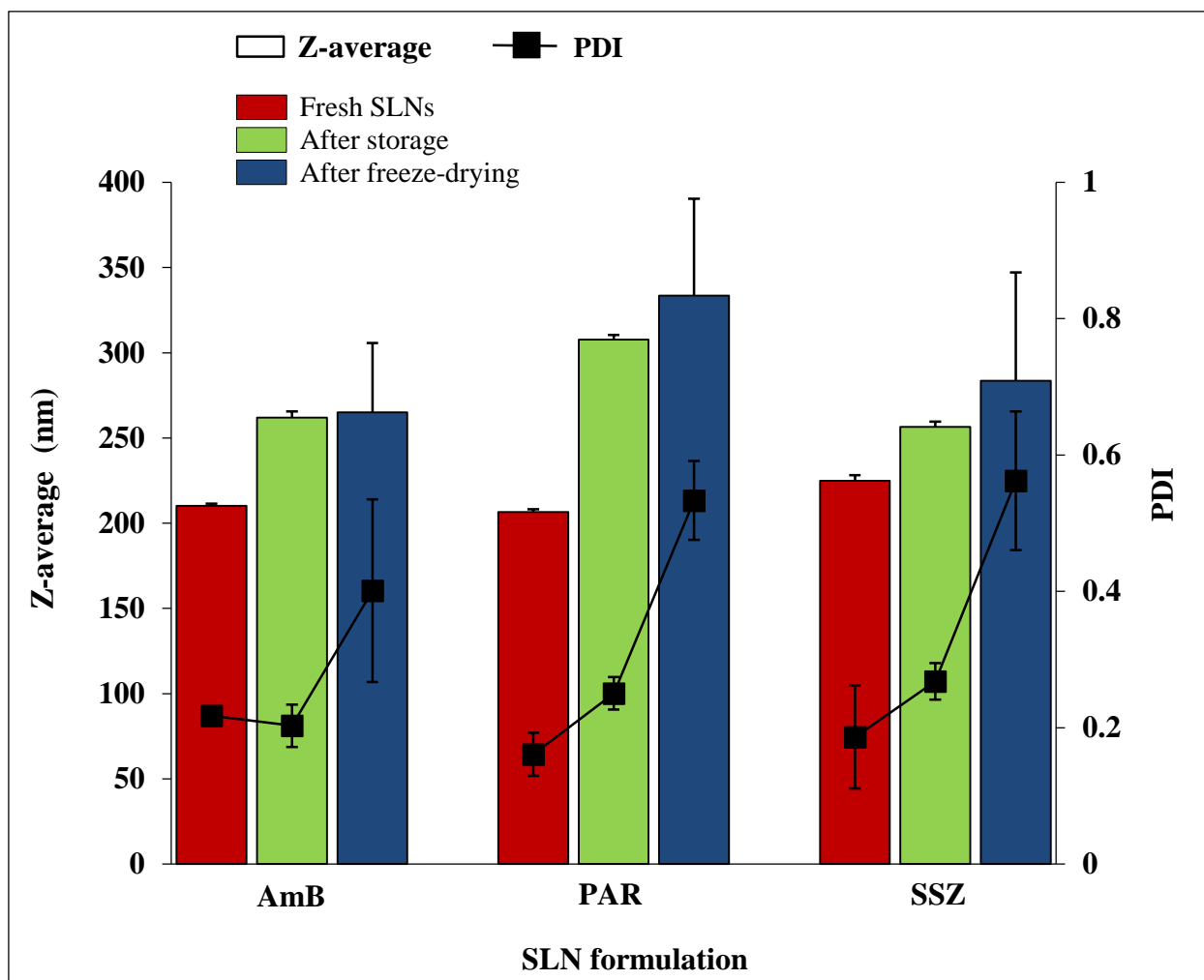


Figure 2.27 Z-averages and PDIs of the fresh SLNs, after storage for 24 months, and after freeze-drying (n = 3)

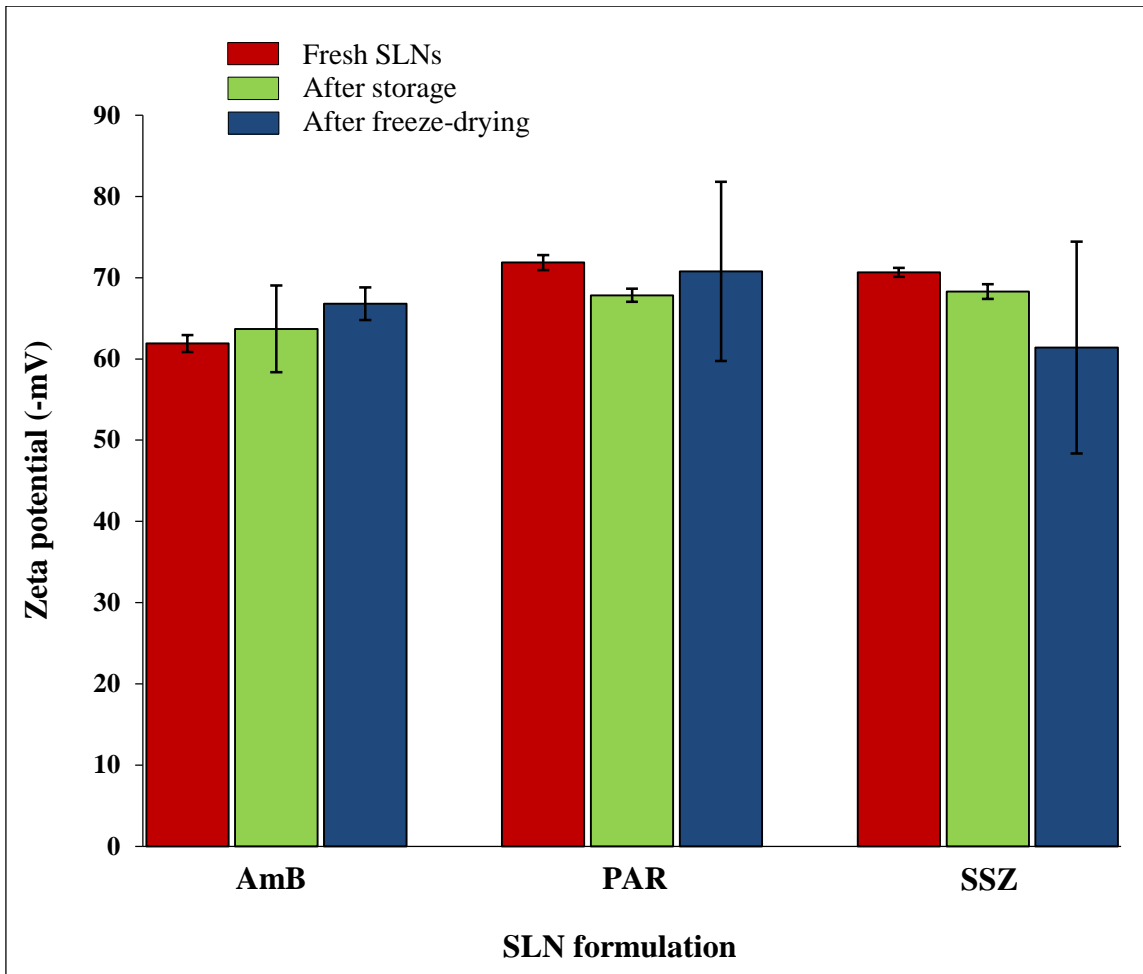


Figure 2.28 ZPs of the fresh SLNs, after storage for 24 months, and after freeze-drying (n = 3)

Another stability consideration of SLN formulations is the effect of light. In the present study, the storage containers for the AmB, PAR and SSZ SLNs were wrapped in aluminium foil to serve as a barrier against light. Coupled with being stored in the refrigerator, direct exposure to light was avoided to a large extent.

A study by Reddy *et al.* (2006) showed more than a 4-fold increase in mean particles size of tamoxifen citrate-loaded SLNs after exposure of the dispersion to artificial light (40 W) and daylight. The high energy of light radiations cause an increase in the kinetic energy of particles in the same way that high temperature does, which causes increase in particle collisions resulting in particle growth. The study by Reddy *et al.* (2006) showed that daylight caused gelation in the dispersions and resulted in a higher destabilising effect (faster particle growth) than artificial light, which is not unusual due to the higher energy of UV radiations in natural light. These findings were in line with those of Freitas and Müller (1998) who also found that exposure of a Compritol SLN formulation to light resulted in gelation while storage of the SLNs in siliconised glass vials in darkness at 8°C prevented any particle growth. With the aforementioned conditions, they achieved an aqueous SLN dispersion which was stable (as regards measured particle size and ZP) over 3 years [Freitas and Müller, 1998; Reddy *et al.*, 2006]. The results from the present study clearly indicate that storage of the SLNs in the refrigerator at 4-8°C was appropriate and prevented any physical or chemical instabilities in the formulations.

2.5 Conclusions

In conclusion, individual SLN formulations containing AmB, PAR or SSZ were successfully formulated using an identical method and good encapsulation efficiencies were obtained. The SLNs had matching physical characteristics as regards particle size, shape, morphology, surface charge, *in vitro* drug release and mobility propensities, which indicate the suitability of employing the PAR and SSZ SLNs as markers in the GI absorption study to be conducted on the AmB SLNs (Chapters 5 and 6). Storing the SLNs for up to 24 months at 4-8°C, as well as freeze-drying did not significantly change the physical characteristics of the SLNs or the chemical nature of the drug load. High ZP values of magnitudes > 60 mV were obtained for all the SLNs, which show that very stable formulations had been prepared. AmB SLNs exhibited low *in vitro* drug release, which is favourable in pursuit of an AmB formulation with improved tolerability and free from systemic toxicity. A slow AmB release also assures that the drug load may be significant during GI transit and subsequent uptake by Peyer's patches along the gut, all of which point to an improved oral bioavailability. The similarities in the properties of the three SLNs indicate the suitability of the preparation method for formulating SLNs containing drugs with different physicochemical properties.

CHAPTER 3

STABILITY OF THE SOLID LIPID NANOPARTICLES AND SURFACE CHEMISTRY ANALYSES IN SIMULATED GASTROINTESTINAL FLUIDS

3.1 Introduction

Estimating the stability of nanoparticulate formulations in biological media can provide critical information for optimising such preparations that are meant for systemic delivery. Stability studies conducted in appropriate simulated gastrointestinal (GI) media may give information on the fate of formulations after oral administration. Generally, the stability of nanoparticulate formulations can be assessed with reference to their chemical and pharmaceutical/storage stabilities [Muthu and Feng, 2009]. The latter has been discussed in the preceding chapter.

After oral administration, dosage forms must initially overcome the physical and chemical dynamics within the GI tract. The drug must traverse the intestinal epithelium efficiently in order to register any meaningful bioavailability. Lipid-based delivery systems comprising biodegradable materials are susceptible to digestion/degradation by gastric and intestinal enzymes, prior to their absorption. They can be absorbed by enterocytes as micelles, a process which serves to improve the absorption of hydrophobic drugs [Müller *et al.*, 1996; Pouton, 2000; Subramanian and Ghosal, 2004; Roger *et al.*, 2009]. In addition, the nanometre dimension of SLNs gives them a large surface area; therefore, they are prone to aggregation, which may reduce particle interaction with the intestinal mucosa [Jani *et al.*, 1990].

The slow and controlled drug release characteristics exhibited by SLN systems assure evasion of gastric and intestinal degradation of susceptible drugs; however, these may depend on the rate of degradation of the particles, which is also governed by the type of stabiliser and lipid used in

formulating the SLNs [Damgé *et al.*, 1990; Olbrich *et al.*, 2002(a,b)]. A study by Zhang *et al.* (2013) revealed that the use of SLNs averted the gastric irritation caused by triptolide, which indicates the intactness of the delivery system in the stomach; however, the composition of the lipid matrix varies among formulations hence each SLN formulation must be tested. In the following, the various techniques that were used in this study to investigate the stability of AmB, PAR and SSZ SLNs when challenged by various simulated GI media are reviewed.

Dynamic light scattering (DLS), also referred to as photon correlation spectroscopy (PCS) is a technique used for measuring particle size in the submicron region up to 10 µm, as well as the size distribution of particles. Useful applications of DLS include characterising particles, emulsions or molecules that are suspended or dissolved in a liquid. In DLS, the Brownian motion of particles in suspension causes scattering of laser light at different intensities, which is analysed using the Stokes-Einstein relationship (below) to obtain particle size.

Stokes-Einstein equation:

$$\overline{(x, y)^2} = \frac{2k_B T}{3r_h \pi \eta} \dots \dots \dots \text{Equation 3.1}$$

Where: k_B is the Boltzmann constant, $\overline{(x, y)^2}$ is the mean squared speed of a particle with a hydrodynamic radius r_h , at a temperature T, and in a medium of viscosity η .

Electrophoretic light scattering (ELS) is a technique that measures the migration of suspended particles having a net charge, towards an oppositely charged electrode within an electric field. The velocity of the particles is known as their electrophoretic mobility and this is related to their zeta potential [Malvern Instruments, 2015].

Nanoparticle tracking analysis (NTA) uses both light scattering and Brownian motion to achieve the size distributions of particles in a suspension. In NTA, a laser beam is passed through a sample chamber and particles in the path of the beam scatter light so that they can be easily visualised through a magnification microscope, onto which a charge-coupled device (CCD) video camera is mounted. The camera captures a video file of the particles undergoing Brownian motion to provide real-time monitoring of changes in the characteristics of the particle populations. The NTA software is then used to track particles individually and using the Stokes-Einstein equation, the hydrodynamic diameter of a sample is computed. A fluorescence mode could also be used in the analysis to obtain data for specifically labelled particles. NTA can be used for analysing particles with sizes ranging from 30 to 1000 nm [Filipe *et al.*, 2010; Malvern Instruments, 2015].

Time-of-flight secondary ion mass spectroscopy (ToF-SIMS) is a technique in which ion beams are used to extract molecular information about functional groups on particle surfaces, as well as the composition of materials. SIMS can therefore be used to obtain information regarding contamination on samples. ToF-SIMS analyses basically involve bombarding a substrate with primary ion beams of Ga^+ , Ar^+ , O_2^+ , Cs^+ , C_{60}^+ , Au^+ , Bi^+ or other atomic, molecular or cluster ions with energies between 3 and 20 keV. This results in the ejection of secondary atomic and molecular ions, which are drawn into a tube for mass analyses [Postawa *et al.*, 2004; Shimizu, 2005; Baer *et al.*, 2010].

ToF-SIMS has a depth profiling capability, in which the surface of a sample is eroded away by rastering a high primary ion dose across the surface to create a flat-bottomed crater. Mass spectral data giving information on the variation in the composition of a sample with depth below its immediate surface is then obtained as a function of sputtering time. Spectroscopy and imaging in SIMS are performed in static mode whereas depth profiling makes use of dynamic SIMS [Briggs

and Seah, 1992]. Dynamic and static SIMS are distinguished by the dose of the primary ions used during an analysis; the latter involves low density and low total dose of ions with minimal surface damage and sample alteration. Depth profiling on the other hand is a destructive technique and results in significant surface damage therefore, spectral or image data for a particular sample area must be performed, if needed, prior to running the instrument in dynamic mode [Briggs and Seah, 1992; Ratner *et al.*, 2009; Vickerman and Gilmore, 2009; Nolan, 2013].

Specifically, PCS, NTA and ToF-SIMS were used to characterise and estimate the stability of AmB, PAR and SSZ SLNs in various simulated salt solutions mimicking GI fluids as regards pH and temperature.

3.2 Materials

The same materials and solvents listed in Section 2.2 were used in formulating the SLNs. Simulated gastric fluid and simulated intestinal fluid were purchased from Sigma-Aldrich (St. Louis, MO, USA) and appropriately diluted with deionised water to obtain the media at pH 1.2 and pH 6.6, respectively.

3.3 Methods

3.3.1 Preparation of drug-free, AmB, PAR and SSZ SLN formulations

The AmB, PAR and SSZ SLNs were prepared according to the procedure described in Section 2.3.3. The drug-free formulation was similarly prepared as the other SLNs except that no drug was added to the formulation.

3.3.2 Stability of the SLNs in simulated GI fluids

All the SLN formulations were evaluated for stability in simulated gastric fluid (SGF) and simulated intestinal fluid (SIF), at 37°C. A 1-mL sample of each formulation was added to SGF-only and SIF-only, each in a separate tube to produce a 1 in 250 dilution, which was incubated for 2 hr. In a parallel study, the formulations were incubated in SGF for 2 hr followed by transfer into SIF and incubation for an additional 2 hr to mimic gastric emptying (SGF+SIF). All the samples were diluted with the appropriate GI fluid or deionised water to obtain a final dilution of 1 in 500. The samples were then evaluated using PCS and NTA. ToF-SIMS was used to qualitatively evaluate the surface chemistries of the fresh particles, as well as to observe changes in the relative drug intensities at the surface of the particles after the various treatments.

3.3.3 PCS studies

PCS studies on the SLNs were carried out using a Zetasizer Nano ZS[®] (Malvern, UK) and the parameters measured were z-average diameter, zeta potential (ZP) and polydispersity index (PDI). Sample analyses were done using a clear disposable zeta cell. Each analysis was carried out at 37°C and performed in triplicate. The data obtained have been expressed as mean \pm standard deviation (SD).

3.3.4 NTA studies

The NTA measurements were performed using a NanoSight LM10 (NanoSight, Amesbury, United Kingdom) equipped with a sample chamber and a 640-nm laser. The samples were injected into

the sample chamber using sterile syringes, until some sample drops reached the tip of the exit nozzle to ensure the chamber was completely filled with the sample. All measurements were done at 37°C. Each video was captured at 30 frames/sec for 1 min 30 sec and analysed using the NTA software version 3.1 Build 3.1.46. Triplicate measurements were performed for each sample and the data obtained expressed as mean \pm SD.

3.3.5 ToF-SIMS analyses

Surface chemistry analyses were carried out on the samples using a ToF-SIMS (ION-ToF GmbH, Münster, Germany) equipped with a liquid metal bismuth ion gun (LMIG). Prior to analyses, the SLNs were washed by centrifuging 1 mL samples at 13 000 rpm for 60 min, after which the supernatants were discarded and deionised water added to the samples. The washing was done to exclude ions from the simulated GI media from the particles, as the ions can affect signals in the spectra; and to remove traces of unassociated drug. The precipitated particles were resuspended in water by shaking and the centrifugation process was repeated thrice. The washed SLNs were redispersed in deionised water and about 40 μ L samples placed on labelled silicon wafers and air-dried prior to analyses. The analyses were carried out using 25 keV Bi₃⁺ primary ions. Depth profiles for the fresh SLNs were obtained by sputtering a 2.5 KeV Ar-cluster beam randomly on a 200 μ m \times 200 μ m area over a sputter time of 500 s. Data analyses were performed on the negative ion spectra for each sample using the Ion-ToF software.

3.4 Results and discussion

3.4.1 PCS analyses

The z-average values obtained from PCS measurements correspond to the hydrodynamic diameters of particles in a sample, whilst the PDI is a measure of the width of the particle size distribution.

PDI values of 0.0-0.1 point to a narrow monodisperse distribution, 0.1-0.4 indicate a moderate polydisperse distribution system, whilst values greater than 0.4 indicate a broadly polydispersed system [NanoComposix, 2012]. Generally samples with mean particle sizes above 500 nm and PDIs greater than 0.5 are considered as “big and agglomerated” however, such data may not be given much consideration. This is because few large particles present in a sample usually dominate the light scattering signal in PCS and give rise to large PDI values, which could render the results unreliable.

In addition, nanoparticles with ZP up to $|10 \text{ mV}|$ are considered to have a neutral charge, whereas those with ZP greater than $|30 \text{ mV}|$ are considered as being strongly charged [Clogston and Patri, 2011].

Figure 3.1 shows the particle size distribution by intensity of drug-free SLNs before and after exposure to simulated GI fluids. Figures 3.2 and 3.3 illustrate the z-averages and PDIs, and ZPs of all the SLNs, respectively, before and after exposure to the simulated fluids. The z-average, PDI and ZP of drug-free SLNs in SGF-only were obtained as $737.4 \pm 41.8 \text{ nm}$, 1.00 ± 0.00 and $2.4 \pm 0.3 \text{ mV}$, respectively, however, the values for the freshly prepared particles were $195.4 \pm 3.1 \text{ nm}$, 0.17 ± 0.01 and $-67.6 \pm 1.7 \text{ mV}$, respectively.

Drug-free SLNs

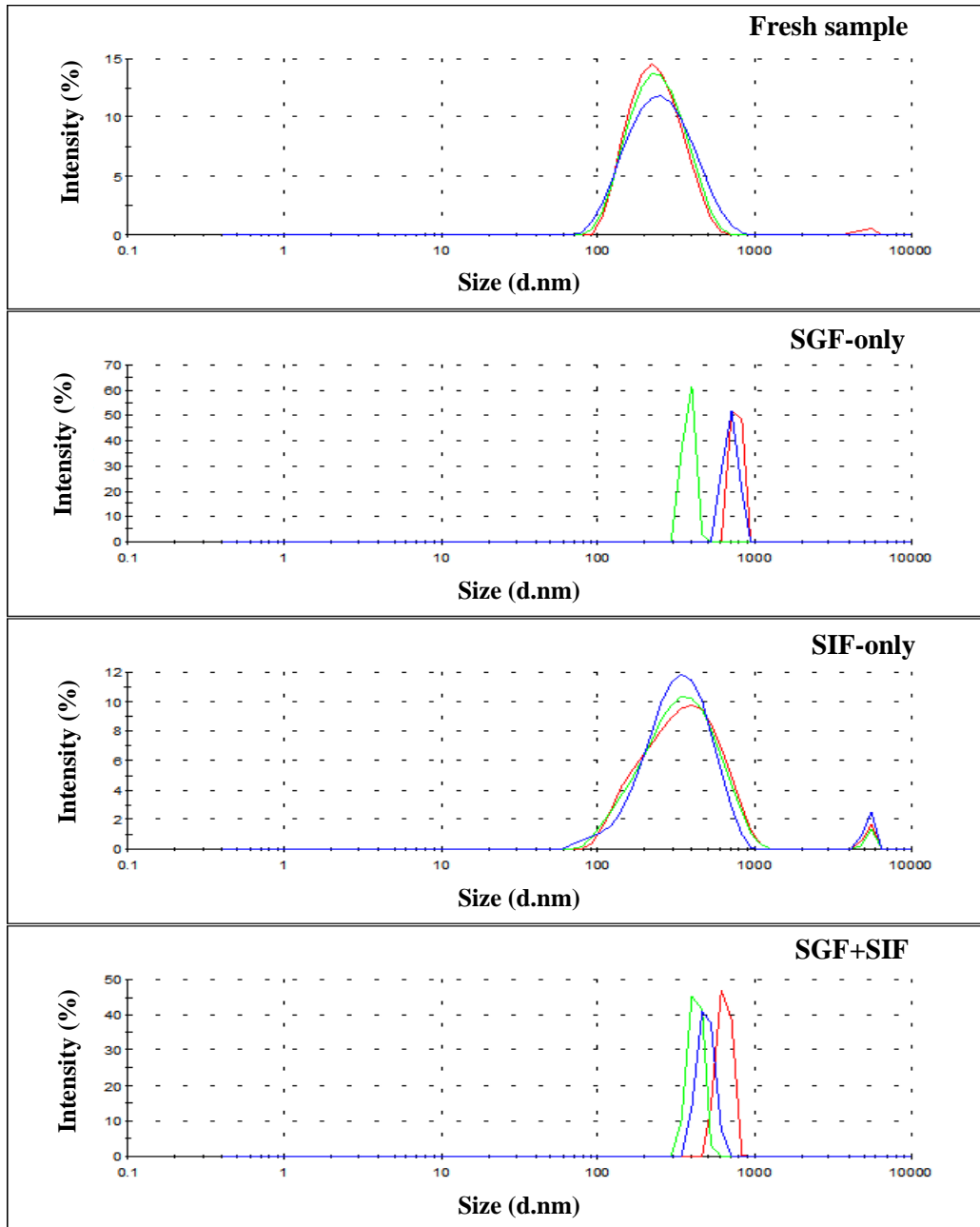


Figure 3.1 Particle size distribution by intensity of drug-free SLNs, before (fresh sample) and after their incubation in simulated GI fluids (n = 3)

The SGF contains approximately 2.0 g/L of NaCl and 2.917 g/L of HCl according to the specifications in the United States and European Pharmacopoeias. SGF is less complex as compared with *in vivo* gastric fluid; however, the dominant features of stomach fluid are its acidity and ionic content, and these properties of the simulated fluid match well with the *in vivo* condition.

There was an approximately 3.8-fold increase in the z-average of the drug-free particles in SGF-only, which points to massive aggregation of the particles in the medium. The marked drop in the magnitude of ZP, as well as the change in surface charge from negative to positive (-67.6 ± 1.7 mV to 2.4 ± 0.3 mV) were due to the presence of H^+ ions in the SGF and their neutralisation of the negative charge on the fresh SLNs. This reduction in ZP favoured van der Waals inter-particle interactions and resulted in particle aggregation.

SIF contains approximately 0.616 g/L of NaOH and 6.8 g/L of KH_2PO_4 . In SIF-only, the z-average, PDI and ZP of the drug-free SLNs were 342.5 ± 1.3 nm, 0.38 ± 0.03 and -28.9 ± 0.6 mV, respectively, indicating a 1.75-fold increase in particle size and a 2.33-fold decrease in the ZP after exposure of the particles to the medium. The PDI value indicates a relatively narrower size distribution of the particles in SIF-only than in SGF-only, and no aggregation of the SLNs due to retention of an adequate surface charge (-28.9 mV) above the threshold attendant for agglomeration of colloidal particles ($|15$ mV) [Riddick, 1968].

The composition and volume of fluid along the GI tract, the motility of the GI tract as well as the transit of dosage forms within it are highly variable [Roger *et al.*, 2009]. As a result, there is no perfect representative model of GI fluid; however, the process of gastric contents being emptied into the small intestine is a consistent characteristic of the gut. Simulation of gastric emptying in respect of exposure to GI fluids was therefore replicated by exposing the SLNs to SGF and then to SIF. The z-average, PDI and ZP obtained were 517.0 ± 113.0 nm, 0.54 ± 0.22 and -0.4 ± 0.1 mV,

respectively. Although the very low ZP magnitude is suggestive of maximum particle agglomeration and precipitation, the PDI and mean particle size are intermediate between the values obtained for the particles in SGF-only and SIF-only, which suggests that the aggregates of the SLNs in SGF are held loosely as floccules, which become deaggregated on exposure to SIF. If this was the case, then the same is to be expected *in vivo*. A high ZP value is essential for long-term storage stability of colloidal formulations. After oral administration however, only a sufficient ZP magnitude is necessary to maintain electrostatic repulsion among the particles prior to their absorption. As a result, a low ZP of nanoparticles after contact with GI fluids is not crucial if their final size is optimum for absorption.

A study by Shakweh *et al.* (2005) showed that the uptake of neutral and negatively charged nano- and microparticles by Peyer's patches in mice occurs to a greater extent as compared with positively charged particles. Their investigation also revealed that particle uptake by Peyer's patches is highly size-dependent. They observed a much larger number of particles with mean diameters of approximately 300 to 1000 nm in the patches than larger-sized particles. Again, particles with negative or close to neutral ZP did not interact with the intestinal mucus gel layer due to electrostatic repulsion; this allowed such particles to reach the follicle-associated epithelium for uptake by M cells through endocytosis. Positively charged particles on the other hand were found to interact strongly with the mucus layer as the latter is negatively charged, thereby resulting in a delayed uptake [Shakweh *et al.*, 2005].

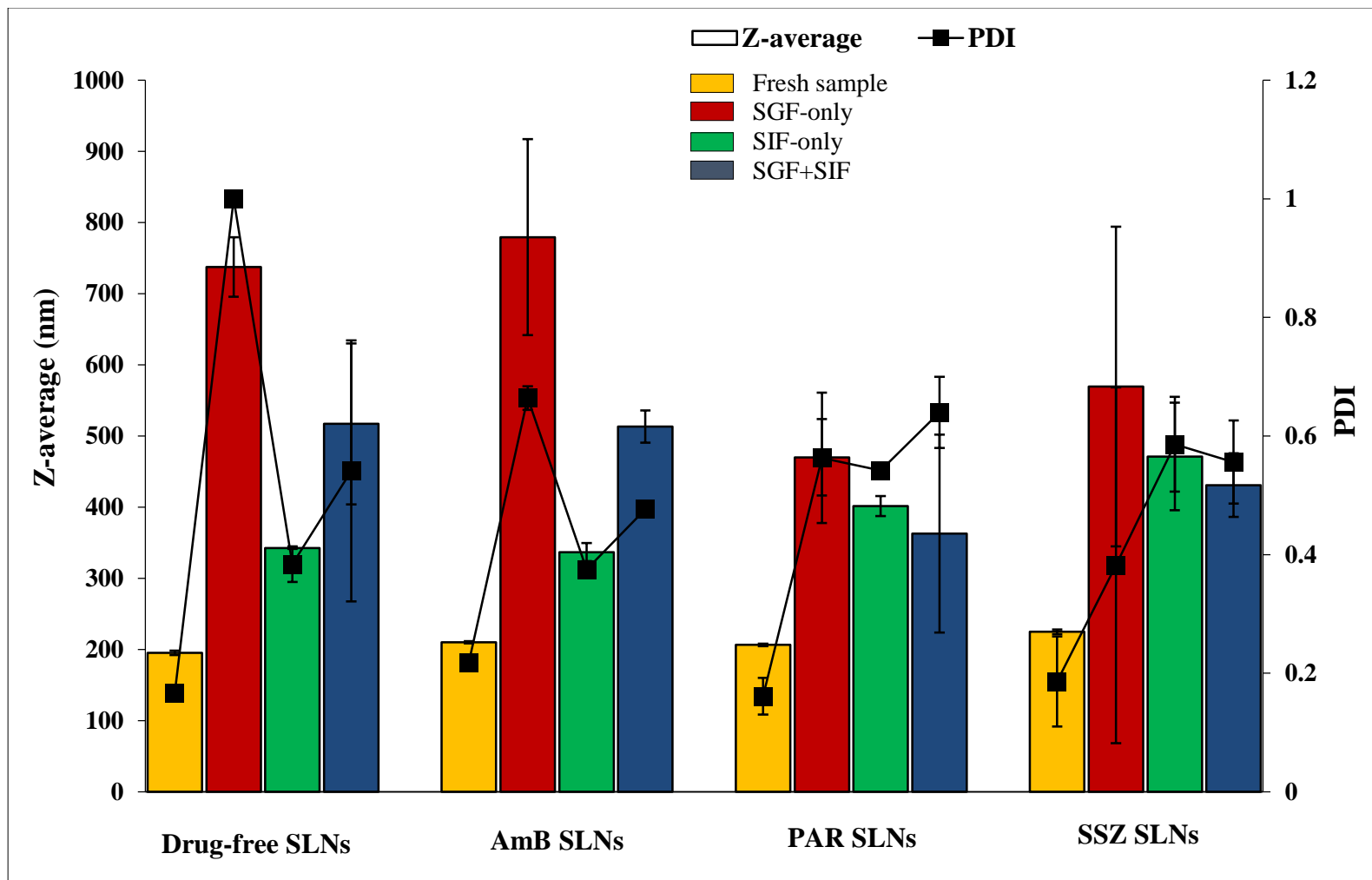


Figure 3.2 Z-averages and PDIs of the SLNs before (fresh sample) and after their incubation in simulated GI fluids (n = 3)

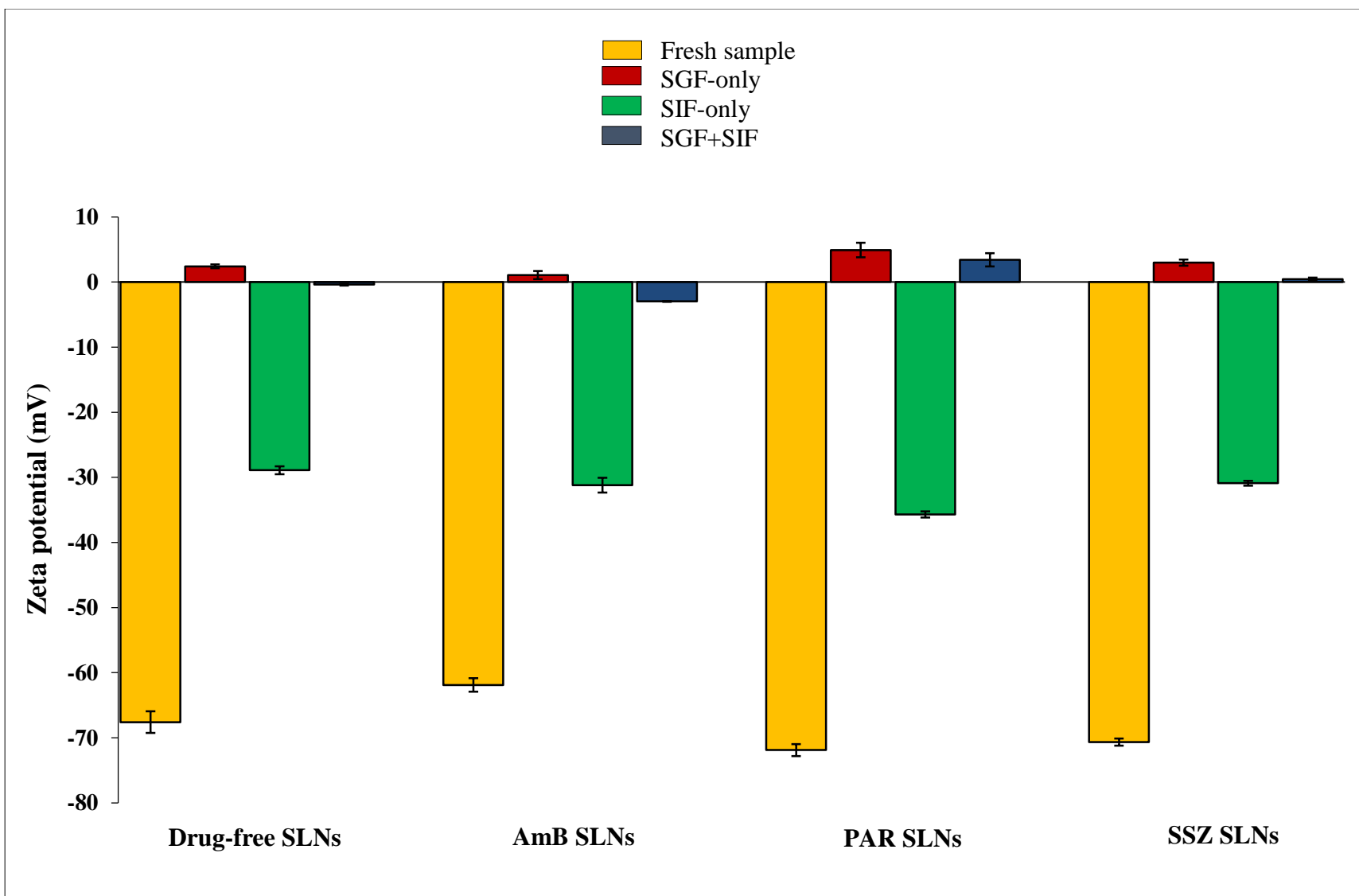


Figure 3.3 ZPs of the SLNs before (fresh sample) and after their incubation in simulated GI fluids (n = 3)

The aforementioned results therefore suggest that after exposure to SGF+SIF, the drug-free particles still retained their integrity, as regards size and surface charge, for absorption via endocytosis as well as lymphatic transport [Jani *et al.*, 1989; Jani *et al.*, 1994; Shakweh *et al.*, 2005]. The increase in size observed after exposure of the particles to the media may be a result of either aggregation or ingress of the dissolution media into the particles or both.

Figure 3.4 shows the particle size distribution by intensity of AmB SLNs before and after placement in simulated GI fluids. The z-averages of the AmB SLNs in SGF-only, SIF-only and SGF+SIF were 779.3 ± 137.7 nm, 336.7 ± 12.8 nm and 513.2 ± 22.8 nm; the PDIs were 0.66 ± 0.02 , 0.38 ± 0.01 and 0.48 ± 0.01 ; and the ZPs were 1.1 ± 0.6 mV, -31.2 ± 1.2 mV and -3.0 ± 0.1 mV, respectively, as depicted in Figures 3.2 and 3.3. The size distribution profile of the particles in the SGF-only showed a bimodal distribution with the two particle populations having mean sizes of 115.3 nm and 737.7 nm.

As with the drug-free particles, it can be said that the AmB SLNs aggregated in SGF and after transfer from SGF into SIF, some deaggregation occurred. Prior to incubation, the AmB SLNs had z-average of 210.1 ± 1.4 nm, PDI of 0.22 ± 0.01 and ZP of -61.9 ± 1.0 mV. According to the findings of Shakweh *et al.* (2005), the uptake of the AmB SLNs via endocytosis and M cells after oral delivery would not be significantly affected as the mean particle size after exposure to SGF+SIF remained below 1000 nm although there had been an increase of about 2.4-fold.

There were no marked differences between the PCS results obtained for drug-free and AmB SLNs. Interestingly, both formulations showed the same pattern of size changes in the respective media; with size increase being highest in SGF-only, followed by SGF+SIF and then SIF-only.

AmB SLNs

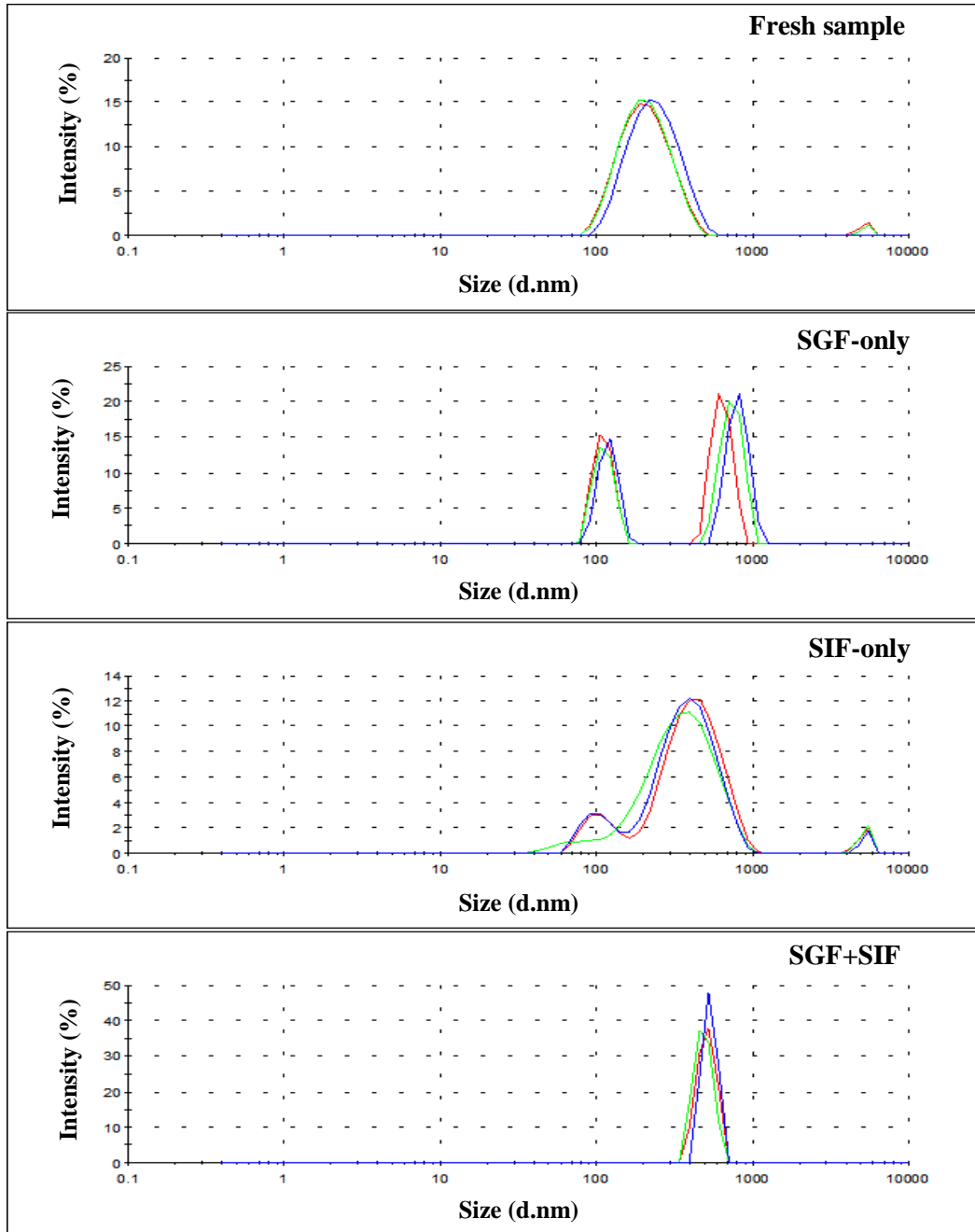


Figure 3.4 Particle size distribution by intensity of AmB SLNs, before (fresh sample) and after their incubation in simulated GI fluids (n = 3)

The increase in particle size in SGF-only and SGF+SIF could be attributed mainly to aggregation while the comparatively less marked size increase in SIF-only could be the result of influx of dissolution medium into the particles. The aggregation of the SLNs in SGF is likely to result in a reduced release of AmB from the particles due to a decrease in effective surface area. It then follows that, aside from slow drug release from SLNs due to the hydrophobic nature of the lipid matrix, which retains most of the encapsulated drug within the matrix, particle aggregation in acidic medium as observed above may augment slow drug release in the stomach. This attribute is advantageous in view of the fact that the small intestine is the probable site for uptake of the SLNs and that it has a high expression of Peyer's patches.

Figure 3.5 shows the particle size distribution by intensity of PAR SLNs before and after their exposure to the simulated GI fluids. The z-averages of the fresh PAR SLNs and after exposure to SGF-only, SIF-only and SGF+SIF were 206.5 ± 1.7 nm, 469.9 ± 53.7 nm, 401.5 ± 14.1 nm and 362.8 ± 139.1 nm; the PDIs were 0.16 ± 0.03 , 0.56 ± 0.11 , 0.54 ± 0.01 and 0.64 ± 0.06 ; and the ZPs were -71.9 ± 0.9 mV, 4.9 ± 1.1 mV, -35.7 ± 0.5 mV and 3.4 ± 1.0 mV, respectively, in each case (Figures 3.2 and 3.3). The PAR SLNs also showed a bimodal distribution in SIF-only with mean sizes of 156.07 nm and 596.5 nm.

It was observed that the size of the PAR SLNs was highest in SGF-only, followed by SIF-only and then SGF+SIF. Generally, the increase in SLN size after incubation in the media was lower for PAR SLNs as compared with the drug-free and AmB SLNs.

PAR SLNs

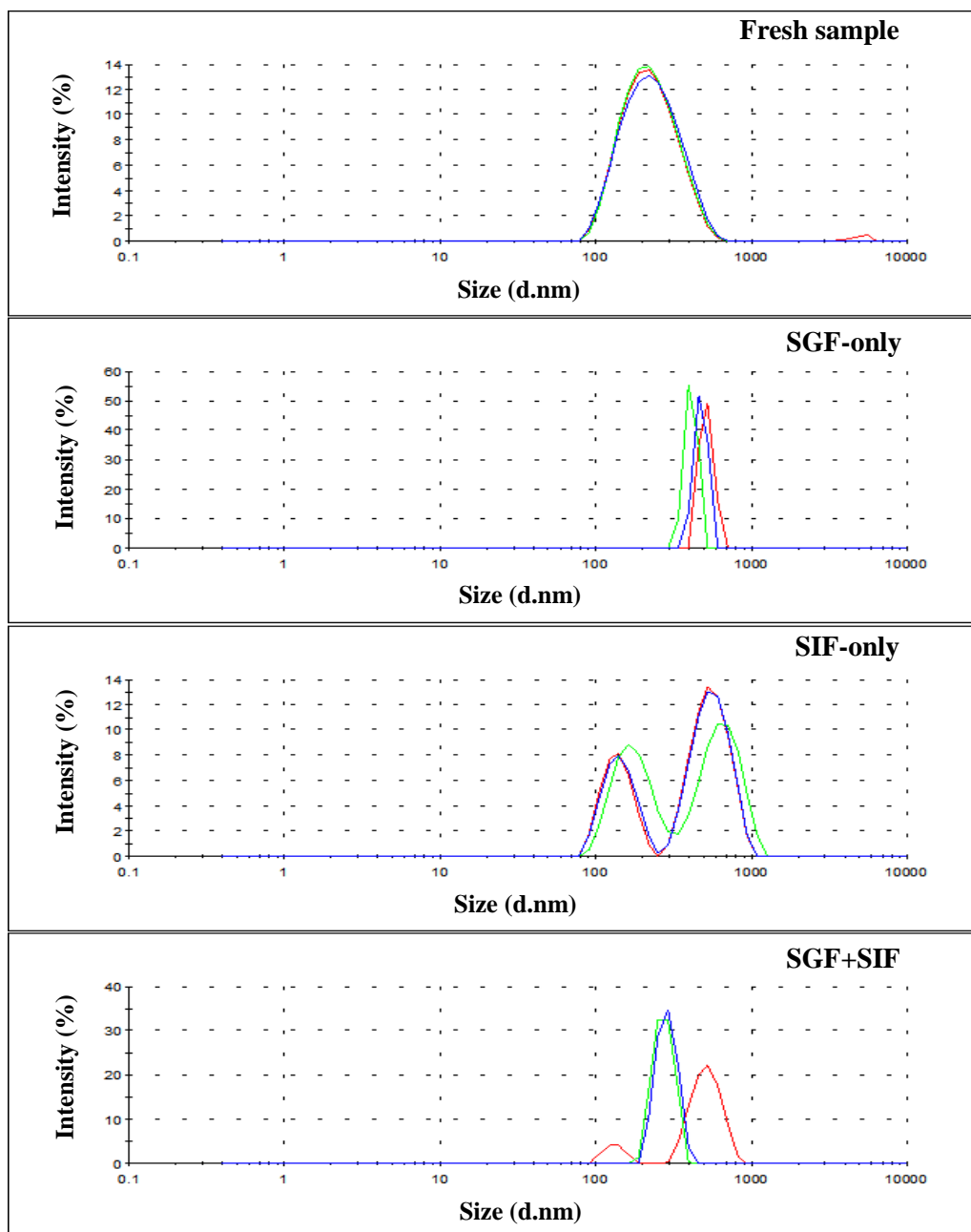


Figure 3.5 Particle size distribution by intensity of PAR SLNs, before (fresh sample) and after their incubation in simulated GI fluids (n = 3)

Figure 3.6 shows the particle size distribution by intensity of SSZ SLNs, before and after their incubation in the simulated fluids. Figures 3.2 and 3.3 show the z-averages obtained for the fresh SSZ SLNs and after their incubation in SGF-only, SIF-only and SGF+SIF, as 224.8 ± 3.3 nm, 569.4 ± 224.7 nm, 471.2 ± 75.5 nm and 431 ± 44.6 nm; the PDIs were 0.19 ± 0.08 , 0.38 ± 0.30 , 0.59 ± 0.08 and 0.56 ± 0.07 ; and the ZPs were -70.7 ± 0.6 mV, 2.9 ± 0.5 mV, -30.9 ± 0.4 mV and 0.5 ± 0.2 mV, respectively. The SSZ SLNs also showed the same pattern of size increase as the PAR SLNs: fresh sample < SGF+SIF < SIF-only < SGF-only, and a bimodal distribution in SIF-only with mean sizes of 132.9 nm and 706.8 nm.

Using DLS, and after a 2 hr-incubation period in SGF-only, Roger *et al.* (2009) found that the size of paclitaxel lipid nanoparticles which had an initial diameter of 51 nm was not affected as there was less than a 10 nm increment in the size of the particles. Laserra *et al.* (2015) also investigated lipoyl-memantine SLNs and found essentially no change in the size of the particles indicating no aggregation in SGF, both in the absence and presence of pepsin. Zhang *et al.* (2013) similarly observed an insignificant decrease (< 30 nm) in the size of triptolide SLNs in SGF-only. Gelatin-coated polymer-lipid nanoparticles having an initial size of 253 nm have also been shown to decrease by 68 nm after incubation in SGF [Jain *et al.*, 2012].

SSZ SLNs

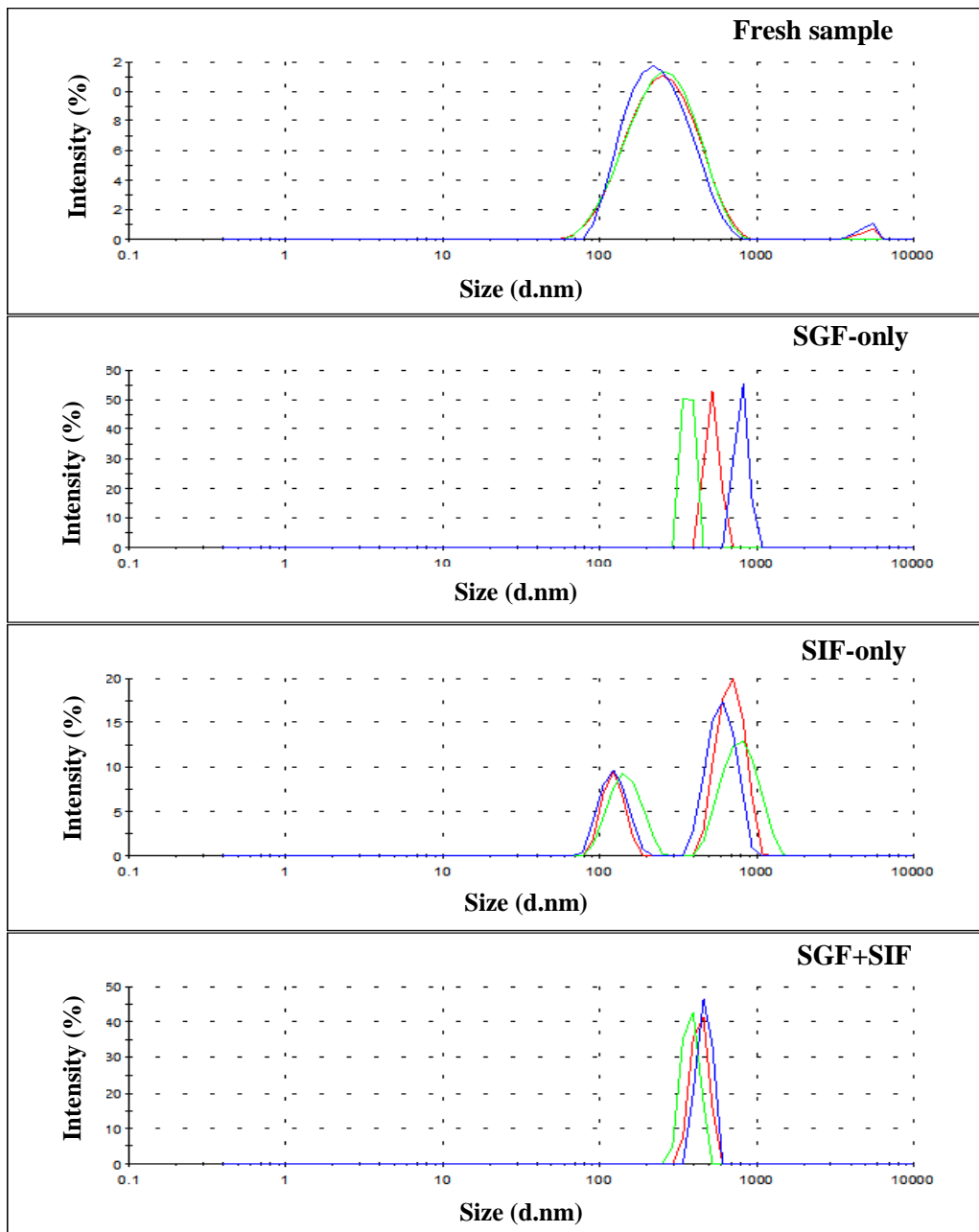


Figure 3.6 Particle size distribution by intensity of SSZ SLNs, before (fresh sample) and after their incubation in simulated GI fluids (n = 3)

On the other hand, in SIF-only, paclitaxel lipid nanoparticles have shown an increase in size of only up to 10 nm after 3 hr incubation with and without pancreatin in the medium [Roger *et al.*, 2009]. An increase in size by 192.6 nm has also been observed after incubating pegylated SLNs [Yuan *et al.*, 2013] in SIF-only, while lipoyl-memantine SLNs after 2 hr of incubation had an increase in size of 157.4 nm and 221.8 nm in the absence and presence of pancreatin, respectively [Laserra *et al.*, 2015]. Jain *et al.* (2012) on the other hand observed a 21 nm decrease in the size of gelatin lipid nanoparticles after 6 hr of incubation in SIF. On exposing the gelatin nanoparticles to SGF+SIF, a 36 nm decrease in size was observed. Only the data obtained by Yuan *et al.* (2013) and Laserra *et al.* (2015) are comparable with those obtained in the present study for the SLNs in SIF-only.

From the foregoing, it appears that either a decrease or no change in the size of various lipid nanoparticulate formulations was observed in SGF-only while in SIF-only, either an increase or a decrease in size was observed. It is likely that the composition of the SLNs may contribute to their propensity to aggregate as a function of the GI media. In the present work, an increase in size or aggregation of both drug-free and drug-loaded SLNs was observed in the simulated GI fluids and this was manifested more in SGF-only.

The hydrodynamic size obtained from DLS measurements can be affected by the salt concentration in the suspending medium, due to the electrical double layer (EDL) surrounding charged particles in an aqueous medium. The EDL is a layer of oppositely charged ions that moves with a nanoparticle having a net surface charge. Even at very low salt concentrations such as in demineralised water, an additional drag is induced by the salts through the extension of the double layer resulting in a decrease in diffusion coefficient and an increase in size [Hackley and Clogston, 2011].

One drawback of DLS is that the technique determines particle size from fluctuations in scattered light intensity, and is biased towards larger particles within a sample. The intensity of scattered light is proportional to the square of the particle diameter thus, larger particles or clusters of smaller particles scatter light more strongly than smaller particles. Again, in DLS the hydrodynamic diameter depends not only on the size of the particle core but also on any surface structures which may be present on the particles [Balog *et al.*, 2015].

The marked increase in size of the SLNs observed in the present work as compared with the other studies could therefore be attributed to the few aggregated or large particles having approximate sizes of 5000 nm, as seen in each of the size distribution profiles for the fresh SLN samples (Figures 3.1, 3.4-3.6). These large particles or aggregates can perturb the light scattering signals and mask the presence of smaller particles, leading to biased and inaccurate size measurements.

It is also noteworthy that z-average is only very useful for characterising particle size of monomodal (single peak), spherical or near-spherical and monodisperse (very narrow distribution width) samples. Consequently, for samples containing significant differences in size populations such as the bimodal distributions obtained for: the AmB SLNs in SGF-only, as well as the PAR and SSZ SLNs in SIF-only, the calculated z-averages do not convey very accurate size information. Although the DLS software has been designed to correct this aberration in multimodal distributions, the results may not reflect true particle size distributions as such, other particle sizing techniques can be used in addition to DLS in such instances [NanoComposix, 2012; Lim *et al.*, 2013].

Overall, ZP was highest for the fresh SLN samples as depicted in Figure 3.3. This is because the initial dispersion medium of the SLNs is deionised water. Additionally, the negative charge on the fresh particles is solely due to sodium cholate, which was the anionic surfactant used during

formulation of the SLNs. Incubating the SLNs in the simulated fluids caused a decrease in their ZPs owing to the pH changes caused by the electrolytes in SGF and SIF. However, the decrease was more marked in SGF-only and SGF+SGF media.

The ZP of a particle is highly dependent on the pH and conductivity of the suspending medium; therefore, different ZP values will be obtained as the two parameters are varied [Clogston and Patri, 2011]. The change from negative to positive surface charge observed in SGF-only for all the samples and in SGF+SIF for PAR and SSZ SLNs was due to charge neutralisation by the high concentration of H⁺ ions in SGF.

In SGF+SIF, all the three drug-loaded SLNs had sizes ranging from 362.8 nm to 513.2 nm. Their surface charges were also neutral as their ZPs ranged from -10 mV and +10 mV. These properties favour the absorption of the SLNs via the M cells of the Peyer's patches [Shakweh *et al.*, 2005; Clogston and Patri, 2011]. It may be concluded that the SLNs exhibit ideal physical properties necessary for absorption, following oral delivery and transit from the stomach to the intestines.

3.4.2 NTA studies

In order to investigate the size variation of the SLNs in simulated GI fluids, free from the bias of DLS, the particle-by-particle approach for determining size using NTA was used. Unlike DLS, NTA is not biased towards larger particles as such, the latter was used to estimate the stability of the SLN formulations in simulated GI fluids in order to obtain more accurate results.

Figure 3.7 shows the size distribution by particle concentration of drug-free SLNs, before and after their incubation in the simulated GI fluids. Figure 3.8 shows the mean particle size for the drug-

free and drug-loaded SLNs in the simulated GI fluids. The mean size of drug-free particles prior to and after incubation in SGF-only, SIF-only and SGF+SIF were 172.3 ± 11.9 nm, 181.9 ± 101.7 nm, 232.5 ± 15.0 nm and 266.4 ± 12.4 nm, respectively. As with the DLS results, it can be observed that there was an increase in size after incubation in the simulated media however, the current results are suggestive of particle size increase due to ingress of the media into the particles than of particle aggregation. The largest increase recorded was 94.1 nm and observed in SGF+SIF.

Drug-free SLNs

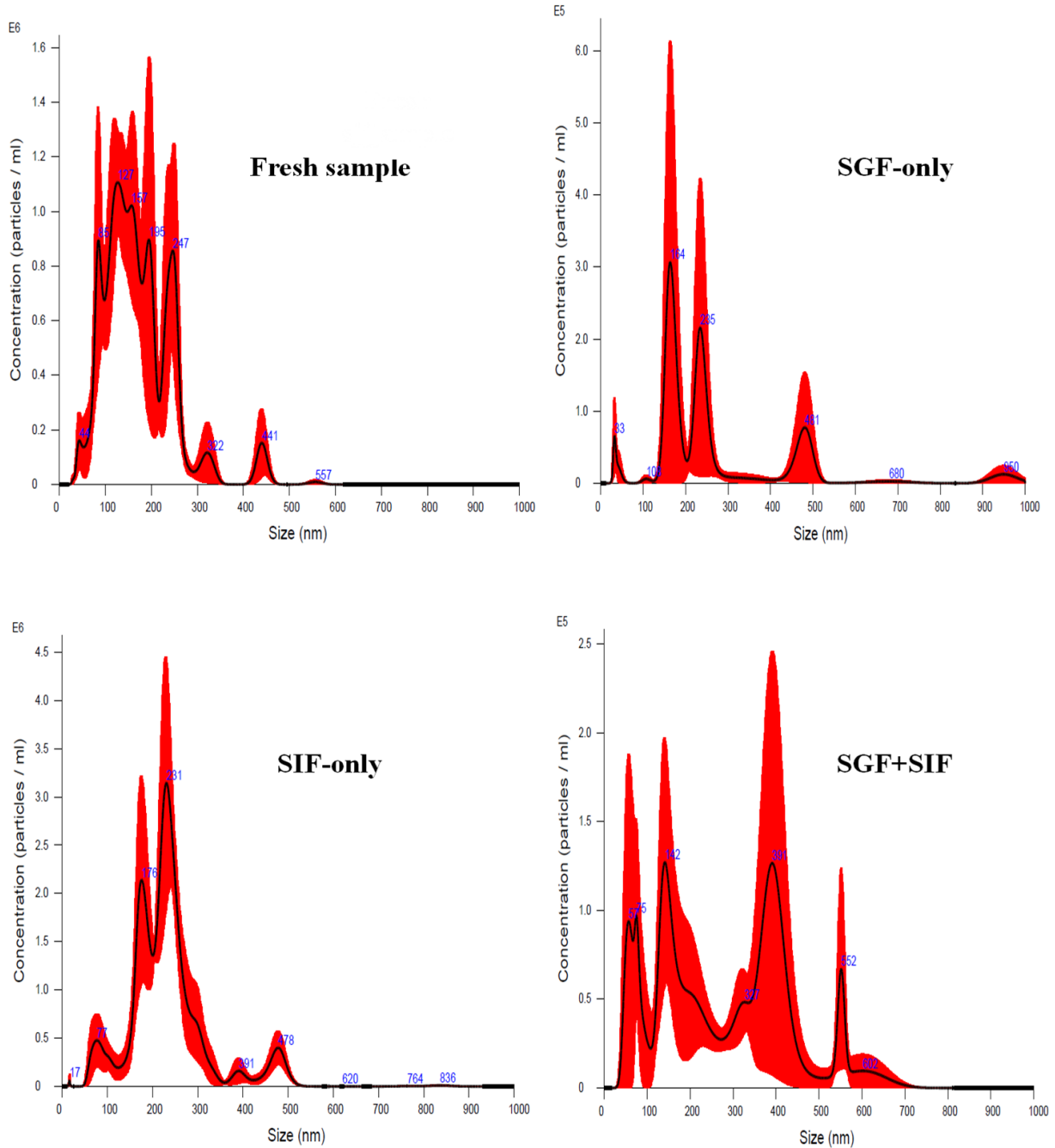


Figure 3.7 Size distribution by particle concentration of drug-free SLNs, before (fresh sample) and after their incubation in simulated GI fluids (n = 3)

[Red profile shows the range of the distributions of particle size and concentration from triplicate measurements; black line signifies the average distribution]

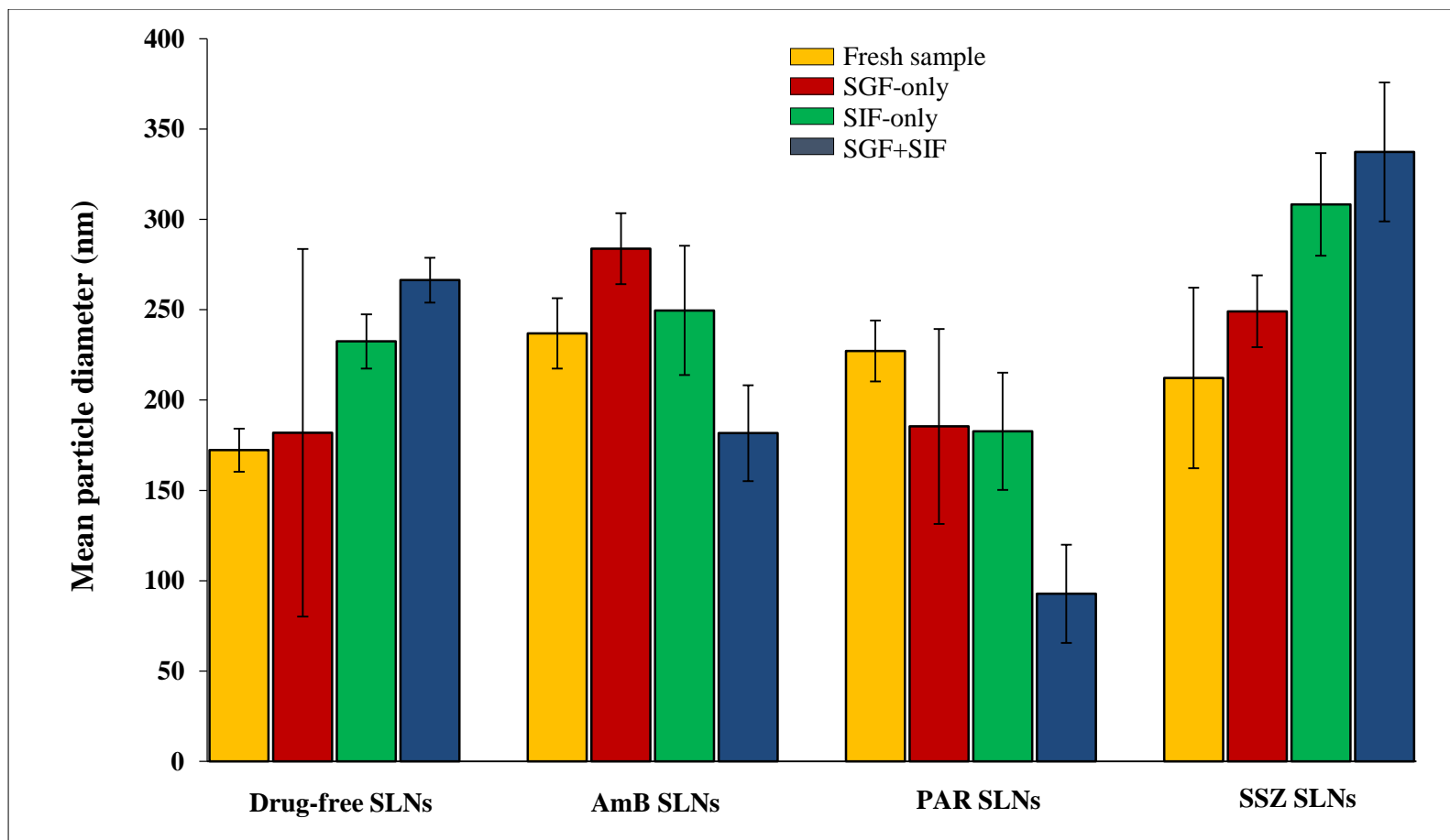


Figure 3.8 Mean particle sizes (using NTA) of the SLNs, before (fresh sample) and after their incubation in simulated GI fluids (n = 3)

Figure 3.9 illustrates the size distribution by particle concentration of AmB SLNs, before and after incubation in the simulated GI fluids. The mean size of the SLNs prior to and after incubation in SGF-only, SIF-only and SGF+SIF were 236.9 ± 19.4 nm, 283.8 ± 19.7 nm, 249.6 ± 26.5 nm and 181.7 ± 35.8 nm, respectively.

There was an increase in size in SGF-only and SIF-only, and a decrease in SGF+SIF. AmB is insoluble in water at pH 6-7 but soluble at pH 2 or 11 due to its amphoteric nature. It seems the SGF+SIF, which has an approximate pH of 1.5, served as a better dissolution medium for AmB thereby causing the decrease in particle size due to outward diffusion of dissolved drug, as opposed to the increase in size in the other media.

AmB SLNs

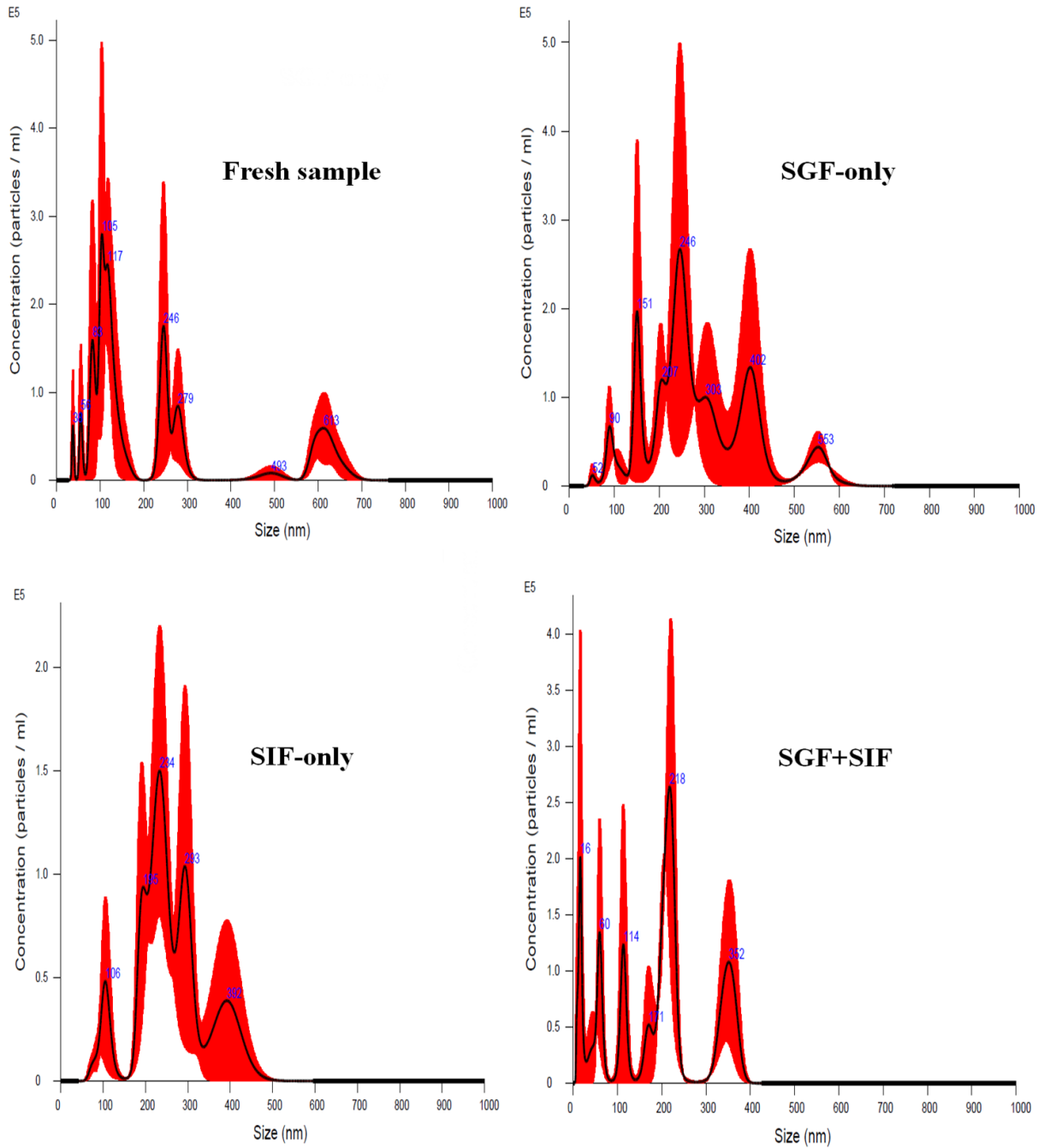


Figure 3.9 Size distribution by particle concentration of AmB SLNs, before (fresh sample) and after their incubation in simulated GI fluids (n = 3)

[Red profile shows the range of the distributions of particle size and concentration from triplicate measurements; black line signifies the average distribution]

Figure 3.10 shows the size distribution by particle concentration of fresh PAR SLNs and after their incubation in simulated GI fluids. The mean sizes of the SLNs prior to and after incubation in SGF-only, SIF-only and SGF+SIF were 227.2 ± 16.9 nm, 185.4 ± 53.9 nm, 182.7 ± 27.2 nm and 92.8 ± 32.5 nm, respectively. There was a decrease in particle size in all three media and the highest observed in SGF+SIF. PAR is a hydrophilic drug that exhibits increasing aqueous solubility as temperature is raised. PAR is also weakly acidic and forms a salt in the presence of a strong acid (SGF) or base however, the solubility of this salt depends on the ionic content of the dispersion medium. Again, the dissolution of weakly acidic drugs is minimal in strong acids. It can be observed that the size of the PAR SLNs in SGF-only and SIF-only was similar (185.4 nm versus 182.7 nm), possibly indicating similar solubility characteristics of the drug as a salt and in its unionised form at the two pHs respectively. The dissolved drug in the particles then freely diffused into the surrounding fluid resulting in the observed decrease in particle size.

PAR SLNs

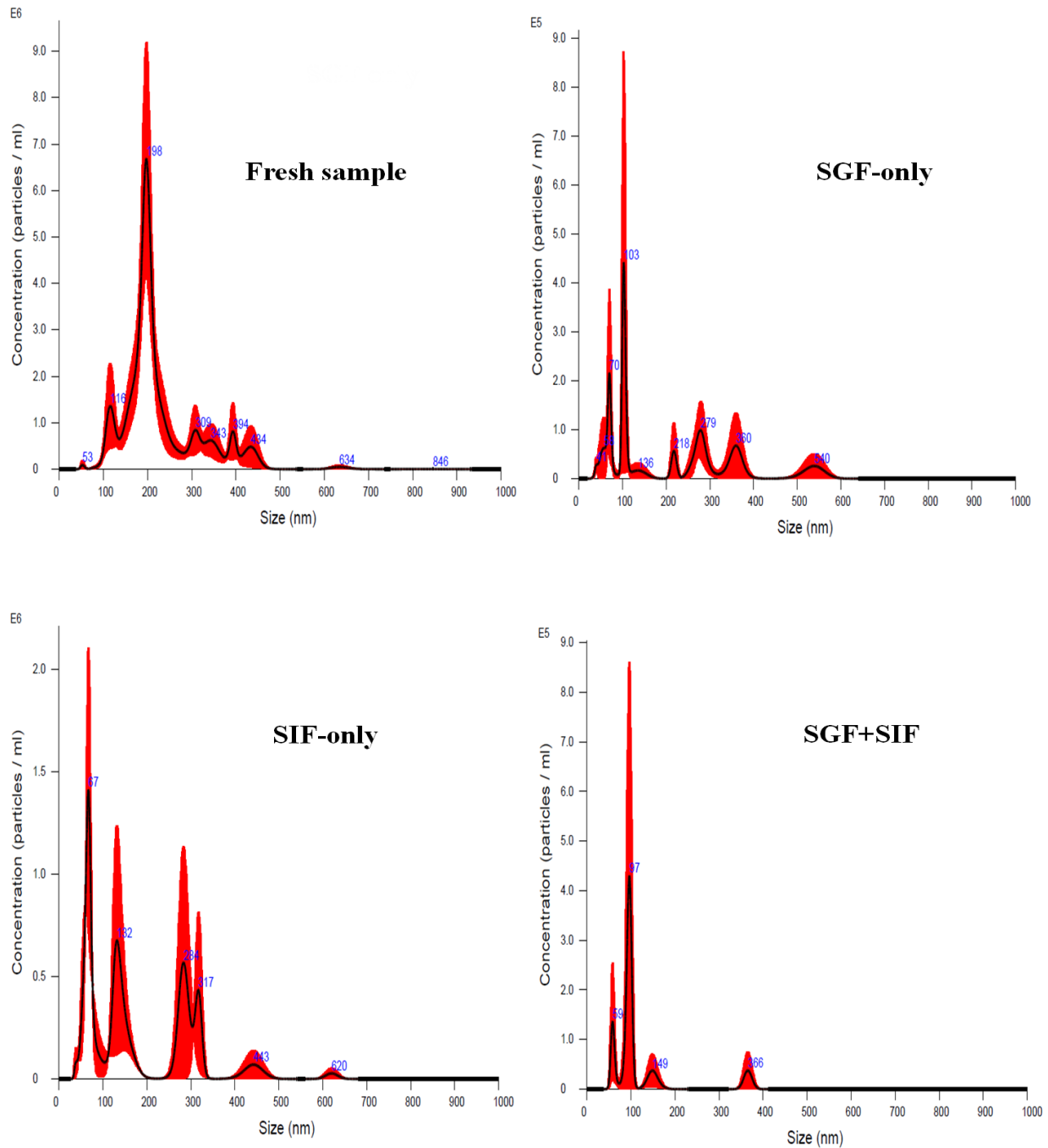


Figure 3.10 Size distribution by particle concentration of PAR SLNs, before (fresh sample) and after their incubation in simulated GI fluids (n = 3)

[Red profile shows the range of the distributions of particle size and concentration from triplicate measurements; black line signifies the average distribution]

Figure 3.11 shows the size distribution by particle concentration of fresh SSZ SLNs and after their incubation in GI fluids. The mean SLN sizes prior to and after exposure to SGF-only, SIF-only and SGF+SIF were 212.2 ± 50.0 nm, 249.1 ± 19.9 nm, 308.3 ± 38.4 nm and 337.3 ± 28.4 nm, respectively.

Of the three drugs, SSZ has the highest $\log P$ value (Section 2.4.13) and hence, it is the most hydrophobic; which could be the reason the SSZ SLNs showed a similar pattern of size change in the various media as the drug-free SLNs (Figure 3.8). This is because the two formulations have the most hydrophobic cores compared with the AmB and PAR SLNs.

Comparing DLS and NTA, the latter is time-consuming and requires more operational skills but it clearly has benefits over DLS. NTA allows for sample visualisation, it gives an approximate concentration of the particles in a sample, and it produces size data based on the Brownian motion of individual particles.

Furthermore, NTA is very accurate for sizing both monodisperse and polydisperse samples and has a considerably better resolution for different particle populations. The presence of few large particles in a sample also has little impact on the sizing accuracy of the NTA technique [Filipe *et al.*, 2010]. This is evident in the present study as much larger particle sizes were obtained using DLS as compared with NTA, although all the samples were similarly treated in the various media. Additionally, NTA proved more suitable in the present study for analysing the stability of the SLN formulations in simulated GI fluids.

SSZ SLNs

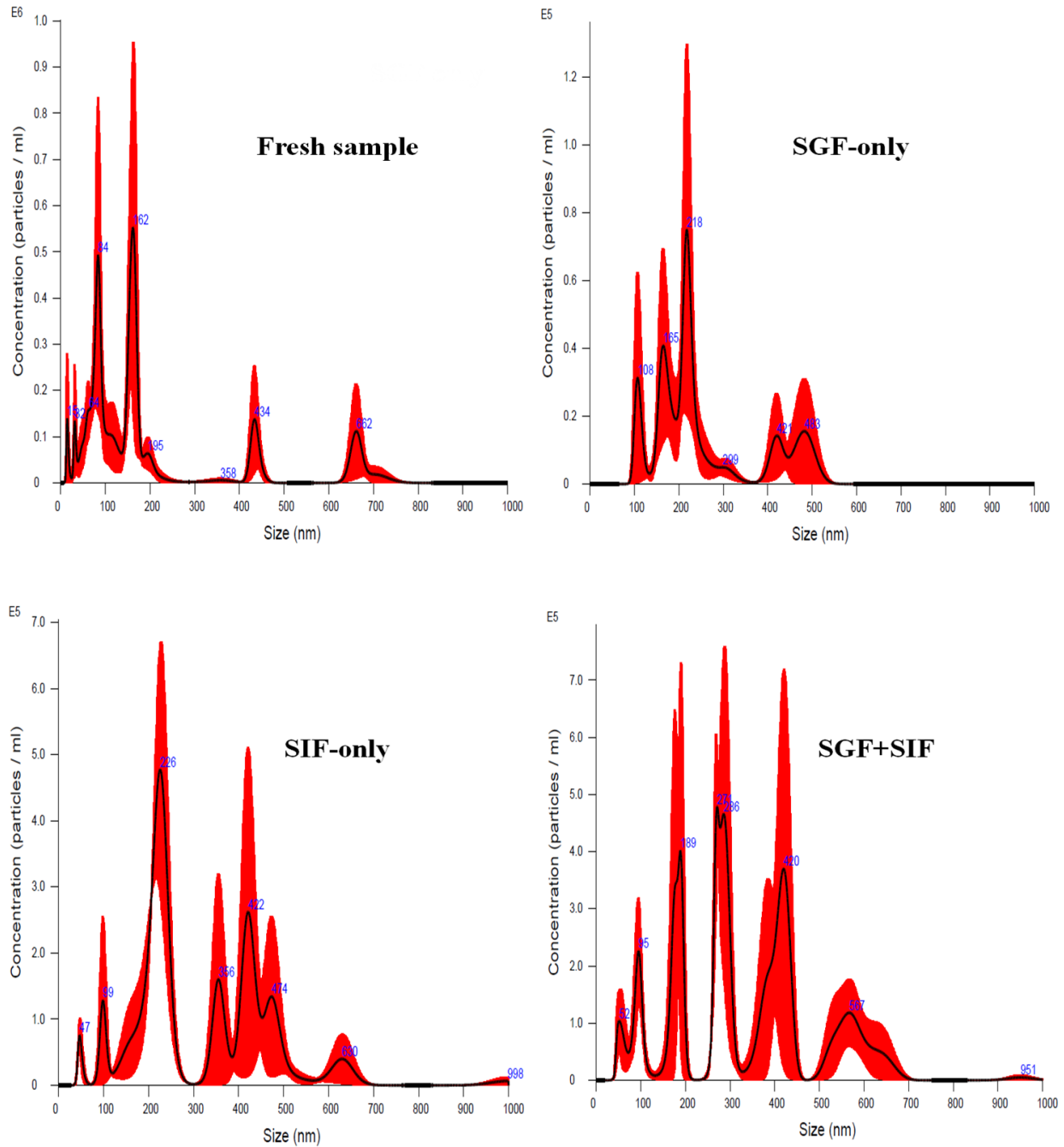


Figure 3.11 Size distribution by particle concentration of fresh SSZ SLNs, before (fresh sample) and after their incubation in simulated GI fluids (n = 3)

[Red profile shows the range of the distributions of particle size and concentration from triplicate measurements; black line signifies the average distribution]

In summary, contrasting patterns of size changes were observed for the drug-loaded SLNs in the various media. It appears that size changes were mainly based on the solubility of the incorporated drug in the simulated fluids such that, entry of the dissolution media into the SLNs caused some swelling of the particles, followed by drug dissolution in the fluid. The diffusion rate of the dissolved drug out of the particles then depended on the aqueous solubility of the drug, which resulted in the varying size changes as observed. Therefore, with PAR being the most hydrophilic, the PAR SLNs manifested a larger decrease in size due to the efflux of the drug from the SLN matrices.

Particle size is a very important factor because uptake of particulates within the GI tract is governed by size, whereby smaller particles are taken to a greater extent compared to larger ones. Particles with sizes below 10 μm are well taken up in the GI tract but uptake occurs more favourably when sizes are below 1000 nm [Jani *et al.*, 1989; Kreuter, 1991; Shakweh *et al.*, 2005]. In addition, the mesh-pore spacing of the intestinal mucosal barrier is 50-1800 nm; however, nanoparticles with sizes below 200 nm diffuse more effectively through the mucus [Lai *et al.*, 2010; Primard *et al.*, 2010].

The three SLN formulations were found to be stable in the simulated GI fluids and can therefore be deemed to be stable *in vivo* as well. The mean particle sizes and ZPs for all three formulations in the simulated media were also optimal for GI absorption meaning that the different particles would respond similarly with GI mucus and epithelia.

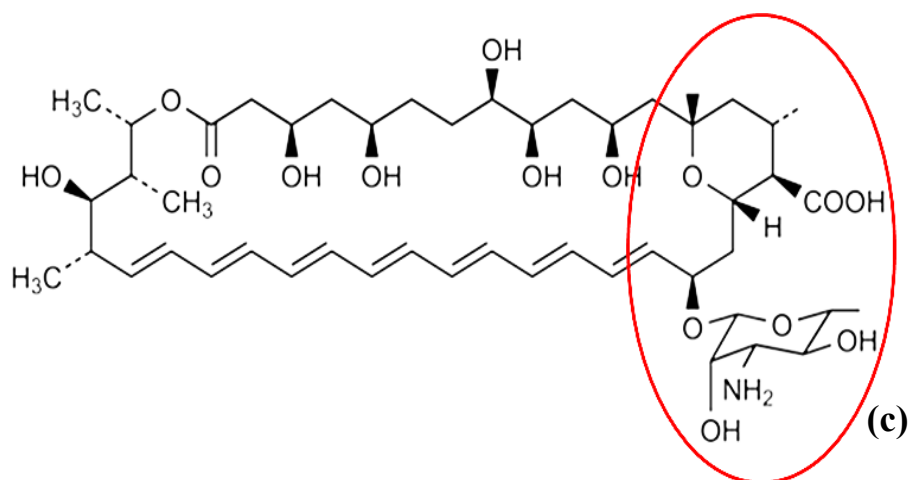


Figure 3.12 The chemical structure of AmB with the portions representing the diagnostic peaks demarcated: (a) [C₂₀H₂₇O₂]⁻ at *m/z* 299.20; (b) [C₂₀H₂₉O₂]⁻ at *m/z* 301.22; and (c) [C₁₇H₂₁NO₄]⁻ at *m/z* 303.23

Comparing pure AmB with AmB SLN, the peak intensities of the diagnostic ions in Figure 3.13 indicate that the drug is present only in a small quantity on the surface of the freshly prepared SLNs. This is a reflection of the high encapsulation efficiency of 91.2±3.04% that was obtained for the formulation in Section 2.4.12, as more of the drug is encapsulated within the matrix. As there was no drug incorporated in the drug-free particles, it could be said that the peaks corresponding to the diagnostic ions in the spectrum for the drug-free SLNs are due to the other ingredients used in preparing the nanoparticles. As a result, the peaks at *m/z* 299.20, 301.22 and 303.23 in the spectrum for the AmB SLNs could be due to the excipients in the formulation, especially since the peak intensities are higher for the drug-free particles. This further points to a very low or no AmB count on the surface of the particles untreated in the media.

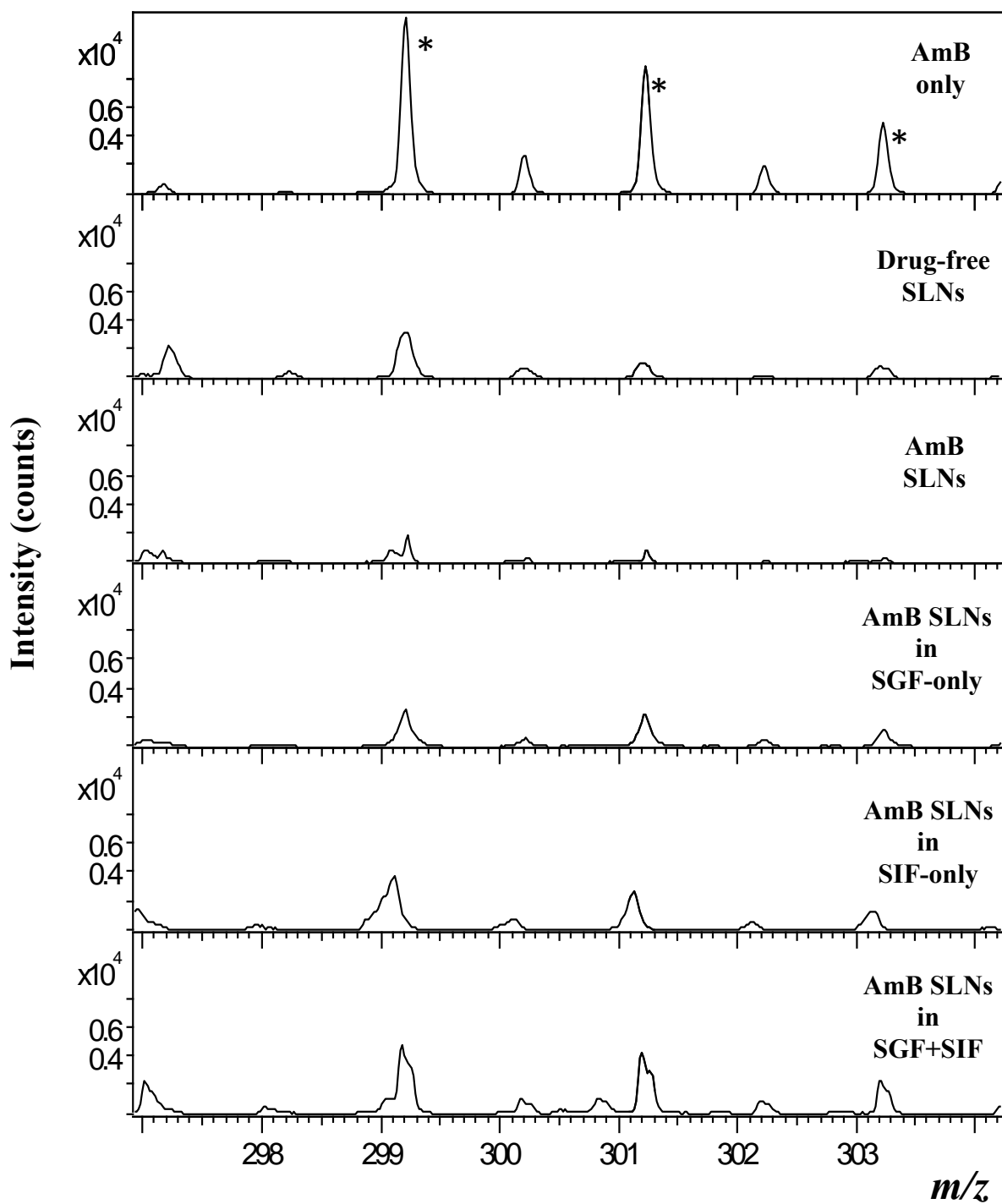


Figure 3.13 Negative ion ToF-SIMS spectra of pure AmB, drug-free SLNs, fresh AmB SLNs and AmB SLNs incubated in simulated GI fluids

Figure 3.14 compares the relative intensities of AmB on the surfaces of the fresh SLNs and after their exposure to the various media. It can be seen that higher drug counts were detected on the particles after their exposure to the media in the following order: SGF+SIF > SIF-only > SGF-only. This trend is in reverse order for decrease in the particle size of the AmB SLNs in the corresponding media (Section 3.4.2). The higher intensities of the reference peaks for the media-exposed SLNs compared to the fresh sample points to the diffusion of AmB towards the surfaces of the SLNs. It is apparent that this diffusion to the surface is most effective in SGF+SIF and least so in SGF-only. Furthermore, this observation is in concert with the assertion that the efflux of AmB from the SLN matrix results in size shrinkage.

The SLNs were washed in deionised water prior to the ToF-SIMS analyses in order to remove any free drug residing on the surface of the particles. Therefore, the ToF-SIMS data represents AmB directly associated with the matrix of the SLNs at their surfaces.

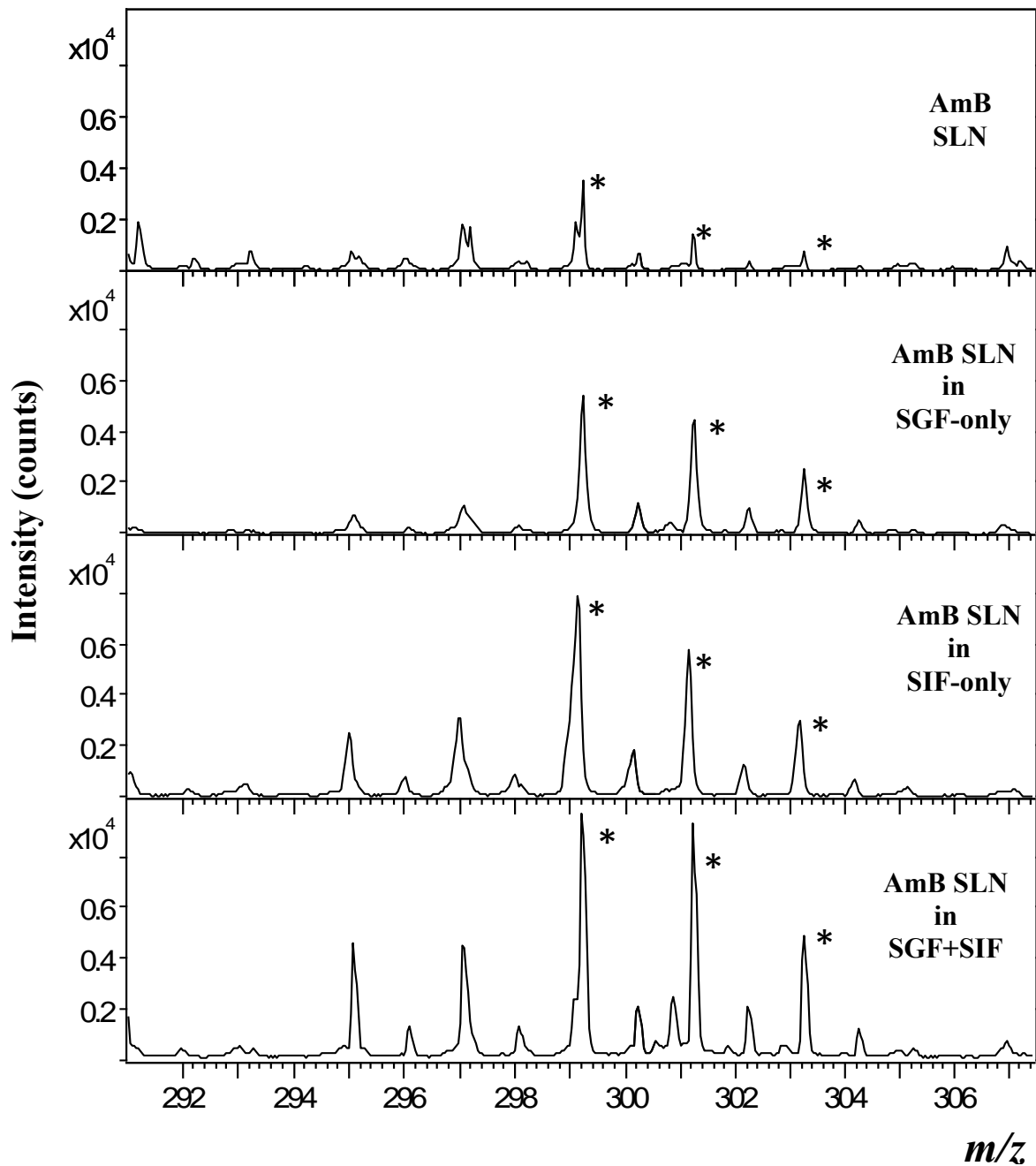


Figure 3.14 Negative ion ToF-SIMS spectra showing AmB on the surface of AmB SLNs, before and after their incubation in simulated GI fluids

The molecular formula and mass of PAR are $C_8H_9NO_2$ and 151.163 g/mol respectively. Figure 3.15 shows the chemical structure of PAR outlining the portion representing the diagnostic peak $[C_7H_7O]^-$ with m/z of 107.05.

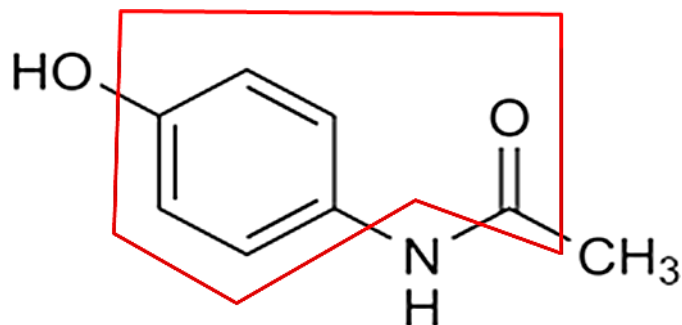


Figure 3.15 The chemical structure of PAR with a demarcation of the portion representing the diagnostic peak $[C_7H_7O]^-$ at m/z 107.05

Figure 3.16 also shows that very minimal amount of PAR was on the surface of the fresh PAR SLNs, just as was observed for the AmB SLNs. The peak at m/z 107.05 in the spectrum of the drug-free SLNs is attributable to the other ingredients within the formulation. The intensity of the diagnostic peak was higher on the PAR SLNs than on the drug-free particles; which indicates that the peak intensity observed on the fresh PAR SLNs is a combination of that for the drug itself, and that as a result of the excipients. This observation is the reverse of that detected in Figure 3.13 for AmB. Regardless, the results indicate that for the SLNs untreated in media, there is a minimal amount of PAR on the PAR SLNs unlike the AmB SLNs, which possibly had no AmB on them.

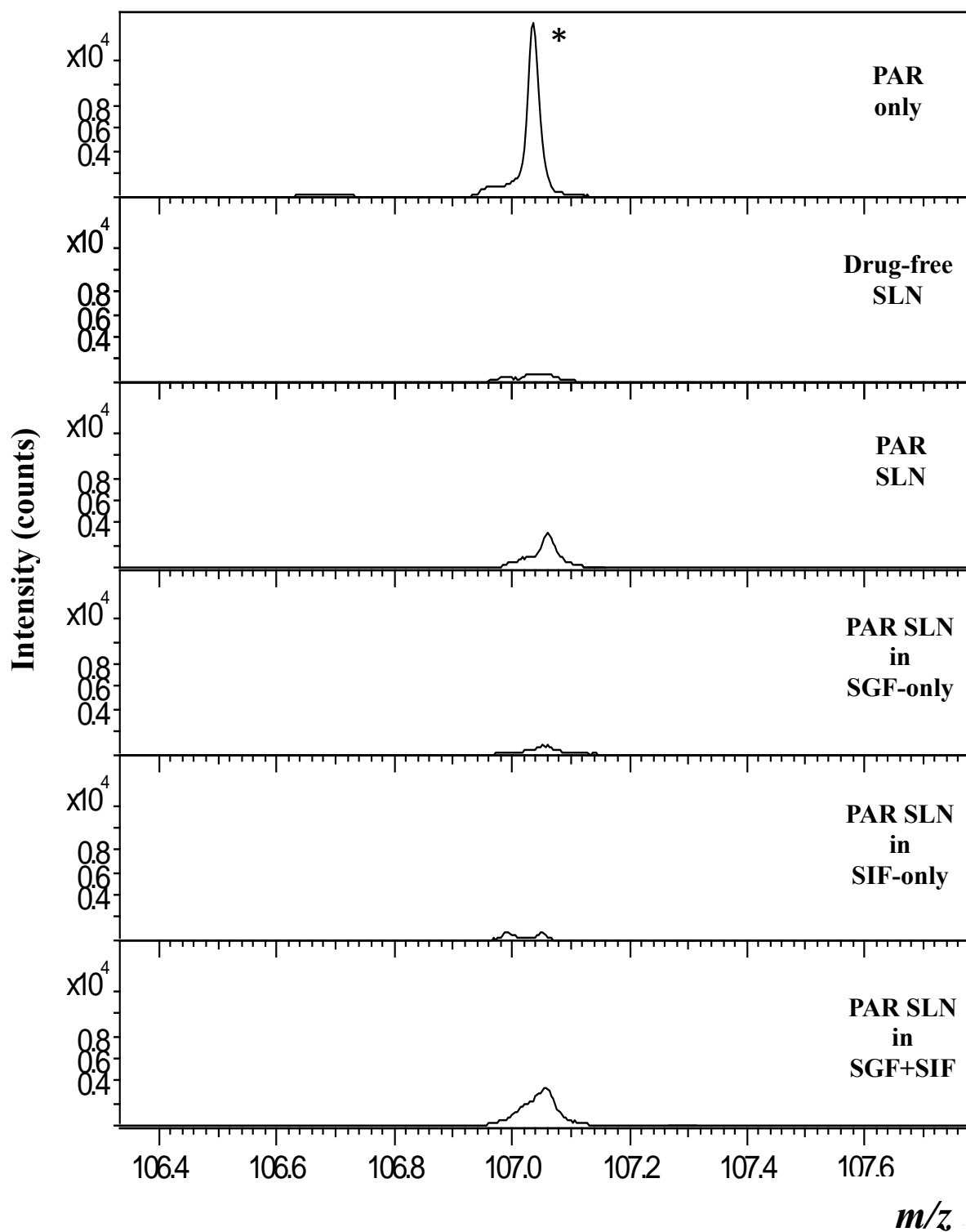


Figure 3.16 Negative ion ToF-SIMS spectra of pure PAR, drug-free SLNs, fresh PAR SLNs and PAR SLNs incubated in simulated GI fluids

Unlike the AmB SLNs, which presented a high drug count on the SLNs after exposure to the simulated media, the spectra in Figure 3.17 show a much intense PAR count on the fresh particles in comparison to those incubated in the media. The PAR SLNs had a lower encapsulation efficiency of $60.7 \pm 0.26\%$ (Section 2.4.12), which may have resulted in saturation of the unencapsulated drug attached to the surface of the fresh SLNs and hence the high drug intensity seen in the spectrum.

PAR is hydrolysed in acidic solutions to produce 4-aminophenol and acetic acid; however, these products have different masses and would therefore not contribute to the signal intensity at m/z 107.05. This would manifest as low PAR intensity on the particles in SGF-only as compared with the fresh particles. PAR is very soluble at the pH of SIF, which favours drug release and dissolution in the medium resulting in an equally low drug count on the particles. As with the AmB SLNs, the highest drug intensity was detected on the PAR SLNs after incubation in SGF+SIF which indicates the latter as the best dissolution medium for both drugs, and also explains why the two SLNs had the smallest size in that medium (Figure 3.8).

The mean size (based on the NTA data) of the PAR SLNs after exposure to the media decreased in the order, SGF-only > SIF-only > SGF+SIF, and drug intensity on the SLNs was in the order, SIF-only < SGF-only < SGF+SIF. From Figures 3.8 and 3.17, the mean sizes of the PAR nanoparticles in SGF-only and SIF-only are comparable (185.4 ± 53.9 nm and 182.7 ± 27.2 nm, respectively). In addition, the intensity of the diagnostic peak is similar in the two media albeit slightly lesser in SIF-only, unequivocally signifying that amount of drug released from the particles in a medium is inversely related to the ultimate size of the particles.

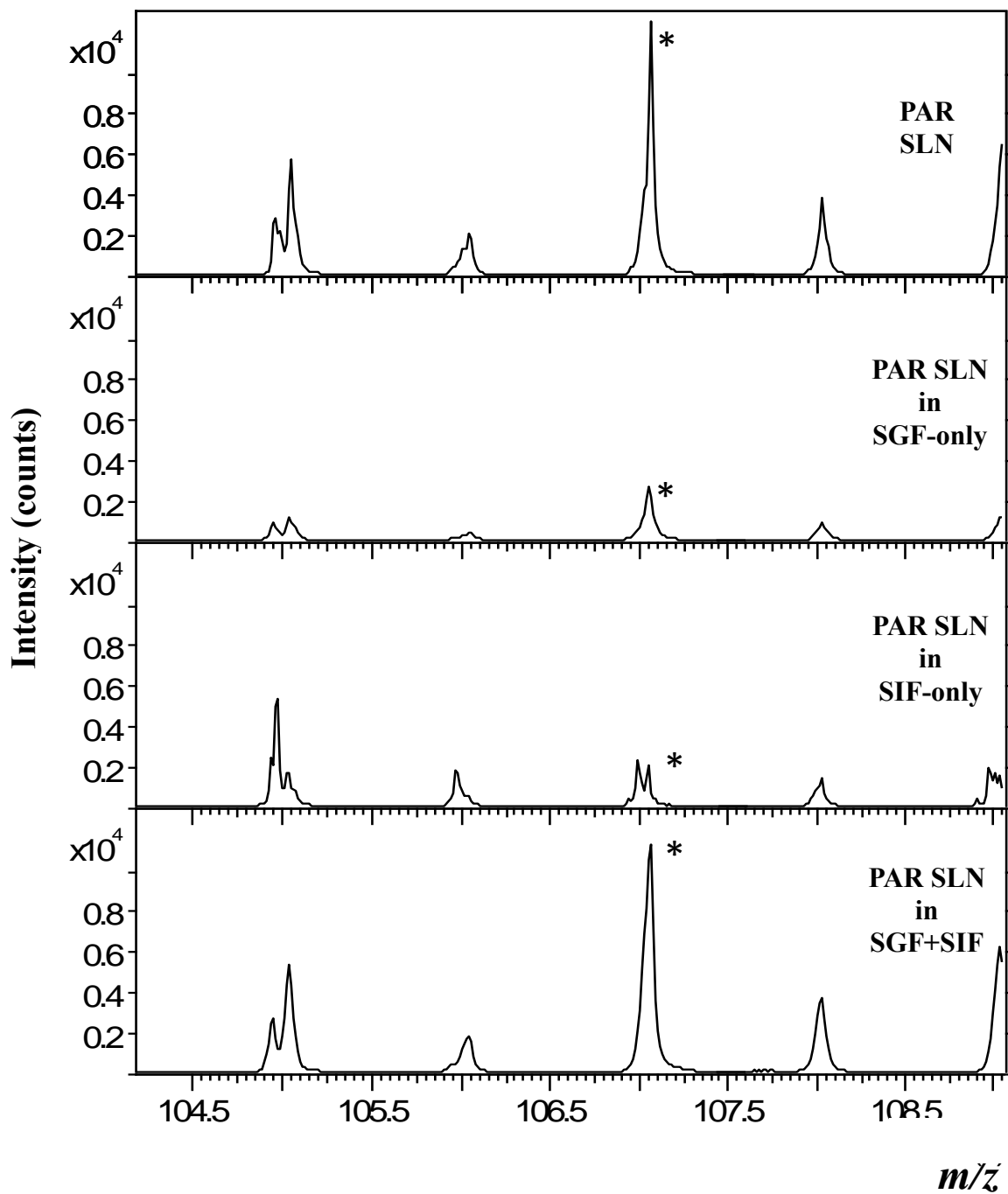


Figure 3.17 Negative ion ToF-SIMS spectra showing PAR on the surface of PAR SLNs, before and after their incubation in simulated GI fluids

In the case of SSZ, the entire molecular ion was used as the diagnostic anion as it was the most intense peak on observing the whole mass spectrum of the drug. The molecular formula and mass of SSZ are $C_{18}H_{14}N_4O_5S$ and 398.393 g/mol, respectively, therefore its molecular ion is $[C_{18}H_{13}N_4O_5S]^-$ and the peak location is m/z 397.09. The fresh SSZ SLNs showed minimal amount of drug on the particle surface as seen in Figure 3.18, just as was the case for the other formulations.

After incubation in the media, it could be seen from Figure 3.19 that the SSZ diagnostic peak was absent in the mass spectrum for the particles in SIF-only, and there was a higher drug intensity on the particles in SGF+SIF than in SGF-only. The signal intensity was highest on the fresh SLNs pointing to a strong SSZ-lipid hydrophobic interaction after the particles were formulated. The absence of any burst release as evidenced in the *in vitro* release study in Section 2.4.13 further suggests that the drug was not loosely attached at the SLN surface.

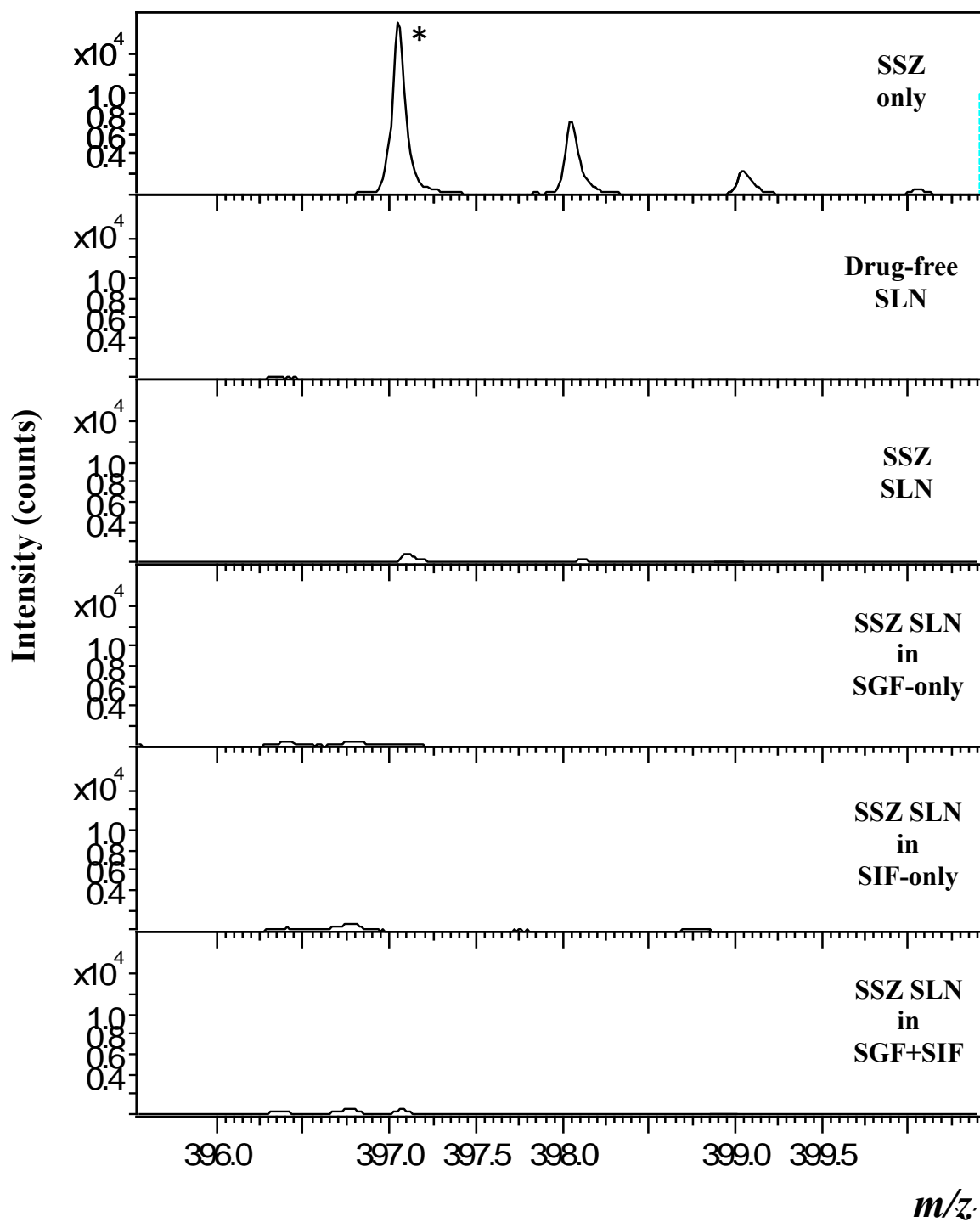


Figure 3.18 Negative ion ToF-SIMS spectra of pure SSZ, drug-free SLNs, fresh SSZ SLNs and SSZ SLNs incubated in simulated GI fluids

In ToF-SIMS analyses, there could be suppression or enhancement of the signal of one molecule in a mixture due to the presence of other molecules or perhaps due to interactions among the compounds present. The ionisation of a molecule can therefore be affected to a large extent by its chemical environment, which is known as “the matrix effect” however, this is exploited in matrix-enhanced SIMS (ME-SIMS).

There are a number of techniques used to address signal suppression, with applications to film and cell preparations, such as washing samples with ammonium formate, ethanol or water prior to analyses. Samples could also be prepared and analysed in a frozen-hydrated state, which is the only procedure that has shown the most useful results [Jones *et al.*, 2007; Jones *et al.*, 2008; Piwowar *et al.*, 2009]. In the present study, using ammonium formate was avoided to prevent the introduction of more ions into the samples. Ethanol was also not used because PAR is completely soluble in it and SSZ has partial solubility in it; which would negatively affect the signal intensities of the diagnostic ions. The samples could not be frozen-hydrated as well as that would have made incubation in the simulated media unfeasible, leaving washing with water as the only choice. In a study by Piwowar *et al.* (2009), washing with water or ammonium formate was however found to reduce secondary ion yield from arginine films which were not exposed to any chemical environment and did not therefore require washing (i.e. control samples), showing that washing may be deleterious and not suitable for all sample types.

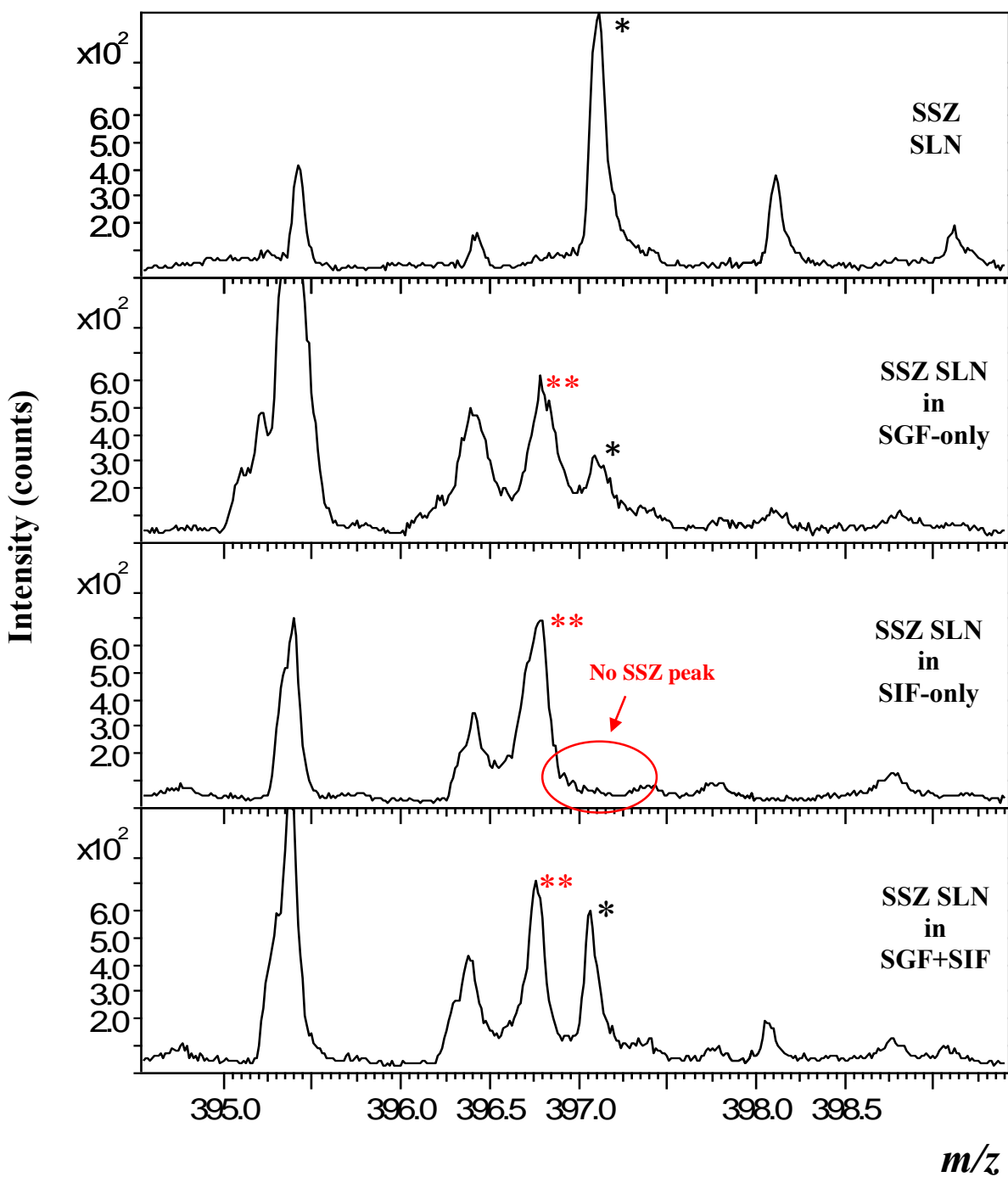


Figure 3.19 Negative ion ToF-SIMS spectra showing SSZ on the surface of SSZ SLNs, before and after their incubation in simulated GI fluids

[** - New peak appearing in spectrum possibly due to a “matrix effect”]

This “matrix effect” could be the reason the $[\text{C}_{18}\text{H}_{13}\text{N}_4\text{O}_5\text{S}]^-$ ion was not detected in the spectrum for the SSZ SLNs in SIF-only. SGF contains NaCl (2.0 g/L) and HCl (2.917 g/L), while SIF contains NaOH (0.616 g/L) and KH_2PO_4 (6.8 g/L). Since Na^+ ions are present in either medium and SGF+SIF contains some amount of KH_2PO_4 , the massive suppression of the SSZ ion signal in SIF-only resulting in its absence in the spectrum could be due to the presence and high concentration of the K^+ and H_2PO_4^- ions.

In a study by Yang *et al.* (2013), none of the cluster primary ions [C_{60}^+ , Ar_n^+ or Bi_3^+] used in sputtering Au/ SiO_2 nanoparticles produced SIMS profiles that were easily explicable. The authors observed the appearance of other structures; some of which were not related to any of the ingredients used to prepare the nanoparticles. A similar observation is recorded here for the SSZ SLNs in the simulated media where there is a peak occurring at m/z 396.7 in each spectrum (red asterisks), close to the position of the diagnostic peak but this is absent in the spectra for the pure drug and the drug-free and fresh SSZ SLNs (Figures 3.18 and 3.19). This could be the result of a “matrix effect”. In the study by Yang *et al.* (2013), the main issue of concern was that melting of the nanoparticles occurred during ion bombardment as were also evident from the SEM images they took before and after sputtering. Meaningful ToF-SIMS analyses on heat sensitive samples therefore requires efficient interventions of controlling any heat (heat sinking) produced due to the kinetic energy of the ion beam, in order to prevent melting and thereby obtain more reliable data [Yang *et al.*, 2013].

Depth profiling of samples is used to obtain ion concentration/intensity data as a function of depth within a sample. In this study, depth analyses were conducted on the fresh SLN formulations. Figure 3.20 shows the molecular ion depth profiles of the three diagnostic ions for AmB. All the three profiles are seen to generally decrease in concentration with increasing sputtering time,

which suggests that the drug is more concentrated closer to the shell of the particles, and decreases towards the core. For the $[\text{C}_{20}\text{H}_{29}\text{O}_2]^-$ and $[\text{C}_{17}\text{H}_{21}\text{NO}_4]^-$ ions however, a more random pattern in drug counts was observed. The intensity of $[\text{C}_{20}\text{H}_{27}\text{O}_2]^-$ was highest of the three diagnostic ions as was observed in the mass spectrum in Figure 3.13. Although the three ions are all representative of the drug, they did not exhibit the same profile because they represent different portions of the drug's structure, corresponding to the ions from different functional groups, and are therefore likely to interact differently with the excipients in the formulation. In this case, the ingredients in the formulation aside the drug could be considered as causing artifacts in the data resulting in a "matrix effect".

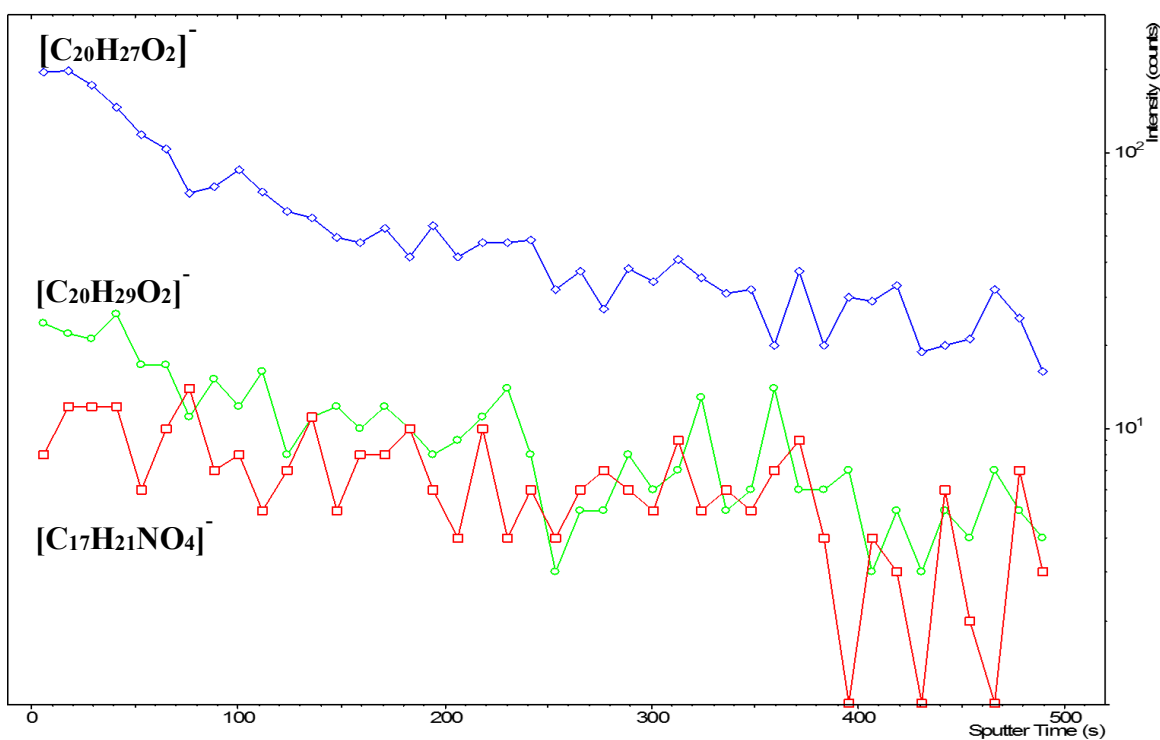


Figure 3.20 Molecular ion depth profiles of $[\text{C}_{20}\text{H}_{27}\text{O}_2]^-$, $[\text{C}_{20}\text{H}_{29}\text{O}_2]^-$ and $[\text{C}_{17}\text{H}_{21}\text{NO}_4]^-$ obtained from the AmB SLNs

Figure 3.21 depicts the profile for $[C_7H_7O]^-$, which also shows a random pattern in PAR concentration across the sample however, the trend is more of a decrease in drug intensity with sputtering.

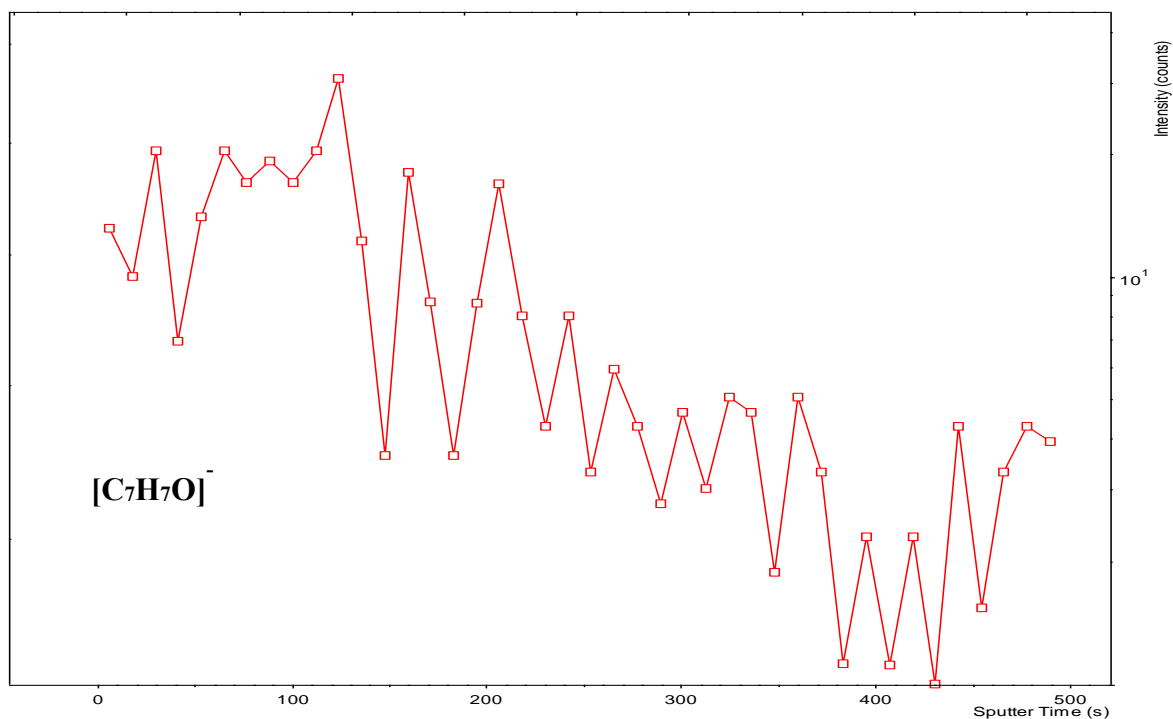


Figure 3.21 Molecular ion depth profile of $[C_7H_7O]^-$ obtained from the PAR SLNs

The depth profile of $[C_{18}H_{13}N_4O_5S]^-$, which is diagnostic of SSZ, as depicted in Figure 3.22 shows a different pattern as compared with those for AmB and PAR. The intensity of $[C_{18}H_{13}N_4O_5S]^-$ initially decreases and rises gradually, forming a crater-like appearance and this was followed by an irregular but increase in drug concentration till the end of the sputtering.

The sputtering of particles occurs differently from that of films or bulk materials, and this is particularly true for smaller particles such as nanoparticles. As such, the sputter depth profiling did not seem to be the optimum approach to obtain layer or depth information on the SLNs.

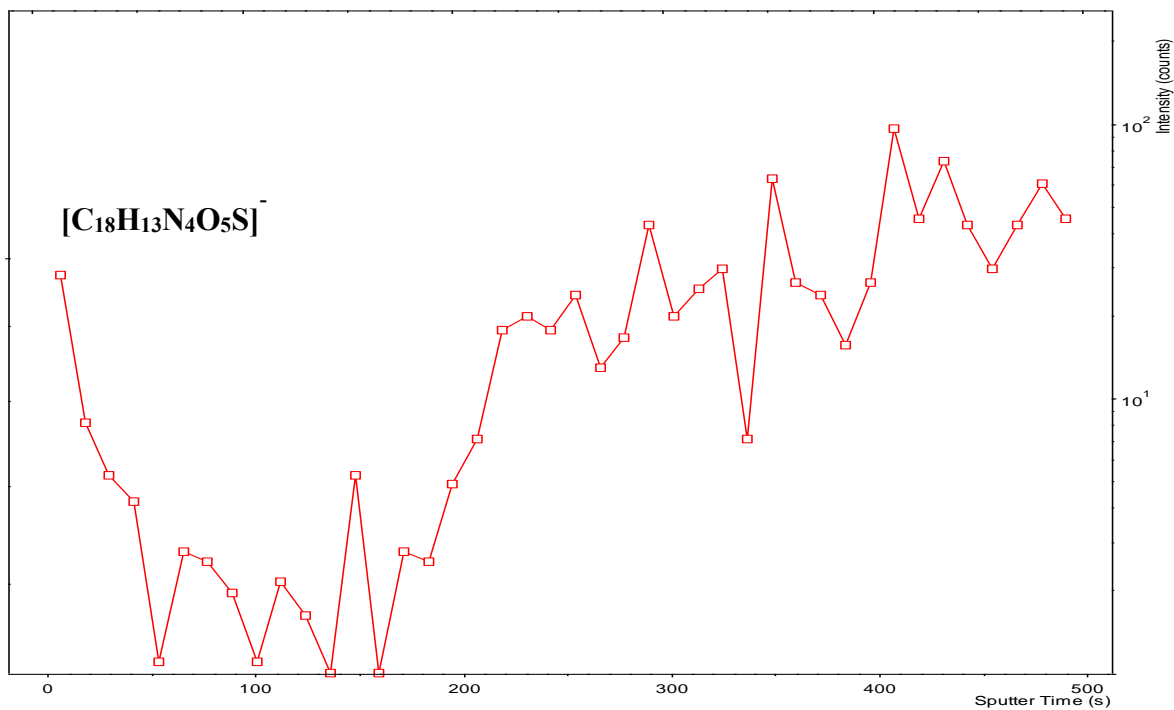


Figure 3.22 Molecular ion depth profile of $[C_{18}H_{13}N_4O_5S]^-$ obtained from the SSZ SLNs

This is because nanoparticles and the bulk forms of their ingredients are different in terms of optical properties, reactivity and electrical conductivity among others, which are caused by the differences in size, shape or molecular arrangements, surface area, agglomeration state and surface or bulk chemistry [Baer *et al.*, 2008; Yang *et al.*, 2013]. This variation may be what accounts for the peak-trough phenomenon observed. The properties of nanoparticles may also be altered in a medium or during a particular process and result in unintended consequences [Grassian, 2008] for instance, the ion beam in SIMS could be destructive in analysing lipid nanoparticles because melting and resolidification may occur and cause significant structural changes [Yang *et al.*, 2013].

In the depth profiling, it was expected that drug intensity counts would increase with sputtering time because *in vitro* studies had revealed a slow rate of drug release in PBS for all three SLNs,

especially for AmB and SSZ (Section 2.4.13). The AmB SLNs showed a high drug intensity on the surface after exposure to the simulated media, according to the ToF-SIMS spectra in Figure 3.14; however, the depth profiles did not show increasing drug intensity with sputtering time. PAR and SSZ SLNs also showed higher drug intensities on the surface of their respective fresh SLNs as compared with after incubation in simulated media yet, both formulations showed different depth profile patterns. Again, for the PAR SLNs, drug count on the particles before and after incubation in SGF+SIF was similar and suggestive of a somewhat constant drug release; as well as a drug-concentrated particle core however, this was not reflected in the depth profile.

The peak and trough pattern in drug intensity observed in the depth profiles is attributable to the roughness or non-uniform nature of the layer of deposited particles when a drop of SLN suspension was placed on the silicon wafer. As the dispersion medium evaporates prior to the analyses, the particles pack to form an uneven layer so that layer-by-layer scans give a variable expression of drug deposition. A depth profile similar to those obtained in the present study was reported by Cheng and Winograd (2005) for a peptide-trehalose film sample, which had an irregular surface due to crystallisation.

As the top (a few nm) of the SLN samples were etched off in the depth analyses, different surfaces and heights of the packed particles were encountered, containing varying drug amounts that could have resulted in the profiles obtained. It could therefore be concluded that a single layer of particles tightly packed together to form a film-like layer and having a fairly flat surface would be more suitable for a depth profile study of nanoparticles. Notwithstanding, the depth profile analyses coupled with the spectral data have provided us with some indication of mass transfer of the drugs within the SLNs when these are placed in simulated GI media.

3.5 Conclusions

The data obtained indicate that after placement of the SLNs in the simulated GI media, there was an inflow of the fluids into the SLNs followed by outward diffusion of the dissolved drug. The rate of the diffusion however depended on the solubility of the loaded-drug in the particular medium. As a result of this, there was an increase in the size (NTA) of the drug-free SLNs since the main mass transfer was the diffusion of the media into the SLNs and no drug diffusion out of the particles. In the case of the SLNs containing SSZ, which is the most hydrophobic drug, there was an increase in size due to a slow rate of dissolution and diffusion of the drug payload while the reverse was true for PAR, which has the highest aqueous solubility of the three drugs. The study showed NTA to be a more suitable technique for analysing the stability of the SLNs in the various media as compared with PCS, which was biased towards larger particles and produced data suggestive of high particle aggregation particularly in SGF-only. The data obtained indicate that the SLNs may aggregate in the stomach after oral ingestion; however, on reaching the small intestine, both size and surface charge of the particles would be optimal for absorption, which indicates good stability.

The mass spectra coupled with the depth profiles obtained from the ToF-SIMS analyses indicated that drug loading into the SLNs possibly followed the core-shell model, and that the AmB SLNs may have a drug-enriched core.

CHAPTER 4

DEVELOPMENT AND VALIDATION OF A HIGH-PERFORMANCE LIQUID CHROMATOGRAPHY METHOD

4.1 Introduction

Validation of analytical methods is an important regulatory requirement in pharmaceutical analyses. High-performance liquid chromatography (HPLC) is commonly used as an analytical technique in developing and validating assay methods for drug products and drug substances [Shabir, 2004].

HPLC is an advanced form of liquid chromatography that may be used in separating a mixture of compounds by passing a solution of the compounds through a column of very packed particles called the stationary phase, in order that the analytes are retained individually [Crawford Scientific, 2015(b)]. Compound separation occurs because each constituent has a different affinity for the stationary phase. Stronger interactions result in longer retention times and hence, slower movement of an analyte through the column and vice versa.

In reversed-phase HPLC (RP-HPLC), a mobile phase more polar than the stationary phase is used as opposed to normal phase HPLC in which a polar stationary phase is used with a less polar mobile phase [Crawford Scientific, 2015(b)]. Stationary phases for RP-HPLC are hydrophobic and usually chemically bonded to the surface of silica support particles. For neutral analytes, the mobile phase consists of water, and an organic solvent that is used to modify the retention of analytes by reducing the polarity of the mobile phase. Analysis of ionisable compounds requires the use of buffers and other additives in the aqueous phase to control retention and peak shape.

Increasing the water content in the mobile phase results in repulsion of hydrophobic analytes out of the mobile phase and onto the non-polar stationary phase, on which they reside until they partition out into the mobile phase again.

The development of an analytical method comprises evaluation and optimisation of the various stages in the sample preparation, chromatographic separation, detection and quantification of the analytes [Shah *et al.*, 1992]. On the other hand, validation of the method is essential as it serves as documented evidence that a specifically developed analytical method is suitable for its planned use, and involves a set of procedures for the collection, processing, storing and analysis/quantitative determination of an analyte or group of analytes in a matrix. Validation test methods have to basically document the accuracy, sensitivity, specificity, reproducibility, linearity and range among other attributes. Ideally, the sample extraction procedure has to be time-economical and give the highest possible recovery with acceptable accuracy and precision. Method performance is determined primarily by the quality of the developed procedure itself [Shah *et al.*, 1992].

An internal standard (IS) is usually employed in bioanalytical assays to compensate for losses during sample extraction and to eliminate the error caused by possible disparities in injection volumes; because variations in the latter significantly affect results especially when the injection volume is small [Jones, 2009]. A fixed volume of an IS of no critical concentration is usually added to all standards and samples with the principle that, if a smaller or larger injection volume is used, the ratio of the peak response of analyte to IS will be the same. Selection of a suitable IS is based on the following: it must be detected/excited at the same wavelength as the analyte, in the case of UV/fluorescence detection; it must be soluble in the same sample solvents; and it must not be a degradation product of the analyte [Jones, 2009].

Data on the transit behaviour of dosage forms through the GI tract is essential in determining possible absorption windows of the drug payload. This information can in turn be used to optimise desirable properties from the dosage form with a view to improving drug bioavailability. The GI transit properties of dosage forms can be studied directly using gamma scintigraphy, nuclear magnetic resonance and other radiographic methods but all these require the use of expensive equipment or harmful radiation. An indirect means of studying GI transit properties of dosage forms using marker drugs provides a less costly alternative and has been used successfully by researchers [Peh and Yuen, 1996; Kondo *et al.*, 2003(a,b); Rahman *et al.*, 2005].

A vital component in utilising the indirect GI transit estimation of dosage forms based on the use of marker drugs is that a suitable analytical method is developed and validated to be sufficiently sensitive to detect minute drug concentrations. A further desirable requirement is the simplicity of the method, given that several drugs would have to be analysed. This chapter focusses on the development of a simple and sensitive RP-HPLC method for the simultaneous assay of AmB, PAR SP and an IS in rat plasma, for use in a subsequent study to determine the GI transit and pharmacokinetic data of AmB following oral administration of AmB SLNs to rats.

4.2 Materials

Acetonitrile was purchased from Duksan Pure Chemicals Co. Ltd. (Ansan, Korea). Paracetamol, dimethyl sulphoxide (DMSO) and sulphapyridine were purchased from Sigma-Aldrich (St. Louis, MO, USA), and amphotericin B from Nacalai Tesque (Kyoto, Japan). Methanol and ethanol were purchased from Thermo Fisher Scientific. Water was Milli-Q 18.2 M Ω ·cm at 25°C (Millipore Corp., Bedford, USA). Acetic acid and sodium acetate trihydrate were purchased from R & M

Chemicals (Essex, UK). All reagents and solvents used were of analytical and HPLC grades respectively.

4.3 Methods

4.3.1 HPLC instrumentation and conditions

A Perkin Elmer HPLC system (Series 200 auto-sampler, Series 200 UV/VIS detector, Waltham, MA, USA) configured to TotalChrom[®] Navigator software was used to analyse drug samples in the rat plasma. Separation of peaks was achieved using a ZORBAX Eclipse Plus[®] C18 (250 x 4.6 mm, 5 μ m) column (Agilent Technologies, Santa Clara, CA, USA). The mobile phase comprised of: acetate buffer (pH 4) [A], prepared by mixing 847 mL of 0.1 M acetic acid and 153 mL of 0.1 M sodium acetate trihydrate [Lambert and Muir, 1955], and the resulting mix vacuum filtered with a 0.2 μ m filter paper; and acetonitrile [B]. The mobile phase was run at a flow rate of 1 mL/min in gradient mode as follows: 100% A from 0-0.5 min; 60% A from 0.5-7 min; 20% A from 7-9 min; 60% A from 9-12 min and 100% A from 12-15 min. The HPLC was run in a two-step injection mode to detect PAR and SP at 254 nm and then AmB at 405 nm. A 5- μ g/mL piroxicam solution in a 1:1 methanol-ethanol mixture was used as internal standard (IS). The IS was detectable at both wavelengths. The methanol-ethanol mixture also served as the deproteinising agent for the plasma samples.

4.3.2 Plasma standards

Stock rat plasma solutions containing AmB, PAR and SP at 100 µg/mL, 200 µg/mL and 1000 µg/mL, respectively, were prepared by spiking the appropriate amounts of the respective drug solutions into the appropriate volumes of rat plasma. The stock solutions were further diluted with blank rat plasma to prepare the calibration standards for each drug. The samples were prepared at three concentration levels for each drug representing low (LC), mid-range (MC) and high (HC) concentrations. The LC, MC and HC for AmB were 0.05, 0.25 and 10 µg/mL; for PAR were 0.5, 2.5 and 100 µg/mL; and for SP were 0.1, 0.5 and 20 µg/mL, respectively.

4.3.3 Plasma sample preparation

Samples for drug analyses were prepared by transferring 100 µL of plasma and 150 µL of the IS solution into microcentrifuge tubes. The tubes were vortex-mixed for 5 min and the extracts centrifuged at 14 000 rpm for 10 min. The clear supernatants were aspirated and filtered through a 0.20 µm syringe filter followed by direct injection onto the HPLC system.

4.3.4 Specificity

The specificity of the analysis was first performed by visually observing the chromatograms for individual as well as combined solutions (drug dissolved in solvent) of pure AmB, PAR, SP and the IS at their respective detection wavelengths. This was followed by examining chromatograms for blank plasma samples to detect any possible peak interferences at the retention times of the analytes. The final step of this procedure involved obtaining chromatograms of the analytes spiked

in plasma. These steps are necessary to ensure that the analytes, both as pure drug solutions or spiked into plasma elute at similar times and that the elution of one component is not affected by the other, to indicate that the method is specific for the analytes.

4.3.5 Linearity and range

Calibration curves for AmB, PAR and SP in drug spiked-plasma were obtained over the following concentration ranges: 0.05-10 µg/mL, 0.5-100 µg/mL and 0.1-20 µg/mL, respectively. The calibration curves were constructed using the ratio of the peak signal of each drug concentration to that of the internal standard, versus the corresponding drug concentration. Each analysis represents a replica of six runs.

4.3.6 Precision

The within-day and between-day precision of the analyses at each concentration for each drug was determined to investigate the repeatability and reproducibility of the method, as a measure of the percentage coefficient of variation (%CV) using the following relationship:

$$\%CV = \frac{\text{Standard deviation (SD)}}{\text{Mean concentration}} \times 100\% \dots \dots \dots \text{Equation 4.1}$$

Each mean value represents a replica of six determinations.

4.3.7 Accuracy

The within-day and between-day accuracy of the analyses is a measure of the disparity between the actual and measured concentrations of the drugs to estimate the reliability of the results obtained from using the assay method. This was determined as the relative error at each concentration for each drug using the following relationship:

$$\text{Relative error (E}_r\text{)} = \frac{\bar{x} - x_t}{x_t} \times 100\% \dots \dots \dots \text{Equation 4.2}$$

Where: \bar{x} = measured concentration (average) and x_t = true concentration

4.3.8 Recovery

The recoveries of AmB, PAR and SP from spiked plasma following the extraction procedure were determined by comparing the peak signal of each drug from the prepared plasma samples with that of pure drug samples in a solvent mixture of DMSO and methanol. Six determinations were done for each drug covering the three concentration levels stated in Section 4.3.2. The percentage recovery was determined using the following relationship:

$$\% \text{Recovery} = \frac{\text{Concentration of drug in spiked plasma}}{\text{Concentration of pure drug solution}} \times 100\% \dots \text{Equation 4.3}$$

4.3.9 Limits of detection and quantification

The sensitivity of the method was estimated in terms of limit of detection (LOD) and limit of quantification (LOQ), which were determined as the lowest amount of each analyte at which the peak signal to noise ratios (S:N) were 3:1 and 10:1, respectively [Shabir, 2004].

4.4 Results and discussion

4.4.1 Selection of internal standard (IS)

As previously mentioned, an IS must absorb UV light at the same wavelength as an analyte and have similar solvent solubility characteristics with the analyte [Jones, 2009]. This means that a compound with similar structural properties as the analyte may be the quickest choice. N-acetyl-AmB was used as IS for AmB in an HPLC analysis by Granich *et al.* (1986) however, the former is costly and not readily available. Due to the absorption wavelengths of PAR and SP being different from that of AmB, N-acetyl-AmB or other compounds with structural similarities as AmB would be unsuitable for the present analyses because the ideal IS would be a compound detectable at both 254 and 405 nm.

Internal standards that have been used in HPLC analysis of AmB as a single entity include natamycin [Lambros *et al.*, 1996], piroxicam [Campanero *et al.*, 1997; Echevarría *et al.*, 1998], 1-amino-4-nitronaphthalene [Eldem and Arican-Cellat, 2001], α -naphthol [Italia *et al.*, 2009(b)] and lornoxicam [Chakrabarty and Pal, 2011]. Natamycin, lornoxicam and 1-amino-4-nitronaphthalene were excluded because they do not absorb UV light at 254 nm. Piroxicam and α -naphthol were therefore selected for analyses. HPLC chromatograms of piroxicam and α -naphthol showed the former to be a better choice as it produced more prominent peak responses.

Figure 4.1 shows a representative chromatogram of a solution containing 125 $\mu\text{g/mL}$ each of α -naphthol and piroxicam. The peak response for piroxicam is 8.8-fold greater than that for α -naphthol. The retention times obtained were 8.8 and 9.7 min for piroxicam and α -naphthol, respectively. The chromatogram is representative of the peak responses of the compounds at both 254 and 405 nm and clearly shows piroxicam to be a better IS option, as it has a better response

compared to α -naphthol at an equivalent concentration. Piroxicam was therefore selected as IS for the subsequent analyses.

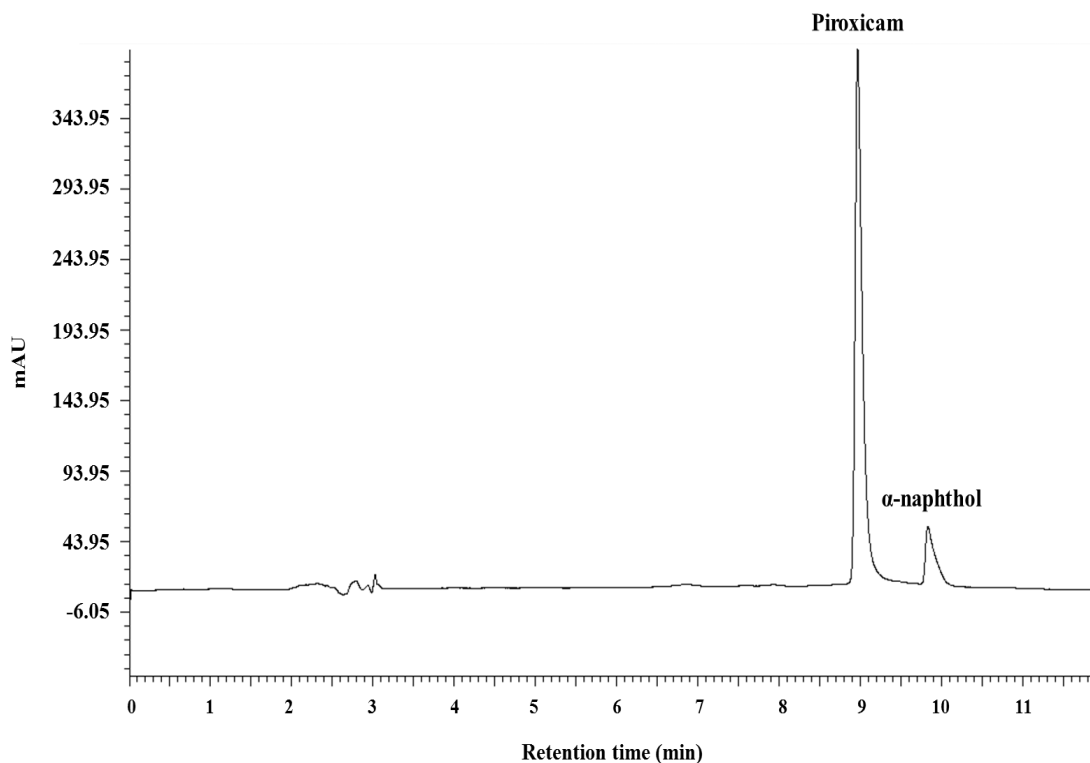


Figure 4.1 Chromatogram for piroxicam and α -naphthol (125 $\mu\text{g}/\text{mL}$ each), showing piroxicam as the preferred IS for the HPLC analyses

4.4.2 Mobile phase composition and elution method

Isocratic elution is the term used if the composition of a mobile phase system in an HPLC analysis remains constant throughout the separation of the analytes, while the reverse is true for gradient elution [Barkovich, 2015]. In the latter, all the compounds in a sample mix can be eluted in a shorter time as compared with isocratic elution. This is because maintaining the same proportion of solvents in a mobile phase system for HPLC analysis of compounds with different solvent solubilities requires a long run time, sufficient to allow interaction of hydrophobic analytes with

the stationary phase prior to their elution or partitioning back into the mobile phase. On the other hand, by changing the ratio of polar to non-polar solvents in the mobile phase during a sample run, various compounds covering a wide range of polarities can interact faster with the stationary phase with shorter retention times. In general, isocratic or gradient elution can be used for separating a mix of analytes and provided that all other conditions are optimal, peak resolution can be maintained in both methods. This leaves the technique of choice to the results from preliminary studies as well as the polarity range of the analytes. As non-polar compounds interact strongly with the stationary phase resulting in long retention times, gradient elution is a better choice for HPLC analyses of polar and non-polar compounds since this has the capability of allowing for a shorter run time while ensuring that peaks are well resolved.

A search through literature revealed an HPLC method using 1.8% tetrahydrofuran in 0.01 M sodium acetate buffer adjusted to pH 4.5 with glacial acetic acid as the mobile phase for analysing PAR and SP [Rahman and Niaz, 2004]. For AmB, organic solvents such as methanol and acetonitrile have been used together with aqueous solutions such acetate or phosphate buffers [Lambros *et al.*, 1996; Campanero *et al.*, 1997; Italia *et al.*, 2009(b); Chakrabarty and Pal, 2011], or acetic acid and water [Echevarría *et al.*, 1998] as the mobile phase. A study by Italia *et al.* (2009b) revealed acetonitrile to be better than methanol as the organic modifier in the mobile phase mix for HPLC analyses of AmB because acetonitrile produced peaks with better symmetry. Methanol was therefore excluded from the mobile phase system in the present study.

Using the aforementioned studies as a guide, a solvent system of sodium acetate buffer (pH 4) as the aqueous phase [A] and acetonitrile as the organic phase [B] was selected as the mobile phase for the current study. Using this solvent mix in isocratic mode and varying the ratios of A to B,

from 90:10 to 10:90 over various ranges of run times, analyte peaks were either not properly resolved or absent from the resulting chromatograms.

On running the mobile phase in gradient mode according to Table 4.1 and injecting a mixture of all the analytes onto the HPLC, the chromatograms in Figures 4.2(a) and (b) were obtained. In order to identify the peaks, each analyte was run separately.

Table 4.1 Gradient elution method for analysing AmB, PAR, SP and IS

Step	Time (min)	% A (acetate buffer, pH 4)	% B (acetonitrile)
Equilibration	2	80	20
1	2	80	20
2	4	20	80
3	2	20	80
4	2	60	40

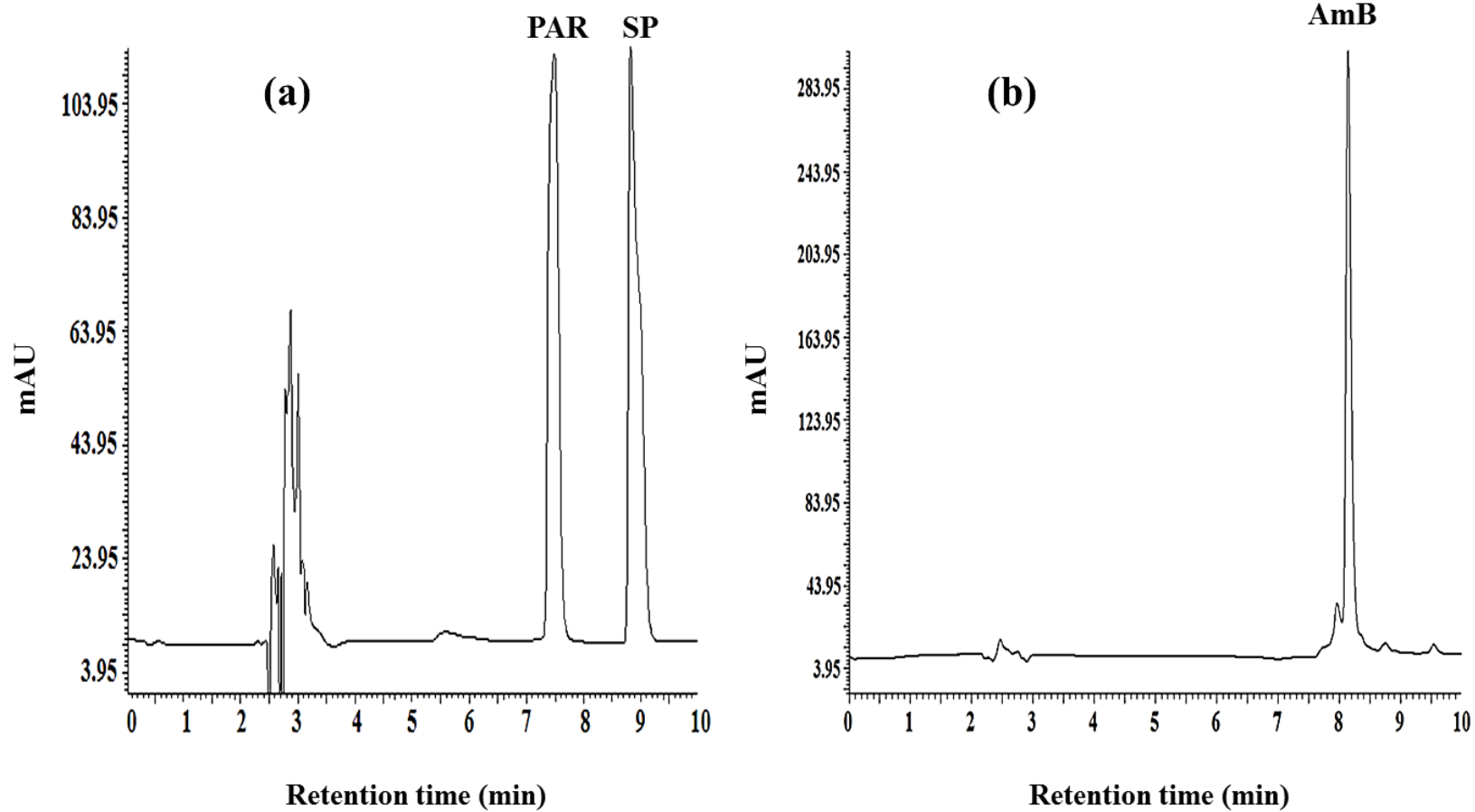


Figure 4.2 Chromatograms for (a) PAR and SP at 254 nm and (b) AmB at 405 nm, using the gradient method in Table 4.1

There was no peak corresponding to the IS in either of the chromatograms. The retention times were 7.5 and 8.8 min for PAR and SP, respectively, at 254 nm and 8.1 min for AmB at 405 nm. The run time of the method was therefore extended from 10 min to 15 min to allow for elution of the IS, and the gradient elution method was also revised so as to obtain more distinct retention times as those for SP and AmB were not well resolved although the compounds are detected at different wavelengths.

The mobile phase gradient was modified by increasing the percentage and run time of the aqueous phase as shown in Table 4.2 to obtain the chromatograms in Figure 4.3. The retention times for the analytes were 7.5, 8.8 and 12.1 min for PAR, SP and the IS, respectively, at 254 nm, and 11.7 and 12.2 min for AmB and the IS, respectively, at 405 nm. These results were an improvement on the previous method (Table 4.1) as it can be seen that the IS was eluted at both wavelengths at approximately the same time, and each analyte had a distinctive retention time. However, only the peaks for PAR and SP were of good symmetry while those for AmB and IS showed some splitting.

The HPLC column was flushed with distilled water, methanol, acetonitrile, methanol and the mobile phase (in that order) to remove any particles such as salts that may have precipitated from the sodium acetate buffer and may have resulted in the split peaks. The gradient method was then again adjusted until the method shown in Table 4.3 was obtained, which resulted in chromatograms with well-resolved peaks for the analytes as are evident in the subsequent chromatograms (Figure 4.5).

Table 4.2 Improved gradient elution method for HPLC analyses of AmB, PAR, SP and IS

Step	Time (min)	% A (acetate buffer, pH 4)	% B (acetonitrile)
Equilibration	2	60	40
1	7	60	40
2	2	20	80
3	2	60	40
4	4	100	0

Table 4.3 Optimum gradient elution method for the HPLC analyses

Step	Time (min)	% A (acetate buffer, pH 4)	% B (acetonitrile)
Equilibration	2	100	0
1	0.5	100	0
2	6.5	60	40
3	2	20	80
4	3	60	40
5	3	100	0

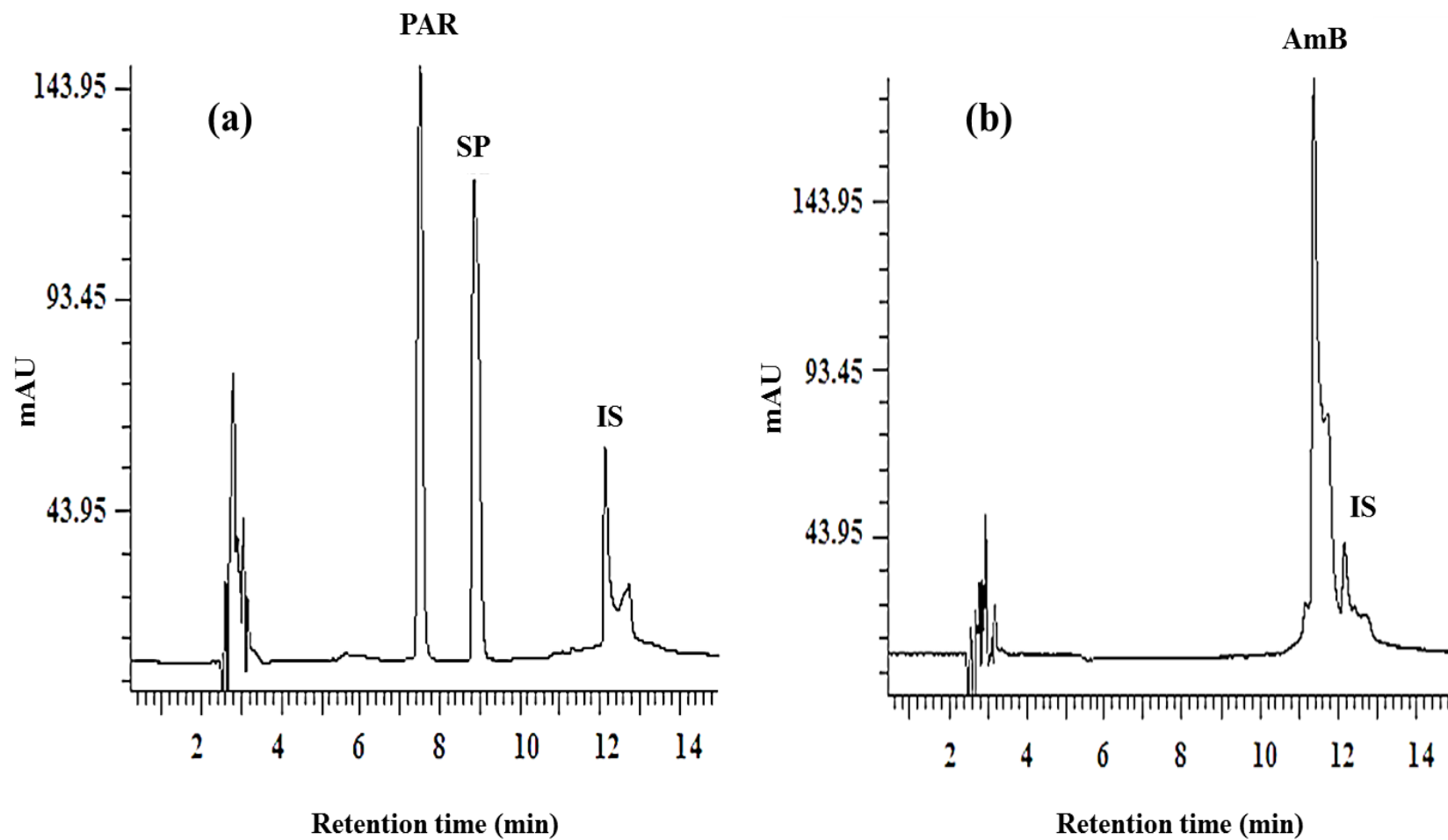


Figure 4.3 Chromatograms for (a) PAR, SP and IS at 254 nm; and (b) AmB and IS at 405 nm, using the gradient method in Table 4.2

4.4.3 Effect of deproteinising agent

Proteins are usually removed from biological samples to allow for qualitative or quantitative analysis of drugs and their metabolites, as well as other non-protein compounds [Polson *et al.*, 2003]. In order to exclude responses due to proteins, deproteinising agents/protein precipitants are normally used to treat the samples prior to such analyses.

Protein solubility in biological fluids is due to polar interactions with the aqueous solvent, ionic interactions with salts, and repulsive electrostatic forces between similar charged molecules. At the isoelectric point (pI), proteins have no net charge and hence they have minimum solubility in aqueous solvents. Above the pI, a protein has a net negative charge and vice versa.

Protein precipitation is a simple purification method of denaturing proteins using strong acids or bases, heat, organic solvents, salts (e.g. ammonium sulphate) and metal ions to disrupt protein-drug binding [Englard and Seifter, 1990; Kole *et al.*, 2011; Oh and Lee, 2013]. The aforementioned agents facilitate protein precipitation differently: organic solvents lower the dielectric constant of the plasma protein solution, which increases the attraction between charged molecules. Organic solvents also displace water molecules around the protein surface, which results in attractive electrostatic interactions and then protein aggregation. Acids on the other hand form insoluble salts with the positively charged amino groups of protein molecules. Addition of high amounts of salts to proteins in solution draw water away from the proteins to become hydrated which in turn results in aggregation of protein molecules by enhancing protein-protein hydrophobic interactions. Positively charged metal ions on the other hand bind with proteins and reduce protein solubility by changing the pI. Metal ions in solution also compete with protons for binding sites on amino acids and displace bound protons thereby lowering the pH of the solution. The alteration of the pI and reduction in pH result in protein precipitation. Heating also alters intramolecular hydrogen

bonds in proteins, which are responsible for the secondary and tertiary structures of proteins thereby denaturing the proteins [Polson *et al.*, 2003].

The use of salts, acids and heat result in trapping of analytes in protein aggregates and causes a reduction in analyte concentration in the supernatant leading to erroneous results. Acids and metal ions (e.g. zinc sulphate) also require a prior evaluation of an analyte's stability in them in order to detect possible degradation and analyte loss through binding with the metal cations. As a result, most bioanalytical protein precipitation methods use water miscible organic solvents for protein denaturation, most of which achieve up to 90-96% protein precipitation [Chamberlain, 1995; Polson *et al.*, 2003; Chang *et al.*, 2007].

Organic solvents used as deproteinising agents include methanol, ethanol and acetonitrile. However, when acetonitrile was used both as deproteinising agent and solvent for the IS in the present study, distortions such as peak broadening, splitting and tailing (Figure 4.4(a)) were obtained on repeated analyses at 254 nm. On using methanol and ethanol in equal proportions as the deproteinising agent and maintaining acetonitrile as the solvent for the IS, the peaks for PAR and the IS became sharper with better symmetry while the SP peak remained distorted and off the baseline of the chromatogram as depicted in Figure 4.4(b).

As a result of the peak improvements after using the methanol/ethanol mix for deproteinising, the latter was employed as the solvent for the IS as well. The chromatogram in Figure 4.4(c) shows all the analyte peaks to be well resolved, sharp and symmetrical without any splitting. As well, all the peaks were on the baseline, clearly indicating methanol/ethanol (1:1) as the optimal deproteinising agent for the plasma samples. Subsequent analyses were therefore conducted using methanol/ethanol (1:1) as both solvent for the IS and as deproteinising agent. In doing so, further dilution of analytes in the plasma samples was avoided, as would have been the case if different

solvents were used for both purposes, while ensuring that sufficient deproteinising solvent is used for effective protein precipitation. The peaks for AmB and the IS at 405 nm were largely unaffected by the choice of solvent for deproteinisation.

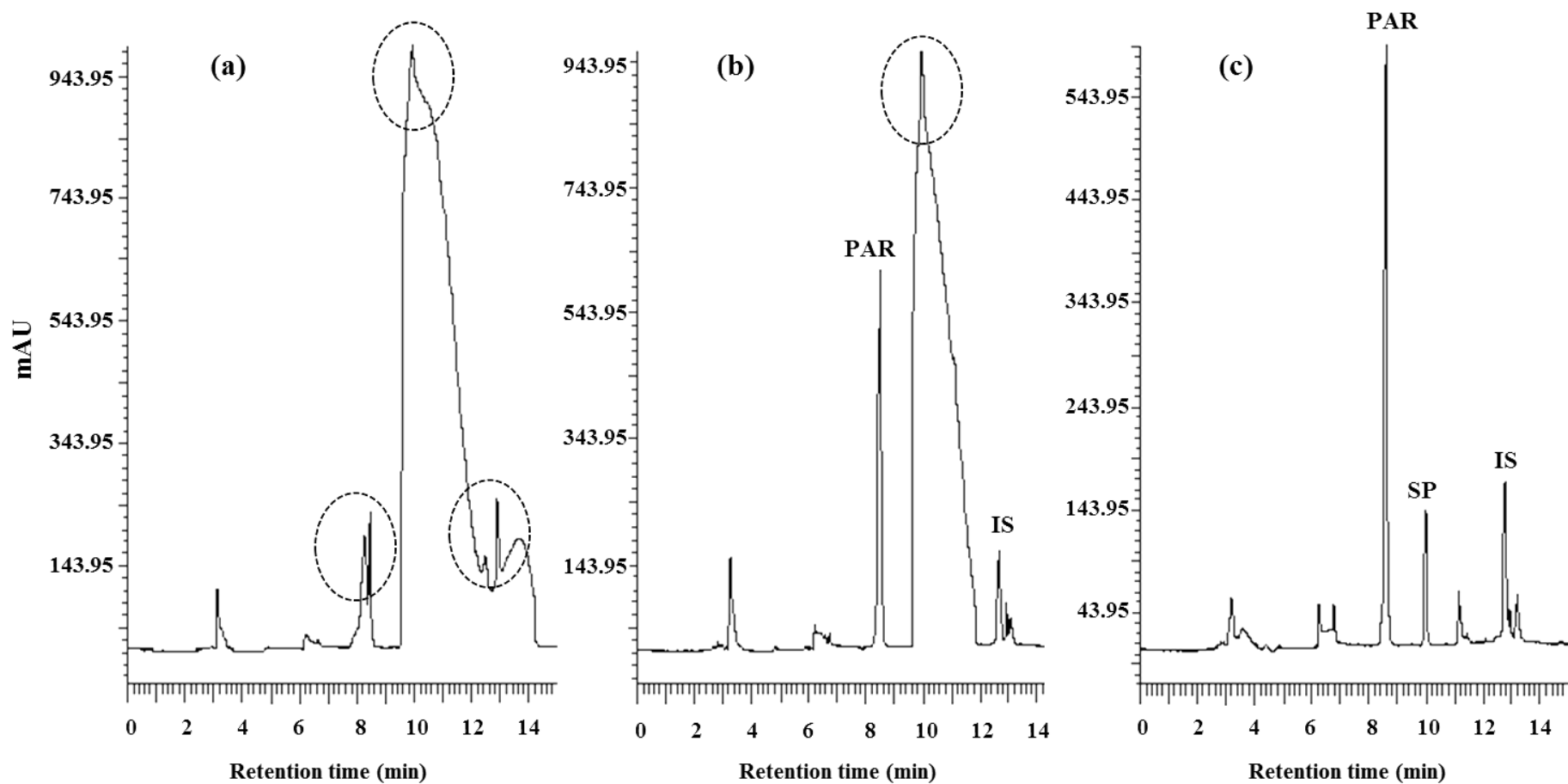


Figure 4.4 Chromatograms showing the effects of deproteinising agent on peak shape and symmetry at 254 nm

- (a) Using acetonitrile containing IS (10 µg/mL) for deproteinisation
- (b) Using acetonitrile containing IS (10 µg/mL) + methanol/ethanol (1:1) for deproteinisation
- (c) Using methanol/ethanol (1:1) containing IS (10 µg/mL) for deproteinisation

4.4.4 HPLC method validation

A number of HPLC methods specific to the detection of AmB and suitable internal standards in biological fluids have been reported [Lambros *et al.*, 1996; Campanero *et al.*, 1997; Echevarría *et al.*, 1998; Italia *et al.*, 2009(b); Chakrabarty and Pal, 2011]. In the present study, a method for the simultaneous analyses of AmB, PAR and SP, which would be suitable for the GI transit monitoring and absorption of AmB, using PAR and SP as marker drugs was developed. Piroxicam was employed as the IS in the present study because it was found to absorb considerably at the two detection wavelengths used (254 and 405 nm).

The results for the method validation parameters investigated for AmB, PAR and SP are summarised in Tables 4.4-4.6 respectively.

4.4.4.1 Specificity

Firstly, it had to be ensured that the method was specific for the drugs in the study so pure solutions of the individual drugs were injected onto the HPLC system separately to obtain the individual retention times of the analytes for the purpose of peak identification. The Eclipse Plus C18 column, mobile phase composition and the simple gradient elution method employed in the study were found to be suitable for the simultaneous analysis of AmB, SP, PAR and the IS. Figures 4.5(a) and (b) show the chromatograms obtained when pure drug solutions containing identical concentrations (22.22 µg/mL each) of PAR, SP and the IS were analysed at 254 nm; and AmB and the IS at 405 nm, respectively.

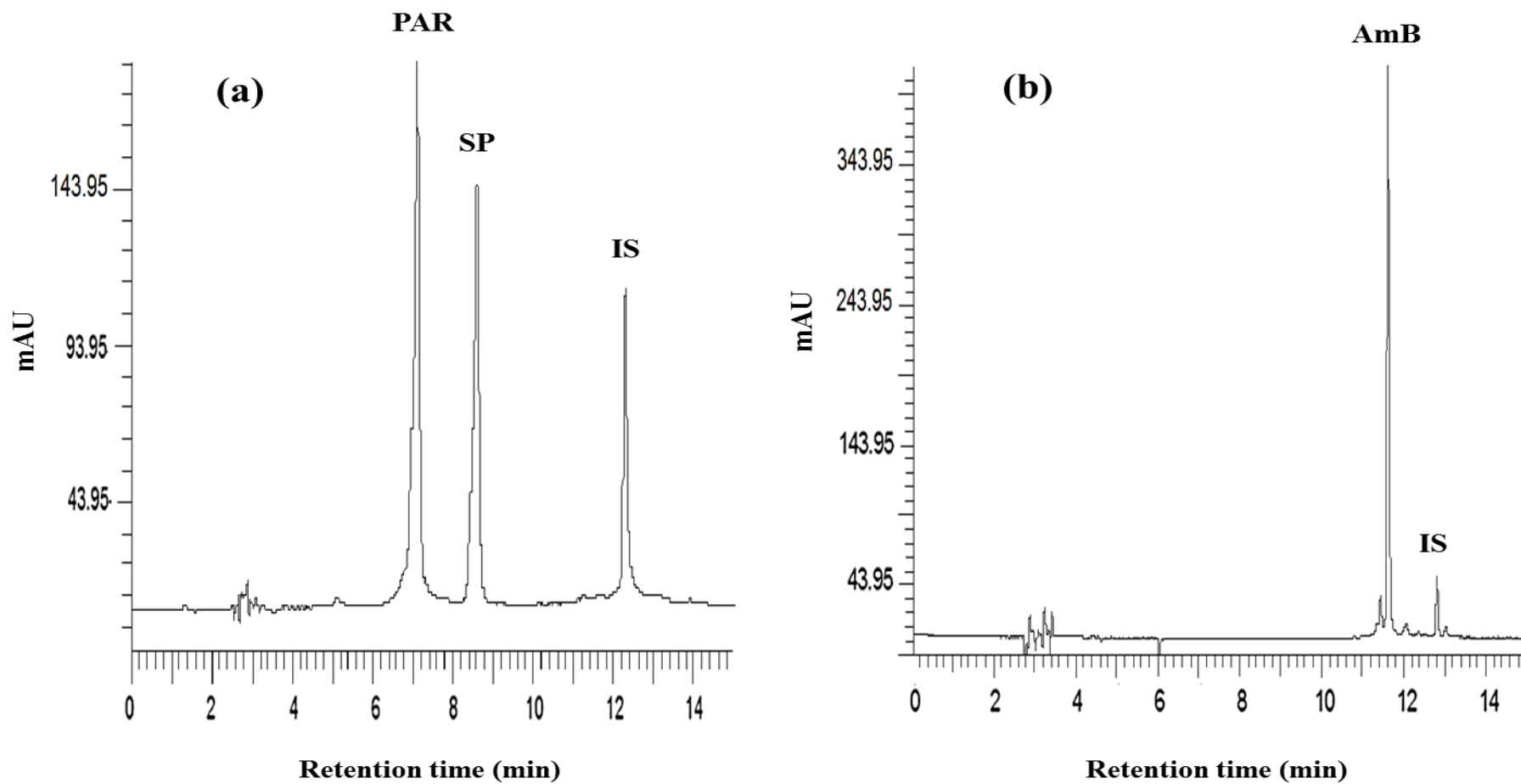


Figure 4.5 Chromatograms of a pure solution of the analytes showing (a) PAR, SP and IS at 254 nm; and (b) AmB and IS at 405 nm

The retention times obtained were 7.1, 8.6 and 12.3 min for PAR, SP and the IS at 254 nm; and 11.7 and 12.9 min for AmB and the IS at 405 nm, respectively. The chromatograms obtained clearly show no interfering peaks, which indicate the absence of degradation products or synthetic precursors, as well as the specificity of the method for the analytes. It is also clear from the chromatograms how different wavelengths affect an analyte's signal [Harvey, 2015] as is seen for the IS.

The hydrophobicity of a compound is the primary indicator of its retentivity in RP-HPLC; that is, retention time is higher for more hydrophobic compounds [Crawford Scientific, 2015(b)]. $\log P$ is a measure of how an analyte in its unionised form partitions between two immiscible solvents (usually octanol and water) under standard conditions, and is used to express hydrophobicity. The higher the value of $\log P$, the more hydrophobic a compound is. The order of elution of analytes is therefore governed by their chemical structures and hence, their solubility in water, as well as their carbon content in the case of an analogous series.

In RP-HPLC, hydrophilic molecules adsorb less to the hydrophobic stationary phase and are eluted first while less polar and non-polar molecules are more strongly held by the hydrophobic stationary phase and are eluted later [Crawford Scientific, 2015(b)]. Polarity however is not the only factor involved in the order of elution. Analyte retention may also be affected by other conditions such as the mobile phase, stationary phase and column temperature.

The $\log P$ values for PAR, SP, AmB and the IS are 0.48, 0.47, 1.16 and 2.67, according to the ACD/ $\log P$ model predictions. It is observed that the analytes eluted in the order of their $\log P$ values except that SP would have been expected to elute before PAR however, this is not concerning as the peaks are well resolved.

Separation of compounds varies for different mobile phases at various solvent ratios. This is because of differences in the chemical properties of organic solvent molecules [Shimadzu, 2015]. The elution order depends on which organic solvent is used in the mobile phase as well as the amount of water present or the pH of the aqueous solvent. The retention time for each analyte is therefore affected differently by the choice of organic solvent. For instance, changing from acetonitrile to tetrahydrofuran or methanol will result in different elution orders for a given set of analytes, leaving the choice of organic solvent to the one which gives the best peak resolution [Harvey, 2015; Shimadzu, 2015].

From Figure 4.6 for instance, it is evident how the elution order of phenol and benzoic acid is reversed due to change in mobile phase composition. The order of elution could however remain the same for two different mobile phases for a given mixture of compounds however, each analyte's retention time would be affected differently; some analytes would elute earlier or more slowly [Harvey, 2015].

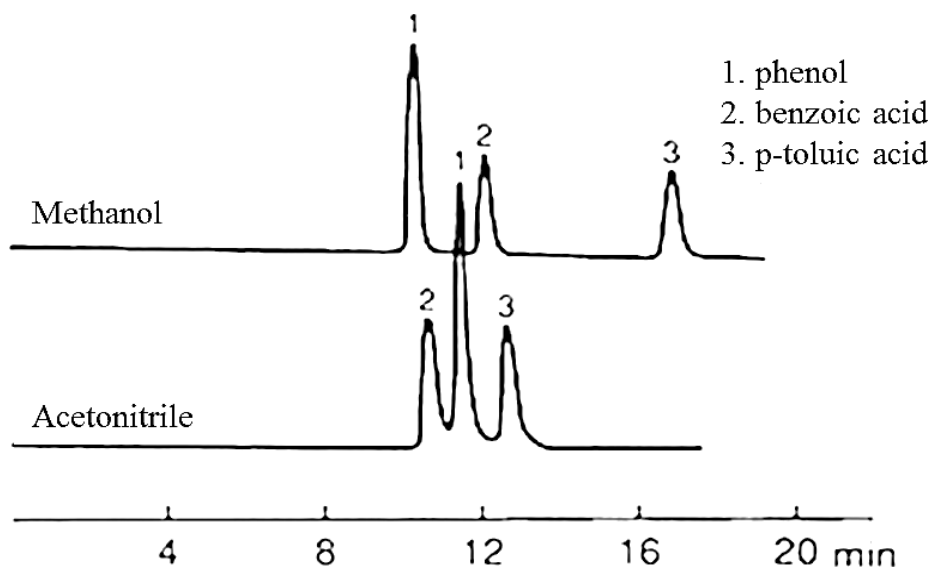


Figure 4.6 Chromatograms showing the separation selectivity of phenol, benzoic acid and p-toluic acid for acetonitrile and methanol [Shimadzu, 2015]

4.4.4.2 Effect of plasma (matrix effect)

Injecting blank plasma onto the HPLC showed no interfering peaks at the retention times of all the analytes at both detection wavelengths as depicted in Figures 4.7(a) and (b), further indicating the specificity of the HPLC method for the analytes. The baselines also showed low noise at the same attenuation of the detector.

Plasma samples spiked with the analytes and IS, treated according to the sample preparation procedure in Section 4.3.3 and injected onto the HPLC system produced the chromatograms shown in Figures 4.8(a) and (b). It can be seen that the peaks for all the drugs remained very well resolved and symmetrical in plasma, with slight increases in some of the retention times. At 254 nm, retention times increased from 7.1 to 8.5 min for PAR; from 8.6 to 9.9 min for SP; and from 12.3 to 12.9 min for the IS, compared with the respective peaks obtained from the pure drug solutions in Figure 4.5. The peaks in Figure 4.8 were obtained by spiking the same solution used to obtain the chromatograms in Figure 4.5 into an equal volume of blank plasma. The differences in the relative peak signals/intensities are attributable to the effect of the plasma matrix; however, this effect remains constant as all subsequent analyses were conducted in plasma. The differences in the peak signals of the analytes relative to each other (i.e. PAR > SP > IS in Figure 4.5 as compared with IS > PAR > SP in Figure 4.8) further indicate that the matrix effects of plasma vary for different analytes. At 405 nm however, the retention times for AmB and the IS remained essentially unchanged.

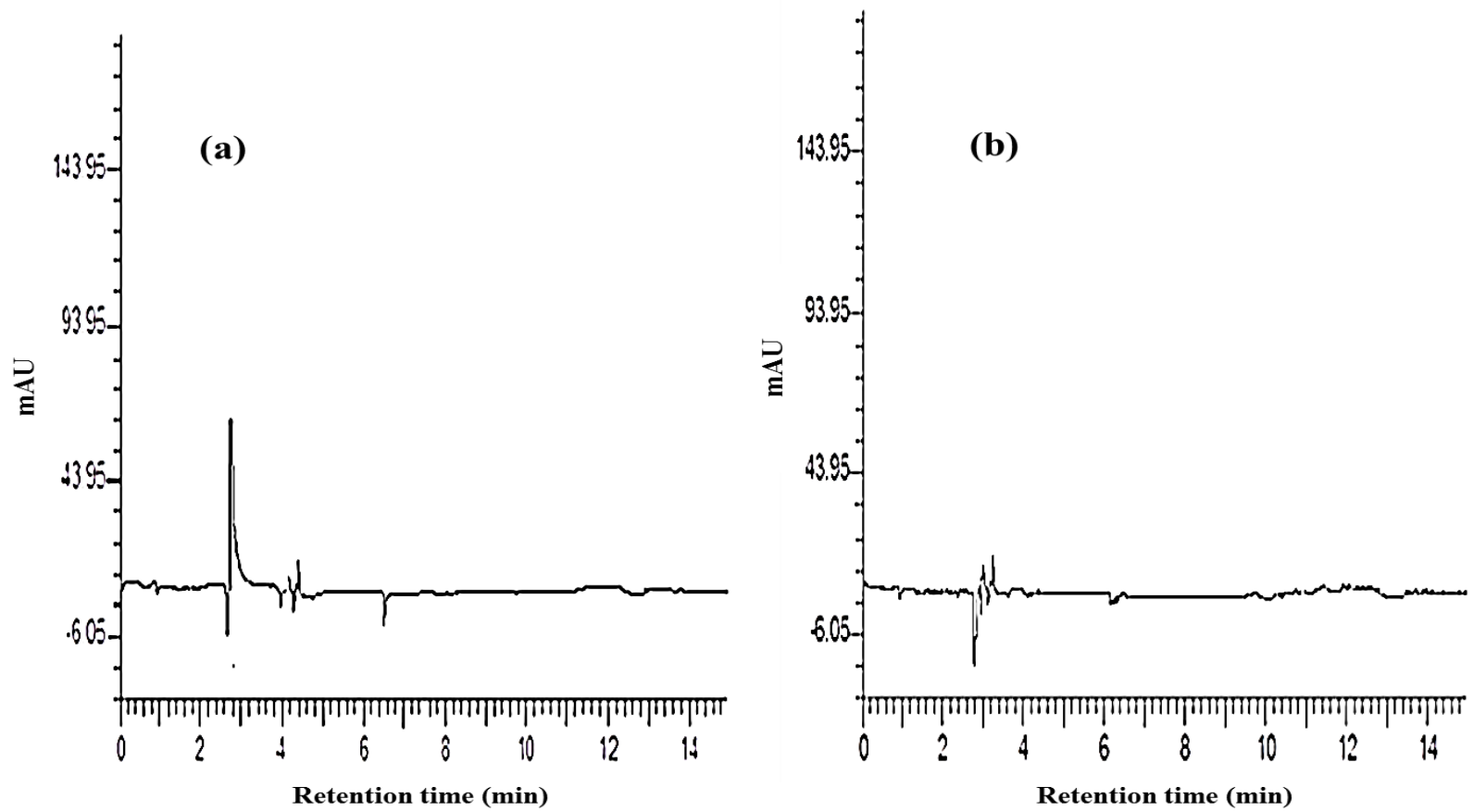


Figure 4.7 Chromatograms of the methanol-ethanolic extract of blank rat plasma at (a) 254 nm and (b) 405 nm

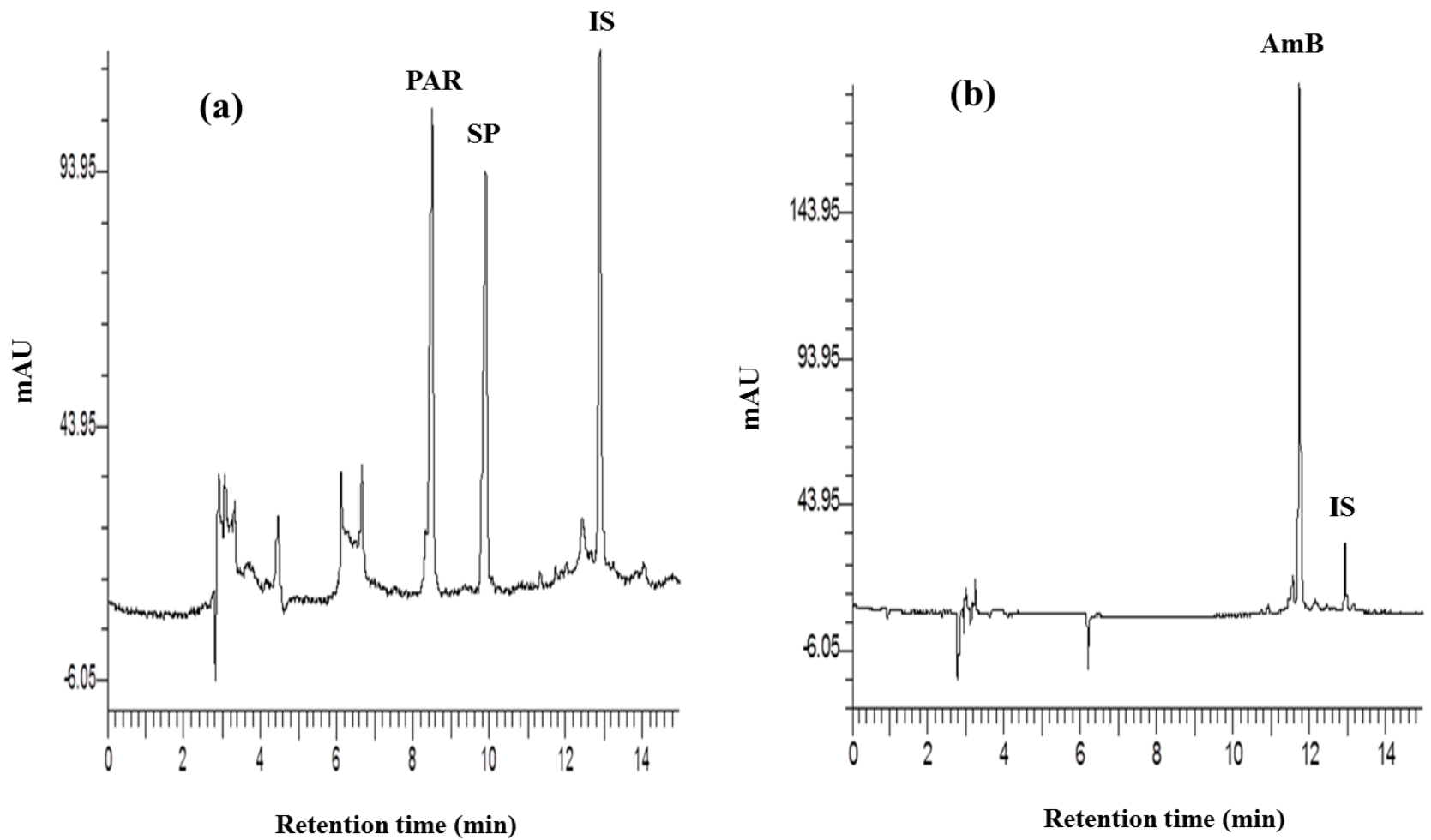


Figure 4.8 Chromatograms of spiked plasma showing (a) PAR, SP and IS at 254 nm; and (b) AmB and IS at 405 nm

HPLC is a useful analytical technique for quantifying drugs, their metabolites and endogenous compounds in biological samples however, “matrix” effects may be encountered [Hall *et al.*, 2012]. Matrix refers to all the constituents of a sample other than the analyte of interest. Plasma samples may contain unknown components however, the known components also vary in amounts in different subjects based on genetics and disease state, as well as the presence of any medications being taken and their metabolites. As a result, matrix effects may differ among subjects. Plasma comprises proteins, amino acids, peptides, glucose, carbohydrates, vitamins, electrolytes, hormones and lipids, all of which contribute to matrix effects.

The Sprague-Dawley rats used in the present study were reared solely for the project and were not given any drug substances except food and water prior to the study. As a result, plasma matrix effects were minimised to the presence of endogenous biological components and metabolites such as phospholipids and carbohydrates, and to interactions such as covalent binding between analytes and plasma proteins [Hall *et al.*, 2012].

A matrix effect can be detected if a peak co-elutes with an analyte and causes a suppression or enhancement in the chromatographic peak properties of the analyte [Polson *et al.*, 2003]. Some matrix components are removed during sample “clean-up” processes such as protein precipitation, liquid-liquid extraction and solid-phase extraction. The use of internal standards also helps to minimise matrix effects. Organic solvent-based deproteinisation efficiently removes majority of proteins from plasma samples hence, further processing of plasma samples can be avoided to reduce analyte losses and ensure accuracy of results [Polson *et al.*, 2003; Hall *et al.*, 2012].

It has been reported that polar analytes are usually more affected by endogenous matrix effects than non-polar analytes, which is clearly manifested in the present study. After the analytes were spiked into plasma, a reduction in the relative peak heights for the polar analytes, PAR and SP,

was observed compared with the peak signal for the hydrophobic IS which remained unchanged (Figure 4.5 versus Figure 4.8). This is due to the fact that most of the constituents of biological matrices are water-soluble compounds. The latter are detectable within the UV range and usually elute early during RP-HPLC [Bonfiglio *et al.*, 1999; Müller *et al.*, 2002] as observed in the initial 7 min of the chromatogram at 254 nm (Figure 4.8), and may affect peak properties of polar analytes as observed for PAR and SP.

The results obtained however clearly showed that the developed HPLC method was suitable for the simultaneous assay of the three drugs and IS in the presence or absence of a biological matrix such as plasma.

4.4.4.3 Linearity and range

The linearity of the method was tested to establish proportionality between peak response and analyte concentration over the working drug concentration ranges. The calibration curves for AmB, PAR and SP in plasma as illustrated in Figures 4.9(a)-(c) were found to be linear over the concentration ranges of 0.05-10 µg/mL, 0.5-100 µg/mL and 0.1-20 µg/mL, respectively. The coefficients of determination were also found to be 0.9999, 0.9991 and 0.9999, respectively, indicating good linearity in each case.

The concentration ranges were selected based on literature on the C_{\max} values obtained after oral administration of formulations of the analytes as single entities to rats. For AmB, doses of 4.5-200 mg/kg resulted in C_{\max} values of 0.071-1.469 µg/mL [Risovic *et al.*, 2003; Gershkovich *et al.*, 2009; Patel and Patravale, 2011; Jain *et al.*, 2012]. For PAR, 10-30 mg/kg doses produced C_{\max} values ranging 3.5-16.9 µg/mL [García-López *et al.*, 1997; Adzu *et al.*, 2001; Qinna *et al.*, 2014].

Lastly, for SP, 20-60 mg/kg oral doses of SSZ resulted in C_{\max} values for SP in the range of 4.764-37.6 $\mu\text{g/mL}$ [Chungi *et al.*, 1989; Zamek-Gliszczyński *et al.*, 2012].

In the present study, it was intended that 10 mg/kg doses of each of the three nanoparticle formulations containing AmB, PAR and SSZ, would be orally administered to rats, implying that the selected concentration ranges would be suitable to detect the plasma concentration levels of the analytes in rat plasma.

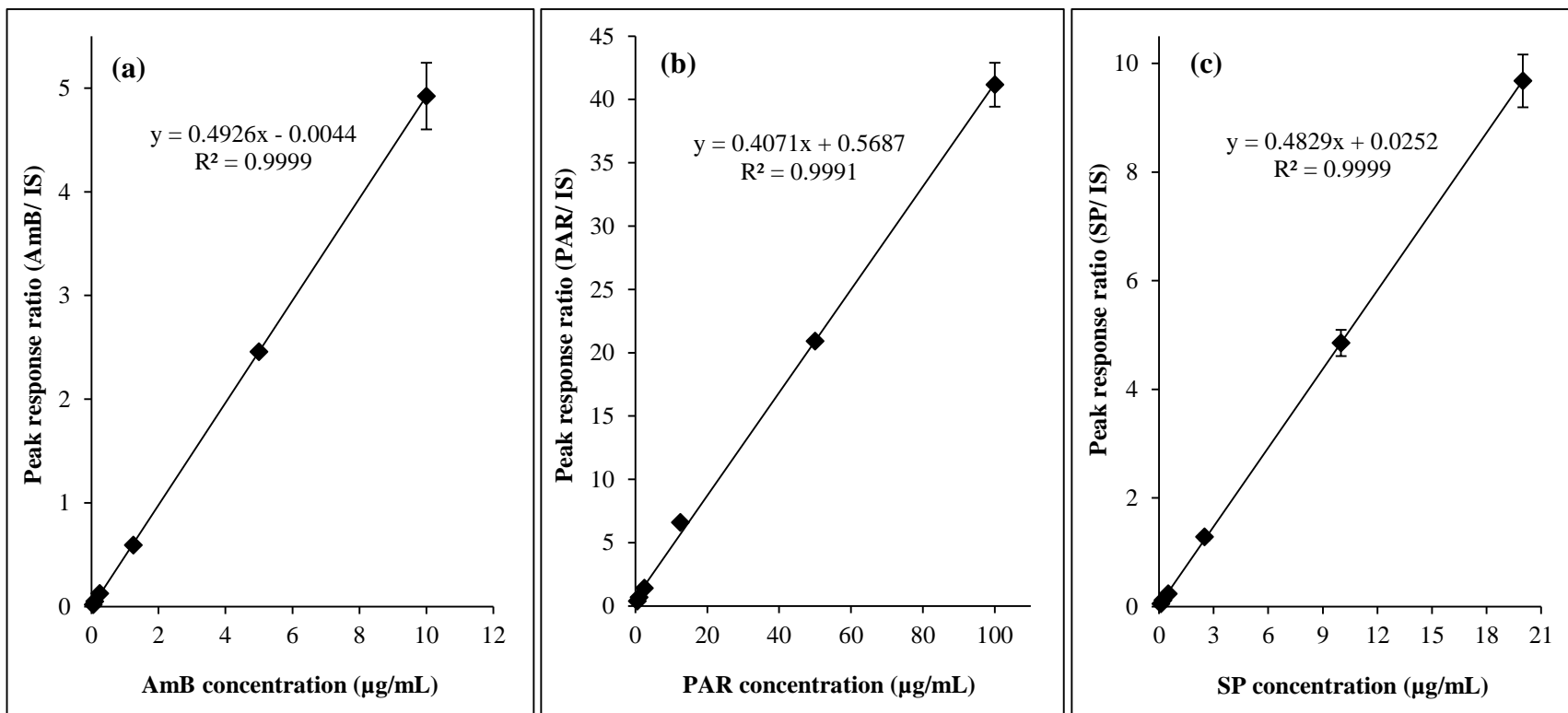


Figure 4.9 Standard calibration curve of the peak response ratios of (a) AmB to IS, (b) PAR to IS, and (c) SP to IS, each versus the corresponding concentration of AmB, PAR or SP (µg/mL) in rat plasma

4.4.4.4 Precision

Precision is a measure of the degree of repeatability of the developed HPLC method [Shabir, 2004]. The within-day assay is the results of the reproducibility of the HPLC method during a short time period, under the same conditions. The between-day runs on the other hand estimates the inter-day variation due to within-laboratory changes resulting from random events such as the effects of different days on performances by the same or different analysts or equipment. The within-day precision determination gave values of 4.39-7.17% for AmB, 2.54-4.28% for PAR and 3.77-9.89% for SP. The variabilities for between-day run on the other hand were in the ranges of 0.93-9.41% for AmB, 2.87-6.08% for PAR and 1.13-4.79% for SP. The precisions were found to be less than 10% in all cases indicating an acceptable degree of variation for all the analytes. To be acceptable, %CV values must be less than 15% at all concentration levels [Bressolle *et al.*, 1996; Campanero *et al.*, 1997].

Other precision values that have been obtained in HPLC analyses of AmB and PAR in rat plasma are 1.02-13.93% [Lambros *et al.*, 1996; Echevarría *et al.*, 1998; Italia *et al.*, 2009(b); Chakrabarty and Pal, 2011] and 3.48-15% [Qinna *et al.* 2014; Alolga *et al.*, 2015], respectively, for both intra- and inter-day assays. The data from the present study are therefore either comparable with those reported in the aforementioned studies or better.

4.4.4.5 Accuracy

The percentage accuracy of an analytical method estimates the closeness between observed/actual and expected/nominal concentrations [Shabir, 2004]. Accuracy was measured in terms of percentage relative error and was found to be as follows for the within-day run; 0.20-3.20% for

AmB, 0.27-1.44% for PAR and 0.08-1.60% for SP. For the between-day run, 0.27-3.90% was obtained for AmB, 1.81-5.06% for PAR and 1.29-7.50% for SP. Comparing the results for all the analytes, the maximum error obtained was 7.50%, which is very minimal. A relative error value less than 15% at all concentrations is an acceptable level of accuracy [Bressolle *et al.*, 1996; Campanero *et al.*, 1997] for an assay method, which indicates that the current HPLC method is accurate for the analysis of the analytes in rat plasma. The studies by Lambros *et al.* (1996) and Echevarría *et al.* (1998) produced maximum relative error levels of 4.4% and 6.4%, respectively, for AmB as a single entity in rat plasma/serum, which agree with the results obtained in the current study. An HPLC method developed by Alolga *et al.* (2015) to assay PAR produced a relative error value of up 13.4% for both intra- and inter-day assays over a concentration range of 0.03-15 µg/mL, to which the current results are superior. A search through published studies revealed no recent data on the accuracy of an HPLC assay of SP in rat plasma.

Precision and accuracy together estimate the error of an analytical method and are the primary criteria used to assess the quality of analytical methods [Bressolle *et al.*, 1996]. The results therefore indicate that the developed HPLC method is of good quality, repeatable and reproducible.

4.4.4.6 Recovery

The percentage recoveries of the analytes from plasma estimate the efficiency of the plasma treatment procedure and the extraction of the drugs spiked in plasma for analysis. Recovery also serves as an indicator of the level of plasma matrix effect. The recovery values obtained were 92.09-98.39% for AmB, 98.73-100.10% for PAR and 91.69-99.20% for SP. These values are all above 91%, indicating that the rat plasma matrix affected the extraction and quantitation of the analytes by 9% or less, which points to good analyte recovery from plasma. Recovery values of

AmB as a single entity from rat plasma/serum have been obtained to be up to 96%, 95%, 97%, 108.5% and 96.5% in other studies by Lambros *et al.* (1996), Campanero *et al.* (1997), Echevarría *et al.* (1998), Italia *et al.* (2009b) and Chakrabarty and Pal (2011), respectively. Mean recovery values of 78.1%, 96.47% and 99.6% were obtained for PAR by Abu-Qare and Abou-Donia (2001), Alolga *et al.* (2015) and Qinna *et al.* (2014), respectively; however for the former, PAR was in an analyte mixture containing pyridostigmine bromide, acetylsalicylic acid and caffeine as well. The recoveries of AmB and PAR obtained in the current study are either superior to or comparable with those obtained in literature, which indicates a minimal matrix effect, as well as the suitability of the HPLC method for the simultaneous assay of the drugs in rat plasma.

4.4.4.7 LOD and LOQ

LOD can be defined as the lowest amount of an analyte that is detectable above the baseline noise, and is normally estimated to be three times the noise level while LOQ is the lowest amount of the analyte that can be reproducibly measured quantitatively above baseline noise [Shabir, 2004]. LOQ is normally estimated as ten times the noise level and at least twice the value of the LOD [Bressolle *et al.*, 1996]. LOD and LOQ were 5.70 ng/mL and 19.05 ng/mL for AmB; 13.44 ng/mL and 44.82 ng/mL for PAR; and 15.30 ng/mL and 51.02 ng/mL for SP, respectively. Some LOD and LOQ values from published HPLC data are 1-5 ng/mL and 10 ng/mL, respectively, for AmB [Lambros *et al.*, 1996; Echevarría *et al.*, 1998; Italia *et al.*, 2009(b); Chakrabarty and Pal, 2011], and 100-200 ng/mL and 150-199 ng/mL, respectively, for PAR [Abu-Qare and Abou-Donia, 2001; Qinna *et al.*, 2014].

The LOQ values obtained for the analytes are lower than the respective plasma analyte concentrations, obtained at the first blood sampling times in pharmacokinetic studies after oral administrations of the following doses to rats: AmB at 4.5-200 mg/kg [Risovic *et al.*, 2003; Gershkovich *et al.*, 2009; Patel and Patravale, 2011; Jain *et al.*, 2012], PAR at 10-30 mg/kg [García-López *et al.*, 1997; Adzu *et al.*, 2001; Qinna *et al.*, 2014] or SSZ at 60 mg/kg [Chungi *et al.*, 1989].

The LOQ values are therefore sufficiently low to allow detection and quantification of expected plasma analyte concentrations following planned (discussed in the next chapter) oral administration of AmB, PAR and SSZ SLNs to rats, each at a dose of 10 mg/kg. It can be observed that the LOD and LOQ values obtained in this study are comparable with those in the stated reports however, for PAR and SP, better values were obtained in the present study.

Table 4.4 Summary of HPLC method validation parameters for AmB

Parameter	Concentration ($\mu\text{g/mL}$)		Intra-day	Inter-day
Precision (% CV)	Low	0.05	4.39	9.41
	Medium	0.25	7.17	2.36
	High	10.00	5.78	0.93
Accuracy (%)	Low	0.05	2.40	0.27
	Medium	0.25	3.20	3.90
	High	10.00	0.20	1.20
Recovery (%)	Low	0.05	97.77 \pm 3.15	
	Medium	0.25	95.60 \pm 6.12	
	High	10.00	92.09 \pm 0.58	
Sensitivity	LOD	5.70 ng/mL		
	LOQ	19.05 ng/mL		
Linearity range	0.05-10 $\mu\text{g/mL}$			

Table 4.5 Summary of HPLC method validation parameters for PAR

Parameter	Concentration ($\mu\text{g/mL}$)		Intra-day	Inter-day
Precision (% CV)	Low	0.50	2.53	6.08
	Medium	2.50	4.01	2.87
	High	100.00	4.28	5.13
Accuracy (%)	Low	0.50	0.90	5.06
	Medium	2.50	1.44	1.81
	High	100.00	0.27	2.90
Recovery (%)	Low	0.50	98.73 \pm 1.53	
	Medium	2.50	100.10 \pm 5.33	
	High	100.00	99.35 \pm 1.34	
Sensitivity	LOD	13.44 ng/mL		
	LOQ	44.82 ng/mL		
Linearity range	0.5-100 $\mu\text{g/mL}$			

Table 4.6 Summary of HPLC method validation parameters for SP

Parameter	Concentration ($\mu\text{g/mL}$)		Intra-day	Inter-day
Precision (% CV)	Low	0.10	7.31	1.13
	Medium	0.50	9.89	4.79
	High	20.00	3.77	3.16
Accuracy (%)	Low	0.10	1.55	1.29
	Medium	0.50	1.60	7.50
	High	20.00	0.08	1.67
Recovery (%)	Low	0.10	97.48 \pm 5.42	
	Medium	0.50	99.20 \pm 4.76	
	High	20.00	91.69 \pm 1.82	
Sensitivity	LOD	15.30 ng/mL		
	LOQ	51.02 ng /mL		
Linearity range	0.1-20 $\mu\text{g/mL}$			

4.5 Conclusions

The results show that the validated HPLC method has the advantage of a simple sample preparation procedure as compared to solid-phase extraction. It can be concluded that the HPLC method is simple, rapid, accurate and reliable for determining the concentrations of AmB, PAR and SP in plasma using piroxicam as the IS. In addition, the method produced data that were comparable with or better than those obtained in other studies. The peaks for all the analytes are well resolved and separated from each other and also, the 15 min run time is relatively short considering that four different compounds (including the IS) can be simultaneously analysed. Again, the volume of plasma used in the analyses is small, which is necessary for pharmacokinetic studies in rodents since only small blood volumes can be sampled for analyses due to their small size.

CHAPTER 5

PILOT GASTROINTESTINAL TRANSIT STUDY

5.1 Introduction

The formulation of pharmaceutical products is carried out with the key aim of enhancing the bioavailability of the therapeutic agent, which presents a challenging prospect for poorly water-soluble drugs. For dosage forms intended for oral delivery, the balance between a drug's solubility in gastrointestinal (GI) fluids and its permeation across the lipophilic membrane of the enterocytes determines its rate and extent of absorption [Pramod *et al.*, 2010; Kalepu *et al.*, 2013].

Amphotericin B (AmB) is poorly absorbed from the GI tract when administered orally due to its low aqueous solubility. There is therefore growing interest by formulation scientists in developing alternative delivery systems to address this constraint. Lipid-based drug delivery systems (LBDDS) are a useful technology designed to address this challenge. This is because encapsulating or solubilising drugs in lipid excipients can promote absorption and improve bioavailability [Pouton, 2006]. In the past decade, researchers have focused their interest on lipids as carrier systems for hydrophobic drugs.

One LBDDS that has received much attention lately is the solid lipid nanoparticle (SLN). After oral administration, lipids are digested by gastric and pancreatic lipases and then incorporated into micellar and vesicular colloidal structures. The presence of exogenous lipids in the small intestine also stimulates the secretion of bile salts which aid in solubilisation and absorption of the lipids. Lipids impact oral drug absorption and bioavailability in a variety of ways including: increasing membrane fluidity which enhances transcellular absorption; allowing paracellular transport via opening of tight junctions; increased intracellular concentration and residence

time by surfactants due to inhibition of P-gp and/or CYP450; and stimulation of lipoprotein/chylomicron production [Humberstone and Charman, 1997; Porter and Charman, 1997; Driscoll, 2002]. LBDDS enhance drug transport into systemic circulation *via* the extensive drainage network of the intestinal lymphatic system when given orally. SLNs also have the potential to be taken up by Peyer's patches along the GI tract, which drain into the lymph. Drug association with chylomicrons in enterocytes is the important step in lymphatic drug absorption. Advantages of lymphatic drug transport include avoidance of first-pass metabolism and targeting specific diseases that spread via the lymphatics [Charman *et al.*, 1997; Driscoll, 2002; Porter *et al.*, 2007].

AmB is currently delivered intravenously but this route of administration is associated with adverse effects like fever, chills, rigors, malaise, headache, generalised aches, nausea, vomiting and hypoxia [Patel, 2000]. There is evidence that lipid-based AmB formulations present reduced renal toxicity [Risovic *et al.*, 2003; Gershkovich *et al.*, 2009; Jain *et al.*, 2012] in addition to enhanced bioavailability when delivered orally [Patel and Patravale, 2011; Jain *et al.*, 2012]. Aside the infusion-related side effects of AmB, other general drawbacks of intravenous administration include drug or blood extravasation, catheter infections and thrombosis, which makes oral delivery the most popular route of drug administration. However, oral delivery may be limited by drug properties such as poor solubility, low permeability, instability and rapid metabolism.

Designing and developing pharmaceuticals aimed at achieving maximum oral bioavailability is best ascertained through monitoring the absorption profile of the drug payload, as well as assessing the GI transit properties of the dosage form. These are particularly crucial for hydrophobic drugs.

In this study, paracetamol (PAR) is used as a marker drug for estimating the gastric emptying rate of AmB SLNs based on the rate of appearance of PAR in the blood following oral administration [Heading *et al.*, 1973; Clements *et al.*, 1978]. Sulphasalazine (SSZ) is partially and irregularly absorbed after oral administration however, a larger proportion of the dose passes unchanged into the colon where it is metabolised by bacteria to produce sulphapyridine (SP) and 5-aminosalicylic acid [Moffat *et al.*, 2005]. The SP is very rapidly and almost completely absorbed from the colon into the blood and can therefore serve as an estimate for the arrival time of an SSZ-containing formulation at the caecum [Kellow *et al.*, 1986; Staniforth *et al.*, 1987]. PAR and SP have been used as marker drugs to estimate gastric emptying and oro-caecal transit times, respectively, of pellet-filled capsules in humans [Peh and Yuen, 1996; Rahman *et al.*, 2005], liquids in monkeys [Kondo *et al.*, 2003(a,b)], and provide a cheaper, safer and more appropriate alternative to direct methods such as gamma scintigraphy in experimental animals like rats.

Prior to administration, AmB, PAR and SSZ were formulated into SLNs using identical methods. These were then characterised to ensure similarity in their physical disposition as reported in Chapter 2, with the assumption that when administered simultaneously, all three SLNs would respond similarly to the hydrodynamics within the GI tract. After this assumption was ascertained *in vitro* (Chapter 2), the stage was now set to conduct a GI transit study on the AmB SLNs.

A pilot or background study is a small-scale version of a main study run to assess if the components and processes involved in the study can efficiently generate an outcome [FDA, 2013]. Generally, pilot studies are conducted prior to full bioequivalence studies in order to obtain clinically relevant data. A pilot study can therefore be used to validate an analytical methodology, assess variability, optimise sample collection time intervals and obtain other

useful information. In the present study, a pilot GI transit investigation on the AmB SLNs was conducted using rat as the animal model.

5.2 Materials and methods

5.2.1 Preparation of AmB, PAR and SSZ SLN formulations

AmB, PAR and SSZ SLNs were individually prepared according to the procedure stated in Section 2.3.3 and freeze-dried using trehalose (10% w/v).

5.2.2 *In vivo* study

5.2.2.1 Animals

Pharmacokinetic studies on AmB, PAR and SSZ, and GI transit studies on the SLNs were performed using three 2-month-old disease-free male Sprague-Dawley rats (300-350 g), fasted overnight. The use of the animals, the protocol for their care, as well as the study protocol used were reviewed and approved by the Animal Ethics Committee of the University Sains Malaysia. The animals were obtained from the Animal Holding Unit of University Sains Malaysia and the study conducted at the School of Pharmaceutical Sciences of the same university.

The rats were housed in ventilated cages, maintained under a 12/12 hr light/dark cycle at ambient temperature and humidity, and supplied with food and water *ad libitum*. The animals were acclimatised for 7 days before the study.

5.2.2.2 Procedural care of the rats

The tail end of each rat was clipped once during the initial blood sampling time. The rats were allowed to move freely in their cages throughout the study period except for being restrained in metabolic cages during the blood sampling periods. After each sampling time, the wounds were monitored for approximately 3 min to ensure that there was no excessive bleeding.

In addition, the wounded tails were swabbed with cotton wool rinsed with 70% ethanol to reduce infection upon completion of the study. Normal food and water supply were resumed to the rats after the study before they were euthanised.

5.2.2.3 Drug administration and blood sampling

The study commenced after a 12 hr overnight fast. Each rat in the treatment group received a dose containing an equivalent of 10 mg/kg each of the three SLNs dispersed in 1 mL of distilled water, which was administered by oral gavage. The control rat was given a suspension of pure AmB, PAR and SSZ in distilled water each at 10 mg/kg. Water and food were withdrawn from all the animals until 2 hr and 4 hr, respectively, post dose administration. Blood samples (300 µL) were collected from the tail end of the rats before and at 1, 2, 4, 8, 12 and 24 hr post dose administration into heparinised microcentrifuge tubes.

The first blood samples were taken by clipping the tail end of the rats while subsequent samples were collected by removing the clotted blood with cotton rinsed with 100 IU of heparin solution. Blood samples were centrifuged at 13 800 rpm for 15 min to obtain plasma, which was immediately harvested and frozen till analyses for drug content using the validated HPLC method described in Chapter 4. Plasma samples were treated and analysed using piroxicam as the internal standard as outlined in Sections 4.3.1 and 4.3.3.

5.2.3 Data and statistical analyses

A plasma concentration (ng/mL) versus time (hr) curve was plotted for each drug, from which the peak plasma concentration (C_{\max}) and time of its occurrence (T_{\max}) were directly obtained. The area under the plasma drug concentration-time curve (AUC), which measures the extent of drug absorption was calculated according to the linear trapezoidal method using GraphPad Prism 5 software.

Statistical analyses were also performed using the same software by means of analysis of variance (ANOVA). Statistical significance was set at $p < 0.05$.

5.3 Results and discussion

5.3.1 Selection of animal model

Small laboratory animals such as rats, mice, guinea pigs and rabbits are mostly suitable for GI transit studies of drugs. They are used to obtain valuable data on the mechanisms of drug absorption and bioavailability of powder or solution formulations, while larger animals such as dogs, pigs and monkeys are used to determine drug absorption from other oral dosage forms. It is imperative to understand the physiological, anatomical and biochemical differences between the GI tracts of the aforementioned laboratory animals to aid the selection of the most suitable model to mimic the bioavailability of compounds in humans [Kararli, 1995].

A study by Cao *et al.* (2006) in human and rat small intestines revealed a correlation in oral drug bioavailability between the two species for drug intestinal permeability by carrier-mediated absorption and passive diffusion. In general, passive diffusion is the main mechanism for the absorption of many lipophilic compounds or particulates, which means that rats are the

more suitable model for the present study. Furthermore, rats and humans exhibit similar drug absorption profiles and transporter expression patterns in the small intestine; therefore, rat models can be used to predict oral drug absorption in the small intestines of humans [Cao *et al.*, 2006].

Another study by Zhao *et al.* (2003) on the absorption of 111 compounds showed that the extent of absorption of the drugs presented as tablets or capsules in humans was similar when these were presented as solutions or suspensions in rats; 94% of the drugs showed less than 20% difference in absorption between the two species while 98% of drugs showed a difference of less than 30%. The results strongly suggested that oral *in vivo* absorption studies in rats could be used to predict the extent of intestinal absorption in humans following oral administration [Zhao *et al.*, 2003].

At the microscopic level, humans and rats have a strong morphological similarity in their intestinal tracts but for obvious reasons such as size difference, there is a gross anatomical dissimilarity in the relative absorptive surface areas [DeSesso and Jacobson, 2001]. This makes the human GI tract capable of absorbing materials relatively faster and to a greater extent than that of the rat.

Adult male Sprague-Dawley rats were selected for the study as male rats are less susceptible to physiological changes than female rats, as exemplified by hormonal fluctuations during the oestrous cycle in female rats [Kulkarni *et al.*, 2012]. Such physiological changes could affect the pharmacokinetics of drugs and induce more variables into a study. In addition, Sprague-Dawley rats are a common rat species and are preferred over mice because of their bigger size. Due to the latter, a relatively higher dose of the test formulation can be administered and larger blood volumes can be sampled to produce quantifiable plasma drug concentrations to facilitate an oral absorption study [Ciccone and Holdcroft, 1999; Kulkarni *et al.*, 2012].

5.3.2 Improved absorption of AmB after its incorporation into SLNs

Figure 5.1 depicts the plasma concentration-time profile of AmB after simultaneous oral administration of AmB, PAR and SSZ SLNs to the rats. The figure also shows the profile for the control rat, which received only a suspension of the pure drugs in distilled water. Table 5.1 shows the pharmacokinetic data as obtained from the plasma drug profiles.

As can be seen in Figure 5.1, the plasma concentration of AmB was higher in rats given the SLNs at each time point. The AUC_{0-24} values were 7638.5 ± 440.5 ng.hr/mL and 5649.0 ng.hr/mL for the rats receiving the SLNs and suspension, respectively, which clearly shows the superior attribute of the SLNs in improving bioavailability. The T_{max} values were obtained as 8 hr for both the SLN and suspension however, a small peak at 2 hr was obtained in the SLN profile. The C_{max} for the SLN formulation was 1.3 times higher than that of the suspension, 446.8 ± 23.5 ng/mL versus 332.9 ng/mL.

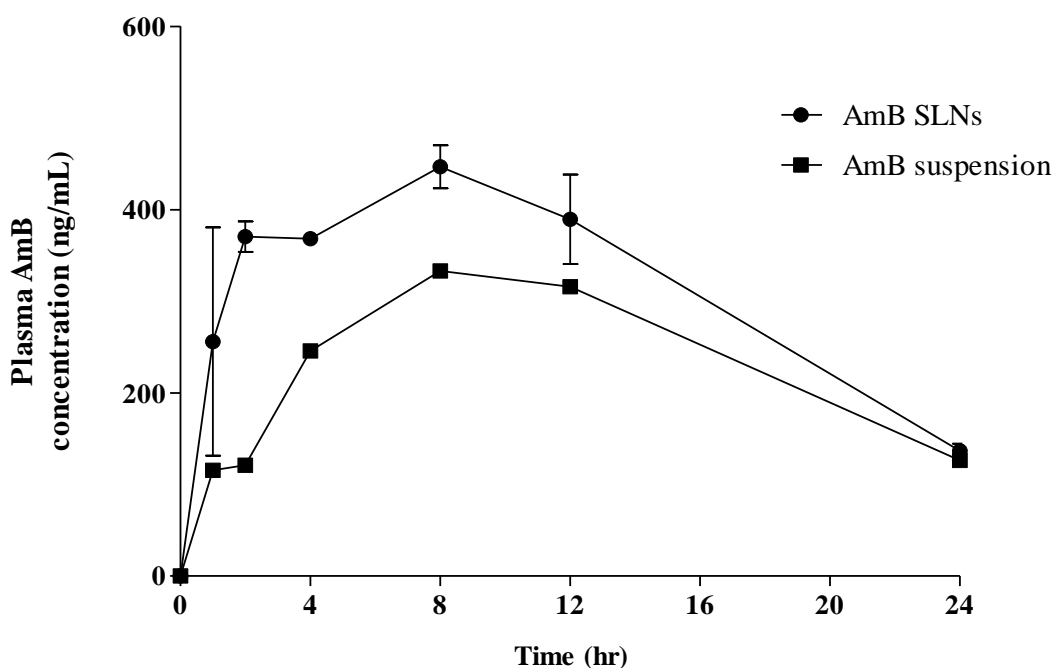


Figure 5.1 Mean plasma concentration-time curves of AmB after a single oral dose administration of AmB SLNs, PAR SLNs and SSZ SLNs; and a suspension of AmB, PAR and SSZ to fasted rats (n = 3)

Table 5.1 Pharmacokinetic data for AmB SLNs and AmB suspension in rat plasma

Formulation	Dose (mg/kg)	T _{max} (hr)	C _{max} (ng/mL)	AUC ₀₋₂₄ (ng.hr/mL)
AmB SLNs	10	8	446.7±23.6	7638.5±440.5
AmB control	10	8	332.9	5649.0

Lymphatic transport of drug-loaded SLNs is highly supported as there have been several studies in which intact SLNs have been found circulating in lymph after oral or intraduodenal administration of SLNs. In these studies, lymph was sampled from cannulated lymph ducts of rats to assess the presence of the SLNs [Bargoni *et al.*, 1998; Cavalli *et al.*, 2003; Yuan *et al.*, 2007; Paliwal *et al.*, 2009]. The presence of the second and main peak at 8 hr in the SLN profile could therefore be attributed to lymphatic absorption of the SLNs prior to drug release into the blood, which takes time to occur. Another reason for the second peak could be due to the prolonged absorption of AmB SLNs due to the possible mucoadhesion of the SLNs in the gut [Luo *et al.*, 2011].

Some oral lipid-based AmB formulations which have been studied include the following: Risovic *et al.* (2003) prepared AmB lipid formulations by dispersing the drug in either Peceol[®] or Intralipid[®], and conducted pharmacokinetic studies in male Sprague-Dawley rats weighing 380-450 g. Peceol[®] is an oily vehicle containing glycerol and glyceryl monooleates and used in self-emulsifying lipid preparations, while Intralipid[®] is a fat emulsion prepared mainly for intravenous administration and contains soybean oil, egg yolk phospholipids and glycerin. At an AmB oral dose of 50 mg/kg, the AUC₀₋₂₄, C_{max} and T_{max} obtained were 5984 ng.hr/mL, 769 ng/mL and 2 hr for the Intralipid[®] formulation. For the Peceol[®] formulation, a 5 mg/kg dose

gave AUC_{0-24} , C_{max} and T_{max} of 4415 ng.hr/mL, 1187 ng/mL and 2 hr; while for a 50 mg/kg dose, the values were 11 407 ng.hr/mL, 1469 ng/mL and 4 hr, respectively.

Gershkovich *et al.* (2009) have prepared an AmB lipid formulation in Peceol®/distearoylphosphatidylethanolamine-poly (ethylene glycol)₂₀₀₀ (DSPE-PEG₂₀₀₀). The authors administered the formulation by oral gavage to fasted male Sprague-Dawley rats (330-350 g) at two concentrations; 4.5 mg/kg and 10 mg/kg, and obtained AUC_{0-24} as 991 ng.hr/mL and 1534 ng.hr/mL, C_{max} as 71 ng/mL and 96 ng/mL and T_{max} at 6.3 hr and 12.5 hr, respectively.

Patel and Patravale (2011) used the microemulsion-based nanoprecipitation technique to formulate AmB SLNs and obtained AUC_{0-24} , C_{max} and T_{max} as 1906.8 ng.hr/mL, 124.94 ng/mL and 9 hr, respectively, after administering an oral dose of 200 mg/kg to fasted male Wistar rats weighing 200-250 g.

Jain *et al.* (2012) used a two-step desolvation method to prepare AmB polymer-lipid hybrid nanoparticles and obtained AUC_{0-72} to be 2813 ng.hr/mL, C_{max} as 94.38 ng/mL and T_{max} at 8 hr after a dose of 10 mg/kg was orally administered to fasted male Sprague-Dawley rats weighing 200-250 g.

In the study by Patel and Patravale (2011), a very high dose of AmB was administered to the rats which was 20 times what was used in the present work however, the C_{max} obtained in the present study is 4.5-fold higher than that reported by the former. The AmB SLNs formulated in the present study is therefore superior in terms of bioavailability. Furthermore, the SLN preparation method utilised in the present work is much simpler and timesaving, employing cheap, readily available and natural lipids in the formulation. The formulation method reported by Patel and Patravale (2011) lasts over 6 hr. The same can be said of the method used by Jain *et al.* (2012) which requires more than 12 hr of preparation time. Gershkovich *et al.* (2009) on the other hand prepared a relatively simple formulation involving only three steps however, the

whole process lasts not less than 5 hr. Alternatively, the AmB lipid preparations by Risovic *et al.* (2003) required merely stirring the drug in Peceol[®] or Intralipid[®] with gentle heating if needed however, the two vehicles are very expensive. The authors obtained a better AmB bioavailability in the Peceol[®] vehicle.

The C_{\max} values obtained by Risovic *et al.* (2003) for AmB in Peceol[®] were higher than those obtained in the present study; the 5 mg/kg formulation for instance gave a value 2.7 times higher than that obtained in the present study. Again, for the AUC_{0-24} , they obtained a value of 4415 ng.hr/mL for the 5 mg/kg dose, and a value of 11 407 ng.hr/mL when the dose was increased 10-fold to 50 mg/kg, clearly depicting a lack of dose proportionality. The AUC_{0-24} obtained in the present study however was 7638.5 ng.hr/mL for a 10 mg/kg AmB dose, which is in line with the values obtained in the former study.

It can be observed that the aforementioned results show wide variations in the data from the various studies except for those obtained by Risovic *et al.* (2003), which showed somewhat comparable AUC_{0-24} values to that obtained in the present study. Although Risovic *et al.* (2003) and Gershkovich *et al.* (2009) dispersed AmB in Peceol[®], the former group had higher AUC_{0-20} and C_{\max} values, which could be attributed to the different methods they used to prepare the formulations. Risovic *et al.* (2003) merely dissolved AmB in the vehicle with gentle heating while Gershkovich *et al.* (2009) used DSPE-PEG₂₀₀₀ and ethanol in addition to the Peceol[®] although the solvent was evaporated off in the last step of the procedure.

In cross-study comparisons, where the blood concentration-time curve of a particular drug product in one study is compared with the blood concentration-time curve of the same drug in another study, misleading conclusions can be made. The credibility of any bioavailability study involving the assay of drug levels in plasma and urine is the analytical methodology used to determine the drug levels, in addition to the study design and subject controls. In the review of

the studies conducted on oral AmB lipid formulations on animals, it can be observed that there were sizable differences in the plasma AmB levels and hence AUC values from the different studies. Usually, such differences are attributable to different subject populations (species and gender), differences in the various study conditions, as well as the different assay methods or varying modifications of the same assay technique employed [Malinowski and Johnson, 2006].

5.3.3 Absorption of PAR from SLNs and suspension

The encapsulation of hydrophilic drugs into the hydrophobic matrix of SLNs is challenging. This is because such drugs tend to quickly partition into the aqueous phase during and after production of the SLNs because of their low affinity for, and weak interaction with the lipids. With the emulsification solvent diffusion technique used in the present study however, an encapsulation efficiency of 60.7% was achieved for PAR (Section 2.4.12), which is a hydrophilic compound.

Figure 5.2 shows the plasma concentration-time curves for PAR from SLNs and suspension. The curves show a higher concentration for the PAR suspension than the SLNs. Both curves however showed a similar pattern of absorption with T_{max} occurring at 1 hr in both cases, followed by a decreasing concentration over the study period. The C_{max} for the PAR suspension was obtained as 1337.0 ng/mL, being about 2.2 times higher than that obtained for the SLNs. The AUC_{0-24} however remained essentially unchanged for both formulations; 5146.0 ± 356.4 ng.hr/mL as against 5727.0 ng.hr/mL for the SLNs and suspension, respectively, albeit slightly higher for the latter.

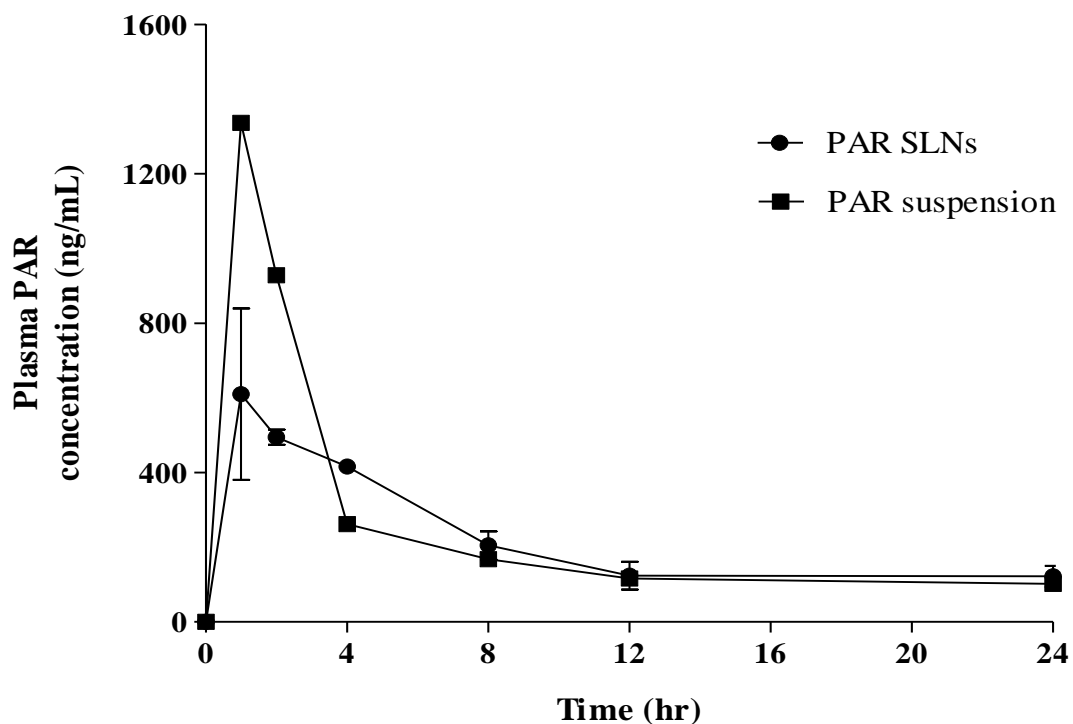


Figure 5.2 Mean plasma concentration-time curves of PAR after a single oral dose administration of AmB SLNs, PAR SLNs and SSZ SLNs; and a suspension of AmB, PAR and SSZ to fasted rats (n = 3)

Table 5.2 Pharmacokinetic data for PAR SLNs and PAR suspension in rat plasma

Formulation	Dose (mg/kg)	T _{max} (hr)	C _{max} (ng/mL)	AUC ₀₋₂₄ (ng.hr/mL)
PAR SLNs	10	1	609.9±229.5	5146.0±356.4
PAR control	10	1	1337.0	5727.0

The reason for the observed disparity of higher AmB absorption from SLNs than from the AmB suspension, as opposed to the reverse situation for PAR can be explained by the fact that PAR has much higher aqueous solubility than AmB, which is practically insoluble in water. In addition, PAR is favourably absorbed in the small intestine after oral delivery [Heading *et al.*, 1973; Clements *et al.*, 1978], which was why a rapid absorption, reflected in a high C_{\max} was observed for the PAR suspension. In the *in vitro* release study (Section 2.4.13), more than 65% of the encapsulated PAR was released from the SLNs within 8 hr. This is reflected in the plasma PAR concentration profile which projects that majority of the drug had been absorbed into blood by 8 hr. Several authors have found intact SLNs circulating in blood; at 30 min and 21 hr after intraduodenal administration [Bargoni *et al.*, 1998; Cavalli *et al.*, 2003], and at 2 hr after oral delivery [Yuan *et al.*, 2007] of the SLNs to rats, using TEM analyses and fluorescence imaging, respectively. Since blood is an aqueous environment as well, PAR release from absorbed SLNs circulating in blood was a continuous process by passive diffusion.

The T_{\max} for AmB SLNs occurred at a later time as compared with that for the PAR SLNs because of the very slow rate of AmB release from the SLNs into the surrounding aqueous medium so that, most of the AmB would be absorbed via uptake of the intact SLNs, which is a slow process. Furthermore, the presence of food (4 hr after dose administration) in the GI tract of the animals slowed down the uptake of the SLNs, resulting in increased release of PAR in the GI tract prior to its absorption as opposed to the AmB, which was preferentially encapsulated within the hydrophobic lipid matrix of the particles. As a result, a higher proportion of the AmB SLNs were likely to have been taken up intact and transported via lymph resulting in the longer T_{\max} .

5.3.4 Absorption of SP from SSZ

SP is a product of the hydrolytic activity of azoreductase enzyme-producing bacteria in the colon, on the azo link in SSZ as depicted in Figure 5.3; and virtually all the SP produced is quickly absorbed [Peppercorn and Goldman, 1973]. Figure 5.4 shows representative HPLC chromatograms in one rat depicting the initial detection of SP at 2 hr, signalling the arrival at and hydrolysis of SSZ in the caecum, and also the peak plasma SP concentration obtained at 8 hr.

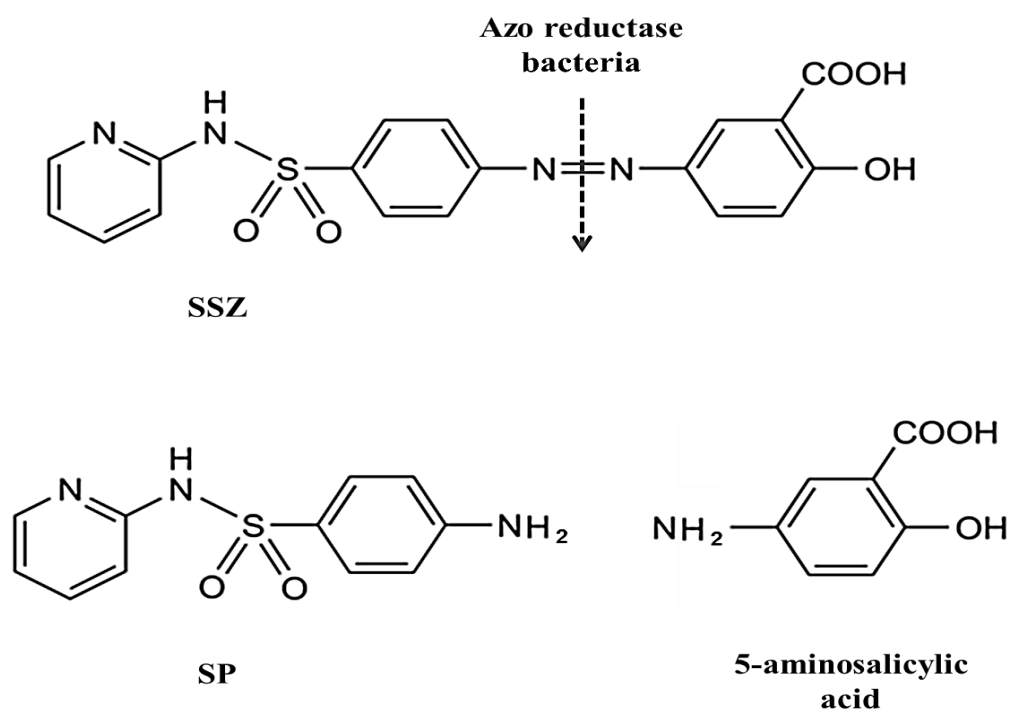


Figure 5.3 Splitting of the azo bond in SSZ by colonic bacteria to release SP and 5-aminosalicylic acid

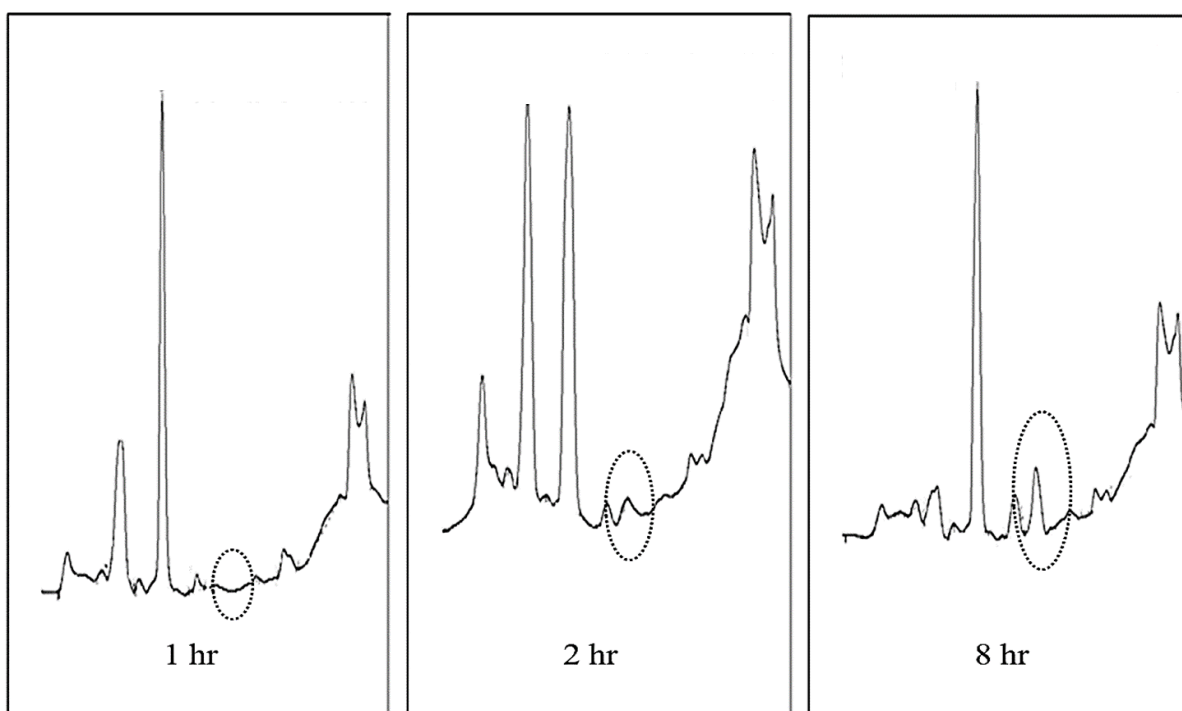


Figure 5.4 Representative HPLC chromatograms showing the appearance of SP in plasma at 2 hr and peaking at 8 hr post dosing in one rat

The plasma concentration-time profiles for SP released from SSZ SLNs and suspension are depicted in Figure 5.5. The pharmacokinetic data in Table 5.3 show that the AUC_{0-24} for SP from the SLNs was higher than that for the suspension; 5095.0 ng.hr/mL as against 3307.0 ng.hr/mL. The C_{max} was however slightly higher for SP from the SSZ suspension; 362.4 ng/mL as opposed to 341.8 ng/mL, while T_{max} was the same in both cases.

Both plasma concentration-time profiles showed a similar pattern of increase in SP concentration followed by a decrease. The large error bars are indicative of a wide variation in SP production and absorption since the level of SP in the plasma mainly depends on the presence and amount of the azoreductase-producing bacteria in the colon, the rate of activity of the bacteria, as well as the variable arrival rates of the SSZ SLNs at the caecum. These factors are influenced by individual differences in the animals [Staniforth *et al.*, 1987; Gramatte

and Terhaag, 1991]. Nonetheless, the use of SP in the present study is chiefly to mark the arrival of SSZ at the caecum using the initial detection of the former in plasma.

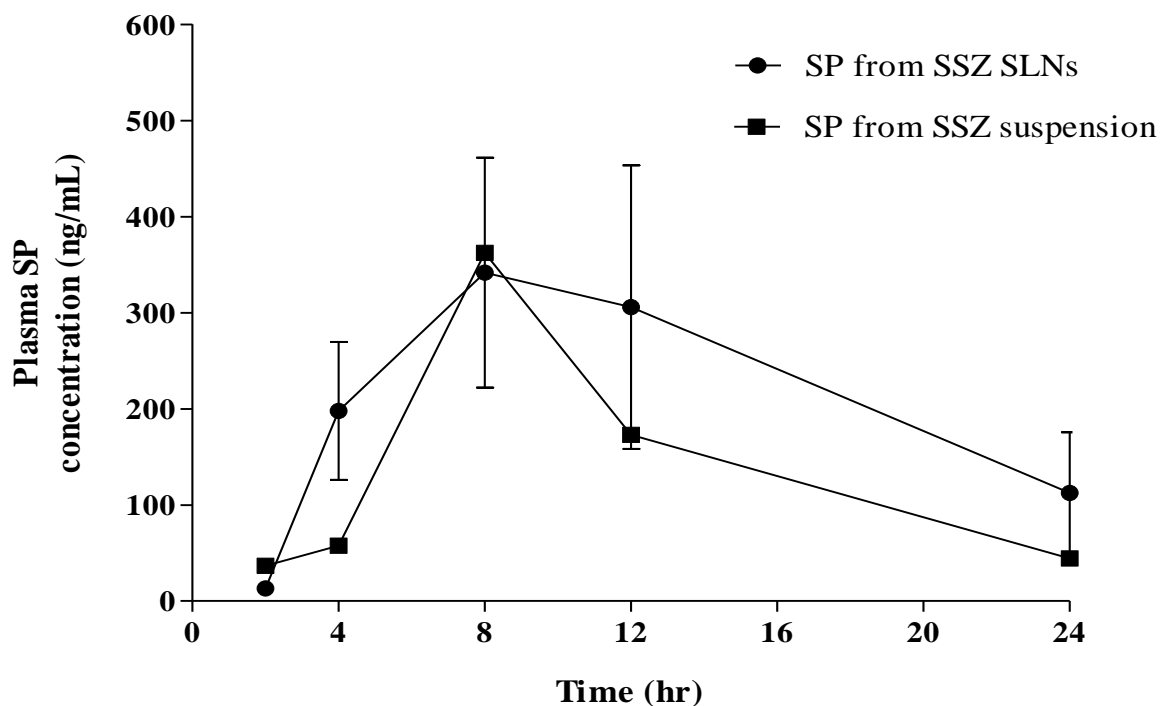


Figure 5.5 Mean plasma concentration-time curves for SP after a single dose oral administration of AmB SLNs, PAR SLNs and SSZ SLNs; and a suspension of AmB, PAR and SSZ to rats (n = 3)

Table 5.3 Pharmacokinetic data for SP from SSZ SLNs and SSZ suspension in rat plasma

Formulation	Dose (mg/kg)	T _{max} (hr)	C _{max} (ng/mL)	AUC ₀₋₂₄ (ng.hr/mL)
SP (from SSZ SLNs)	10	8	341.8±169.1	5095.0±3186.2
SP (from SSZ suspension)	10	8	362.4	3307.0

5.3.5 Pilot GI transit study

In order to test the viability of the indirect method for estimating the GI transit and absorption of AmB SLNs using PAR and SP as markers, this pilot GI study was conducted. The three SLNs exhibited identical physicochemical characteristics as discussed in Chapter 2. Figure 5.6 shows the plasma drug concentration-time profiles for AmB, PAR and SP following simultaneous oral administration of AmB, PAR and SSZ SLNs to the rats.

The T_{max} of about 1 hr observed for PAR indicates a rapid PAR release and absorption in the small intestine and therefore serves as a good estimate of the gastric emptying time of the SLNs. AmB SLNs were slowly absorbed from the GI tract most likely via lymphatic transport and Peyer's patches, which are located mainly in the ileum, prior to drug emptying into systemic circulation and reaching T_{max} at 8 hr.

There was a lag time of about 2 hr prior to appearance of SP in the plasma, which estimates the caecal arrival time (CAT) of the SLNs. The delay in the absorption of SP is due to a combined delay in the arrival of the SLNs at the colon, as well as the delay in the microbial degradation of SSZ, followed by SP absorption. It then follows that the estimated small intestinal transit time (SITT) of the SLNs is 1 hr, which is the difference between CAT and the time of initial detection of PAR in the plasma, which was also found to be 1 hr.

The AUC_{0-24} for AmB SLNs was 1.6 times more than that for PAR, indicating a more favourable albeit slow uptake process as well as the suitability of using SLNs to improve the bioavailability of AmB. However, PAR had the highest magnitude of C_{max} (609.9 ng/mL) among the three analytes, which is indicative of a rapid rate of absorption from the small intestine, and more likely to be as a result of released PAR than due to uptake of the PAR SLNs followed by drug emptying into blood.

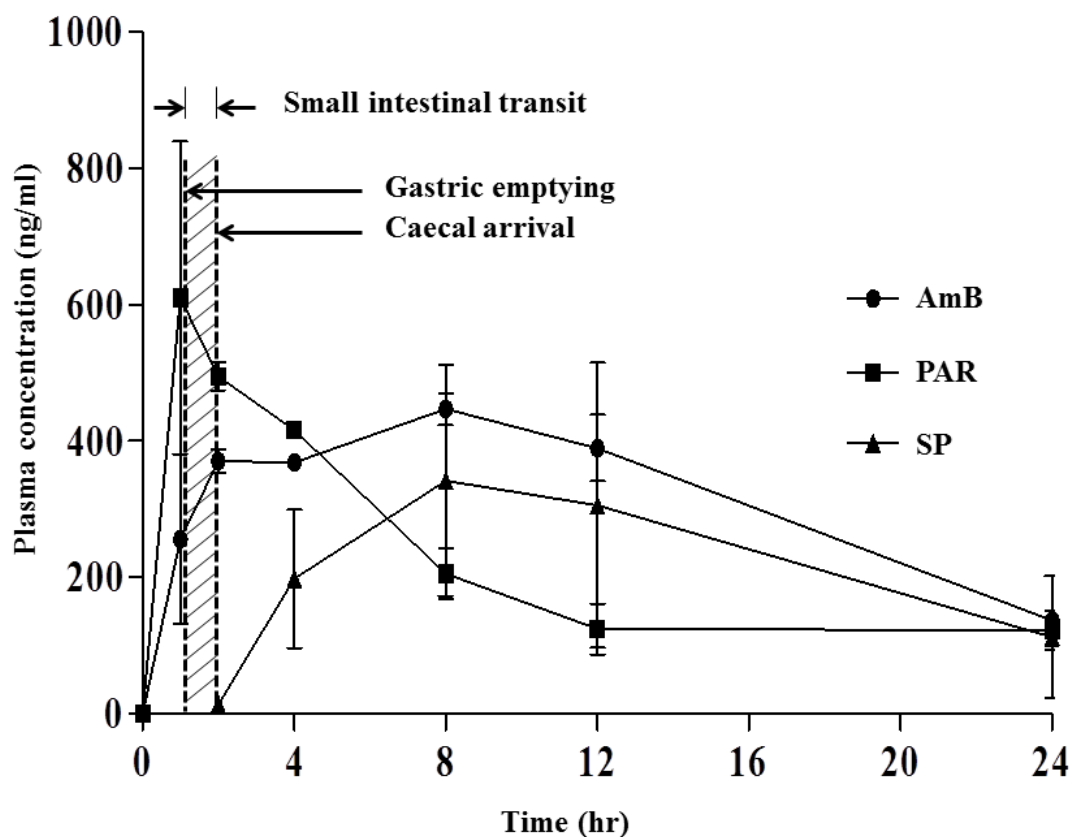


Figure 5.6 Plasma drug concentration-time profiles for AmB, PAR, and SP following simultaneous administration of AmB SLNs, PAR SLNs and SSZ SLNs at a dose of 10 mg/kg each (n = 3)

5.3.6 Considerations for the main GI transit study

The plasma PAR profiles showed the C_{max} of PAR for both the SLNs and suspension as the first point in the respective curves. As a result of this, more sampling points during the first hour post dose administration will be considered to ensure a more accurate estimate of T_{max} and hence, gastric emptying.

For the AmB SLN formulation, the 10 mg/kg dose used produced suitable plasma concentrations and the results obtained were comparable with or better than some published data. For PAR and SSZ as well, the 10 mg/kg dose seems favourable as PAR produced very

high plasma concentrations within the initial two hours of the study, and the SP from the SSZ was also quantifiable. The dose was therefore maintained in the main GI transit study.

In the subsequent GI transit study (Chapter 6), the control rat group were given a dose of only AmB suspended in distilled water. Pure PAR and SSZ were excluded from the control dose as the pharmacokinetic data from PAR and SSZ were deemed not relevant in the control group.

Lastly, since most of the studies conducted on the oral bioavailability of AmB in literature are in fasted rats, it was an objective to study the effect of food on the GI transit and absorption of the AmB SLNs in the subsequent study. As a result, the fasting period post dose delivery was extended as well in the fasted group.

The results obtained in this pilot study strongly indicate that the HPLC method developed and validated in the preceding chapter is very suitable for the simultaneous assay of AmB, PAR and SP, using piroxicam as the internal standard. The HPLC method may therefore be employed in pharmacokinetic studies on these drugs as well as in the indirect estimation of the GI transit properties of oral dosage forms, using PAR and SP as marker drugs.

5.4 Conclusions

Oral pharmaceuticals are more economical to formulate because they do not require sterile manufacturing conditions. Oral drug administration is most preferred for reasons such as patient convenience and compliance, which increase the therapeutic efficacy of a drug. The AmB SLNs therefore serve to produce a triple benefit of convenience of oral administration, improved bioavailability and potential for reduced renal toxicity.

The pilot GI transit study indicates that AmB in SLNs is absorbed slowly but significantly from the small intestines. Therefore, development of dosage forms for delivery of AmB via the oral route may exploit this attribute.

The previously validated HPLC method can potentially be applied to simultaneously assay AmB, PAR, SP and piroxicam in rat plasma, and the indirect approach of studying the GI transit properties and pharmacokinetics of AmB SLNs has been successfully applied in the present study. The data from this pilot study has been useful as a better study protocol can be developed to achieve a better outcome from the main transit study.

CHAPTER 6

EFFECT OF FOOD STATUS ON THE GASTROINTESTINAL TRANSIT OF AMPHOTERICIN B-CONTAINING SOLID LIPID NANOPARTICLES

6.1 Introduction

The administration of drug products with food can alter drug bioavailability by either affecting the drug substance directly or indirectly, or by affecting the drug product, and may result in clinically important outcomes. In reality, the exact mechanism by which food changes bioavailability of drugs is difficult to determine without conducting specific mechanistic studies [FDA, 2002]. Generally, significant food effects on bioavailability occur less with most drug products containing BCS class I drugs (highly soluble/rapidly dissolving and highly permeable drugs). This is because the absorption of such drugs is usually pH and site-independent and thus insensitive to differences in dissolution [FDA, 2002]. However, for some drugs in this class, food can influence bioavailability if the drug is unstable in the GI tract, or if the drug undergoes extensive first-pass metabolism, adsorption or complexation. The type of excipients used in a product, interactions between excipients, as well as food-induced changes in the physiology of the gut can also affect bioavailability. Drug-food interactions present problems particularly for oral controlled-release products that are single unit dosage forms because a significant effect by food on systemic availability may have serious and prolonged consequences [Welling, 1996; Singh, 1999; FDA, 2002].

For drugs that show enhanced bioavailability with food intake, high fat meals are recommended as fatty meals affect GI physiology and maximise drug transfer into systemic circulation. For immediate-release drug products containing BCS class II, III and IV drugs, and modified-release products, food effects most likely result from more complex combinations of factors that influence the *in vivo* dissolution of the drug product and/or absorption of the drug. In such

instances, the effect of type and magnitude of food on bioavailability are difficult, if not impossible to predict without conducting a fed study [FDA, 2002].

The effects of food on drug bioavailability may manifest due to changes in drug dissolution prior to absorption, changes in GI residence time of the dosage form, modification in membrane permeability of the drug and inhibition of efflux transporters. Furthermore, the type and quantity of food, as well as the time interval between food intake and dosing may reduce, delay, increase or accelerate drug absorption. In addition, different dosage forms of the same drug may be affected differently by food [Welling, 1996; Singh, 1999; Benet *et al.*, 2004].

It is important to know how orally administered drug products respond to GI physiology during their transit through the GI tract. The transit of dosage forms through the oesophagus is dependent on the dosage form type and the patient's posture; however, most dosage forms administered in an upright position transit quickly through the oesophagus in less than 15 sec. Gastric residence time, gastric emptying time or gastric emptying rate are synonymous terms used to refer to the time it takes a dosage form to travel through the stomach. Gastric emptying (GE) of pharmaceutical products is highly variable depending on the dosage form and fed/fasted states. Normal gastric residence times in humans range from 5 min to 2 hr however, longer times have been observed for large single dosage units [Nimmo *et al.*, 1973; Ashford, 2001].

In the small intestine, there are propulsive and mixing movements; the former primarily determines the intestinal transit rate and hence the residence time of a dosage form. As this is the main site of absorption in the GI tract for most drugs, small intestinal transit time (SITT) (transit time between the stomach and the caecum) is an important factor with respect to drug bioavailability, and particularly important for dosage forms that slowly release the incorporated drug as they pass along GI tract [Ashford, 2001].

Colonic transit of pharmaceuticals is long, variable and dependent on the type of dosage form as well as the diet, eating pattern and disease state of an individual. Contractile activity in the colon consists of propulsive contractions or mass movements away from the mouth and segmental or haustral contractions, which serve to mix the luminal contents. Segmental contractions are brought about by circular muscles and predominate whereas propulsive contractions, which are due to contractile activity of longitudinal muscles occur only 3-4 times daily in normal individuals. Colonic transit is therefore characterised by short bursts of activity followed by long periods of stasis and can vary from 2 to 48 hr. In most individuals, mouth-to-anus transit times are longer than 24 hr [Ashford, 2001].

It has been shown in humans that SITT of dosage forms is more consistent than gastric transit time (GTT), and the former is less affected by the nature (physical state or size) of the dosage form and the presence of food [Davis *et al.*, 1986].

The importance of the transit times of dosage forms in the various regions of the GI tract makes it necessary for investigations involving the effect of food on drug absorption from dosage forms to be conducted. This allows for appropriate assessment of the resulting pharmacokinetic data, which in turn can be used in optimising the formulation to maximise bioavailability.

Peh and Yuen (1996) have monitored the GI transit and absorption of theophylline pellets in human volunteers, applying the indirect estimation method using PAR and SP as markers. The results they obtained were consistent with the findings of Yuen *et al.* (1993), who monitored pellets of approximately similar size and density using gamma scintigraphy. The results were also in agreement with previous gamma scintigraphic studies [Christian *et al.* 1980; Davis *et al.* 1984; Devereux, 1987], which indicate the suitability of the indirect method for a harmless and less expensive GI transit study.

AmB has two important physicochemical characters: amphiphilic behaviour due to the apolar and polar sides of its lactone ring; and amphoteric behaviour due to the presence of ionisable carboxyl and amine groups. As a consequence of its amphiphilic and zwitterionic nature, and the asymmetrical distribution of hydrophobic and hydrophilic groups, AmB is poorly soluble in all aqueous solvents and in many organic solvents. Although it is water soluble at a pHs 2 and 11, the solubilised drug tends to show a loss of activity with pronounced instability [Torrado *et al.*, 2008]. AmB, a BCS class IV drug, is poorly absorbed not only orally but also after intramuscular and subcutaneous administrations as well. It is slowly excreted in the urine and traces are still detectable 2 months after cessation of treatment [Moffat *et al.*, 2005].

The absorption of small oral doses of PAR occurs readily while that of larger doses varies considerably and is influenced by the rate of gastric emptying, the presence of food and the time of day. PAR is widely distributed throughout most body fluids and is present in saliva at concentrations paralleling those in plasma. PAR undergoes first-pass metabolism, and about 70 to 90% of the administered dose is bioavailable [Moffat *et al.*, 2005].

SSZ is partially and irregularly absorbed after oral administration however, the absorbed amount is not metabolised but excreted unchanged in urine. The greater part of the dose passes unchanged into the colon and is metabolised by bacteria to SP and 5-aminosalicylic acid, which is thought to be the active moiety [Moffat *et al.*, 2005].

In previous chapters, an AmB-containing SLN formulation has been successfully developed and subjected to extensive characterisation. A pilot GI transit study of the formulation has also been performed in fasted rats. In this chapter, the pharmacokinetics of AmB and the GI transit of AmB SLNs as a consequence of food status is described by means of the indirect estimation method, using PAR and SP as markers.

6.2 Methods

6.2.1 Preparation of SLN formulations

The proportions of ingredients described in the optimised procedure for formulating the SLNs in Section 2.3.3 were used for preparing individual lipid nanoparticle formulations containing AmB, PAR or SSZ.

6.2.2 Animals

Twelve (12) disease-free male Sprague-Dawley rats weighing 250 ± 20 g were obtained from the Animal Holding Unit of the University Sains Malaysia and used for the study. The study protocol complied with the recommendations of and was approved by the Animal Ethics Committee of the University Sains Malaysia. The animals were maintained under a 12/12 hr dark/light cycle and housed in cages at ambient temperature and humidity. They were allowed free access to food and water and acclimatised for 7 days before the study. The procedural care of the animals was as described in Section 5.2.2.2.

The rats were randomly divided into fasted-SLNs, fasted-control, fed-SLNs and fed-control groups. Water was withdrawn from all the animals until 2 hr post dose administration. The fasted group was fasted overnight and allowed access to food 8 hr after dosing with the SLNs.

6.2.3 Drug administration and blood sampling

The rats in the fasted-SLNs and fed-SLNs groups were given single-dose oral gavages containing 10 mg/kg of each SLN (AmB, PAR and SSZ) dispersed in distilled water. Blood samples (300 μ L) were collected from the tail end of the rats before dosing and at 0.25, 0.5,

0.75, 1, 2, 4, 8, 12, 24 and 30 hr post dose administration into heparinised microcentrifuge tubes. Plasma was immediately separated from the blood samples by centrifugation and frozen till analysis using the HPLC method described in Sections 4.3.1 and 4.3.3.

6.2.4 Estimation of gastric transit time (GTT)

The parameters for estimating the time elapsed for GE or GTT were obtained from the plasma PAR absorption-time profiles and based on the assumption that the percentage of PAR absorbed is directly related to the percentage of PAR SLNs emptied from the stomach into the duodenum [Peh and Yuen, 1996]. This serves as a fairly good estimate for GE of the AmB and SSZ SLNs as well. This is because all three SLNs shared identical physical characteristics (Chapters 2 and 3) and were administered simultaneously to the rats; therefore, the assumption is that all three SLNs would transit similarly within the GI tract. The time for complete emptying of the SLNs (T_{90P}) from the stomach was estimated using the time for 90% of PAR absorption in the small intestine, which was also considered the GTT. Another parameter obtained from the plasma PAR absorption-time profile was the time for 10% PAR absorption (T_{10P}), which was used to signal the arrival of the SLNs at the small intestine.

6.2.5 Estimation of small intestinal transit time (SITT)

The SITT was estimated as the time difference between the caecal arrival time of the SLNs and the start of emptying of the SLNs into the small intestines (T_{10P}). SITT was therefore approximately the difference between T_{10S} (the time taken for 10% SP absorption in the caecum) and T_{10P} .

6.2.6 Estimation of caecal arrival time (CAT) and colonic transit time (CTT)

Data obtained from plasma SP concentration-time curves were used to determine the CAT of the AmB SLNs. The CAT by definition is the time taken for the SLNs to arrive at the caecum and has been estimated as the time for the initial detection of SP in the plasma using the indirect method of estimation [Staniforth, 1989]. Due to the time lapse in SP production from SSZ released from SSZ SLNs reaching the caecum, CAT was estimated to be approximately T_{10S} . T_{10S} serves as a better estimate for CAT of the SLNs than the first SP detection in plasma as the latter may be mainly due to free SSZ released from the SLNs prior to caecal arrival, rather than SSZ released from the intact SSZ SLNs within the caecum. The CTT was estimated as the time for 90% SP absorption (T_{90S}).

6.2.7 Estimation of AmB absorption in the stomach, small intestine and colon

The percentage of AmB SLNs absorbed in the stomach, small intestine and the colon were estimated from the plasma AmB absorption-time profiles using the respective transit times (GTT and SITT). The percentage AmB absorbed during gastric transit or GTT was estimated from the time of dose administration to T_{10P} . The time from T_{10P} to T_{10S} , or SITT was used to estimate the percentage absorption in the small intestine while the remaining percentage of AmB SLNs absorbed after this point was considered as summation of both colonic and progressed lymphatic absorption.

6.2.8 Statistical analyses

The data have been presented as mean \pm standard deviation (SD) where indicated. Statistical analyses were performed using GraphPad Prism 5 software. The various parameters were

analysed using analysis of variance (ANOVA) which distinguishes effects due to subject/group and treatment. Statistical significance was considered when p value < 0.05 .

6.3 Results and discussion

6.3.1 Improved oral bioavailability of AmB from the SLNs

Figure 6.1 shows the plasma concentration versus time profiles of AmB suspension and freshly prepared AmB SLNs in fasted rats and Table 6.1 gives the pharmacokinetic parameters of AmB in both fasted and fed rats. The peak plasma concentration (C_{\max}) for AmB from the SLNs was 564.7 ± 122.5 ng/mL and the T_{\max} was 8 hr, both values being significantly higher ($p < 0.05$) than those obtained for the AmB suspension, 205.3 ± 9.6 ng/mL and 1.50 ± 0.71 hr, respectively, as shown in Table 6.1. Furthermore, the extent of absorption (AUC_{0-30}) of AmB was significantly higher ($p < 0.05$) for the AmB SLNs compared to the suspension; 7953.0 ± 551.2 ng.hr/mL against 4412.5 ± 376.9 ng.hr/mL.

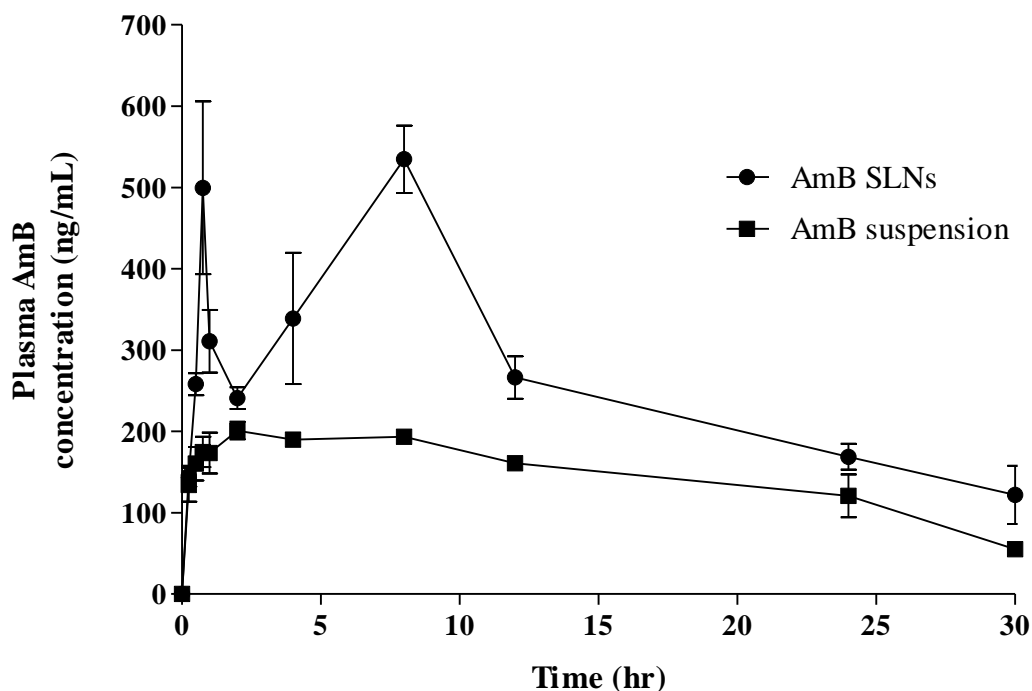


Figure 6.1 The mean plasma concentration-time curve of AmB in fasted rats after a single 10 mg/kg oral dose of AmB suspension; and 10 mg/kg dose each of AmB SLNs, PAR SLNs and SSZ SLNs

Table 6.1 Pharmacokinetic data for AmB SLNs and AmB suspension in fasted and fed rats

Group	Dose (mg/kg)	T _{max} (hr)	C _{max} (ng/mL)	AUC ₀₋₃₀ (ng.hr/mL)	
Fasted	AmB SLNs	10	8.00±0.00*	534.7±122.5*	7953.0±551.2*
	AmB suspension	10	1.50±0.71	205.3±9.6 [#]	4412.5±376.9
Fed	AmB SLNs	10	9.33±4.62**	323.2±44.0 **	7565.3±1390.6 **
	AmB suspension	10	0.38±0.18	173.8±27.9	3343.0±209.3

* $p < 0.05$ - significantly different from AmB suspension in fasted rats

** $p < 0.05$ - significantly different from AmB suspension in fed rats

$p < 0.05$ - significantly different compared with fed rats

In the case of the SLNs however, a rate-limiting step defined by the rate of AmB diffusion within the SLN matrix followed by drug release precedes absorption. The significant improvement in the extent of AmB absorption from SLNs points to an alternative route of absorption into the systemic circulation, most likely through uptake of intact SLNs since the GI epithelium is capable of taking up submicron to micron-sized particulates.

Figure 6.2 depicts plasma AmB concentration in the fed rats. A similar observation was made in the fed rats as in the fasted rats, where C_{max} , T_{max} and AUC_{0-30} obtained from the rats administered the AmB SLNs were significantly ($p < 0.05$) higher as compared with the corresponding values obtained from the rats administered the suspension of pure drug only.

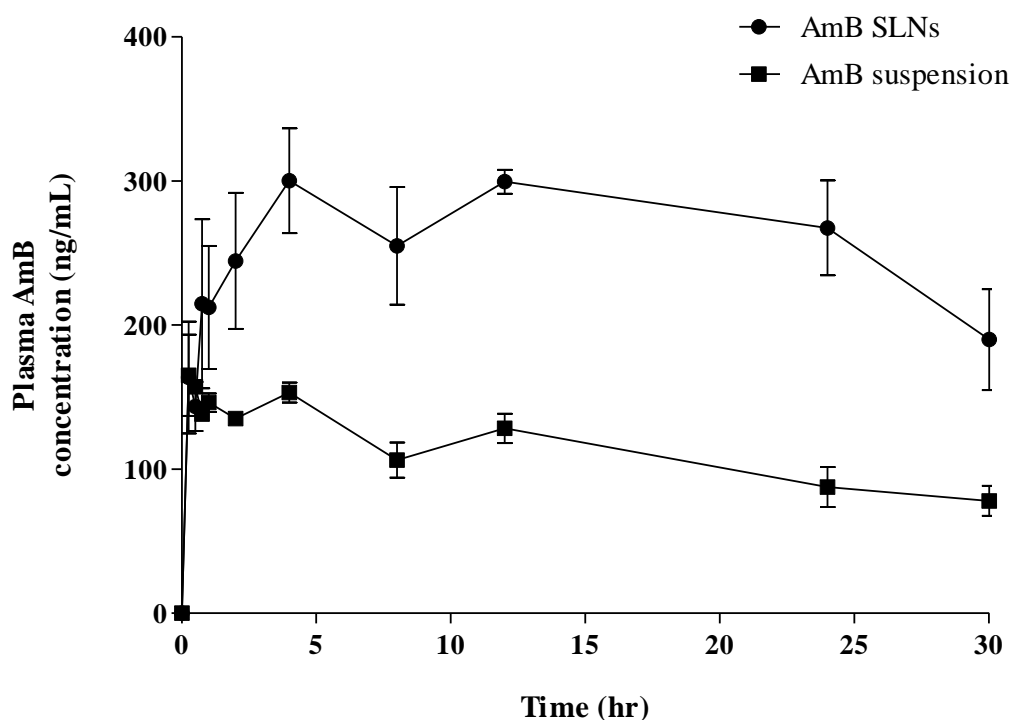


Figure 6.2 The mean plasma concentration-time curve of AmB in fed rats after a single 10 mg/kg oral dose of AmB suspension; and 10 mg/kg dose each of AmB SLNs, PAR SLNs and SSZ SLNs

For the fed rats, the C_{\max} , T_{\max} and AUC_{0-30} were 323.2 ± 44.0 ng/mL, 9.33 ± 4.62 hr and 7565.3 ± 1390.6 ng.hr/mL, respectively, for the SLN formulation; and for the suspension, the values were 173.8 ± 27.9 ng/mL, 0.38 ± 0.18 hr and 3343.0 ± 209.3 ng.hr/mL, respectively. These results clearly indicate improved oral absorption and bioavailability of AmB after incorporation into SLNs in both the fasted and fed states.

From Figures 6.1 and 6.2, two peaks in both the fasted (0.75 and 8 hr) and fed (4 and 12 hr) states are noted after administration of the AmB SLNs, with those in the fasted rats being more prominent. A similar observation was made by Yang *et al.* (1999), Luo *et al.* (2011) and Jain *et al.* (2012) who reported bi-phasic plasma peak concentrations for camptothecin SLNs, puerarin SLNs and AmB gelatin-lipid nanoparticles. The first peak was due to absorption of free AmB particles released from the AmB SLNs and loosely adsorbed AmB on the surface of the SLNs. Free AmB may also be contributed by digestion of the lipid component of the SLNs by lipases followed by the action of bile salts to produce mixed micelles and chylomicrons containing solubilised AmB [Müller *et al.*, 2006; Porter *et al.*, 2007]. However, contribution of free AmB by this mode is expected to be modest. A further contribution of free AmB would come from released drug from the SLNs. Finally, absorption of free AmB is buoyed by surfactant (sodium cholate) effects within the SLNs.

The AUC_{0-30} and C_{\max} values obtained for the fasted rats in the main study were 7953.0 ± 551.2 ng.hr/mL and 534.7 ± 122.5 ng/mL, respectively, and were slightly higher than those obtained in the pilot study, 7638.5 ± 440.5 ng.hr/mL and 446.8 ± 23.5 ng/mL, respectively, which was also conducted in fasted rats although the sampling period in the main study was 6 hr longer. The more prominent peaks in the plasma AmB profiles obtained in the main study seem to reflect the effect of length of fasting period post SLN dosing on AmB bioavailability. In the pilot study, the animals were fasted for 4 hr as opposed to the 8 hr fast in the main study. It can also

be observed that the initial peak at 0.75 hr in the main study is obviously masked in the pilot study due to fewer sampling times during the initial phase. The minor differences are solely due to the different blood sampling times and normal experimental variables in cross-study comparisons and not actually due to differences in bioavailability [Malinowski and Johnson, 2006]. Although the rats used in the pilot study were slightly bigger (325 ± 25 g versus 250 ± 20 g), the adjustments made in the administered doses as per weight of each animal corrected for this. Therefore, the data obtained from the pilot and the main studies are essentially identical and indicate the success and importance of the pilot study.

6.3.2 Gastric transit of the AmB SLNs

The mean plasma PAR concentration-time profiles in both fasted and fed rats are presented in Figure 6.3 and the pharmacokinetic data obtained from the profiles are presented in Table 6.2. In both fasted and fed states, a rapid PAR absorption was observed albeit a slower rate in the fed state. Furthermore, multiple peaks were observed within the first four hours of the PAR concentration-time profile for the fed rats, possibly due to the effect of food.

A later peak occurred at 8 hr post dose administration in the fasted rats and can be attributed to possible uptake of intact SLNs by Peyer's patches and via lymph [Bargoni *et al.*, 1998; Yuan *et al.*, 2007] followed by assimilation and PAR release into blood. This is a slow process and therefore expected to manifest late. In the fed rats however, no such late sharp peak is observed as the presence of food significantly slowed the absorption rate of the intact SLNs. The plasma PAR profile pattern in the fasted rats was very much similar to that for the AmB in the fasted rats, and seems to be an inherent feature of the SLNs formulated in this study.

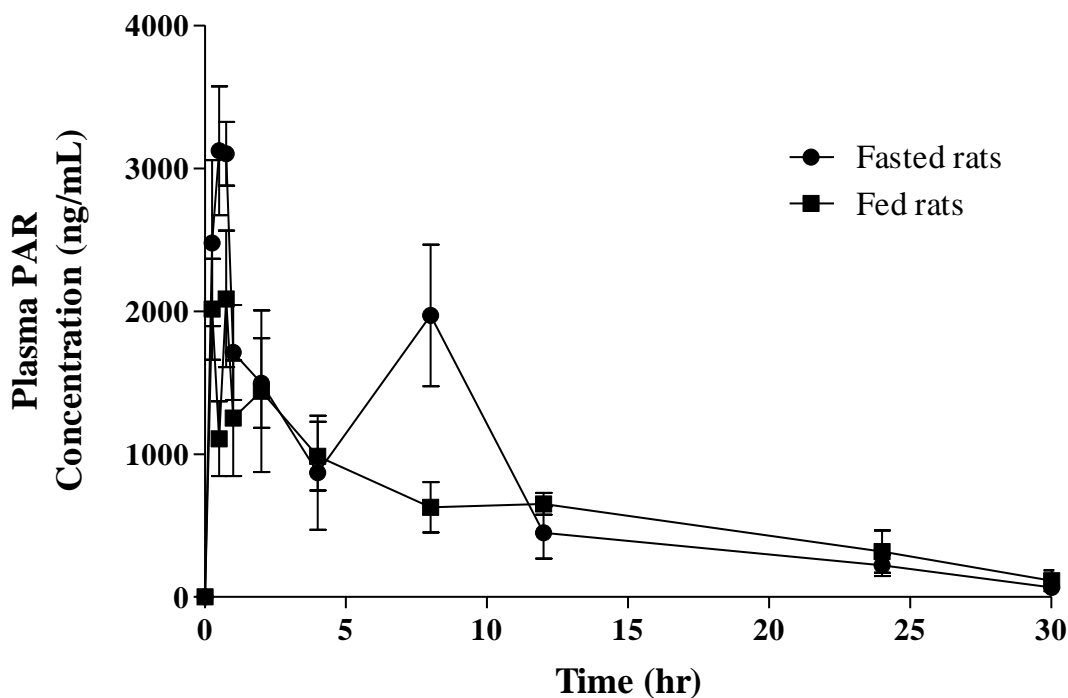


Figure 6.3 Effect of food on the absorption of PAR SLNs in fasted and fed rats (n = 3)

Table 6.2 Pharmacokinetic data for PAR SLNs and PAR suspension in fasted and fed rats

Group	Dose (mg/kg)	T _{max} (hr)	C _{max} (ng/mL)	AUC ₀₋₃₀ (ng.hr/mL)
Fasted	10	0.50±0.25	3616.3±68.4*	21 786.0 ± 5879.8
Fed	10	0.75±0.29	2383.3±747.9	18 135.7±5712.2

* $p < 0.05$ - difference between fasted and fed groups is statistically significant

The main difference between the two profiles was that the initial peak for PAR was much higher than the second peak unlike for the AmB curve. This higher initial peak observed for PAR SLNs is due to the fast release of PAR from the SLNs followed by rapid uptake in the

small intestine. Furthermore, the encapsulation efficiency of PAR was less than that for AmB so that a lower PAR payload is assimilated by the epithelia from uptake of the SLNs. The C_{\max} and AUC_{0-30} values for the PAR SLNs obtained in this study were 3616.3 ± 68.4 ng/mL and 21786.0 ± 5879.8 ng.hr/mL, which were significantly higher than the respective values obtained in the pilot study: 609.85 ± 229.5 ng/mL and 5146.0 ± 356.4 ng.hr/mL. This is because significant absorption of PAR SLNs occurred within the first hour of dose administration resulting in a T_{\max} at 0.50 hr, an observation that was absent in the pilot study because the first blood sample was taken at 1 hr.

PAR has better aqueous solubility than AmB hence PAR favourably partitions out into the more aqueous GI fluids than into the hydrophobic lipid matrix of the SLNs, leaving a lower drug load within any absorbed SLNs in the rats: an effect that was more pronounced in the fed rats. The presence of food caused an insignificant reduction in C_{\max} ($p = 0.05$) and AUC_{0-30} ($p > 0.05$), and a delay in T_{\max} ($p > 0.05$) in the absorption of PAR from SLNs. It is clear from the mean values that a delayed T_{\max} was caused by the presence of food through a slowed gastric emptying process of the SLNs.

In both fasted and fed groups, no lag time in PAR absorption was observed as can be seen from Figure 6.4; however, this phenomenon is most likely a result of the rapid emptying of PAR solution released from the SLNs within the administered dose and subsequent absorption in the small intestine. The absorption of this PAR solution therefore occurred almost instantly after dose administration to the rats and emptying of this solution into the small intestines occurred unobstructed. PAR absorption in patients with pyloric stenosis has been found to be hindered and may cause a delay in GE [Heading *et al.*, 1973]; however, the data obtained in the present study suggest unimpeded emptying into the small intestine. The statistical analyses indicate that although the patterns of absorption of the PAR SLNs in fasted and fed states were different

according to the profiles in Figure 6.3, GE was not markedly slowed by food. This is in agreement with previous studies in which food did not affect the extent of absorption of PAR from tablets but slowed the rate of absorption [McGilveray and Mattok, 1972; Divoll *et al.*, 1982; Digenis and Sandefer, 1994].

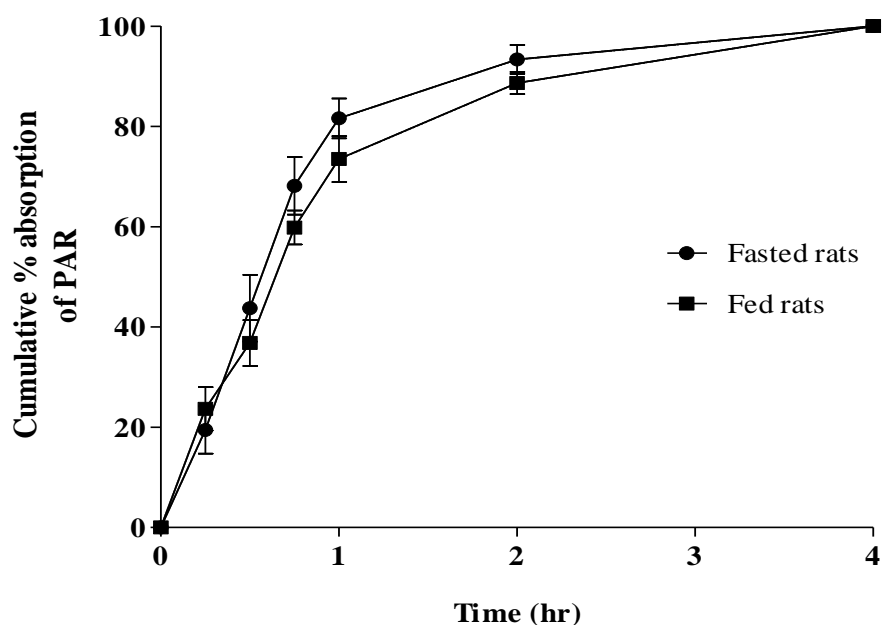


Figure 6.4 Mean PAR absorption versus time curves in the fasted and fed rats (n = 3)

Due to significant lymphatic absorption of lipid-based formulations as evidenced by the two-peak plasma profiles, only the initial four hours of the plasma concentration-time curves of the PAR SLNs were used in estimating T_{10P} and T_{90P} . On observing the profiles, it can be said that the second peak occurring at 8 hr in the fasted rats is due to drug emptying into systemic circulation from the lymphatic vessels, while the initial peak is likely due to direct PAR absorption into blood from the gut. Using the whole absorption profile for the PAR SLNs over the 30 hr study period to determine the values of T_{10P} and T_{90P} would therefore result in an overestimation. The first four hours of the profiles give a better approximation of uptake of intact and digested PAR SLNs by the enterocytes into blood, and excludes SLN absorption via

lymph as much as possible in order to obtain a better estimate of GE. A similar approximation was done by Peh and Yuen (1996) who used the first 10 hr of PAR absorption in estimating GE as opposed to the total 24 hr blood-sampling period they used in human subjects. T_{10P} and T_{90P} were calculated from Figure 6.4, which depicts the cumulative percentage absorption of PAR in the rats.

Quini *et al.* (2012) employed magnetic monitoring using alternating current biosusceptometry as a direct method to estimate GE in rats (equivalent to T_{90P} in the present study), and found it be approximately 1.67 hr and 2.34 hr after liquid (ferrofluid) and solid (ferrite powder pellets and laboratory chow) meals, respectively, were orally administered. These values are comparable with those observed in the present study, which were 1.71 hr and 2.25 hr for the fasted and fed rats, respectively, as presented in Table 6.3, and indicate the suitability of using PAR as an indirect marker for GE.

Table 6.3 Individual values of T_{10P} , T_{90P} and GTT, estimated from plasma PAR profiles under fasted and fed states (n = 3)

Rat No.	Fasted		Fed	
	T_{10P} (hr)	T_{90P} (GTT) (hr)	T_{10P} (hr)	T_{90P} (GTT) (hr)
1	0.16	1.56	0.08	1.74
2	0.18	2.38	0.16	2.38
3	0.09	1.19	0.10	2.63
Mean	0.14	1.71	0.11	2.25
SD	0.04	0.61	0.04	0.46

6.3.3 Small intestinal transit of the AmB SLNs

The mean SITT of the SLNs in the fasted rats was 1.65 ± 0.86 hr, and 1.79 ± 1.29 hr in the fed group as shown in Table 6.4, giving a time difference of only about 0.14 hr and $p > 0.05$, indicating that the difference between the two values is not statistically significant. This shows that the transit of the SLNs in the small intestines was similar in both states. In the study conducted by Quini *et al.* (2012), an identical mean value of approximately 1.71 hr was obtained as SITT in both liquid-meal and solid-meal fed Wistar rats, using magnetic monitoring. In another study by Myagmarjalbuu *et al.* (2013), SITT in mice was found to be approximately 1.60 hr. In the latter study, the authors used fluoroscopic imaging to monitor the transit of radio-opaque markers in the form of 0.5 mm metal balls in the animals. The mice were deprived of food 1 hr before the experiment and allowed access to food 1 hr after administration of the markers. They also used barium to determine the anatomical locations in the GI tract.

The similarities among the values obtained from the two studies and in the present work are in concert with the established notion that transit of liquids and solids [Quini *et al.*, 2012], and suspensions of nano-sized (SLNs in the current work) or larger particles (0.5 mm) [Myagmarjalbuu *et al.*, 2013], in the small intestine is identical. They also indicate that the indirect and inexpensive means of estimating SITT using PAR and SP as marker drugs is reliable, and produces data identical with direct techniques such as the magnetic and fluoroscopic imaging methods used by the other authors. These studies suggest that physiological discrimination between solids and liquids may exist in the stomach but not in the small bowel [Davis *et al.*, 1986; Yuen *et al.*, 1993; Peh and Yuen, 1996].

Table 6.4 Individual values of T_{max} , T_{10S} , CAT and SITT, estimated from plasma SP profiles under fasted and fed states (n = 3)

Rat No.	Fasted				Fed			
	T_{max} (hr)	T_{10S} (CAT) (hr)	SITT (hr)	CTT (hr)	T_{max} (hr)	T_{10S} (CAT) (hr)	SITT (hr)	CTT (hr)
1	8	1.92	1.76	19.9	8	0.92	0.84	23.6
2	12	0.93	0.75	13.9	12	1.42	1.26	22.7
3	8	2.54	2.45	18.8	12	3.36	3.26	27.5
Mean	9.30	1.80	1.65	15.50*	10.70	1.90	1.79	24.60
SD	2.30	0.81	0.86	3.20	2.30	1.29	1.29	2.60

* $p < 0.05$ - Difference between fasted and fed groups is statistically significant

SITT values ranging from 2.70 to 4.58 hr have been obtained in humans using various direct techniques employing materials such as radiolabelled fibre particles [Malagelada *et al.*, 1984] and dosage forms [Davis *et al.*, 1986; Yuen *et al.*, 1993; Billa *et al.*, 2000], a magnetic pill [Worsøe *et al.*, 2011] and a video capsule endoscope [Fischer and Fadda, 2015]. Using the indirect method, SITT has been obtained as approximately 4.1-6.0 hr in both fasted and fed subjects [Peh and Yuen, 1996; Rahman *et al.*, 2005].

The above-mentioned studies in both humans and mice/rats appear to support the proposal of Hofmann *et al.* (1983) that drugs, whether as a molecular solution, micellar preparation or a particulate dispersion, may be considered to be moved along the small intestine at the same net propulsive rate as food particles.

6.3.4 CAT and CTT of the AmB SLNs

The human colon has over 400 distinct species of bacteria as resident flora, with a possible population of up to 10^{10} bacteria per gram of colonic contents [Chien, 1992]. Among the reactions carried out by these floras are azoreduction and enzymatic cleavage. The distribution of azoreductase and glucuronidase activity in the GI tracts of rats and rabbits has been found to be comparable with that in humans [Mooter and Kinget, 1995]. Metabolism of azo compounds by intestinal bacteria is one of the most extensively studied bacterial metabolic processes [Friend and Chang, 1985]. Colon targeted drug delivery systems have attracted considerable attention in developing drug delivery systems that are able to release drugs specifically in the colon in a predictable and reproducible manner, based mainly on the activity of flora in the colon. This makes the colon a site for both local and systemic delivery of drugs [Philip and Philip, 2010].

A number of transit studies on pellets or suspensions have estimated caecal arrival time as the time for the initial detection of SP in plasma [Peh and Yuen, 1996; Kondo *et al.*, 2003(a,b); Rahman *et al.*, 2005]. In the present study, T_{10S} was used to estimate CAT of the AmB SLNs instead of the time for the first appearance of SP in plasma, which with most certainty is a result of SSZ released from the SLNs as solution and arriving at the caecum ahead of the SLNs. The arrival of this SSZ solution would lead to the hydrolysis of free SSZ and not the SSZ released from intact SLNs reaching the caecum and therefore will underestimate the CAT. The most accurate CAT estimation using initial SP detection in plasma would require more frequent blood sampling during the first few hours of the study, which is the main constraint in the use of the indirect approach.

Figure 6.5 and Table 6.4 show the mean SP concentration-time profiles in plasma and the individual data obtained from the profiles, respectively. Both curves showed a similar

absorption pattern. Initially, there was a slight drop in plasma SP concentrations in both food statuses after which the plasma SP level rose and attained a T_{max} at 8 hr.

The first concentration point in each food status is due to the absorption of SP after colonic bacteria activity on released SSZ, which arrives at the colon relatively earlier than the SSZ SLNs. The slight drop in SP concentration thereafter can be attributed to a depleted source of this dissolved SSZ that arrived ahead of the SLNs, as well as the time lapse required for the release of SSZ from the SSZ SLNs, followed by microbial action by colonic bacteria when the SLNs were resident in the colon. The mean CAT was obtained as 1.80 ± 0.81 hr in the fasted rats, and found to be 0.10 hr shorter than in the fed rats ($p > 0.05$).

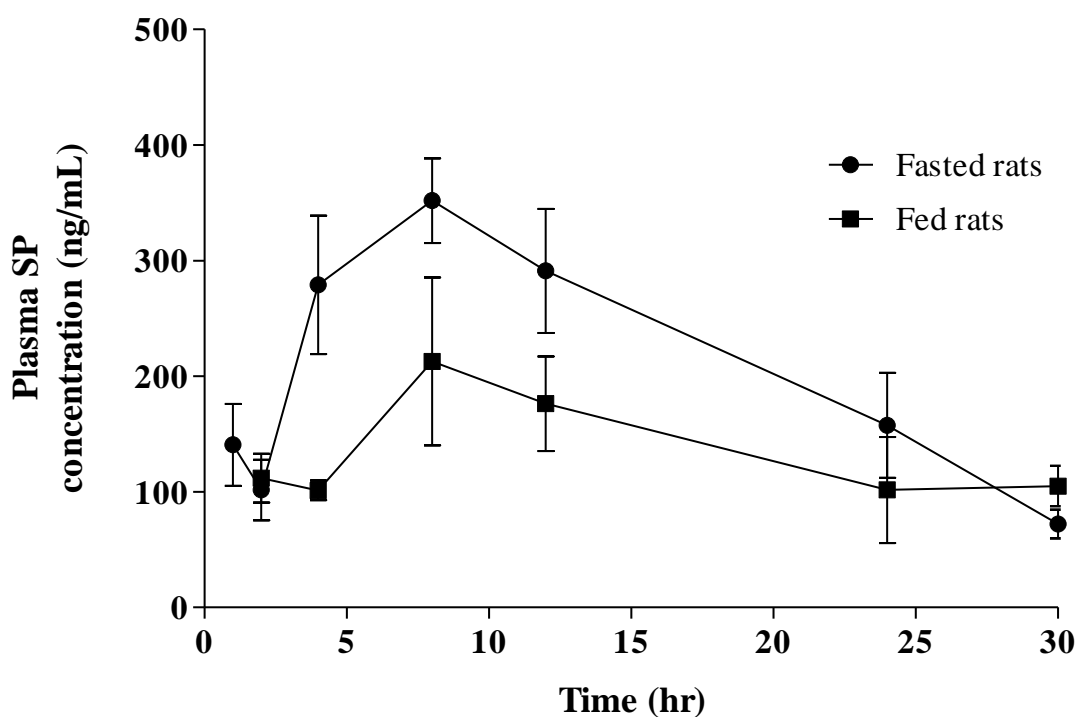


Figure 6.5 Effect of food on the absorption of SP from SSZ SLNs in rat colon (n = 3)

Figure 6.6 shows the percentage SP absorption versus time curves in the fasted and fed conditions, from which T_{10S} and T_{90S} were obtained. A number of methods have been employed in measuring CTT in humans including the use of radio-opaque markers [Evans *et al.*, 1999; Pomerri *et al.*, 2007] and gamma scintigraphy [Burton *et al.*, 1997; Bonapace *et al.*, 2000], which involve tracking the time it takes for ingested markers to travel along the large bowel. In a study by Enck *et al.* (1989), a mean CTT value of 15.5 hr was obtained in rats fed *ad libitum*. In that study, a carmine red solution was infused into the caecum of the rats and the time for the first discharge of a red coloured faecal pellet was considered as CTT.

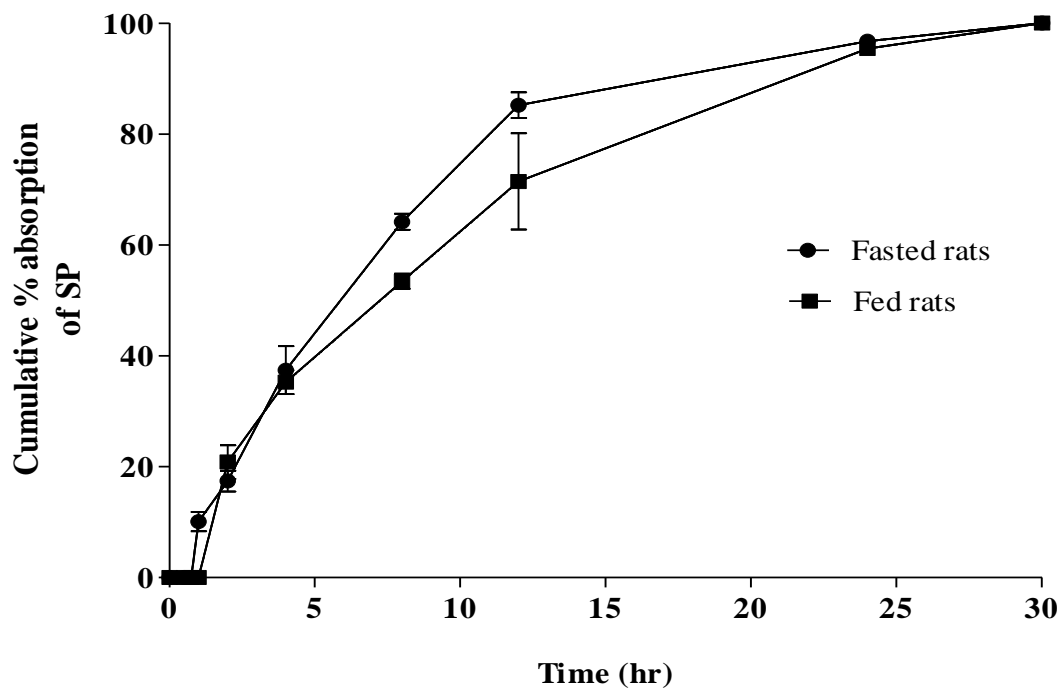


Figure 6.6 Mean SP absorption versus time curves in the fasted and fed rats (n = 3)

Usually in CTT determination, subjects or animals are allowed to maintain their usual dietary intake and medications if any, provided the latter do not interfere with intestinal motility. In the present study, the mean CTT in the fasted rats was found to be 15.50 hr, which was

statistically shorter ($p < 0.05$) than that observed for the fed rats, which was 24.60 hr. The difference in CTT values observed in the present study with those reported by Enck *et al.* (1989) can be attributed to differences in the markers/methods used. In the present study, a suspension of nanoparticles was studied whereas Enck *et al.* (1989) used faecal discharge from the digestion of food administered to the animals to estimate CTT. This confirms that CTT varies for solids and liquids, and physiological variability exists in the colonic movements in different individuals [Ashford, 2001].

6.3.5 Estimated AmB absorption in the stomach, small intestine and colon

In a preliminary formulation study, it has been shown that AmB is molecularly dispersed within the lipid matrix of the SLNs [Tan *et al.*, 2014]. The data presented in the preceding chapters also showed that the three SLNs (AmB, PAR and SSZ) share identical physical characteristics; therefore, they were expected to respond similarly to the hydrodynamics of the GI tract. A molecularly dispersed arrangement of AmB within the lipid matrix favours prior interaction of the lipid with the intestinal epithelia and assimilation of the SLNs in the enterocytes and Peyer's patches for lymphatic absorption [Bargoni *et al.*, 1998; Müller *et al.*, 2006; Li *et al.*, 2009].

The mean plasma AmB concentration-time profiles in the fasted and fed rats are depicted in Figures 6.7 and 6.8, respectively, and the pharmacokinetic data obtained from them have already been presented in Table 6.1. The first and second boundaries demarcated in the figures represent T_{10P} and T_{10S} , respectively, and the various regions within the profiles correlate the extent of absorption of AmB within the respective regions.

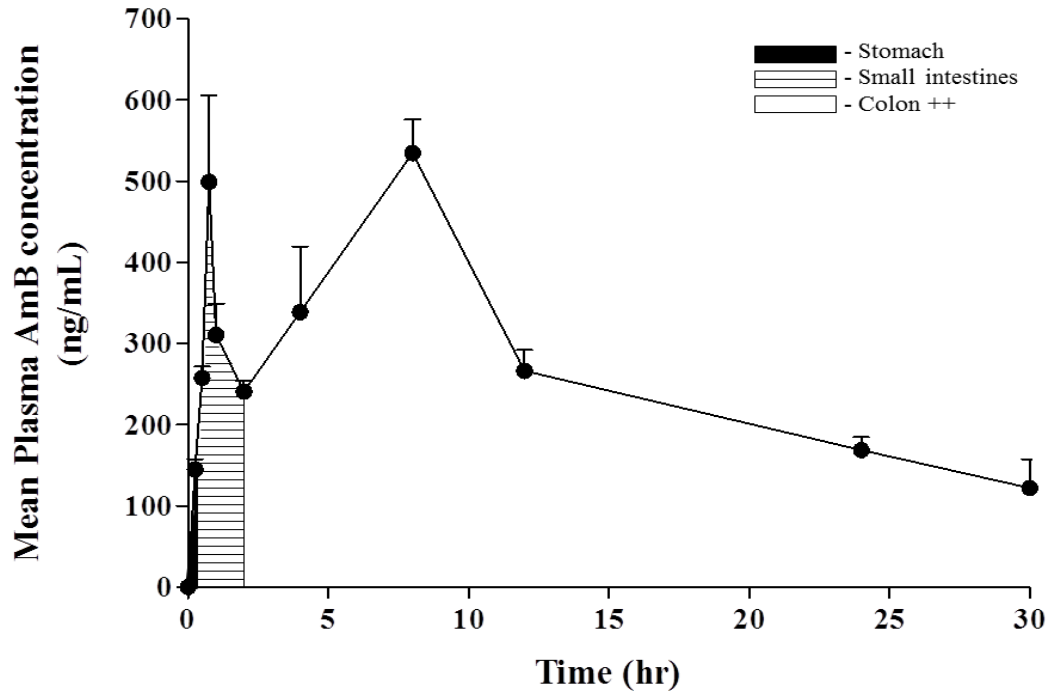


Figure 6.7 Absorption of AmB SLNs in the stomach, small intestine and colon in fasted rats

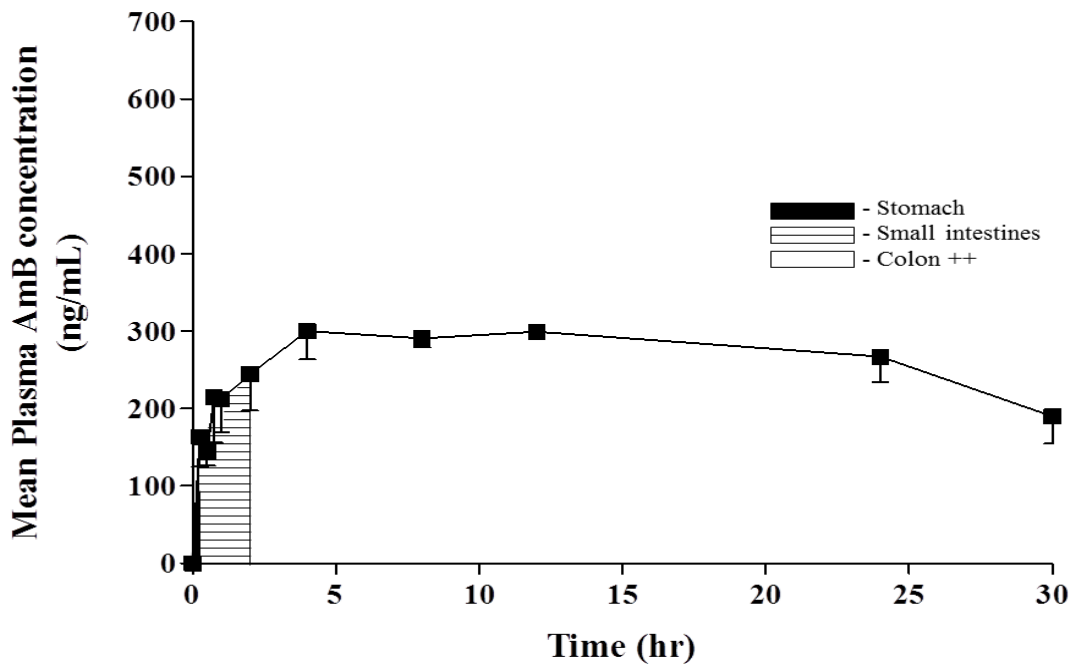


Figure 6.8 Absorption of AmB SLNs in the stomach, small intestine and colon in the fed rats

Using TEM analysis, intact SLNs have been observed circulating in lymph and blood 30 min post duodenal administration of SLNs to rats [Bargoni *et al.*, 1998]. Lymph contents are transported via lymph vessels into lymph nodes prior to emptying through the subclavian veins into blood. SLNs or drug particles in lymph will therefore appear in blood later although they may be detected in both lymph and blood at the same time. This is the reason the appearance of the second peak in the drug plasma profiles after oral administration of the SLNs in the present study is attributed to the process of particle uptake by Peyer's patches and lymph, prior to drug emptying into the blood. This process is thus slow and hence AmB only appears in blood after a finite time. The latter is the basis for the "colon⁺⁺" designated in Figures 6.7 and 6.8.

Absorption of the AmB SLNs in the colon⁺⁺ regions is therefore attributable to a combination of absorption processes in the colon *per se* as well as the continued absorption process via lymph in the small intestines explained earlier. This means that plasma AmB concentration post CAT is not attributed solely to colonic drug absorption. At the present time, the proportion of AmB absorption occurring only in the colon against the same via lymph has not been established.

The C_{max} for AmB obtained from the fasted rats was well defined and significantly higher ($p < 0.05$) than that in the fed group, signifying a more rapid rate of absorption of AmB from SLNs in the fasted state. There was no significant difference ($p > 0.05$) between the AUC_{0-30} values in the two groups. The absence of sharp peaks in the AmB absorption profile for the fed rats, and the relatively steady plasma concentration during the study period is a feature that can be exploited for controlled AmB delivery.

Table 6.5 shows the estimated percentage absorptions of AmB from the SLNs in the various GI regions during the fasted and fed conditions, as obtained from Figure 6.9. In both cases, the

highest percentage absorption occurred in the colon⁺⁺ region, indicating major colonic and lymphatic absorption. There was no statistically significant difference ($p > 0.05$) between the fasted and fed groups with regard to percentage absorptions in the respective GI regions (pair-wise comparisons), confirming that although the presence of food slowed the rates of absorption of AmB SLNs, the extent of AmB absorption remained unchanged in either food status. The stomach presented the poorest percentage absorption of AmB albeit slightly higher in the fasted state. A significantly higher level of absorption occurred in the small intestines compared to the stomach; and slightly higher in the fasted state ($44.1 \pm 10.7\%$ and $37.2 \pm 16.0\%$ obtained for the fasted and fed rats respectively). These findings agree with those obtained by Li *et al.* (2009) who indicated that the ileum and colon were the main GI segments where the absorption of quercetin-containing SLNs occurred.

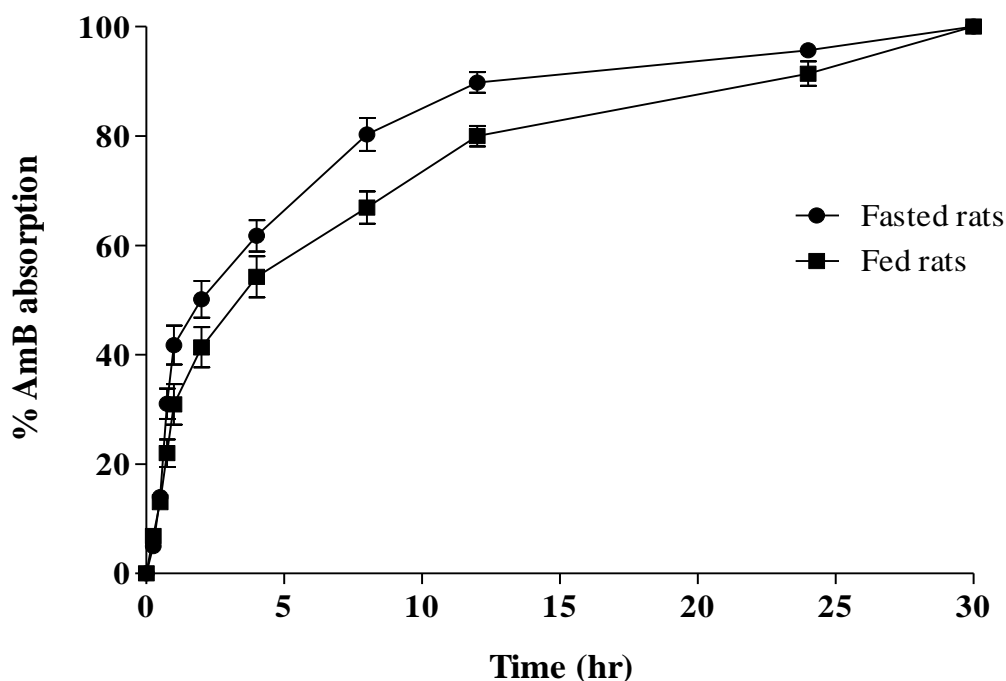


Figure 6.9 Cumulative percentage absorption of AmB under fasted and fed conditions

Table 6.5 Estimated percentage absorption of AmB from SLNs in the stomach, small intestine and colon (n = 3)

Rat No.	Fasted			Fed		
	Stomach (%)	Small intestine (%)	Colon ⁺⁺ (%)	Stomach (%)	Small intestine (%)	Colon ⁺⁺ (%)
1	3.4	53.5	43.1	1.9	19.8	78.3
2	3.4	32.4	64.2	3.8	40.4	55.8
3	1.5	46.4	52.1	4.0	51.3	44.7
Mean	2.8	44.1	53.1	3.2	37.2	59.6
SD	1.1	10.7	10.6	1.2	16.0	17.1

Generally, little drug absorption occurs in the stomach due to its relatively smaller surface area however, gastric emptying can be rate limiting to the onset of drug absorption from the small intestine [Ashford, 2001]. The small intestine has a very large surface area provided by the villi and microvilli, and the intestinal wall is enriched with a network of blood and lymphatic vessels, all of which aid in absorption. The lymphatic system is important in the absorption of fats from the GI tract. Blood leaving the small intestine flows into the hepatic portal vein and into systemic circulation via the liver; therefore, drugs that are metabolised by the liver reach systemic circulation in lower concentrations. The colon, unlike the small intestine has no specialised villi; however, the microvilli of the absorptive epithelial cells, the presence of crypts, and the irregularly folded mucosae serve to increase the surface area of the colon. The surface area nevertheless remains approximately $\frac{1}{30}$ th that of the small intestine.

In addition, because of the high water absorption capacity of the colon, colonic contents are considerably viscous and their mixing is not efficient, thus availability of most drugs to the absorptive membrane is low [Chien, 1992]. As a result of these anatomical differences, the small intestine is generally better suited for drug absorption.

As previously mentioned, the “colon⁺⁺ absorption” is a summation of AmB absorption in the colon and lymphatic absorption from the small intestine. From the late detection of AmB that resulted in the second peak in the plasma profiles, it could be inferred that further AmB SLN absorption via lymphatic tissue in the colon may lead to significant blood levels of AmB after the 30th hour sampling time.

Lymphatic tissues in the colon, rectum and appendix vermiformis are fewer and not discrete like the Peyer’s patches and isolated lymphoid follicles in the small intestine but rather, they occur diffusely in aggregated masses at irregular intervals, with the exception of the proximal colonic patches in rodents [Owen *et al.*, 1991]. Uchida *et al.* (1988) observed the presence of M cells in the colon, which suggests that particles that are micron-sized or smaller may also be absorbed in this region of the GI tract.

Although the absorption of particulates is mostly investigated in the small intestine, there are a few reports documenting lymphatic uptake of particulate material from the large intestine. Earlier studies have shown the absorption of colloidal gold in normal and inflamed colonic tissues of patients as well as in the rectal area [D’Addabbo *et al.*, 1969; Fukai *et al.*, 1987].

Other studies on particulate absorption further suggest that while micron-sized particles cannot breach the intestinal barrier effectively, once in the sub-mucosal tissue, they are able to enter both capillaries and lymphatics leading to systemic dissemination. Some studies in rats have shown colonic absorption of both uncoated and surface-modified nanoparticles to also be a size-dependent process [Jani *et al.*, 1990; Jani *et al.*, 1994; Hillery *et al.*, 1994].

These studies indicate that the high percentage of AmB SLN absorption of more than 53% that was observed in the colon⁺⁺ in both fasted and fed conditions may be inclusive of particulate absorption via lymphoid tissues in the colon.

6.4 Conclusions

An indirect method was used to study the GI transit of AmB SLNs and the data obtained indicate that, the presence of food slowed the rate of absorption of AmB from SLNs but the extent of absorption remained essentially unchanged as AUC was not significantly different in fasted and fed rats. Furthermore, the percentage AmB absorption was lowest in the stomach region but significantly higher in the small intestine, and this process was slow to manifest but continued post caecal arrival of the SLNs. Some absorption of AmB appears to occur in the colon however, this amount is masked by the continued lymphatic absorption process in the small intestine resulting in late AmB appearance in the plasma.

Specifically, the percentage AmB absorption during the fasted state in the stomach, small intestine and colon were not significantly different from absorption within the respective regions in the fed state. In both states however, absorption was highest in the colon and appeared to be a combination of lymphatic absorption from the small intestine plus absorption proper within the colon. Absorption of the SLNs via lymphoid tissues in the colon is also postulated.

The study suggests that AmB SLNs irrespective of food status are slowly but well taken up in lymph, making the small intestine the most favourable site for the delivery of the AmB SLNs. As a result, a formulation process aimed at slowing down the transit time of the AmB SLNs in the small intestine would be beneficial to obtain a higher oral bioavailability.

CHAPTER 7

SUMMARY AND GENERAL CONCLUSIONS

Presently, there is no oral AmB product for clinical use, which makes research into oral AmB formulations as alternatives to the currently available yet costly intravenous formulations a growing interest. This is because AmB is a very useful antifungal agent but with serious side effects and as a result, is only used in severely ill patients who are usually immunocompromised. AmB is practically insoluble in water therefore, studies using lipid-based delivery systems to make the drug orally bioavailable with better tolerability are developing. In this project, AmB has been formulated into SLNs to achieve the aforementioned benefit. There is limited research on the GI transit behaviour of oral AmB preparations, a need that has been met in the present study. SLN formulations containing either AmB, PAR or SSZ were successfully formulated using an identical method based on the emulsification solvent diffusion technique, with the aim of using the latter two drugs as indirect markers to investigate the transit of the AmB SLNs. The effectiveness of the preparation method resulted in good encapsulation efficiencies ($> 60\%$), with AmB having the highest of $91.2 \pm 3.04\%$. The z-average diameters of the freshly made particles ranged from 206.5 to 224.8 nm and the PDI values were 0.161-0.218. All three SLNs showed very good colloidal stability evident from the high zeta potential values which were $> |60 \text{ mV}|$. The SLNs had other matching physical characteristics as regards shape and morphology, investigated using SEM and AFM. The mobility propensities of the particles were also determined using their migration time in a gel electrophoresis study, in which all three SLNs were observed to move similarly through the gel. The images obtained from the study showed that all the three SLNs travelled a similar distance of 22.2-22.4 mm after voltage application. This together with other similarities in physical properties was a clear indication of the suitability of employing the markers in

investigating the GI transit and absorption of the AmB SLNs. DSC studies showed that the drugs were in their amorphous forms in the lipid matrices and no polymorphic transitions had occurred. These further pointed to the stability of the systems. Storage of the SLNs at 4-8°C for 24 months, and freeze-drying did not significantly change the physical characteristics of the SLNs as their final properties as regards size, PDI and zeta potential were optimum for absorption via the oral route. The data obtained from *in vitro* release studies showed the AmB SLNs exhibited the lowest drug release (< 20% over 8 hr) among the three formulations. Such low drug release was very favourable in the quest for an AmB formulation with improved oral bioavailability via absorption of intact SLNs containing a high drug load, improved tolerability, and reduced or no systemic toxicity. The SLNs were subjected to tests in simulated gastrointestinal media in order to assess the stability of the particles after contact with GI fluids following oral administration. Using PCS, NTA and ToF-SIMS in the analyses, the data obtained indicated an inflow of the fluids into the SLNs followed by outward diffusion of the dissolved drug from the particles. The study showed NTA as a more suitable technique for analysing the stability of the SLNs in the various media as compared with PCS, as the latter showed bias towards larger particles and produced data suggestive of high particle aggregation. Overall, the data obtained indicated that the SLNs after oral ingestion may aggregate or increase in size after contact with GI fluids particularly in the stomach, possibly due to the low pH. However, on reaching the small intestine, both size and surface charge of the particles would be optimal for absorption indicating good stability; this is because the formulations had mean sizes < 350 nm and were either neutral or negatively charged after exposure to simulated gastric fluid followed by simulated intestinal fluid, which mimics GE. The mass spectra obtained from the ToF-SIMS analyses indicated that drug loading into the SLNs possibly followed the core-shell model, and that the AmB SLNs may have a drug-enriched core. Generally, the spectra corroborated the data obtained from the NTA, in that, a higher drug

count was observed on particles which had decreased in size as a result of drug diffusion from within the particles to the surfaces after incubation in a medium and vice versa, demonstrating that particle size is proportional to drug load. A two-step HPLC method that was developed and validated for the simultaneous assay of AmB, PAR and SP in rat plasma was found to be simple, rapid, accurate and reliable. Piroxicam was found to be a suitable internal standard for the analyses. Significantly, the method required a small volume of plasma, which is important for pharmacokinetic studies in rats, which were used as the animal model. A pilot study was conducted to validate the HPLC method and optimise sample collection time intervals. The data obtained indicated that AmB in SLNs was absorbed slowly but significantly from the small intestine. In the main study, the effect of food on the GI transit and absorption of the AmB SLNs was studied. The results from both fasted and fed rats showed a significant increase in bioavailability after incorporating AmB into SLNs as C_{max} and AUC values from the SLNs were statistically higher than the respective values for AmB suspended in water only. Food slowed the rate of AmB absorption from the SLNs; however, it was observed that the extent of absorption remained essentially unchanged as it was not significantly different in fasted and fed rats. It was also noted that percentage AmB absorption in the fasted state in the stomach, small intestine and colon were not significantly different from absorption in the respective regions in the fed state. In both states however, absorption was highest in the colon and appeared to be a combination of lymphatic absorption from the small intestine plus absorption proper within the colon. Absorption of the SLNs via lymphoid tissues in the colon was also postulated. The study suggested that AmB SLNs, irrespective of food status, are slowly but well taken up via lymph, making the small intestine the most favourable site for the delivery of the AmB SLNs. As a result, a formulation process aimed at slowing the transit time of the SLNs in the small intestine would result in a higher oral bioavailability. It could be concluded that the use of SLNs eliminated any variabilities in AmB absorption due to fasted and fed states.

CHAPTER 8

SUGGESTIONS FOR FUTURE WORK

The research on improving the oral bioavailability of amphotericin B (AmB) using lipid-based drug delivery systems is gaining a lot of interest. The solid lipid nanoparticulate formulation of AmB presented herein shows a lot of promise for use in clinical settings as such, listed below are some suggestions for future work:

- **Effect of the AmB SLN formulation on renal toxicity in rats**

The nephrotoxicity caused by AmB manifests as renal vasoconstriction with substantial decrease in glomerular filtration rate and renal blood flow, and also renal potassium and magnesium wasting [Barton *et al.*, 1984; Sawaya *et al.*, 1995]. Some lipid-based AmB preparations have already been shown to exhibit less or no nephrotoxicity when compared with the free drug or AmB deoxycholate [Risovic *et al.*, 2003; Gershkovich *et al.*, 2009; Jain *et al.*, 2012] however, future work aimed at evaluating the AmB SLNs in reducing renal toxicity caused by AmB has to be conducted.

Blood urea nitrogen and plasma creatinine levels can be used as biochemical markers to evaluate the nephrotoxicity. Risovic *et al.* (2003) have used a 50% increase in plasma creatinine concentration from the baseline as the criterion for detecting renal toxicity; however, a statistically significant increment in plasma creatinine after dose administration may signify renal toxicity.

- **Modifications in the formulation procedure to further improve oral bioavailability**

The encapsulation efficiency of the AmB SLNs obtained in this study (91.2%) was a significant improvement on the lipid formulation previously prepared, which was less than 50%. This indicates that further modifications in the nanoparticle production parameters could result in a higher encapsulation efficiency, which with most certainty will translate to a higher oral bioavailability.

It was observed in this study that the transit of the SLNs in the GI tract was similar to that of food particles and other dosage forms. It has also been shown that there is major lymphatic absorption of the SLNs. These indicate that slowing down the transit of the SLNs in the GI tract is likely to result in a higher lymphatic uptake. The addition of mucoadhesive agents to the formulation, preferably as a coating around the SLNs, could be used to achieve this.

- **Studies to ascertain the proportion of AmB SLNs absorbed in the colon only**

The results from the present study indicate significant absorption of the AmB SLNs after arrival of the particles in the colon, pointing to a combination of continuous lymphatic absorption and colonic absorption itself. It would therefore be valuable to investigate the proportion of SLN absorption that occurs only in the colon using rats as the animal model.

Monitoring plasma AmB levels after dose administration into the duodenum [A], followed by a suitable washout period, and then a separate pharmacokinetic study after caecal delivery of the SLNs [B] would give useful data on colonic absorption. A suitable protocol has to be developed for surgery in the animals to aid dose administration and also, the blood sampling period in study A should be a summation of the sampling time in study B and the caecal arrival time of the SLNs, in order to obtain accurate results.

- **Bioequivalent studies with commercially available formulations**

As an alternative to the currently available formulations of AmB are being sought due to the associated side effects, cost and the general inconvenience of intravenous drug delivery, it would be worthwhile to conduct bioequivalence studies to compare the bioavailability of the oral AmB SLNs with those of the parenteral products which are presently in clinical use.

- **Investigating the long term effects of the AmB SLNs**

The treatments of fungal infections such as aspergillosis, severe invasive candidiasis and other mycoses, as well as leishmaniasis often last several days to several months. AmB is usually the drug of choice for treating these systemic infections. It is therefore necessary that possible toxic effects of the AmB SLNs due to long-term use be investigated.

- **Improving the storage stability of the AmB SLNs**

The AmB SLN suspension was found to be stable over a 24-month storage period at 4-8°C, and the freeze-dried product was also found to possess similar physical properties as the freshly prepared formulation. These two situations indicate that an optimised freeze-dried SLN product will have a reasonably long shelf life if a careful study of the variables in the freeze-drying process is done, and an appropriate cryoprotectant is selected for use. Trehalose has been found in many studies to be the most suitable cryoprotectant for several SLN formulations [Cavalli *et al.*, 1997; Schwarz and Mehnert, 1997; Heiati *et al.*, 1998; Mehnert and Mäder, 2001] therefore, preliminary studies may be conducted using trehalose.

LIST OF PUBLICATIONS FROM THE PRESENT WORK

1. H. Amekyeh, N. Billa, C.J. Roberts, K.H. Yuen. Improved oral bioavailability of Amphotericin B (AmB) using solid lipid nanoparticles (SLNs): Effect of food on absorption. 6th APS International PharmSci, 7th-9th September, 2015, East Midlands Conference Centre, Nottingham, United Kingdom. Poster presentation.
2. Amekyeh, H., Billa, N., Yuen, K.H. & Chin, S.L.S. 2015. A gastrointestinal transit study on amphotericin B-loaded solid lipid nanoparticles in rats. *AAPS PharmSciTech*, 16(4), 871-877.
3. Amekyeh, H., Billa, N. & Yuen, K.H. 2015. Simultaneous HPLC assay of paracetamol and sulphapyridine as markers for estimating gastrointestinal transit of amphotericin B-containing nanoparticles in rat plasma. *Journal of Bioequivalence*, 1(1), 104 (7 pages).
4. Amekyeh, H., Billa, N., Yuen, K.H. & Lim, S.C. 2015. Effect of food status on the gastrointestinal transit of amphotericin B-containing solid lipid nanoparticles in rats. *AAPS PharmSciTech*, 1-5.
5. Hilda Amekyeh, Nashiru Billa, Kah-Hay Yuen, Sherlyn Lim Sheau Chin. Using marker drugs to study the gastrointestinal transit behaviour of amphotericin B-containing solid lipid nanoparticles. 25th Federation of Asian Pharmaceutical Associations (FAPA) Congress, 9th-12th October, 2014, Sutera Harbour Resort, Kota Kinabalu, Malaysia. Poster presentation.

REFERENCES

- Abu-Qare, A.W. & Abou-Donia, M.B. 2001. A validated HPLC method for the determination of pyridostigmine bromide, acetaminophen, acetylsalicylic acid and caffeine in rat plasma and urine. *Journal of Pharmaceutical and Biomedical Analysis*, 26, 939-947.
- Adzu, B., Garba, M., Haruna, A., Maman, M. & Wambebei, C. 2001. Effect of Niprisan® on single oral dose pharmacokinetics of paracetamol in rats. *European Journal of Drug Metabolism and Pharmacokinetics*, 26(3), 201-204.
- Alba, F., Crawley, G.M., Fatkin J., Higgs, D.M.J., Kippax, P.G. & South, S.L. 1999. Acoustic spectroscopy as a technique for the particle sizing of high concentration colloids, emulsions and suspensions. *Colloids and Surfaces A: Physicochemical and Engineering Aspects*, 153, 495-502.
- Almeida, A.J. & Souto, E. 2007. Solid lipid nanoparticles as a drug delivery system for peptides and proteins. *Advanced Drug Delivery Reviews*, 59, 478-490.
- Alolga, R.N., Assanhou, A.G., Onoja, V., Muyaba, M., Amadi, S. & Kakila, J.L. 2015. Effect of a chinese herbal formulation on the pharmacokinetics of paracetamol in rats. *World Journal of Pharmacy and Pharmaceutical Sciences*, 4(3), 1433-1443.
- AL-Quadeib, B.T., Radwan, M.A., Siller, L., Horrocks, B. & Wright, M.C. 2015. Stealth amphotericin B nanoparticles for oral drug delivery: *In vitro* optimisation. *Saudi Pharmaceutical Journal*, 23(3), 290-302.
- Amidon, G.L., DeBrincat, G.A. & Najib, N. 1991. Effects of gravity on gastric emptying, intestinal transit, and drug absorption. *Journal of Clinical Pharmacology*, 31(10), 968-973.
- Amidon, G.L., Lennernäs, H., Shah, V.P. & Crison, J.R. 1995. A theoretical basis for a biopharmaceutic drug classification: the correlation of in vitro drug product dissolution and in vivo bioavailability. *Pharmaceutical Research*, 12(3), 413-420.
- Antoniadou, A. & Dupont, B. 2005. Lipid formulations of amphotericin B: where are we today? *Journal of Medical Mycology*, 15, 230-238.
- Aprahamian, M., Michel, C., Humbert, W., Devissaguet, J.P. & Damge, C. 1987. Transmucosal passage of polyalkylcyanoacrylate nanocapsules as a new drug carrier in the small intestine. *Biology of the Cell*, 61, 69-76.
- Arning, M., Kliche, K., Heersonderhoff, A. & Wehmeier, A. 1995. Infusion related toxicity of three different amphotericin B formulations and its relation to cytokine plasma levels. *Mycoses*, 38, 459-65.
- Artifin, D.Y., Lee, L.Y. & Wang, C.H. 2006. Mathematical modeling and simulation of drug release from microspheres: implication to drug delivery systems. *Advanced Drug Delivery Reviews*, 58, 1274-1325.
- Asher, I.M. & Schwartzman, G. 1977. Amphotericin B. *Analytical Profiles of Drug Substances*, 6, 1-42.

- Ashford, M. 2001. The gastrointestinal tract - physiology and drug absorption. *In: Aulton, M.E. (ed.), Pharmaceutics: The Science of Dosage Form Design, 2nd Ed.*, London: Churchill Livingstone, 217-233.
- Attwood, D. 2001. Disperse systems. *In: Aulton, M.E. (ed.), Pharmaceutics: The Science of Dosage Form Design, 2nd Ed.*, London: Churchill Livingstone, 98.
- Auvillain, M., Cavé, G., Fessi, H. & Devissaguet, J.P. 1989. Lyophilisation of submicron colloidal carriers. *STP Pharma Sciences*, 5, 738-744.
- Baer, D.R., Amonette, J.E., Engelhard, M.H., Gaspar, D.J., Karakoti, A.S., Kuchibhatla, S. *et al.* 2008. Characterisation challenges for nanomaterials. *Surface and Interface Analysis*, 2008, 40, 529-537.
- Baer, D.R., Gaspar, D.J., Nachimuthu, P., Techane, S.D. & Castner, D.G. 2010. Application of surface chemical analysis tools for characterisation of nanoparticles. *Analytical and Bioanalytical Chemistry*, 396(3), 983-1002.
- Baginski, M. & Czub, J. 2009. Amphotericin B and its new derivatives-mode of action. *Current Drug Metabolism*, 10, 459-469.
- Baginski, M., Resat, H. & Borowski, E. 2002. Comparative molecular dynamics simulations of amphotericin B-cholesterol/ergosterol membrane channels. *Biochimica and Biophysica Acta (BBA)-Biomembrane*, 1567, 63-78.
- Balamuralikrishna, K. & Syamasundar, B. 2010. Validated RP-HPLC method for the estimation of amphotericin b in bulk and pharmaceutical dosage form. *International Journal of Research in Pharmaceutical and Biomedical Sciences*, 1(2), 147-151.
- Balog, S., Rodriguez-Lorenzo, L., Monnier, C.A., Obiols-Rabasa, M., Rothen-Rutishauser, B., Schurtenberger, P. & Petri-Fink, A. 2015. Characterizing nanoparticles in complex biological media and physiological fluids with depolarized dynamic light scattering. *Nanoscale*, 14, 7(14), 5991-5997.
- Bargoni, A., Cavalli, R., Caputo, O., Fundaro, A., Gasco, M.R. & Zara, G.P. 1998. Solid lipid nanoparticles in lymph and plasma after duodenal administration to rats. *Pharmaceutical Research*, 15(5), 745-750.
- Barkovich, M. 2015. *High performance liquid chromatography*, UC Davis ChemWiki-USA. Available at: http://chemwiki.ucdavis.edu/Analytical_Chemistry/Instrumental_Analysis/Chromatography/High_performance_liquid_chromatography [Accessed August 9, 2015].
- Barton, C.H., Pahl, M., Vaziri, N.D. & Cesario, T. 1984. Renal magnesium wasting associated with amphotericin B therapy. *American Journal of Medicine*, 77(3), 471-474.
- Benet, L.Z., Cummins, C.L. & Wu, C.Y. 2004. Unmasking the dynamic interplay between efflux transporters and metabolic enzymes. *International Journal of Pharmaceutics*, 277, 3-9.
- Bentley, J., Gilliss, S. R., Carter, C. B., Al-Sharab, J. F., Cosandey, F., Anderson, I. M. & Kotula, P. J. 2005. Nanoscale EELS analysis of oxides: composition mapping, valence determination and beam damage. *Journal of Physics: Conference Series*, 26, 69-72.
- Billa, N., Yuen, K.H., Khader, M.A.A. & Omar, A. 2000. Gamma-scintigraphic study of the gastrointestinal transit and in vivo dissolution of a controlled release diclofenac sodium

- formulation in xanthan gum matrices. *International Journal of Pharmaceutics*, 201(1), 109-120.
- Boistelle, R. 1988. Fundamentals of nucleation and crystal growth. In: Garti, N. & Sato, K. (eds.), *Crystallization and Polymorphism of Fats and Fatty Acids*, Marcel Dekker, Inc., New York, 189-226.
- Bonapace, E., Maurer, A., Davidoff, S., Krevsky, B., Fisher, R.S. & Parkman, H.P. 2000. Whole gut transit scintigraphy in the clinical evaluation of patients with upper and lower GI symptoms. *The American Journal of Gastroenterology*, 95(10), 2838-2847.
- Bonfiglio, R., King, R.C., Olah, T.V. & Merkle, K. 1999. The effects of sample preparation methods on the variability of the electrospray ionization response for model drug compounds. *Rapid Communications in Mass Spectrometry*, 13(12), 1175-1185.
- Bosch, H., Pruitt, J., Ryde, N., Ryde, T. & Wertz, C. 2003. Low viscosity liquid dosage forms. Patent US 20040105889 A1.
- Bowden, R., Ckandrasekar, P., White, M., Li, X., Pietrelli, L., Gurwith, M., van Burik, J., Laverdiere, M., Safrin, S. & Wingard, J.R. 2002. A double-blind, randomized, controlled trial of amphotericin B colloidal dispersion versus amphotericin B for the treatment of invasive aspergillosis in immunocompromised patients. *Clinical Infectious Diseases*, 35, 359-366.
- Bressolle, F., Bromet-Petit, M. & Audran, M. 1996. Validation of liquid chromatographic and gas chromatographic methods Applications to pharmacokinetics. *Journal of Chromatography B*, 686, 3-10.
- Briggs, D. & Seah, M. 1992. *Practical surface analysis: Ion and neutral spectroscopy, Vol. 2*, 2nd ed., Wiley and Sons Ltd., Chichester, England.
- Bunjes, H., Koch, M.H.J. & Westesen, K. 2000. Effect of particle size on colloidal solid triglycerides. *Langmuir*, 16, 5234-5241.
- Bunjes, H., Siekmann, B. & Westesen, K. 1998. Emulsions of super-cooled melts-a novel drug delivery system. In: Benita, S. (ed.), *Submicron Emulsions in Drug Targeting and Delivery*, Harwood Academic Publishers, Amsterdam, 175-204.
- Burton, D.D., Camilleri, M., Mullan, B.P., Forstrom, L.A. & Hung, J.C. 1997. Colonic transit scintigraphy labeled activated charcoal compared with ion exchange pellets. *Journal of Nuclear Medicine*, 38(11), 1807-1810.
- Cai, Z., Wang, Y., Zhu, L.J. & Liu, Z.Q. 2010. Nanocarriers: A General Strategy for Enhancement of oral bioavailability of poorly absorbed or pre-systemically metabolised drugs. *Current Drug Metabolism*, 11(2), 197-207.
- Calbet, J.A.L. & MacLean, D.A. 1997. Role of caloric content on gastric emptying in humans. *The Journal of Physiology*, 498(Pt 2), 553-559.
- Caliceti, P., Brossa, A., Salmaso, S., Bersani, S., Elvassore, N. & Bertucco, A. 2006. Preparation of protein loaded solid lipid nanoparticles by compressed fluid process. *Control Release Bioactive Materials*, 33, 383.
- Campanero, M.A., Zamarrefio, A.M., Diaz, M., Dios-Vieitez, M.C. & Azanza J.R. 1997. Development and validation of an HPLC method for determination of amphotericin B in

- plasma and sputum involving solid phase extraction. *Chromatographia*, 46(11-12), 641-646.
- Cao, X., Gibbs, S.T., Fang, L., Miller, H.A., Landowski, C.P., Shin, H.-C. *et al.* 2006. Why is it challenging to predict intestinal drug absorption and oral bioavailability in human using rat model. *Pharmaceutical Research*, 23(8), 1675-1686.
- Carr, B., Hole, P., Malloy, A., Weld, A., Nelson, P., Smith, J., *et al.* 2008. The real-time, simultaneous measurement of size, surface charge and fluorescence of populations of nanoparticles in liquids. Proceedings of: Particulate Systems Analysis, Stratford-upon-Avon, UK, September 2-4,
- Cavalli, R., Bargoni, A., Podio, V., Muntoni, E., Zara, G.P. & Gasco, M.R. 2003. Duodenal administration of solid lipid nanoparticles loaded with different percentages of tobramycin. *Journal of Pharmaceutical Sciences*, 92(5), 1085-1094.
- Cavalli, R., Caputo, O., Carlotti, M.E., Trotta, M., Scarnecchia, C. & Gasco, M.R. 1997. Sterilisation and freeze-drying of drug-free and drug-loaded solid lipid nanoparticles. *International Journal of Pharmaceutics*, 148, 47-54.
- Cavalli, R., Marengo, E., Rodriguez, L. & Gasco, M.R. 1996. Effects of some experimental factors on the production process of solid lipid nanoparticles. *European Journal of Pharmaceutics and Biopharmaceutics*, 3, 110-115.
- Cavalli, R., Peira, E., Caputo, O. & Gasco, M.R. 1999. Solid lipid nanoparticles as carriers of hydrocortisone and progesterone complexes with beta-cyclodextrins. *International Journal of Pharmaceutics*, 182(1), 59-69.
- Chacon, M., Molpeceres, J., Berges, L., Guzman, M. & Aberturas, M. R. 1999. Stability and freeze-drying of cyclosporine loaded poly (D, L lactide-glycolide) carriers. *European Journal of Pharmaceutical Sciences*, 8, 99-107.
- Chakrabarty, U.S. & Pal T.K. 2011. Rapid and sensitive high performance liquid chromatography method for the determination of amphotericin b in rat plasma. *Journal of Pharmacy Research*, 4, 3194-3197.
- Chamberlain, J. 1995. The analysis of drugs in biological fluids, 2nd Ed., CRC press, Boca Raton.
- Chandra, R. & Sharma, K.D. 2013. Quantitative determination of paracetamol and caffeine from formulated tablets by reversed phase-HPLC separation technique. *International Journal of Chromatographic Science*, 3(2), 31-34.
- Chandra, R., Verma, D., Sharma, K.D., Kumar, S., Alam, N. & Singh, S. 2013. Comparative quantitative determination of paracetamol by RP-HPLC and UV spectrophotometry from its formulated tablets. *International Journal of Pharmacy and Pharmaceutical Sciences*, 5(3), 863-865.
- Chang, Q., Zhang, J. & El-Shourbagy, T.A. 2007. Historical review of sample preparation for chromatographic bioanalysis: pros and cons. *Drug Development Research*, 68(3), 107-133.
- Charman, W.N., Porter, C.J., Mithani, S. & Dressman, J.B. 1997. Physiochemical and physiological mechanisms for the effects of food on drug absorption: the role of lipids and pH. *Journal of Pharmaceutical Sciences*, 86, 269-282.

- Cheng, J. & Winograd, N. 2005. Depth profiling of peptide films with TOF-SIMS and a C60 probe. *Analytical Chemistry*, 77(11), 3651-3659.
- Chia, J. & McManus, E. 1990. *In vitro* tumor necrosis factor induction assay for analysis of febrile toxicity associated with amphotericin B preparations. *Antimicrobial Agents and Chemotherapy*, 34, 906-908.
- Chien, Y.W. 1992. Oral drug delivery and delivery systems. *In*: Chien, Y.W. (ed.), *Novel drug delivery systems*, New York: Marcel Dekker Inc., 139-196.
- Christensen, F.N., Davis, S.S., Hardy, J.G., Taylor, M.J., Whalley, D.R. & Wilson, C.G. 1985. The use of gamma scintigraphy to follow the gastrointestinal transit of pharmaceutical formulations. *The Journal of Pharmacy and Pharmacology*, 37(2), 91-95.
- Christian, P.E., Moore, J.G., Sorenson, J.A., Coleman, R.E. & Welch, D.M. 1980. Effects of meal size and correction technique on gastric emptying time: studies with two tracers and opposed detectors. *Journal of Nuclear Medicine*, 21, 883-885.
- Chungi, V.S., Dittert, L.W. & Shargel, L. 1989. Pharmacokinetics of sulfasalazine metabolites in rats following concomitant oral administration of riboflavin. *Pharmaceutical Research*, 6(12), 1067-1072.
- Cicccone, G.K. & Holdcroft, A. 1999. Drugs and sex differences: a review of drugs relating to anaesthesia. *British Journal of Anaesthesia*, 82(2), 255-265.
- Clarke, G.M., Newton, J.M. & Short, M.D. 1993. Gastrointestinal transit of pellets of differing size and density. *International Journal of Pharmaceutics*, 100(1-3), 81-92.
- Clements, J.A., Heading, R.C., Nimmo, W.S. & Prescott, L.F. 1978. Kinetics of acetaminophen absorption and gastric emptying in man. *Clinical Pharmacology and Therapeutics*, 24, 420-431.
- Clogston, J.D. & Patri, A.K. 2011. Zeta potential measurement. *In*: McNeil, S.E. (ed.), *Methods in molecular biology: Characterization of nanoparticles intended for drug delivery*, New York: Humana Press, 63-70.
- Collett, J. & Moreton, C. 2001. Modified-release peroral dosage forms. *In*: Aulton, M.E. (ed.), *Pharmaceutics: The Science of Dosage Form Design*, 2nd Ed., London: Churchill Livingstone, 217-233.
- Cortesi, R., Esposito, E., Luca, G. & Nastruzzi, C. 2002. Production of lipospheres as carriers for bioactive compounds. *Biomaterials*, 23, 2283-2294.
- Crawford Scientific. 2015(a). *Quantitative & qualitative HPLC*. Available at: http://www.chromacademy.com/lms/sco9/Theory_Of_HPLC_Quantitative_and_Qualitative_HPLC.pdf [Accessed July 22, 2015].
- Crawford Scientific. 2015(b). *Reversed phase chromatography*. Available at: http://www.chromacademy.com/lms/sco5/Theory_Of_HPLC_Reverse_Phase_Chromatography.pdf [Accessed July 22, 2015].
- D'Addabbo, A., Dammacco, F., Capurso, A. & Damato, V. 1969. Clinical and animal experiment studies of the resorption of dyes and colloidal radiogold in the large intestine. *Fortschritte auf dem Gebiete der Röntgenstrahlen und der Nuklearmedizin*, 111, 565-572.

- D'Mello, S.R., Das, S.K. & Das, N.G. 2009. Polymeric Nanoparticles for Small-Molecule Drugs: Biodegradation of Polymers and Fabrication of Nanoparticles. *In: Pathak, Y. & Thassu, D. (eds.) Drug delivery nanoparticles formulation and characterisation*, London: Informa Healthcare, 16-34.
- Damgé, C., Michel, C., Aprahamian, M., Couvreur, P. & Devissaguet, J.P. 1990. Nanocapsules as carriers for oral peptide delivery. *Journal of Controlled Release*, 13, 233-239.
- Davis, S.S., Hardy, J.G. & Fara J.W. 1986. Alimentary tract and pancreas: Transit of pharmaceutical dosage forms through the small intestine. *Gut*, 27, 886-892.
- Davis, S.S., Hardy, J.G., Taylor, M.J., Whalley, D.R. and Wilson, C.G. 1984. The effect of food on the gastrointestinal transit of pellets and an osmotic device (Osmet). *International Journal of Pharmaceutics*, 21, 331-340.
- Deray, G. 2002. Amphotericin B nephrotoxicity. *Journal of Antimicrobial Chemotherapy*, 49(1), 37-41.
- Desai, M.P., Labhsetwar, V. & Amidon, G.L. 1996. Gastrointestinal uptake of biodegradable microparticles: effect of particle size, *Pharmaceutical Research*, 13, 1838-1845.
- Desai, M.P., Labhsetwar, V., Walter, E., Levy, R.J. & Amidon, G.L. 1997. The mechanism of uptake of biodegradable microparticles in Caco-2 cells is size dependent. *Pharmaceutical Research*, 14 (11), 1568-1573.
- DeSesso, J.M. & Jacobson, C.F. 2001. Anatomical and physiological parameters affecting gastrointestinal absorption in humans and rats. *Food and Chemical Toxicology*, 39(3), 209-228.
- Devereux, J.E. 1987. Gastro-intestinal transit of multiple unit dosage forms. *Ph.D. Thesis*, University of London, UK.
- Dhawan, S., Single, A.K. & Sinha, V.R. 2004. Evaluation of mucoadhesive properties of chitosan microspheres prepared by different methods. *AAPS PharmSciTech*, 5(4), 67.
- Digenis, G.A. & Sandefer, E.P. 1994. The effect of food and gastrointestinal residence on drug absorption: case studies which merit the *in vivo* study of dosage form behavior and its relationship to oral drug absorption. Division of Medicinal Chemistry and Pharmaceutics, College of Pharmacy University of Kentucky, 9-11.
- Divoll, M., Greenblatt, D.J., Ameer, B. & Abernethy, D.R. 1982. Effect of food on acetaminophen absorption in young and elderly subjects. *The Journal of Clinical Pharmacology*, 22(11-12), 571-576.
- Dodiya, S.S., Chavhan, S.S., Sawant, K.K. & Korde, A.G. 2011. Solid lipid nanoparticles and nanosuspension formulation of saquinavir: preparation, characterization, pharmacokinetics and biodistribution studies. *Journal of Microencapsulation*, 28(6), 515-527.
- Dragovic, R.A., Gardiner, C., Brooks, A.S., Tannetta, D.S., Ferguson, D.J., Hole, P., Carr, B., Redman, C.W., Harris, A.L., Dobson, P.J., Harrison, P. & Sargent, I.L. 2011. Sizing and phenotyping of cellular vesicles using Nanoparticle Tracking Analysis. *Nanomedicine*, 7, 780-788.

- Drake, B., Prater, C.B., Weisenhorn, A.L., Gould, S.A.C., Albrecht, T.R., Quate, C.F. *et al.* 1989. Imaging crystals, polymers and processes in water with the AFM. *Science*, 243, 1586-1589.
- Driscoll, C.M.O. 2002. Lipid based formulations for intestinal lymphatic delivery. *European Journal of Pharmaceutical Sciences*, 15, 405-415.
- Dubes, A., Parrot-Lopez, H., Abdelwahed, W., Degobert, G., Fessi, H., Shahgaldian, P. *et al.* 2003. Scanning electron microscopy and atomic force microscopy imaging of solid lipid nanoparticles derived from amphiphilic cyclodextrins. *European Journal of Pharmaceutics and Biopharmaceutics*, 55(3), 279-282.
- Dubois, A. & Castell, D.O. 1984. *Esophageal and gastric emptying*, Florida: CRC Press, 159.
- Dwivedi, P., Khatik, R., Khandelwal, K., Taneja, I., Raju, K.S., Wahajuddin, Paliwal, S.K., Dwivedi, A.K. & Mishra, P.R. 2014. Pharmacokinetics study of arteether loaded solid lipid nanoparticles: An improved oral bioavailability in rats. *International Journal of Pharmaceutics*, 466, 321-327.
- Echevarría, I., Barturen, C., Renedo, M.J. & Dios-Viéitez, M.C. 1998. High-performance liquid chromatographic determination of amphotericin B in plasma and tissue. Application to pharmacokinetic and tissue distribution studies in rats. *Journal of Chromatography A*, 819, 171-176.
- Ekambaram, P., Abdul, H.S. & Priyanka, K. 2012. Solid lipid nanoparticles: A Review. *Scientific Reviews & Chemical Communications*, 2(1), 83-87.
- Eldem, T. & Arican-Cellat, N. 2000. High-performance liquid chromatographic determination of amphotericin B in a liposomal pharmaceutical product and validation of the assay. *Journal of Chromatographic Science*, 38, 338-344.
- Eldem, T. & Arican-Cellat, N. 2001. Determination of amphotericin B in human plasma using solid-phase extraction and high-performance liquid chromatography. *Journal of Pharmaceutical and Biomedical Analysis*, 25, 53-64.
- Ellis, M.E., Al-Hokail, A.A., Clink, H.M., Padmos, M.A., Ernst, P., Spence, D.G., Tharpe, W.N & Hillier, V.F 1992. Double blind randomised study of the effect of infusion rates on toxicity of amphotericin B. *Antimicrobial Agents and Chemotherapy*, 36, 172-179.
- Enck, P., Merlin, V., Erckenbrecht, J.F. & Wienbeck, M. 1989. Stress effects on gastrointestinal transit in the rat. *Gut*, 30(4), 455-459.
- Englard, S. & Seifter, S. 1990. Precipitation techniques. *Methods in Enzymology*, 182, 285-300.
- Escubed Ltd. 2015. *Zeta Potential-Electrophoresis*. Available at: [http://www.escubed.co.uk/sites/default/files/zeta_potential_\(an011\)_electrophoresis.pdf](http://www.escubed.co.uk/sites/default/files/zeta_potential_(an011)_electrophoresis.pdf) [Accessed April 2, 2015].
- Evans, R.C., Kamm, M.A., Hinton, J.M. & Lennard-Jones, J.E. 1992. The normal range and a simple diagram for recording whole gut transit time. *International Journal of Colorectal Disease*, 7(1), 15-17.
- Ezzati, N.D.J., Hamishehkar, H. & Valizadeh, H. 2014. Development of dry powder inhaler formulation loaded with alendronate solid lipid nanoparticles: Solid-state

- characterization and aerosol dispersion performance. *Drug Development and Industrial Pharmacy*, 15, 1-7.
- Fara, J.W. 1985. Gastric emptying and the transit of dosage forms. *In: Prescott, L.F. & Nimmo, W.S. (eds.), Rate control in drug therapy*, Edinburgh: Churchill Livingstone, 144-50.
- Fell, J.T. & Digenis, G.A. 1984. Imaging and behaviour of solid oral dosage forms *in vivo*. *International Journal of Pharmaceutics*, 22(1), 1-15.
- Filipe, V., Hawe, A. & Jiskoot, W. 2010. Critical evaluation of nanoparticle tracking analysis (NTA) by NanoSight for the measurement of nanoparticles and protein aggregates. *Pharmaceutical Research*, 27(5), 796-810.
- Fischer, M. & Fadda, H.M. 2015. The effect of sex and age on small intestinal transit times in humans. *Journal of Pharmaceutical Sciences*, doi 10.1002/jps.24619.
- Food and Drug Administration (FDA). 2002. Food-effect bioavailability and fed bioequivalence studies, food and drug administration. Available at: <http://www.fda.gov/downloads/RegulatoryInformation/Guidances/UCM126833.pdf> [Accessed November 21, 2015].
- Food and Drug Administration (FDA). 2013. Bioequivalence studies with pharmacokinetic endpoints for drugs submitted under an ANDA. Available at: <http://www.fda.gov/downloads/drugs/guidancecomplianceregulatoryinformation/guidances/ucm377465.pdf> [Accessed November 19, 2015].
- Freitas, C. & Müller, R.H. 1998. Effect of light and temperature on zeta potential and physical stability in solid lipid nanoparticle (SLNTM) dispersions. *International Journal of Pharmaceutics*, 168(2), 221-229.
- Friend, D.R. & Chang, G.W. 1985. Drug glycosides: potential prodrugs for colon specific drug delivery. *Journal of Medicinal Chemistry*, 28(1), 51-57.
- Fukai, H., Murakami, M., Yoshikawa, H., Takada, K. & Muranishi, R. 1987. Studies on the promoting effect of lipid-surfactant mixed micelles (MM) on intestinal absorption of colloidal particles. Dependence on particle size and administration site. *Journal of Pharmacobio-dynamics*, 10, 236-242.
- Gangishetty, S. & Verma, S. 2013. RP-HPLC method development and validation for simultaneous estimation of clarithromycin and paracetamol. *ISRN Analytical Chemistry*, Article ID 948547, doi:10.1155/2013/948547.
- García-López, P., Pérez-Urizar, J., Madrazo, I., Guízar-Sahagún, G. & Castañeda-Hernández, G. 1997. Oral paracetamol bioavailability in rats subjected to experimental spinal cord injury. *Biopharmaceutics & Drug Disposition*, 18(3), 203-211.
- Garti, N. & Sato, K. 1988. Crystallization of Fats and Fatty Acids. *In: Garti, N. & Sato, K (eds.), Crystallization and Polymorphism of Fats and Fatty Acids*, Marcel Dekker, New York, 227-266.
- Garud, A., Singh, D. & Garud, N. 2012. Solid Lipid Nanoparticles (SLN): Method, Characterisation and Applications. *International Current Pharmaceutical Journal*, 1(11), 384-393.
- Gasco, M.R. 1993. Method for producing solid lipid microspheres having narrow size distribution: United States Patent, USS 188837.

- Gershkovich, P., Wasan, E.K., Lin, M., Sivak, O., Leon, C.G., Clement, J.G. & Wasan, K.M. 2009. Pharmacokinetics and biodistribution of amphotericin B in rats following oral administration in a novel lipid-based formulation. *Journal of Antimicrobial Chemotherapy*, 64, 101-108.
- Gohla, S. & Dingler, A. 2001. Scaling up feasibility of the production of solid lipid nanoparticles (SLN). *Die Pharmazie*, 56(1), 61.
- Goodacre, R. & Anklam, E. 2001. Fourier transform infrared spectroscopy and chemometrics as a tool for the rapid detection of other vegetable fats mixed in cocoa butter. *Journal of the American Oil Chemists' Society*, 78(10), 993-1000.
- Grainger, D.W. & Castner, D.G. 2008. Nanobiomaterials and nanoanalysis: Opportunities for improving the science to benefit biomedical technologies. *Advanced Materials*, 20, 867-877.
- Gramatte, T.H. & Terhaag, B. 1991. The variability of oro-caecal transit time evaluated by the salicylazosulfapyridine/sulfapyridine method. *International Journal of Clinical Pharmacology, Therapy and Toxicology*, 29, 147-150.
- Granich, G.G., Kobayashi, G.S. & Krogstad, D.J. 1986. Sensitive high-pressure liquid chromatographic assay for amphotericin B which incorporates an internal standard. *Antimicrobial Agents and Chemotherapy*, 29(4), 584-588.
- Grassian, V.H. 2008. When size really matters: Size-dependent properties and surface chemistry of metal and metal oxide nanoparticles in gas and liquid phase environments. *The Journal of Physical Chemistry C*, 112, 18303-18313.
- Gruber, C.M., Ridolfo, A.S. & Rosick, W.A. 1958. An enteric compression coating II. *In vivo* studies with barium sulphate-potassium iodide and barium sulphate tablets. *Journal of the American Pharmaceutical Association*, 47(12), 862-866.
- Gupta, S., Dub, A. & Vyas, S.P. 2013. Development and characterization of amphotericin B loaded solid lipid nanoparticles against experimental visceral leishmaniasis. *Pharmaceutical Nanotechnology*, 1, 54-67.
- Hackley, V.A. & Clogston, J.D. 2011. Measuring the hydrodynamic size of nanoparticles in aqueous media using batch-mode dynamic light scattering. In: McNeil, S.E. (ed.) *Methods in molecular biology: Characterization of nanoparticles intended for drug delivery*, New York: Humana Press, 36-52.
- Hall, T.G., Smukste, I., Bresciano, K.R., Wang, Y., McKearn, D. & Savage, R.E. 2012. *Identifying and overcoming matrix effects in drug discovery and development, tandem mass spectrometry-applications and principles*: Prasain, J. (ed.). Available at: <http://www.intechopen.com/books/tandem-mass-spectrometry-applicationsandprinciples/identifying-and-overcoming-matrix-effects-in-drug-discovery-and-development> [Accessed August 29, 2015].
- Hanafy, A., Spahn-Langguth, H., Vergnault, G., Grenier, P., Tubic Grozdanis, M., Lenhardt, T. & Langguth, P. 2007. Pharmacokinetic evaluation of oral fenofibrate nanosuspensions and SLN in comparison to conventional suspensions of micronized drug. *Advanced Drug Delivery Reviews*, 59(6), 419-426.
- Harde, H., Das, M. & Jain, S. 2011. Solid lipid nanoparticles: an oral bioavailability enhancer vehicle. *Expert Opinion on Drug Delivery*, 8(11), 1407-1424.

- Harvey, D. 2015. *High-performance liquid chromatography*. Available at: http://chemwiki.ucdavis.edu/Analytical_Chemistry/Analytical_Chemistry_2.0/12_Chromatographic_and_Electrophoretic_Methods/12E%3A_High-Performance_Liquid_Chromatography [Accessed July 22, 2015].
- Heading, R.C., Nimmo, J., Prescott, L.F. & Tohill, P. 1973. The dependence of paracetamol absorption on the rate of gastric emptying. *British Journal of Pharmacology*, 47, 415-421.
- Heiati, H., Tawashi, R. & Phillips N.C. 1998. Drug retention and stability of solid lipid nanoparticles containing azidothymidine palmitate after autoclaving, storage and lyophilisation. *Journal of Microencapsulation*, 15, 173-184.
- Herbrecht, R. 2003. The lipid formulations of Amphotericin B. *Expert Opinion on Pharmacotherapy*, 4, 1277-1287.
- Higuchi, T. 1961. Rate of release of medicaments from ointment bases containing drugs in suspension. *Journal of Pharmaceutical Sciences*, 50(10), 874-875.
- Higuchi, W.I., Ho, N.F.H., Park, J.Y. & Komiya, I. 1981. Rate limiting steps in drug absorption. In: Prescott, L.F. & Nimmo, W.S. (eds.), *Drug absorption*. Lancaster: MTP Press, 35-60.
- Hillery, A.M., Jani, P.U. & Florence, A.T. 1994. Comparative, quantitative study of lymphoid and non-lymphoid uptake of 60-nm polystyrene particles. *Journal of Drug Targeting*, 2, 151-156.
- Ho, N.F.H., Park, J.Y., Morozowich, W. & Higuchi, W.I. 1977. Physical model approach to the design of drugs with improved intestinal absorption. In: Roche, E.B. (ed.), *Design of biopharmaceutical properties through prodrugs and analogs*. Washington: American Pharmaceutical Association, 136-227.
- Hofmann, A.F., Pressman, J.H., Code, C.F. & Witztum, K.F. 1983. Controlled entry of orally administered drugs: physiological considerations. *Drug Development and Industrial Pharmacy*, 9, 1077-1109.
- Hölzer, H.H., Turkelson, C.M., Solomon, T.E. & Raybould, H.E. 1994. Intestinal lipid inhibits gastric emptying via CCK and a vagal capsaicin-sensitive afferent pathway in rats. *The American Journal of Physiology*, 267(4 Pt 1), G625-9.
- Honkanen, O., Marvola, J., Kanerva, H., Lindevall, K., Lipponen, M., Kekki, T. Ahonen, A. & Marvola, M. 2004. Gamma scintigraphic evaluation of the fate of hydroxypropyl methylcellulose capsules in the human gastrointestinal tract. *European Journal of Pharmaceutical Sciences*, 21(5), 671-678.
- Hou, D., Xie, C., Huang, K. & Zhu, C. 2003. The production and characteristics of solid lipid nanoparticles (SLNs). *Biomaterials*, 24, 1781-1785.
- Hu, L., Xing, Q., Meng, J. & Shang, C. 2010. Preparation and enhanced oral bioavailability of cryptotanshinone-loaded solid lipid nanoparticles. *AAPS PharmSciTech*, 11(2), 582-587.
- Humberstone, A.J. & Charman, W.N. 1997. Lipid-based vehicles for the oral delivery of poorly water soluble drugs. *Advanced Drug Delivery Reviews*, 25, 103-128.
- Hussain, S., Pezzei, C., Güzel, Y., Rainer, M., Huck, C.W. & Bonn, G.K. 2014. Zirconium silicate assisted removal of residual proteins after organic solvent deproteinization of

- human plasma, enhancing the stability of the LC-ESI-MS response for the bioanalysis of small molecules. *Analytica Chimica Acta*, 852, 284-292.
- Imhof, A., Walter, R.B. & Schaffner, A. 2003. Continuous infusion of escalated doses of amphotericin B deoxycholate: an open-label observational study. *Clinical Infectious Diseases*, 36, 943-951.
- Italia, J.L., Singh, D. & Ravi Kumar, M.N.V. 2009(b). High-performance liquid chromatographic analysis of amphotericin B in rat plasma using alpha-naphthol as an internal standard. *Analytica Chimica Acta*, 634, 110-114.
- Italia, J.L., Yahya, M.M., Singh, D. & Ravi Kumar, M.N.V. 2009(a). Biodegradable nanoparticles improve oral bioavailability of amphotericin B and show reduced nephrotoxicity compared to intravenous Fungizone. *Pharmaceutical Research*, 26, 1324-1331.
- Jahnke, S. 1998. The theory of high pressure homogenization. In: Müller, R.H., Benita, S., Bohm, B. (eds.), *Emulsions and nanosuspensions for the formulation of poorly soluble drugs*, Medpharm Scientific Publishers, Stuttgart, 177-200.
- Jain, S., Valvi, P.U., Swarnakar, N.K. & Thanki, K. 2012. Gelatin coated hybrid lipid nanoparticles for oral delivery of amphotericin B. *Molecular Pharmaceutics*, 9, 2542-2553.
- Jani, P., Halbert, G.W., Langridge, J. & Florence, A.T. 1989. The uptake and translocation of latex nanospheres and microspheres after oral administration to rats. *Journal of Pharmacology and Therapeutics*, 41, 809-812.
- Jani, P., Halbert, G.W., Langridge, J. & Florence, A.T. 1990. Nanoparticle uptake by the rat gastrointestinal mucosa: quantitation and particle size dependency. *Journal of pharmacy and pharmacology*, 42, 821-826.
- Jani, P.U., McCarthy, D.E. & Florence, A.T. 1994. Titanium dioxide (rutile) particle uptake from the rat GI tract and translocation to systemic organs after oral administration. *International Journal of Pharmaceutics*, 105, 157-168.
- Jawahar, N., Meyyanathan, S. N., Reddy, G. & Sood, S. 2012. Solid lipid nanoparticles for oral delivery of poorly soluble drugs. *Journal of Pharmaceutical Science & Research*, 4(7), 1848-1855.
- Jelvehgari, M. & Montazam, S.H. 2012. Comparison of microencapsulation by emulsion-solvent extraction/evaporation technique using derivatives cellulose and acrylate-methacrylate copolymer as carriers. *Jundishapur Journal of Natural Pharmaceutical Products*, 7(4): 144-152.
- Jones, E.A., Lockyer, N.P. & Vickerman, J.C. 2008. Depth profiling brain tissue sections with a 40 keV C₆₀⁺ primary ion beam. *Analytical Chemistry*, 80(6), 2125-2132.
- Jones, E.A., Lockyer, N.P., Kordys, J. & Vickerman, J.C. 2007. Suppression and enhancement of secondary ion formation due to the chemical environment in static-secondary ion mass spectrometry. *Journal of the American Society for Mass Spectrometry*, 18(8), 1559-1567.
- Jones, S. 2009. Chromatography focus. Making an HPLC calibration work (Part 1). Laserchrom HPLC Laboratories Ltd.

- Joresa, K., Mehnert, W., Drechslerb, M., Bunjes, H., Johannnd, C. & Mäder, K. 2004. Investigations on the structure of solid lipid nanoparticles (SLN) and oil-loaded solid lipid nanoparticles by photon correlation spectroscopy, field-flow fractionation and transmission electron microscopy. *Journal of Controlled Release*, 95, 217-227.
- Jovanoviæ, N., Bouchard, A., Hofland, G.W., Witkamp, G.J., Crommelin, D.J.A. & Jiskoot, W. 2004. Stabilization of proteins in dry powder formulations using supercritical fluid technology. *Pharmaceutical Research*, 21, 1955-1969.
- Jung, J. & Perrut, M. 2001. Particle design using supercritical fluids: literature and patent survey. *Journal of Supercritical Fluids*, 20, 179-219.
- Jung, S.H., Lim, D.H., Jung, S.H., Lee, J.E., Jeong, K.-S., Seong, H. & Shin, B.C. 2009. Amphotericin B-entrapping lipid nanoparticles and their in vitro and in vivo characteristics. *European Journal of Pharmaceutical Sciences*, 37(3-4), 313-320.
- Kakkar, V., Singh, S., Singla, D. & Kaur, I.P. 2011. Exploring solid lipid nanoparticles to enhance the oral bioavailability of curcumin. *Molecular Nutrition & Food Research*, 55(3), 495-503.
- Kalepu, S., Manthina, M. & Padavala, V. 2013. Oral lipid-based drug delivery systems - an overview. *Acta Pharmaceutica Sinica B*, 3(6), 361-372.
- Kararli, T.T. 1995. Comparison of the gastrointestinal anatomy, physiology, and biochemistry of humans and commonly used laboratory animals. *Biopharmaceutics & Drug Disposition*, 16, 351-380.
- Kellow, J.E., Borody, T.J., Phillips, S.F., Haddad, A.C. & Brown, M.L. 1986. Sulphapyridine appearance in plasma after salicylazosulphapyridine. *Gastroenterology*, 91, 396-400.
- Kelly, K.A. 1981. Motility of the stomach and gastroduodenal junction. In: Johnson, L.R. (ed.), *Physiology of the gastrointestinal tract*, New York: Raven Press, 393-410.
- Khoo, S. H., Bond, J. & Denning, D.W. 1994. Administering amphotericin B-a practical approach. *Journal of Antimicrobial Chemotherapy*, 33, 203-213.
- Kirby, A.R., Gunning, A.P. & Morris, V.J. 1995. Imaging xanthum gum by atomic force microscopy. *Carbohydrate Research*, 267, 161-166.
- Kleinberg, M. 2006. What is the current and future status of conventional amphotericin B? *International Journal of Antimicrobial Agents*, 27S, S12-S16.
- Klepser, M. 2011. The value of amphotericin B in the treatment of invasive fungal infections. *Journal of Critical Care*, 26(2), 225.e1-225.e10.
- Kole, P.L., Venkatesh, G., Kotecha, J. & Sheshala, R. 2011. Recent advances in sample preparation techniques for effective bioanalytical method. *Biomedical Chromatography*, 25, 199-217.
- Kondo, H., Takahashi, Y., Watanabe, T., Yokohama, S. & Watanabe, J. 2003(a) Gastrointestinal transit of liquids in unfed cynomolgus monkeys. *Biopharmaceutics & Drug Disposition*, 24(3), 131-140.
- Kondo, H., Watanabe, T., Yokohama, S. & Watanabe, J. 2003(a). Effect of food on gastrointestinal transit of liquids in cynomolgus monkeys. *Biopharmaceutics & Drug Disposition*, 24(4), 141-151.

- Korsmeyer, R.W., Gurny, R., Doelker, E., Buri, P. & Peppas, N.A. 1983. Mechanisms of solute release from porous hydrophilic polymers. *International Journal of Pharmaceutics*, 15(1), 25-35.
- Kreuter, J. 1991. Peroral administration of nanoparticles. *Advanced Drug Delivery Reviews*, 7, 71-86.
- Kulkarni, K.H., Yang, Z., Niu, T. & Hu, M. 2012. Effects of estrogen and estrus cycle on pharmacokinetics, absorption, and disposition of genistein in female Sprague-Dawley rats. *Journal of Agricultural and Food Chemistry*, 60(32), 7949-7956.
- Kumar, S. & Randhawa, J.K. 2013. High melting lipid based approach for drug delivery: Solid lipid nanoparticles. *Materials Science and Engineering: C*, 33(4), 1842-1852.
- Kushwaha, A.K., Vuddanda, P.R., Karunanidhi, P., Singh, S.K. & Singh, S. 2013. Development and evaluation of solid lipid nanoparticles of raloxifene hydrochloride for enhanced bioavailability. *BioMed Research International*, Article ID 584549, doi: 10.1155/2013/584549.
- Lai, S.K., Wang, Y.Y., Hida, K., Cone, R. & Hanes, J. 2010. Nanoparticles reveal that human cervicovaginal mucus is riddled with pores larger than viruses. *Proceedings of the National Academy of Sciences*, 107(2), 598-603.
- Lambert, J. & Muir, T.A. 1955. *Practical chemistry*, 3rd ed., Heineman publishing, London, England.
- Lambros, M.P., Abbas, S.A. & Bourne, D.W.A. 1996. New high-performance liquid chromatographic method for amphotericin B analysis using an internal standard. *Journal of Chromatography B*, 685, 135-140.
- Lander, R., Manger, W., Scouloudis, M., Ku, A., Davis, C. & Lee, A. 2000. Gaulin homogenization: a mechanistic study. *Biotechnology Progress*, 16, 80-85.
- Langer, R. 1990. New methods of drug delivery. *Science*, 249, 1527-1533.
- Laserra, S., Basit, A., Sozio, P., Marinelli, L., Fornasari, E., Cacciatore, I. *et al.* 2015. Solid lipid nanoparticles loaded with lipoyl-memantine codrug: Preparation and characterization. *International Journal of Pharmaceutics*, 485(1-2), 183-191.
- Li, H., Zhao, X., Ma, Y., Zhai, G., Li, L. & Lou, H. 2009. Enhancement of gastrointestinal absorption of quercetin by solid lipid nanoparticles. *Journal of Controlled Release*, 133, 238-244.
- Lim, J., Yeap, S.P., Che, H.X. & Low, S.C. 2013. Characterization of magnetic nanoparticle by dynamic light scattering. *Nanoscale Research Letters*, 8(1), 381.
- Lindholm, J. 2004. Development and validation of HPLC methods for analytical and preparative purposes. *Ph.D thesis*, Uppsala University, Sweden.
- Lippacher, A., Müller, R.H. & Mäder, K. 2000. Investigation on the viscoelastic properties of lipid based colloidal drug carriers. *International Journal of Pharmaceutics*, 196, 227-230.
- Lippacher, A., Müller, R.H. & Mäder, K. 2001. Preparation of semisolid drug carriers for topical application based on solid lipid nanoparticles. *International Journal of Pharmaceutics*, 214, 9-12.

- Liu, J., Gong, T., Wang, C., Zhong, Z. & Zhang, Z. 2007. Solid lipid nanoparticles loaded with insulin by sodium cholate-phosphatidylcholine-based mixed micelles: preparation and characterization. *International journal of pharmaceutics*, 340(1), 153-162.
- Lockman, P.R., Oyewumi, M.O., Koziara, J.M., Roder, K.E., Mumper, R.J. & Allen, D.D. 2003. Brain uptake of thiamine-coated nanoparticles. *Journal of controlled release*, 93(3), 271-282.
- Loxley, A. 2009. Solid lipid nanoparticles for the delivery of pharmaceutical actives. *Drug Delivery Technology*, 9, 8.
- Luo, C.F., Yuan, M., Chen, M.S., Liu, S.M., Zhu, L., Huang, B.Y., Liu, X.W. & Xiong, W. 2011. Pharmacokinetics, tissue distribution and relative bioavailability of puerarin solid lipid nanoparticles following oral administration. *International Journal of Pharmaceutics*, 410, 138-144.
- Magenheim, B. & Benita, S., 1991. Nanoparticle characterisation: a comprehensive physicochemical approach. *STP Pharma Sci.*, 1, 221-241.
- Malagelada, J.R., Robertson, J.S., Brown, M.L., Remington, M., Duenes, J.A., Thomforde, G.M. *et al.* 1984. Intestinal transit of solid and liquid components of a meal in health. *Gastroenterology*, 87(6), 1255-1263.
- Malinowski, H.J. & Johnson, S.B. 2006. Bioavailability and bioequivalency testing. *In*: Troy, D.B. & Beringer, P. (eds.) *Remington: The science and practice of pharmacy*, Philadelphia: Lippincott Williams & Wilkins, 1037-1046.
- Malvern Instruments. 2015. *Technology*. Available at: <http://www.malvern.com/en/products/technology/default.aspx> [Accessed September 28, 2015].
- Marangoni, A. 2011. The trouble with crystal polymorphism. *Proceedings of the 102nd AOCS Annual Meeting & Expo*; May 1-11; Cincinnati, Ohio, USA.
- Martin, A., Swarbrick, J. & Cammarata, A. 1983. States of matter and phase equilibria. *In*: *Physical Pharmacy*, Philadelphia: Lea & Febiger, 62-92.
- Martino, R. 2004. Efficacy, safety and cost-effectiveness of amphotericin B lipid complex (ABLC): a review of the literature. *Current Medical Research and Opinion*, 20, 485-504.
- McGilveray, I.J. & Mattok, G.L. 1972. Some factors affecting the absorption of paracetamol. *Journal of Pharmacy and Pharmacology*, 24(8), 615-619.
- Mehnert, W. & Mäder, K. 2001. Solid lipid nanoparticles: production, characterisation and applications. *Advanced Drug Delivery Reviews*, 47(2-3), 165-196.
- Mehnert, W., zur Mühlen, A., Dingler, A., Weyhers, H. & Müller R.H. 1997. Solid Lipid Nanoparticles (SLN) - A novel active drug-carrier for cosmetics and pharmaceuticals, II. Drug incorporation, release and sterilisability. *Pharmazeutische Industrie*, 59(6), 511-514.
- Mei, Z., Li, X., Wu, Q., Hu, S. & Yang, X. 2005. The research on the anti-inflammatory activity and hepatotoxicity of triptolide-loaded solid lipid nanoparticle. *Pharmacological Research*, 51(4), 345-351.

- Mobley, W.C. & Schreier, H. 1994. Phase transition temperature reduction and glass transformation in dehydroprotected lyophilized liposomes. *Journal of Controlled Release*, 31, 73-87.
- Moffat, A.C., Osselton, M.D. & Widdop, B. 2005. Amphotericin B: In Galichet, L.Y. (ed.) *Clarke's Analysis of Drugs and Poisons*, London: Pharmaceutical Press.
- Mooter, V.G. & Kinget, R. 1995. Oral colon-specific drug delivery: A review. *Drug Delivery*, 2, 881-931.
- Mowat, A.M. 2003. Anatomical basis of tolerance and immunity to intestinal antigens. *Nature Reviews Immunology*, 3, 331-341.
- Mukherjee, S. Ray S. & Thakur, R.S. 2009. Solid lipid nanoparticles: a modern formulation approach in drug delivery system. *Indian Journal of Pharmaceutical Sciences*, 71 (4), 349-358.
- Müller, C., Schafer, P., Stortzel, M., Vogt, S. & Weinmann, W. 2002. Ion suppression effects in liquid chromatography-electrospray-ionisation transport-region collision induced dissociation mass spectrometry with different serum extraction methods for systematic toxicological analysis with mass spectra libraries. *Journal of Chromatography B*, 773(1), 47-52.
- Müller, R. H., Ruhl, D. & Runge, S.A. 1996. Biodegradation of solid lipid nanoparticles as a function of lipase incubation time. *International Journal of Pharmaceutics*, 144(1), 115-121.
- Müller, R.H. & Lucks J.S. 1996. Medication vehicles of solid lipid particles (Solid lipid nanospheres-SLN). Patent CA 2119253 A1.
- Müller, R.H. 1996. Zeta potential and particle charge in the laboratory, Scientific Verlags Company.
- Müller, R.H., Mäder, K. & Gohla, S. 2000. Solid lipid nanoparticles (SLN) for controlled drug delivery-a review of the state of the art. *European Journal of Pharmaceutics and Biopharmaceutics*, 50(1), 161-177.
- Müller, R.H., Peterson, R.D., Hommoss, A. & Pardeike, J. 2007. Nanostructured lipid carriers (NLC) in cosmetic dermal products. *Advanced Drug Delivery Reviews*, 59, 522-530.
- Müller, R.H., Radtke, M. & Vissing, S.A. 2002. Solid lipid nanoparticles (SLN) and nanostructured lipid carriers (NLC) in cosmetic and dermatological preparations. *Advanced Drug Delivery Reviews*, 54, S131-S55.
- Müller, R.H., Runge, S., Ravelli, V., Mehnert, W., Thunemann, A.F. & Souto, E.B. 2006. Oral bioavailability of cyclosporine: solid lipid nanoparticles (SLN) versus drug nanocrystals. *International Journal of Pharmaceutics*, 317(1), 82-89.
- Muthu, M.S. & Feng, S.S. 2009. Pharmaceutical stability aspects of nanomedicines. *Nanomedicine*, 4(8), 857-860.
- Myagmarjalbuu, B., Moon, M.J., Heo, S.H., Jeong, S.I., Park, J.-S., Jun, J.Y. *et al.* 2013. Establishment of a protocol for determining gastrointestinal transit time in mice using barium and radiopaque markers. *Korean Journal of Radiology*, 14(1), 45-50.

- Nahar, M. & Jain, N.K. 2009. Preparation, characterization and evaluation of targeting potential of amphotericin B-loaded engineered PLGA nanoparticles. *Pharmaceutical Research*, 26(12), 2588-2598.
- Nahar, M., Mishra, D., Dubey, V. & Jain, N.K. 2008. Development, characterisation, and toxicity evaluation of amphotericin B-loaded gelatin nanoparticles. *Nanomedicine*, 4, 252-261.
- NanoComposix Inc. 2012. *Guidelines for dynamic light scattering measurement and analysis*. Available at: <http://50.87.149.212/sites/default/files/nanoComposix%20Guidelines%20for%20DLS%20Measurements%20and%20Analysis.pdf> [Accessed November 3, 2015].
- NanoComposix Inc. 2015. *Characterization techniques: Zeta potential*. Available at: <http://nanocomposix.com/pages/characterization-techniques#zeta-potential> [Accessed April 2, 2015].
- Nimmo, J., Heading, R.C., Tothill, P. & Prescott, L.F. 1973. Pharmacological modification of gastric emptying: effects of propantheline and metoclopramide on paracetamol absorption. *British Medical Journal*, 1, 587-589.
- Nolan, J.A. 2013. Time of flight mass spectrometry of pharmaceutical systems. *Ph.D thesis*, The University of Nottingham, England.
- Nzai, J.M & Proctor, A. 1998. Determination of phospholipids in vegetable oil by fourier transform infrared spectroscopy. *Journal of the American Oil Chemists' Society*, 75(10), 1281-1289.
- Oh, J.H. & Lee, Y.J. 2013. Sample preparation for liquid chromatographic analysis of phytochemicals in biological fluids. *Phytochemical Analysis*, 25(4), 314-330.
- Olausson, E.A., Alpsten, M., Larsson, A., Mattsson, H., Andersson, H. & Attvall, S. 2008. Small particle size of a solid meal increases gastric emptying and late postprandial glycaemic response in diabetic subjects with gastroparesis. *Diabetes Research and Clinical Practice*, 80 (2), 231-237.
- Olbrich, C., Kayser, O. & Müller, R.H. 2002(a). Enzymatic degradation of Dynasan 114 SLN - effect of surfactants and particle size. *Journal of Nanoparticle Research*, 4(1-2), 121-129.
- Olbrich, C., Kayser, O. & Müller, R.H. 2002(b). Lipase degradation of Dynasan 114 and 116 solid lipid nanoparticles (SLN)-effect of surfactants, storage time and crystallinity. *International Journal of Pharmaceutics*, 237(1-2), 119-128.
- Ostrosky-Zeichner, L., Marr, K., Rex, J. & Cohen, S. 2003. Amphotericin B: Time for a new "Gold Standard". *Clinical Infectious Diseases*, 415-425.
- Owen, R.L., Piazza, A.J. & Ermak, T.H. 1991. Ultrastructural and cytoarchitectural features of lymphoreticular organs in the colon and rectum of adult BALB/c mice. *American Journal of Anatomy*, 190, 10-18.
- Paliwal, R., Rai, S., Vaidya, B., Khatri, K., Goyal, A.K., Mishra, N., Mehta, A. & Vyas, S.P. 2009. Effect of lipid core material on characteristics of solid lipid nanoparticles designed for oral lymphatic delivery. *Nanomedicine*, 5(2), 184-191.

- Panyam, J. & Labhasetwar, V. 2003. Biodegradable nanoparticles for drug and gene delivery to cells and tissue. *Advanced Drug Delivery Reviews*, 55, 329-347.
- Patel, P.A. & Patravale, V.B. 2011. Ambionp: Solid lipid nanoparticles of amphotericin b for oral administration. *Journal of Biomedical Nanotechnology*, 7, 1-8.
- Patel, R. 2000. Amphotericin B colloidal dispersion. *Expert Opinion on Pharmacotherapy*, 1, 475-488.
- Peh, K.K. & Yuen, K. H. 1996. Indirect gastrointestinal transit monitoring and absorption of theophylline. *International Journal of Pharmaceutics*, 139(1-2), 95-103.
- Peppercorn, M.A. & Goldman, P. 1973. Distribution studies of salicylazosulphapyridine and its metabolites. *Gastroenterology*, 64, 240-245.
- Philip, A.K., & Philip, B. 2010. Colon targeted drug delivery systems: a review on primary and novel approaches. *Oman Medical Journal*, 25(2), 79-87.
- Pinto, J.F. & Müller, R.H. 1999. Pellets as carriers of solid lipid nanoparticles (SLNs) for oral administration of drugs. *Die Pharmazie*, 506-509.
- Piwovar, A.M., Lockyer, N.P. & Vickerman, J.C. 2009. Salt effects on ion formation in desorption mass spectrometry: An investigation into the role of alkali chlorides on peak suppression in time-of-flight-secondary ion mass spectrometry. *Analytical Chemistry*, 81(3), 1040-1048.
- Polson, C., Sarkar, P., Incledon, B., Raguvaran, V. & Grant, R. 2003. Optimization of protein precipitation based upon effectiveness of protein removal and ionization effect in liquid chromatography - tandem mass spectrometry. *Journal of Chromatography B*, 785(2), 263-275.
- Pomerri, F., Frigo, A.C., Grigoletto, F., Dodi, G. & Muzzio, P.C. 2007. Error count of radiopaque markers in colonic segmental transit time study. *American Journal of Roentgenology*, 189(2), W56-W59.
- Porter, C.J. & Charman, W.N. 2001. In vitro assessment of oral lipid based formulations. *Advanced Drug Delivery Reviews*, 50(1), S127-S147.
- Porter, C.J., Trevaskis, N.L. & Charman, W.N. 2007. Lipids and lipid based formulations: optimizing the oral delivery of lipophilic drugs. *Nature Reviews. Drug Discovery*, 6(3), 231-248.
- Porter, C.J.H. & Charman, W.N. 1997. Uptake of drugs into intestinal lymphatics after oral administration. *Advanced Drug Delivery Reviews*, 25, 71-89.
- Postawa, Z., Czerwinski, B., Szewczyk, M., Smiley, E.J., Winograd, N. & Garrison, B.J. 2004. Microscopic insights into the sputtering of Ag{111} induced by C-60 and Ga bombardment. *Journal of Physical Chemistry B*, 108, 7831-7838.
- Pouton, C.W. & Porter, C.J.H. 2008. Formulation of lipid-based delivery systems for oral administration: Materials, methods and strategies. *Advanced Drug Delivery Reviews*, 60, 625-637.
- Pouton, C.W. 2000. Lipid formulations for oral administration of drugs: nonemulsifying, self-emulsifying and 'self-microemulsifying' drug delivery systems. *European Journal of Pharmaceutical Sciences*, 11(2), S93-S98.

- Pouton, C.W. 2006. Formulation of poorly water-soluble drugs for oral administration: physicochemical and physiological issues and the lipid formulation classification system. *European Journal of Pharmaceutical Sciences*, 29, 278-287.
- Pramod, K., Peeyush, K., Rajeev, K., Nitish, K. & Rakesh, K. 2010. An overview of lipid based formulation for oral drug delivery. *Drug Invention Today*, 2, 390-395.
- Primard, C., Rochereau, N., Luciani, E., Genin, C., Delair, T., Paul, S. *et al.* 2010. Traffic of poly (lactic-acid) nanoparticulate vaccine vehicle from intestinal mucus to sub-epithelial immune competent cells. *Biomaterials*, 31, 6060-6068.
- Qinna, N.A., Ismail, O.A., Alhussainy, T.M., Idkaidek, N.M. & Arafat, T.A. 2014. Evidence of reduced oral bioavailability of paracetamol in rats following multiple ingestion of grapefruit juice. *European Journal of Drug Metabolism and Pharmacokinetics*, doi:10.1007/s13318-014-0251-4.
- Quini, C.C., Américo, M.F., Corá, L.A., Calabresi, M.F.F., Alvarez, M., Oliveira, R.B. *et al.* 2012. Employment of a noninvasive magnetic method for evaluation of gastrointestinal transit in rats. *Journal of Biological Engineering*, 6:6.
- Quintanar-Guerrero, D., Fessi, H., Allmann, E. & Doelker, E. 1996. Influence of stabilizing agents and preparative variables on the formation of poly (D, L-lactic acid) nanoparticles by an emulsification-diffusion technique. *International Journal of Pharmaceutics*, 143(2), 133-141.
- Rahman, N. & Niaz, U. 2004. HPLC Assay for paracetamol and sulfapyridine in human plasma as markers of gastric emptying and oro-caecal transit. *Journal of Medical Sciences*, 4, 232-235.
- Rahman, N. U., Yuen, K. H. & Woei, W. J. 2005. Gastrointestinal transit monitoring and absorption of controlled-release pellets of Diltiazem. *Pharmaceutical Development and Technology*, 10(3), 371-379.
- Ratner, B.D., Castner, D.G., Brison, J., Barnes, C. & Daneshcvar, R. 2009. *Static SIMS: A powerful tool to investigate nanoparticles and biology*. Available at: http://www.semineddle.com/system/files/BuddyRatner_5-14-09.pdf?snc=5963.
- Read, N.W., Al Janabi, M.N., Bates, T.E. & Barber, D.C. 1983. Effect of gastrointestinal intubation on the passage of a solid meal through the stomach and small intestine in humans. *Gastroenterology*, 84(6), 1568-1572.
- Read, N.W., Miles, C.A., Fisher, D., Holgate, A.M., Kime, N.D., Mitchell, M.A., Reeve A.M., Roche, T.B. & Walker, M. 1980. Transit of a meal through the stomach, small intestine, and colon in normal subjects and its role in the pathogenesis of diarrhea. *Gastroenterology*, 79(6), 1276-1282.
- Reddy L.H., Vivek, K., Bakshi, N. & Murthy, R.S. 2006. Tamoxifen citrate loaded solid lipid nanoparticles (SLNTM): Preparation, characterization, in vitro drug release, and pharmacokinetic evaluation. *Pharmaceutical Development and Technology*, 11, 167-177.
- Riddick, T.M. 1968. Control of colloid stability through zeta potential. Pennsylvania: Livingston Publishing Company.

- Risovic, V., Boyd, M., Choo, E. & Wasan, K.M. 2003. Effects of lipid-based oral formulations on plasma and tissue amphotericin b concentrations and renal toxicity in male rats. *Antimicrobial Agents and Chemotherapy*, 47(10), 3339-3342.
- Rodrigues, M., Peiriço, N., Matos, H., Lobato, M.R., Almeida, A.J. & Gomes de Azevedo, E. 2004. Microcomposites theophylline/hydrogenated palm oil from a PGSS process for controlled drug delivery systems. *Journal of Supercritical Fluids*, 29, 175-184.
- Roger, E., Lagarce, F. & Benoit, J.P. 2009. The gastrointestinal stability of lipid nanocapsules. *International Journal of Pharmaceutics*, 379(2), 260-265.
- Sahoo, S.K. & Labhasetwar, V. 2003. Nanotech approaches to drug delivery and imaging. *Drug Discovery Today*, 8, 1112-1120.
- Saini, B. & Bansal, G. 2014. Degradation study on sulfasalazine and a validated HPLC-UV method for its stability testing. *Scientia Pharmaceutica*, 82, 295-306.
- Sanjula, B., Shah, F.M., Javed, A. & Alka, A. 2009. Effect of poloxamer 188 on lymphatic uptake of carvedilol-loaded solid lipid nanoparticles for bioavailability enhancement. *Journal of Drug Targeting*, 17(3), 249-256.
- Saupe, A. & Rades, T. 2006. Solid lipid nanoparticles. *In: Mozafari, M.R. (ed.), Nanocarrier Technologies: Frontiers of Nanotherapy*. Springer, The Netherlands, 41-50.
- Saupe, A., Wissing, S.A., Lenk, A., Schmidt, C. & Müller, R.H. 2005. Solid lipid nanoparticles (SLN) and nanostructured lipid carriers (NLC) - Structural investigations on two different carrier systems. *Bio-Medical Materials and Engineering*, 15, 393-402.
- Sauto, E.B. & Müller, R.H. 2007. Lipid nanoparticles (solid lipid nanoparticles and nanostructured lipid carriers) for cosmetic, dermal and transdermal applications. *In: Thassu, D., Deleers, M., Pathak, Y. (eds.), Nanoparticulate Drug Delivery Systems*. New York: Informa Health Care, 213-233.
- Sawaya, B.P., Briggs, J.P. & Schnermann, J. 1995. Amphotericin B nephrotoxicity: the adverse consequences of altered membrane properties. *Journal of the American Society of Nephrology*, 6(2), 154-164.
- Schwarz, C. & Mehnert, W. 1997. Freeze-drying of drug-free and drug-loaded solid lipid nanoparticles. *International Journal of Pharmaceutics*, 157(2), 171-179.
- Schwarz, C. 1995. Solid lipid nanoparticle: Production, characterisation, drug incorporation and release, sterilisation and lyophilisation. *Ph.D thesis*, Free University of Berlin, Germany.
- Sellers, S.P., Clark, G.S., Sievers, R.E. & Carpenter, J.F. 2001. Dry powders of stable protein formulations from aqueous solutions prepared using supercritical CO₂-assisted aerosolisation. *Journal of Pharmaceutical Sciences*, 90, 785-797.
- Severino, P., Andreani, T., Macedo, A.S., Fangueiro, J.F., Santana, M.H.A., Silva, A.M. & Souto E.B. 2012. Current State-of-Art and New Trends on Lipid Nanoparticles (SLN and NLC) for Oral Drug Delivery. *Journal of Drug Delivery*, doi: 10.1155/2012/750891.
- Shabir, G.A. 2004. A practical approach to validation of HPLC methods under current good manufacturing practices. *Journal of Validation Technology*, 10, 210-218.

- Shah, P.V, Midha, K.K., Dighe, S., McGilveray, J.I, Skelly, P.J, Yacobi, A., Layloff, T., Viswanathan, C.T., Cook, E.C., Mcdowall, R.D., Pittman, A.K. & Spector S. 1992. Analytical Method Validation: Bioavailability, Bioequivalence and Pharmacokinetics Studies. *Journal of Pharmaceutical Sciences*, 81, 309-312.
- Shakweh, M., Besnard, M., Nicolas, V. & Fattal, E. 2005. Poly (lactide-co-glycolide) particles of different physicochemical properties and their uptake by Peyer's patches in mice. *European Journal of Pharmaceutics and Biopharmaceutics*, 61(1-2), 1-13.
- Shimadzu. 2015. *HPLC: Tips for daily analysis. Differences between using acetonitrile and methanol for reverse phase chromatography*. Available at: <http://www.shimadzu.com/an/hplc/support/lib/lctalk/35/35lab.html> [Accessed July 22, 2015].
- Shimizu, R. 2005. Monte Carlo simulation studies in Japan on interaction of charged particles with solids during those early days in 1960s-1970s. *Nuclear Instruments & Methods in Physics Research Section B-Beam Interactions with Materials and Atoms*, 232, 117-124.
- Siekmann, B. & Westesen, K. 1992. Submicron-sized parenteral carrier systems based on solid lipids. *Pharmaceutical and Pharmacological Letters*, 1, 123-126.
- Siekmann, B. & Westesen, K. 1994. Melt-homogenized solid lipid nanoparticles stabilized by the nonionic surfactant tyloxapol I. Preparation and particle size determination. *Pharmaceutical and Pharmacological Letters*, 3, 194-197.
- Siepmann, J. & Peppas, N.A. 2011. Higuchi equation: Derivation, applications, use and misuse. *International Journal of Pharmaceutics*, 418(1), 6-12.
- Singh, B.N. 1999. Effects of food on clinical pharmacokinetics. *Clinical Pharmacokinetics*, 37(3), 213-255.
- Sinha, V.R., Srivastava, S., Goel, H. & Jindal, V. 2010. Solid Lipid Nanoparticles (SLN'S)- Trends and Implications in Drug Targeting. *International Journal of Advances in Pharmaceutical Sciences*, 1, 212-238.
- Sjöström, B. & Bergenståhl, B. 1992. Preparation of submicron drug particles in lecithin-stabilised o/w emulsions I. Model studies of the precipitation of cholesteryl acetate. *International Journal of Pharmaceutics*, 88, 53-62.
- Smith, D.J. 2007. Characterisation of nanomaterials using transmission electron microscopy. *In: Hutchison, J., Kirkland, A. (eds.), Nanocharacterisation*, Cambridge: The Royal Society of Chemistry, 1-27.
- Soliman, A.A., Mohamed, G.G., Hosny, W.M. & El-Mawgood, M.A. 2005. Synthesis, spectroscopic and thermal characterization of new sulphasalazine metal complexes. *Synthesis and Reactivity in Inorganic, Metal-Organic and Nano-Metal Chemistry*, 35(6), 483-490.
- Staniforth, D.H., Coates, P. & Clarke, J.G.N. 1987. An HPLC assay for sulphapyridine in plasma and its use to assess small bowel transit time after the administration of sulphasalazine. *International Journal of Clinical Pharmacology, Therapy and Toxicology*, 25(7), 406- 409.
- Steingoetter, A., Fox, M., Treier, R., Weishaupt, D., Marincek, B., Boesiger, P., Fried, M. & Schwizer, W. 2006. Effects of posture on the physiology of gastric emptying: a magnetic

- resonance imaging study. *Scandinavian Journal of Gastroenterology*, 41(10), 1155-1164.
- Subramanian, N. & Ghosal, S.K. 2004. Enhancement of gastrointestinal absorption of poorly water soluble drugs via lipid based systems. *Indian Journal of Experimental Biology*, 42, 1056-1065.
- Sugito, K., Ogata, H., Goto, H., Kaniwa, N., Takahata, H. & Samejima, M. 1992. Gastric emptying rate of drug preparations. III. Effects of size of enteric micro-capsules with mean diameters ranging from 0.1 to 1.1 mm in man. *Chemical & Pharmaceutical Bulletin*, 40(12), 3343-3345.
- Suresh, G., Manjunath, K., Venkateswarlu, V. & Satyanarayana, V. 2007. Preparation, characterisation and *in vitro* and *in vivo* evaluation of lovastatin solid lipid nanoparticles. *AAPS PharmSciTech*, 8(1), E1-E9.
- Svilenov, H. & Tzachev, C. 2013. Solid Lipid Nanoparticles-A promising drug delivery system. *Nanomedicine*, 8, 187-237.
- Tan, C.S.W., Billa, N., Roberts, C.J. & Scurr, D.J. 2014. Properties of an oral nanoformulation of a molecularly dispersed amphotericin B comprising a composite matrix of theobroma oil and bee's wax. *Nanomaterials*, 4(4), 905-916.
- Tan, S.W., Billa, N., Roberts, C.R. & Burley, J.C. 2010. Surfactant effects on the physical characteristics of Amphotericin B-containing nanostructured lipid carriers. *Colloids and Surfaces A: Physicochemical and Engineering Aspect*, 372(1-3), 73-79.
- Tarr, B.D. & Yalkowsky, S.H. 1989. Enhanced intestinal absorption of cyclosporine in rats through the reduction of emulsion droplet size. *Pharmaceutical Research*, 6, 40-43.
- Torrado, J.J., Espada, R., Ballesteros, M.P. & Torrado-Santiago, S. 2008. Amphotericin B formulations and drug targeting. *Journal of Pharmaceutical Sciences*, 97(7), 2405-2425.
- Torrado, J.J., Espada, R., Ballesteros, M.P. & Torrado-Santiago, S. 2008. Amphotericin B formulations and drug targeting. *Journal of Pharmaceutical Sciences*, 97, 2405-2425.
- Trotta, M., Debernardi, F., Caputo, O. 2003. Preparation of solid lipid nanoparticles by a solvent emulsification-diffusion technique. *International Journal of Pharmaceutics*, 257(1-2), 153-160.
- Tscharnuter, W. 2000. Photon correlation spectroscopy in particle sizing. In: Meyers, R.A. (ed.), *Encyclopedia of analytical chemistry*, John Wiley & Sons Ltd., Chichester, 5469-5485.
- Tuleu, C., Andrieux, C., Boy, P. & Chaumeil, J.C. 1999. Gastrointestinal transit of pellets in rats: effect of size and density. *International Journal of Pharmaceutics*, 180(1), 123-131.
- Uchida, J. 1988. Electron microscopic study of microfold cells (M cells) in normal and inflamed human appendix. *Gastroenterologia Japonica*, 23, 251-262.
- Uner, M. & Yener, G. 2007. Importance of solid lipid nanoparticles (SLN) in various administration routes and future perspectives. *International Journal of Nanomedicine*, 2(3), 289-300.
- Unruh, T., Bunjes, H., Westesen, K. & Koch, M.H.J. 1999. Observation of size dependent melting in lipid nanoparticles. *The Journal of Physical Chemistry B*, 103, 10373-10377.

- Varshosaz, J., Minayian, M. & Moazen, E. 2010(a). Enhancement of oral bioavailability of pentoxifylline by solid lipid nanoparticles. *Journal of Liposome Research*, 20(2), 115-123.
- Varshosaz, J., Tabbakhian, M. & Mohammadi, M.Y. 2010(b). Formulation and optimization of solid lipid nanoparticles of buspirone HCl for enhancement of its oral bioavailability. *Journal of Liposome Research*, 20(4), 286-296.
- Venkateswarlu, V. & Manjunath, K. 2004. Preparation, characterisation and *in vitro* release kinetics of clozapine solid lipid nanoparticles. *Journal of Controlled Release*, 95(3), 627-638.
- Vickerman, J.C. & Gilmore, I.S. 2009. *Surface analysis: the principal techniques*, 2nd ed., Wiley and Sons Ltd., Chichester, England.
- Vivek, K., Reddy, H. & Murthy, R.S.R. 2007. Investigations of the effect of the lipid matrix on drug entrapment, *in vitro* release, and physical stability of olanzapine-loaded solid lipid nanoparticles. *AAPS PharmSciTech*, 8(4), 16-24.
- Vyas, S.P. & Gupta, S. 2006. Optimizing efficacy of amphotericin B through nanomodification. *International Journal of Nanomedicine*, 1 (4), 417-432.
- Wagner, D., Langguth, H.S., Hanafy, A., Koggela, A. & Langguth, P. 2001. Intestinal drug efflux: formulation and food effects. *Advanced Drug Delivery Reviews*, 50(1), S13-S31.
- Walsh, M., White, L., Atkinson, K. & Enno, A. 1992. Fungal *Pseudoallescheria boydii* lung infiltrates unresponsive to amphotericin B in leukaemic patients. *Australian and New Zealand Journal Medicine*, 22, 265-268.
- Walsh, T.J., Hiemenz, J.W., Seibel, N.L., Perfect, J.R., Horwith, G., Lee, L., Silber, J.L., DiNubile, M.J., Reboli, A., Bow, E., Lister, J. & Anaissie, E.J. 1998. Amphotericin B lipid complex for invasive fungal infections: analysis of safety and efficacy in 556 cases. *Clinical Infectious Diseases*, 26(6), 1383-1396.
- Walsh, T.J., Melcher, G.P., Rinaldi, M.G., Lecciones, J. McGough, D.A., Kelly, P., Lee, J., Callender, D., Rubin, M. & Pizzo P.A. 1990. *Trichosporon beigellii*, an emerging pathogen resistant to amphotericin B. *Journal Clinical Microbiology*, 28, 1616-1622.
- Wang, J.W., Tang, H.F., Shen, M., Wang, L. & Fang, K.Q. 2007. Preparation and quality evaluation of oleanolic acid-loaded solid lipid nanoparticles. *Journal of Fourth Military Medical University*, 28, 472-472.
- Wang, S.L., Lin, S.Y. & Wei, Y.S. 2002. Transformation of metastable forms of acetaminophen studied by thermal fourier transform infrared (FT-IR) microspectroscopy. *Chemical and Pharmaceutical Bulletin*, 50(2), 153-156.
- Welling, P.G. 1996. Effects of food on drug absorption. *Annual Review of Nutrition*, 16, 383-415.
- Westesen, K. & Bunjes, H. 1995. Do nanoparticles prepared from lipids solid at room temperature always possess a solid lipid matrix? *International Journal of Pharmaceutics*, 115(1), 129-131.
- Westesen, K., Siekmann, B. & Koch, M.H.J. 1993. Investigations on the physical state of lipid nanoparticles by synchrotron radiation X-ray diffraction. *International Journal of Pharmaceutics*, 93, 189-199.

- White, M.H., Bowden, R.A., Sandler, E.S., Graham, M.L., Noskin, G.A., Wingard, J.R. *et al.* 1998. Randomised double-blind clinical trial of amphotericin B colloidal dispersion vs. amphotericin B in the empirical treatment of fever and neutropenia. *Clinical Infectious Diseases*, 27, 296-302.
- Wilkinson, J.M., McDonald, C., Parkin, J.E. & Sunderland, V.B. 1998. A high-performance liquid-chromatographic assay for amphotericin B in a hydrophilic colloidal paste base. *Journal of Pharmaceutical and Biomedical Analysis*, 17, 751-755.
- Wilson, C.G. & Mahony, B.O. 1997. The behaviour of fats and oils in the upper G.I. tract. *Gattefossé Bulletin Technique*, 90, 13-18.
- Wilson, C.G., Parr, G.D., Kennerley, J.W., Taylor, M.J., Davis, S.S., Hardy, J.G. & Rees, J.A. 1984. Pharmacokinetics and *in vivo* scintigraphic monitoring of a sustained release acetylsalicylic acid formulation. *International Journal of Pharmaceutics*, 18(1-2), 1-8.
- Wingard, J.R., Kubilis, P., Lee, L., Yee, G., White, M., Walshe, L., Bowden, R., Anaissie, E., Hiemenz, J. & Lister, J. 1999. Clinical significance of nephrotoxicity in patients treated with Amphotericin B for suspected or proven aspergillosis. *Clinical Infectious Diseases*, 29, 1402-1407.
- Wissing, S., Lippacher, A. & Müller, R.H. 2001. Investigations on the occlusive properties of solid lipid nanoparticles (SLN). *Journal of Cosmetic Science*, 52, 313-324.
- Wong-Beringer, A., Jacobs, R.A. & Guglielmo, B.J. 1998. Lipid formulations of amphotericin B: Clinical efficacy and toxicities. *Clinical Infectious Diseases*, 27, 603-618.
- Worsøe, J., Fynne, L., Gregersen, T., Schlageter, V., Christensen, L.A., Dahlerup, J.F. *et al.* 2011. Gastric transit and small intestinal transit time and motility assessed by a magnet tracking system. *BMC Gastroenterology*, 11:145.
- Xue, M., Yang, M.X., Zhang, W., Li, X.M., Gao, D.H., Ou, Z.M., Li, Z.P., Liu, S.H., Li X.J. & Yang, S.Y. 2013. Characterization, pharmacokinetics, and hypoglycemic effect of berberine loaded solid lipid nanoparticles. *International Journal of Nanomedicine*, 8, 4677-4687.
- Yang, L., Seah, M.P., Gilmore, I.S., Morris, R.J.H., Dowsett, M.G., Boarino, L., Sparnacci, K. & Laus, M. 2013. Depth profiling and melting of nanoparticles in secondary ion mass. *The Journal of Physical Chemistry C*, 117, 16042-16052.
- Yang, L., Xu, Y., Su, Y., Wu, J., Zhao, K., Chen, J. & Wang, M. 2005. FT-IR spectroscopic study on the variations of molecular structures of some carboxyl acids induced by free electron laser. *Spectrochimica Acta Part A: Molecular and Biomolecular Spectroscopy*, 62(4-5), 1209-1215.
- Yang, S., Zhu, J., Lu, Y., Liang, B. & Yang, C. 1999. Body distribution of camptothecin solid lipid nanoparticles after oral administration. *Pharmaceutical Research*, 16, 751-757.
- Yang, S.C. & Zhu, J.B. 2002. Preparation and characterization of camptothecin solid lipid nanoparticles. *Drug Development and Industrial Pharmacy*, 28(3), 265-274.
- Yasir, M. & Sara, U.V.S. 2014. Solid lipid nanoparticles for nose to brain delivery of haloperidol: *in vitro* drug release and pharmacokinetics evaluation. *Acta Pharmaceutica Sinica B*, 4(6), 454-463.

- Yuan, H., Chen, J., Du, Y.Z., Hu, F.Q., Zeng, S. & Zhao, H.L. 2007. Studies on oral absorption of stearic acid SLN by a novel fluorometric method. *Colloids and Surfaces. B Biointerfaces*, 58(2), 157-164.
- Yuan, H., Chen, C.-Y. , Chai, G., Du, Y.-Z. & Hu, F.-Q. 2013. Improved transport and absorption through gastrointestinal tract by pegylated solid lipid nanoparticles. *Molecular Pharmaceutics*, 10, 1865-1873.
- Yuen, K.H., Desmukh, A.A., Newton, J.M., Short, M. & Melchor, R. 1993. Gastrointestinal transit and absorption of theophylline from a multiparticulate controlled release theophylline formulation. *International Journal of Pharmaceutics*, 97(1-3), 588-592.
- Zamek-Gliszczyński, M.J., Bedwell, D.W., Bao, J.Q. & Higgins, J.W. 2012. Characterization of SAGE Mdr1a (P-gp), Bcrp, and Mrp2 knockout rats using loperamide, paclitaxel, sulfasalazine, and carboxydichlorofluorescein pharmacokinetics. *Drug Metabolism and Disposition: The Biological Fate of Chemicals*, 40(9), 1825-1833.
- Zhang, C., Gu, C., Peng, F., Liu, W., Wan, J., Xu, H., Lam, C.W. & Yang, X. 2013. Preparation and optimization of triptolide-loaded solid lipid nanoparticles for oral delivery with reduced gastric irritation. *Molecules*, 18(11), 13340-13356.
- Zhang, Y. & Zhang, J. 2005. Surface modification of monodisperse magnetite nanoparticles for improved intracellular uptake to breast cancer cells. *Journal of Colloid and Interface Science*, 283, 352-357.
- Zhang, Z., Gao, F., Bu, H., Xiao, J. & Li, Y. 2012. Solid lipid nanoparticles loading candesartan cilexetil enhance oral bioavailability: in vitro characteristics and absorption mechanism in rats. *Nanomedicine: Nanotechnology, Biology, and Medicine*, 8, 740-747.
- Zhao, Y.H., Abraham, M.H., Le, J., Hersey, A., Luscombe, C.N., Beck, G. *et al.* 2003. Evaluation of rat intestinal absorption data and correlation with human intestinal absorption. *European Journal of Medicinal Chemistry*, 38(3), 233-243.
- Zheng, J., Dobner, A., Babygirija, R., Ludwig, K. & Takahashi, T. 2009. Effects of repeated restraint stress on gastric motility in rats. *American Journal of Physiology. Regulatory, Integrative and Comparative Physiology*, 296(5), R1358-65.
- Zimnicka, B. & Hacura, A. 2006. An investigation of molecular structure and dynamics of crude beeswax by vibrational spectroscopy. *Polish Journal of Environmental Studies*, 15(4), 112-114.
- zur Mühlen, A. & Mehnert, W. 1998. Drug release and release mechanism of prednisolone loaded solid lipid nanoparticles. *Pharmazie* 53(8), 552-555.
- zur Mühlen, A. 1996. Solid Lipid nanoparticles with prolonged drug liberation: long-term stability, characterisation, release behaviour and mechanisms. *Ph.D thesis*, Free University of Berlin, Germany.
- zur Mühlen, A., Schwarz, C. & Mehnert, W. 1998. Solid lipid nanoparticles (SLN) for controlled drug delivery-drug release and release mechanism. *European Journal of Pharmaceutics and Biopharmaceutics*, 45(2), 149-155.
- zur Mühlen, A., zur Mühlen, E., Niehus, H. & Mehnert, W. 1996. Atomic force microscopy studies of solid lipid nanoparticles. *Pharmaceutical Research*, 13, 1411-1416.